Tesis Doctoral

DESIGN AND DYNAMIC ANALYSIS OF STEAM GENERATORS FOR CONCENTRATING SOLAR POWER PLANTS

Autor

Pedro Ángel González Gómez

Director

Domingo Santana Santana

Co-director

Jesús Gómez Hernández

DEPARTAMENTO DE INGENIERÍA TÉRMICA Y DE FLUIDOS

Leganés (Madrid), Octubre 2017

Universidad Carlos III de Madrid
www.uc3m.es

TESIS DOCTORAL

DESIGN AND DYNAMIC ANALYSIS OF STEAM GENERATORS FOR CONCENTRATING SOLAR POWER PLANTS

Autor: Pedro Ángel González Gómez

Director de Tesis: Domingo Santana Santana

Co-director de Tesis: Jesús Gómez Hernández

Firma del Tribunal Calificador:

Firma

Presidente: D. David Sánchez Martínez

Secretario: D. Antonio José Rovira de Antonio

Vocal: D. Rafael Eduardo Guédez Mata

Calificación:

Leganés (Madrid), 4 de Diciembre de 2017

DEPARTAMENTO DE INGENIERÍA TÉRMICA Y DE FLUIDOS

Escuela Politécnica Superior

DESIGN AND DYNAMIC ANALYSIS OF STEAM GENERATORS FOR CONCENTRATING SOLAR POWER PLANTS

Autor

Pedro Ángel González Gómez

Director de Tesis: Domingo Santana Santana

Co-director de Tesis: Jesús Gómez Hernández

Leganés (Madrid), Diciembre 2017

A mi familia.

A Amparo.

Agradecimientos

Ahora que estoy terminando de escribir esta tesis, no puedo evitar acordarme de todos aquellas personas que me han ayudado de forma directa o indirecta durante todo este tiempo. En primer lugar, agradecer a Domingo la confianza depositada en mí para la realización de esta investigación y su apoyo constante durante todos estos años. También agradecer a mi codirector Jesús su inestimable ayuda. A ambos, gracias por haberme guiado en el mundo de la investigación y por vuestra paciencia. Destacar también la colaboración de Javi Villa, Fontina y Antonio Acosta por su gran ayuda y sus valiosos consejos.

También me gustaría agradecer a los doctores del grupo ISE: Mercedes, María, Antonio Soria, Néstor, Ulpiano, Celia, Sergio, Carol, Fernando, Luismi, Reyes, Alberto, Edu y Dani el buen trato y los miles de favores recibidos. Agradecer a todos los miembros del grupo de Mecánica de Fluidos su buena acogida. Agradecer a Cristina su gran ayuda en innumerables ocasiones.

También me gustaría agradecer a los doctorandos y compañeros del departamento: Patri, Alejandro, Dani, Pablo, Juan, Miguel Parrales, Dani Moreno los buenos momentos vividos, y en especial a mis compañeros de despacho: María y Andrés, así como a los compañeros del departamento de Mecánica: Carlos Pons y Miguel.

Gracias a mis amigos, tanto a los de Albacete: Kisko, Paco, Setos, Joserra, Ismael, Rubén, Toni, Jambo, Joseda, Jesusete; como a los del pueblo: Miguel, Josedo, Chema, Ernesto, Lezcano, Xavi, Joni, Vergara y muchos otros. Gracias a todos por los grandes momentos vividos y por lo momentos que vendrán.

Gracias a mi familia. A mis padres: Pedro y Pilar; y a mis hermanos: Jesús y Mari Pili. Gracias por vuestro apoyo incondicional y vuestro cariño. Gracias por ser un ejemplo de humildad y generosidad. Gracias a mis abuelos: Pedro, Carmen, Antonio y Alfonsa. A mis tíos, Antonio y María, Mari y Pedro, Pepi y Vicente, Toni y Chelo, Ángel, Valen y Ana. A mis primos: Mónica, Teresa, Ana, Miguel Ángel, Beatriz, Víctor, Aitor y Yago. En definitiva, gracias familia por haberme dado tanto. Gracias por vuestro ejemplo. Sin vuestro sacrificio yo no hubiera podido realizar muchos de mis sueños.

Gracias a Amparo, mi compañera de vida. Gracias por estar siempre a mi lado y por ser un ejemplo para mí. Gracias por tu paciencia, apoyo y cariño.

Acknowledgments

I would like to thank to Fredrik Haglind and Davide Ferruzza, form Technical University of Denmark, for their hospitality and help during my research stay in summer 2017.

Resumen

Las centrales termosolares normalmente utilizan sistemas de generación de vapor indirectos debido a las ventajas producidas por la utilización de un fluido caloportador, que permite la instalación de eficientes sistemas de almacenamiento térmico. Sin embargo, los sistemas de generación de vapor indirectos están limitados por la diferencia de temperaturas mínima en el evaporador, que fija el caudal de fluido caloportador, y por tanto tiene un gran impacto en el funcionamiento de la planta. Como consecuencia, se obtiene un compromiso entre los costes de inversión de los intercambiadores de calor y los costes de bombeo del fluido caloportador.

El estado actual de los mercados eléctricos promueve la necesidad de incrementar la flexibilidad de las centrales termosolares. El sistema de generación de vapor tiene una gran influencia en la flexibilidad debido al estrés térmico en los componentes de pared gruesa que limitan las rampas de arranque y cambio de carga. Además, la operación cíclica de las centrales termosolares pueden producir daño a fatiga y por tanto conducir a un fallo prematuro del material. Por esta razón, el análisis dinámico del sistema de generación de vapor es necesario para asegurar su vida útil.

Esta tesis doctoral está basada en el diseño y análisis dinámico de sistemas de generación de vapor de centrales termosolares. En primer lugar se ha desarrollado un metodología para el diseño del sistema de generación de vapor de centrales termosolares de 50 MWe de cilindro parabólico, incluyendo también el diseño de los intercambiadores sales-aceite. El diseño de los intercambiadores de calor se ha realizado acorde con la normativa TEMA y el código ASME. El análisis económico se ha realizado tomando la diferencia de temperatura mínima en el evaporador y la temperatura de salida del fluido caloportador como principales variables. De este modo, se tienen en cuenta los costes de bombeo del fluido caloportador y los costes de inversión de los intercambiadores de calor. Por otro lado, dos estrategias de diseño son comparadas: minimización del área de transferencia de calor y minimización de los costes anualizados. Obteniendo con la segunda opción un considerable ahorro de los costes de operación. Además, se ha desarrollado un evaporador de recirculación especialmente diseñado para centrales termosolares de cilindro parabólico.

Por otro lado, también se ha desarrollado una metodología para el diseño del sistema de generación de vapor de una central termosolar de tipo torre. Las condiciones especiales de operación con altas temperaturas y grandes calores de intercambio hacen de esta tarea un problema atípico en el diseño de intercambiadores de calor. Por esta razón, se han tenido en cuenta consideraciones de transferencia de calor y estrés térmico para la selección del tipo de intercambiador para sobrecalentador, recalentador, evaporador y precalentador. El análisis económico se

ha realizado tomando como principal variable la diferencia de temperaturas mínima en el evaporador por su influencia en el funcionamiento global de la central. Dos configuraciones del generador de vapor son estudiadas: con un tren y con dos trenes en paralelo. Los resultados muestran que los valores óptimos se obtienen para diferencias de temperaturas mínimas en el evaporador muy bajas. Además, un análisis económico preliminar se ha realizado para comparar los evaporadores con circulación forzado y natural.

El estudio dinámico comienza con el análisis transitorio del sistema de generador de la central termosolar de tipo torre. Para ello, son desarrollados diferentes modelos dinámicos para los intercambiadores monofásicos, y para el conjunto evaporador y calderín. Además, se han desarrollado modelos para el cálculo de los campos temperaturas y del estrés en partes críticas de intercambiadores de tubo y carcasa como los ligamentos de placa de tubos y las uniones de la placa de tubos. Para el estudio dinámico del arranque del generador de vapor son considerados dos escenarios. El primero considera perfiles de temperatura no isotérmicos en los intercambiadores al principio del arranque, mientras que el segundo considera perfiles isotérmicos. Para ambos escenarios son calculadas las rampas de temperatura del fluido caloportador y del evaporador para operar el generador de vapor por el lado de la seguridad.

Además también se ha presentado el análisis dinámico del sistema de generación de vapor de una central termosolar de cilindro parabólico. Para ello, se han desarrollado modelos dinámicos para intercambiadores TEMA F y TEMA H. Los estreses térmicos son calculados en zonas críticas como: la placa de tubos, uniones de cabeza y tobera, las uniones tipo T del calderín y los tubos en U. Además, los modelos de estrés son validados por medio de diferentes modelos en elementos finitos. El análisis dinámico del arranque del sistema de generación se ha realizado para rampas de temperatura que no sobrepasan los límites de estrés impuestos por la integridad estructural y la protección de la capa de magnetita. Finalmente, se ha realizado un estudio comparando el comportamiento dinámico entre evaporador tipo *kettle* y de recirculación.

En último lugar, se ha realizado el análisis a fatiga del sistema de generación de vapor de una central termosolar de cilindro parabólico. El análisis a fatiga se ha realizado conforme al código ASME para las operaciones de arranque, apagado y cambio de carga del generador de vapor.

Abstract

Commercial concentrating solar power (CSP) plants normally use an indirect steam generation system due to the advantages provided by use of the heat transfer fluid (HTF), which allows the installation of cost-effective storage systems. However, the pinch point temperature difference limitation imposed by the indirect steam generator (SG) systems has a great influence on the overall plant performance because it sets the mass flow rate of the HTF. As a consequence, a trade-off is obtained between the investment cost of the heat exchangers and the operational pump cost of the heat transfer fluid.

CSP plants need to increase their flexibility in order to be competitive in the current electricity markets. The SG has a great influence on the flexibility of CSP plants due to the thermal stresses on thick-walled components that limit the start-up and load changes ramps. Furthermore, the cycling operating conditions of CSP plants may cause fatigue damage. For this reason, the dynamic analysis of SG is mandatory to assure its lifetime.

This PhD thesis consists of the design and dynamic analysis of SG for CSP plants. A methodology for the design of the SG and oil-to-salt heat exchangers of a 50 MWe parabolic trough power plant (PTPP) is presented. The heat exchanger design is made following TEMA standards and ASME Pressure Vessel code. The economic analysis of SG is made using as main variables the evaporator pinch point and the HTF outlet temperature, in order to take into account the total operational HTF pump cost and the investment cost of the SG heat exchangers. The heat exchanger design is made using genetic algorithms to obtain feasible and optimized results. Two design strategies are compared: the minimization of the total heat transfer area and the minimization of the total annualized cost. The results show that the second approach leads to substantial savings. A recirculation evaporator specially designed for PTPP is modeled and compared with kettle design.

A methodology for heat exchanger design of a solar power tower plant (SPTP) is also proposed. The special operating conditions with high fluid temperatures and the high heat duty make this issue a non-typical heat exchanger design problem. For this reason, heat transfer and thermal stress requirements are considered in the heat exchanger selection of superheater, reheater, evaporator and preheater. The economic analysis consists of the evaporator pinch point temperature difference optimization taking into account its impact on the global plant performance. Two SG configurations are studied: with one or two parallel trains of heat exchangers. The results show extremely low optimum pinch point values. A preliminary economic study is also made to compare forced and natural circulation evaporator designs.

The section of the thesis corresponding to dynamic study deals about the off-design analysis of the proposed design of SG for a SPTP. For that purpose, transient models are developed to the single phase heat exchangers and the recirculation evaporator with steam drum. Furthermore, different models are proposed to estimate the transient temperature field and stresses on critical parts of shell-and-tube heat exchangers such as: tubesheets ligaments and tubesheet junction. Two SG start-up initial conditions are studied. The first considers non-isothermal temperature profiles on the heat exchangers at the beginning of the start-up whereas the second considers isothermal initial conditions. For both scenarios are proposed a start-up procedure where the main allowable temperature fluid ramps to operate the SG on safety-side are calculated.

The dynamic analysis of the SG proposed for a PTPP is also presented. The dynamic response of the heat exchangers is estimated developing transient models for TEMA F and TEMA H. The thermal stresses are calculated on the critical zones such tubesheets, head-nozzle junctions, steam drum-downcomer junction and U-bend regions. In addition, the analytical stress models are validated by means of different finite element simulations. A SG start-up is performed using temperature ramps to not overpass the ratcheting and magnetite protection stress limits. Lastly, a study is made to compare the dynamic behavior between kettle and recirculation evaporators.

Finally, it is presented the fatigue analysis of the SG for a PTPP. The fatigue analysis is performed following ASME Pressure Vessel code for the start-up, shutdown and load change of the SG.

Contents

Agradecimientos i

Acknowledgments iii

Resumen v

Abstract vii

Contents ix

List of figures xv

List of Tables xix

1. Introduction 1

1.1. Motivation 1

1.2. Concentrating solar power plants 2

1.2.1. Solar Field 3

1.2.2. Thermal Energy Storage System 4

1.2.3. Steam generator 4

1.2.4. Power Block 6

1.3. SG Design for commercial CSP plants 6

1.4. The importance of the flexibility of CSP plants 7

1.5. Heat exchanger design 7

1.5.1. Process and design specifications 8

1.5.2. Thermal and hydraulic design 8

1.5.3. Mechanical Design 10

1.5.4. Cost estimation 12

1.5.5. Optimization 12

1.6. Objectives of the thesis 12

1.7. Structure of this thesis 13

1.8. References 14

2. Cost-based design optimization of the heat exchangers in a parabolic trough power plant 17

2.1. Abstract 17
2.2. Introduction 18
2.3. Methodology 20
2.3.1. Calculation of heat transfer and pressure drops 20
2.3.2. Economic analysis 22
2.3.3. Genetic algorithm 24
2.4. Initial design of the parabolic trough plant 25
2.5. Mechanical design and TEMA standards 27
2.6. Cost-based design optimization 30
2.6.1. Optimizing the design of the SG 33
2.6.2. Optimizing the design of the oil-to-salt heat exchanger 37
2.7. Conclusions 41
2.8. References 46
3. Thermo-economic optimization of molten salt steam generators 51
3.1. Abstract 52
3.2. Introduction 52
3.3. Initial design of SPTP 54
3.4. Methodology 55
3.4.1. SG design selection 56
3.4.2. Material Selection 61
3.4.3. Thermal-Hydraulic Design 62
3.4.4. Mechanical Design 65
3.4.5. Estimating Cost Models 68
3.4.6. Heat exchanger Optimization using genetic algorithms 70
3.5. Optimization 71
3.5.1. Optimization of the approach point of the SG 71
3.5.2. Results of the approach point optimization 71
3.5.3. Optimization of the pinch point of the SG 72
3.5.4. Global optimization procedure 73

3.5.5. Results of the pinch point optimization....75
3.5.6. SG proposed design....76
3.6. Conclusions....79
3.7. References....83
4. Steam generator daily start-up for solar power tower plants....87
4.1. Abstract....88
4.2. Introduction....88
4.3. System description....90
4.3.1. Turbine operation modes....92
4.3.2. Control system....92
4.3.3. Start-up initial conditions....94
4.4. Modeling and validation....96
4.4.1. Single phase flow heat exchangers....96
4.4.2. Two phase flow model for evaporator and steam drum....98
4.4.3. Stresses on steam drum and SH header....100
4.4.4. Stresses on tubesheet....101
4.4.5. Stresses on U-tubes....108
4.5. Results....109
4.5.1. Feedwater temperature....110
4.5.2. Daily start-up with non-isothermal initial conditions....111
4.5.3. Daily start-up with isothermal initial conditions....114
4.6. Conclusions....118
4.7. References....123
5. Dynamic analysis of the steam generator of parabolic trough power plants....127
5.1. Abstract....128
5.2. Introduction....128
5.3. Plant description....130
5.3.1. Power block model....132
5.3.2. SG control system....132

5.3.3. Start-up initial conditions 134
5.4. Methodology 134
5.4.1. Single phase flow heat exchangers 134
5.4.2. Two phase flow model for EV and steam drum 137
5.4.3. Steam drum and SH nozzle stress calculation 138
5.4.4. Tubesheet stress calculation 142
5.4.5. Tubesheet junction stress calculation 145
5.4.6. U-tube stress calculation 150
5.5. Results and discussion 151
5.5.1. Start-up simulation of the SG 152
5.5.2. Stress analysis 154
5.5.3. Comparison between kettle and TEMA X evaporators 156
5.6. Conclusions 159
5.7. References 162
6. Fatigue analysis of the steam generator of parablic trough power plants 167
6.1. Abstract 167
6.2. Introduction 168
6.3. Methodology for the fatigue analysis 170
6.3.1. Lifetime estimation according ASME Section VIII Div 2 [23] 171
6.4. Results of the fatigue analysis 175
6.4.1. Fatigue analysis for the evaporator temperature ramp operation during the SG start-up 176
6.4.2. Fatigue analysis for the HTF inlet temperature ramp operation during the SG start-up 179
6.4.3. Fatigue analysis for a 50% load change operation of the SG 181
6.5. Conclusions 183
6.6. References 186
Conclusions 189
Appendix 191

Appendix A. Evaporator calculations.....191

Appendix B. Tubesheet stress calculations 193

Appendix C. U-Tube stress calculations.....195

List of Publications 197

List of figures

Figure 1.1: CSP technologies [6]. 3
Figure 1.2: Schematic of the main steps of the heat exchanger design process (Adapted from [23]). 9
Figure 1.3: Stress categories and limits of equivalent stress [27]. 11
Figure 2.1: Schematic of the parabolic trough solar power plant. 26
Figure 2.2: TEMA shell types developed for single-phase heat exchangers. 28
Figure 2.3: Kettle type evaporator. 29
Figure 2.4: TEMA-X shell recirculation evaporator. 30
Figue 2.5: SG configuration. 34
Figure 2.6: SG temperatures versus heat duty. 34
Figure 2.7: SG design optimization: a) evaporator pinch point and b) thermal oil outlet temperature. 35
Figure 2.8: Economic analysis of the SG. 36
Figure 2.9: Proposed design of oil-to-salt heat exchanger with TEMA F shell in series. 39
Figure 2.10: Power block performance under part load conditions. 40
Figure 2.11: Economic analysis of the TES. 41
Figure 3.1: Schematic of a SPTP. 55
Figure 3.2: Schematic of the main heat exchanger calculations. 56
Figure 3.3: Evaporator design: a) Forced circulation evaporator. b) Natural circulation evaporator. The annualized cost against the circulation ratio: c) Forced circulation evaporator; d) Natural circulation evaporator. 59
Figure 3.4: Typical temperature profile for the SG. 60
Figure 3.5: Heat exchanger configuration selected for the SG. 61
Figure 3.6: Shell and baffle types. 63
Figure 3.7: Tubesheet temperatures for different superheater shell types. 66
Figure 3.8: U-tube deformation by thermal expansion. 67
Figure 3.9: Minimal radius against temperature difference between different hot and cold leg overhand differences (ΔS_{h-c}). 68
Figure 3.10: Total annualized cost against approach point. 72
Figure 3.11: Approach point against pinch point. 73
Figure 3.12: Evolution of different costs against the pinch point. 74
Figure 3.13: Schematic of the optimization algorithm. 75
Figure 3.14: SG layout with two trains in parallel. 76

Figure 3.15: Total annualized cost against pinch point. 77
Figure 4.1: Schematic of SPTP. 91
Figure 4.2: Schematic of SG and control system. 93
Figure 4.3: Salt temperature profiles in SG. 95
Figure 4.4: Response comparison between numerical and analytical methods for a temperature step change in the hot fluid: a) cold fluid outlet and b) hot fluid outlet. 97
Figure 4.5: Response of the system for a heat step of 10 MWth: a) steam drum pressure; b) total water volume ; c) evaporator outlet steam mass fraction; d) steam drum level. 99
Figure 4.6: T-junction points selected. 100
Figure 4.7: Tubesheet ligament boundary conditions. 103
Figure 4.8: Transient temperature field in tubesheet ligament zone. 104
Figure 4.9: Schematic of the head-tubesheet-shell junction forces. 105
Figure 4.10: Schematic of the tubesheet junction boundary conditions. 106
Figure 4.11: Transient temperature field in tubesheet junction. 107
Figure 4.12: U-tube deformation by thermal expansion. 108
Figure 4.13: SH U-bend stress for different temperature differences between hot leg and cold leg. 109
Figure 4.14: Feedwater system performance: a, b) without start-up feedwater heater; c, d) with start-up feedwater heater. 111
Figure 4.15: Schematic of the procedure of the start-up with non-isothermal initial conditions. 112
Figure 4.16: Non-isothermal start up simulation: a) salt temperature and mass flow rate, turbine power output; b) SH performance; c) steam drum performance; d) RH performance. 113
Figure 4.18: Schematic of the procedure of the start-up with non-isothermal initial conditions. 115
Figure 4.17: Stress evolution of the main components during non-isothermal start-up: a) tubesheet ligament stresses; b) tubesheet head junction stresses ;c) tubesheet shell junction stresses; d) tubesheet no-tube-lane stresses; e) SH inlet head nozzle junction stresses; f) SH outlet head nozzle junction stresses; g) steam drum downcomer junction stresses; h) U-tube stresses. 116
Figure 4.19: Isothermal start-up simulation: a) salt temperature and mass flow rate, turbine power output; b) SH performance; c) steam drum performance; d) RH performance. 117
Figure 4.20: Stress evolution of the main components during isothermal start-up: a) tubesheet ligament stresses; b) tubesheet head junction stresses ;c) tubesheet shell junction stresses; d) tubesheet no-tube-lane stresses; e) SH inlet head nozzle

junctionstresses; f) SH outlet head nozzle junction stresses; g) steam drum-downcomer junction stresses; h) U-tube stresses. 119
Figure 5.1: Schematic diagram of the PTPP considered. 131
Figure 5.2: Schematic of SG and control system. 133
Figure 5.3: Schematic TEMA H shell heat exchanger. 135
Figure 5.4: Transient responses of the outlet temperatures of the TEMA F and TEMA H shell against an inlet temperature step for different wall capacities. 136
Figure 5.5: Steady-state temperature profiles of the SH. 137
Figure 5.6: Response of the system for a steam mass flow step of 10 kg/s: a) steam drum pressure; b) total water volume; c) evaporator outlet steam mass fraction; d) steam drum level. 139
Figure 5.7: Selected points for stresses calculation of the steam drum-downcomer junction. 140
Figure 5.8: FEA results obtained in SH head-nozzle T-junction. 141
Figure 5.9: RH FEA temperature field results. 144
Figure 5.10: RH FEA stress results in ligaments due to temperature difference across no-tube-lane. 145
Figure 5.11: Force analysis on the tubesheet junction. 146
Figure 5.12: SH Tubesheet junction model. 148
Figure 5.13: Stress results for tubesheet junction at no-tube-lane zone. 148
Figure 5.14: Comparison between the analytical model and FEA results obtained for SH. 150
Figure 5.15: The five points selected for tubesheet stress analysis. 152
Figure 5.16: Schematic of the procedure of the start-up. 153
Figure 5.17: Daily start up simulation: a) thermal oil temperature and mass flow rate, turbine power output; b) SH performance; c) steam drum performance; d) RH performance. 154
Figure 5.18: Stress evolution of the main components of the SG during daily start-up: a) tubesheet ligament stresses; b) tubesheet head junction stresses; c) tubesheet shell junction stresses; d) tubesheet no-tube-lane stresses; e) tubesheet junction at no-tube-lane zone; f) U-tube stresses; g) steam drum downcomer junction stresses; g) SH outlet head nozzle junction stresses. 157
Figure 5.19: Critical points selected for the stress analysis of TEMA X recirculation and kettle evaporator. 158
Figure 5.20: Results of the stress analysis for between TEMA X evaporator and kettle evaporator: a) drum downcomer junction (shell for kettle); b) tubesheet ligament stresses. 159
Figure 6.1: Stress classification according to ASME Section VIII Div 2 [23] 172
Figure 6.2: Possible calculations of the extremes in case of RSE [8]. 173

Figure 6.3: Simulation results for different evaporator temperature ramps. a) Drum pressure; b) Drum temperature; c) HTF mass flow; d) HTF inlet temperature.... 176
Figure 6.4: Stress results for different evaporator temperature ramps: a) Point 1 of the drum-downcomer junction; b) Point 2 of the drum-downcomer junction; c) Point 1 of the SH inlet nozzle-head junction; d) Point 2 of the SH inlet nozzle-head junction. 177
Figure 6.5: Fatigue results for different evaporator temperature ramps. 178
Figure 6.6: Simulation results for different HTF inlet temperature ramps: a) HTF inlet temperature; b) SH outlet steam temperature. 179
Figure 6.7: Stress results for different HTF inlet temperature ramps: a) Point 1 of the SH outlet nozzle-head junction; b) Point 2 of the SH outlet nozzle-head junction. 180
Figure 6.8: Fatigue results for different HTF temperature ramps. 180
Figure 6.9: Simulation results for a 50% load change: a) Drum pressure; b) Drum temperature; c) HTF mass flow; d) HTF inlet temperature..... 181
Figure 6.10: Stress results for 50% load change: a) Point 1 of the drum-downcomer junction; b) Point 2 of the drum-downcomer junction; c) Point 1 of the SH inlet nozzle-head junction; d) Point 2 of the SH inlet nozzle-head junction..... 182
Figure 6.11: Fatigue results for a 50% load change transient case. 183
Figure A.1: Heat exchanger discretization cell model..... 191
Figure A.2: Scheme of the evaporator calculation. 192
Figure B.1: Schematic of Tubesheet zones. 193

List of Tables

Table 2.1: Design variables. 25
Table 2.2: Nominal values of the 55 MWe (gross) steam power cycle. 27
Table 2.3: Proposed designs of heat exchangers. 38
Table 2.4: Proposed designs for the oil-to-salt heat exchanger. 42
Table 3.1: Nominal values of the 110 MWe steam power cycle. 55
Table 3.2: Selected Materials for the main SG components. 62
Table 3.3: Search variables selected for the heat exchanger design 70
Table 3.4: Proposed design of the heat exchangers for the SG layout with one train. ..77
Table 3.5: Proposed design of the heat exchangers for the SG layout with two train. .78
Table 3.6: Proposed design of the steam drums. 79
Table 4.1: Selected Materials for the main SG components. 92
Table 4.2: Main equations for stress calculations proposed by O'Donnell et al. [36]. .102
Table 5.1: Power Block and SG design parameters. 131
Table 5.2: Selected Materials for the main SG components. 132
Table 5.3: Comparison between analytical and FEA results obtained in SH head-nozzle T-junction. 141
Table 5.4: Main equations for stress calculations proposed by O'Donnell et al. [43]. .142
Table 5.5: Comparison between analytical and FEA results obtained for RH. 144
Table 5.6: Comparison between analytical and FEA results obtained for SH tubesheet junction. 149
Table 6.1: Transient cases for SG fatigue analysis. 175
Table B.6.2: Main equations for stress calculations proposed by O'Donnell et al. [36]. 194

CHAPTER

ONE

Introduction

Contents

1.1. Motivation 1
1.2. Concentrating solar power plants 2
1.2.1. Solar Field. 3
1.2.2. Thermal Energy Storage System 4
1.2.3. Steam generator 4
1.2.4. Power Block 6
1.3. SG Design for commercial CSP plants 6
1.4. The importance of the flexibility of CSP plants 7
1.5. Heat exchanger design 7
1.4.1. Process and design specifications 8
1.4.2. Thermal and hydraulic design 8
1.4.3. Mechanical Design 10
1.4.4. Cost estimation. 12
1.4.5. Optimization 12
1.6. Objectives of the thesis 12
1.7. Structure of this thesis 13
1.8. References 14

1.1. Motivation

Climate change problems push to scientific community to sought renewable energy sources. According to the International Energy Agency (IEA) [1], CO_2 levels should reduce the current values by around 50% in 2050 to reach an acceptable level

of emissions. In addition, the instabilities of the oil prices and the interest to reduce the dependency on foreign power sources drive to the development of the local energy sources.

Concentrating solar power (CSP) plants are a promising option to provide the growing demand of energy while reducing CO_2 emissions. These plants convert the solar energy in a high temperature heat source before its conversion to electricity, allowing the possibility of integrate a cost-effective thermal energy store (TES) system or even the hybridization with fossil fuels [2]. Nowadays, CSP plants such Gemasolar with 15 full-load production hours of storage can operate 24 hours a day in summer [3].

Typically, commercial CSP plants use an indirect steam generation system. This is because direct steam generation systems present significant disadvantages such as: problems in the plant operation with high variations due to clouds and the low cost-efficiency of their storage system. The indirect steam generation systems have a great impact in the plant performance due to the pinch point temperature difference limit, which sets the mass flow rate of the heat transfer fluid. In this way, a compromise between the investment cost of the heat exchangers and the operational pump cost of heat transfer fluid is obtained.

The current electricity market push to CSP plants to further increase their flexibility to enhance their competitiveness. The steam generator (SG) plays a key role in terms of flexibility of the CSP plants, since the thermal stress on thick-walled components limits the load changes ramps. To obtain realistic results in the study of different plant operation strategies it is required the development of stress models to estimate the lifetime reduction on the SG components.

1.2. Concentrating solar power plants

Commercial concentrating solar power plants were first built around 1980s in the United States by means of the facilities Solar Electric Generating Station (SEGS) [4]. After 20 years, CSP plants have experimented a great growth in Spain and United States mainly driven by government subsidies and technological improvements. Nowadays, the power installed of the CSP plants in the world is around 4.8 GWe. The most extended technology is the parabolic trough with around 85% of the total power installed, followed by power tower with 10% and fresnel representing 4% [5]. According to the International Energy Agency, it is expected that the total power generated by CSP plants installed in the world will be 1000 GW by 2050 [6].

Concentrating solar power is a technology where the solar energy is concentrated by a collector and/or mirrors to provide a high temperature source to generate heat or electricity. In case of CSP plant, normally a heat transfer fluid is heat-up to produce

steam. Then, as it occurs in a conventional thermal power plant, the steam is used to drive a steam turbine to generate electricity.

The CSP plants can be divided into four sub-systems: solar field, the storage system, the steam generator and the power block.

1.2.1. Solar Field

The solar field is the zone where the solar radiation is concentrated to provide the heat source. CSP plants can be divided into two main groups, depending on the Sun radiation concentration: focal line or single focal point. Focal line technologies include parabolic trough and linear Fresnel. Focal point technologies include solar tower and parabolic dish. Figure 1.1 shows the main CSP technologies.

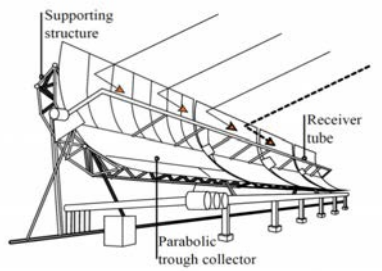

Parabolic trough

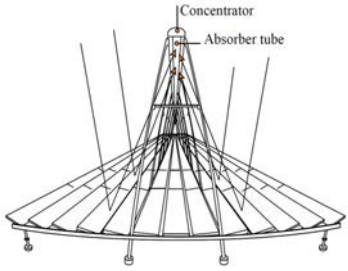

Linear Fresnel

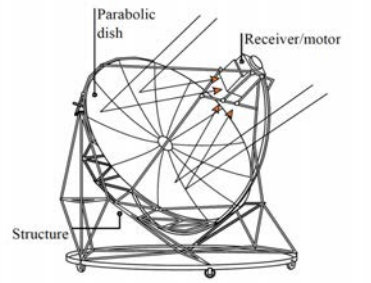

Parabolic dish

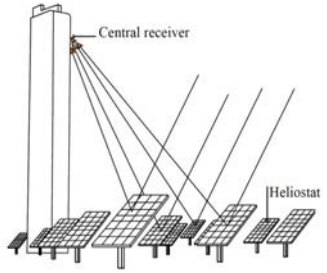

Solar tower

Figure 1.1: CSP technologies [6].

Line focus technologies can concentrate the solar radiation until 100 times obtaining a temperature operation range between 350-450 ºC [5]. At this moderate temperature level the thermal efficiency can be considered low. On the other hand, point focus technologies can achieve a concentration factor around 1000 times and the

temperature operation is ranged between 600ºC-800ºC [5]. At this temperature range the thermal efficiency is high enough to help in the reduction of the cost per unit of energy produced.

1.2.2. Thermal Energy Storage System

CSP plants can be integrated with large store thermal energy systems decoupling the solar source to the electricity production. The thermal energy storage (TES) system presents different advantages [2]:

- Increment of the system reliability: since the energy production can be delivered in a smooth way and within stable limits, a potential reduction of the risk of breakdowns is obtained.
- Increment of generation capacity: the excess of energy during low-demand periods can be stored in order to be delivered during high-demand periods. This increases the effective generation capacity leading to higher competiveness.
- Reduction of cost of generation: although the initial investment cost increases, the synergies obtained due to the increment of the annual energy production and the potential reduction of the maintenance cost provides a lower cost per unit of energy produced.

TES system presents clear advantages compared to other technologies such as battery storage or pumped-storage hydropower, which always increase the cost per unit of energy produced [5]. However, the grade of the potential benefits of TES systems is dependent on the plants layout, the storage temperature, the size and the desired operating strategy.

1.2.3. Steam generator

The SG transfers the thermal energy captured in the solar field by means of solar collectors or central receivers to produce high and low pressure steams. The SG is mainly formed by four different heat exchangers: superheater, reheater, evaporator and preheater. These heat exchangers are normally mounted separate due to the different technical requirements of each heat exchanger. However, other designs include preheater, evaporator and superheater in the same pressure vessel [7].

The function of the evaporator consists of providing heat to generate steam from hot water. The evaporator is main part of SG in terms of size and cost. In the case of recirculation evaporator-type, a closed circulating loop is formed by the steam drum,

the downcomers, the evaporator and the risers. From the steam drum, the saturated water is circulated in downcomer to enter at the evaporator. Then, the water-steam mixture formed in the evaporator is sent to the steam drum by the risers. In the case of kettle evaporator-type, the flow circulation loop occurs only in the shell. In the evaporator design, one of the most important technical constraint is the critical heat flux [8]. This phenomenon has associated flow instabilities that lead to thermal cyclic variations on tube walls driving deposit-corrosion and fatigue damage. A special attention must be paid for horizontal flow since the critical heat flux point has significant decrease due to the potential flow stratification [9].

The function of the preheater consists of heating-up the SG feed-water until achieve the saturation conditions. One of the most important issues in the design and operation of preheater is the phenomenon known as *steaming*. The *steaming* occurs when subcooled flow nucleate boiling is generated [10]. This effect has associated tube vibrations that may lead to failure if it is not considered in the design.

The superheater heats-up the saturated steam from the steam drum until the high pressure turbine inlet conditions. The high temperature and pressure conditions make necessary a high thickness in the head in order to maintain the stresses in allowable ranges. Thus, superheater head is a critical part during SG start-up due to the thermal stresses induced by the high thicknesses.

The reheater provides the heat to reach the steam inlet temperature of the low pressure turbine. Although the working temperatures are normally similar to the superheater, the metal wall thickness is lower due to the low pressure of the steam. Moreover, in the reheater is necessary more heat transfer area than in the superheater due to the low heat transfer coefficient on the steam side. For this reason, a heat exchanger with high thermal efficiency should be required to reduce the heat transfer area.

The steam drum function is to separate the water from steam. The lower part is full of water that comes from preheater. The upper part is filled with steam where its output is regulated by the main valve placed in the top. The critical design constraint of the steam drum is the steam velocity, which should be low enough to assure that the water droplets are not dragged when the steam flows through the chevron dryers [11]. Several boiler types show that the steam drum - downcomer junction is the most limiting point during the SG start-up from the stress point of view [12].

The SG also includes the supporting structure, water circulation pumps, attemperator systems, etc.

1.2.4. Power Block

The power block includes the steam turbine, the feed-water heater system and the condenser. The steam turbine is normally composed by the high and low pressure sections. The feed-water system, formed by low- and high- pressure closed-feed-water-heaters, use the extractions from steam turbine to enhance the plant efficiency. Furthermore, a deaerator is also included in the feed-water system to remove undesired non-condensing gases [13]. Depending on the availability of cooling water, the condenser in CSP plant is cooled with either wet or dry cooling towers. Wet-cooled plants are slightly more efficient than dry ones [14].

1.3. SG Design for commercial CSP plants

Steam generators on CSP plants can be classified in direct o indirect systems. The direct steam generator systems are those where the steam is generated directly using solar radiation.

The main advantages of direct steam generator (DSG) systems are the high working temperatures and the investment cost reduction because of the use of heat transfer fluids and heat exchangers are not necessary [6]. On the other hand, the DSG systems present several problems during the start-up and operation caused by the heat variations such as clouds. The storage system consists of using pressure vessels where the steam is accumulated. However, a storage system to assure a stable operation is not feasible yet due to the high investment cost [4]. This is mainly due to the low volumetric energy density provided by the steam accumulators. At commercial level mainly two technologies have been probed for DSG systems: receiver systems like PS10 [2]; and linear Fresnel like Puerto Errado 1[15].

The indirect steam generator systems have the limitation of the pinch point temperature difference, which sets the mass flow rate of the heat transfer fluid. As a result, a trade-off between the investment cost of the heat exchangers and the operational pump cost of the heat transfer fluid side is obtained.

The most common SG design used in commercial PTPPs in Spain has the capacity to provide steam enough to produce 50 MWe [16]. The SG consists of an indirect steam generator system using thermal oil as heat transfer fluid. The thermal oil enters to the SG at 393 ºC, since higher temperatures lead to thermal oil degradation [17]. The thermal oil outlet temperature is 300 ºC. The outlet temperature of the high and low pressure is around 377 ºC and the respective pressures are 10.5 MPa and 2 MPa. The steam flow rate produced is around 60 kg/s. The steam generator is typically arranged in two parallel lines in order to avoid the plant stop in case of steam generator failure.

The largest commercial SPTP based on an indirect steam generation system consists of 110 MWe plant using molten-salt as heat transfer fluid [4]. The molten salt inlet temperature is 565 ºC whereas the outlet temperature is around 290 ºC. The outlet temperature of high and low pressure is around 540 ºC and the respective pressures are 12.5 MPa and 3 MPa. The steam flow rate produced is around 86 kg/s.

1.4. The importance of the flexibility of CSP plants

The unregulated electricity markets combined with the high growth of the renewable energy sources change the operation of the electricity grid. The unpredictable generation of renewable energies such as wind or photovoltaic leads to unbalancing grid problems. The new market scenario has encouraged to increase the competitiveness of conventional power plants improving its dispatchability [18].

The most important feature of CSP plants is the ability to adapt the production to the electricity market demand. The similarities of CSP plants with conventional plants (steam turbine with synchronous generator, large production capacity) provide a competitive advantage to participate in grid balancing services [19]. This means an increment of the revenues, and thus, an increment of its competitiveness.

However, to be considered as dispatchable, a sufficient flexibility level by means of faster load changes ramps is required [4]. Furthermore, faster start-ups are especially important for CSP plants because lead to higher annual energy production [20]. Nevertheless, the change of the operating conditions produces high thermal stresses on thick-wall components as SG, which also cause fatigue damage. As a result, a good management of the plant requires the study of the compromise between the potential increment of revenues due to dispatchability services and the analysis of the lifetime reduction of the SG components or even the cost due to fatigue failure.

1.5. Heat exchanger design

The SG of commercial solar power plants with indirect steam generation system is based on conventional shell-and-tube heat exchangers [21,22]. The heat exchanger design is a complex process that involves several disciplines such as: thermal and hydraulic design, mechanical design and lifetime estimation, cost estimation and optimization. As a consequence, a rigorous methodology should be followed in order to accomplish the heat exchanger design with successful results. A schematic of the main steps of the design process proposed by Shah and Skulic [23] is shown in Figure

1.2. As it can be seen, the heat exchanger design is a thorough method where an iterative process is required.

1.5.1. Process and design specifications

The process specification is a critical step where experience can play a key role to obtain successful results. In this step are considered the operational data at design and off-design conditions, the environment, fluid types, fouling tendency, corrosion/erosion, etc. Due to that, background knowledge is built and, together with the main constraints, helps in the search of similar process on the available literature. Based on this analysis, the selection of heat exchanger type and its main components (tube type, shell type, head type, baffle type, etc) is made passing to the calculation process.

1.5.2. Thermal and hydraulic design

The objective of the thermal and hydraulic design consists of the estimation of the pressure drop and the total heat transferred in order to size the heat exchanger. The thermal design procedure basically consists of satisfying the enthalpy rate equation ($Q_j = \dot{m}_j \Delta h_j$) and the heat transfer rate equation ($Q = U\, A\, \Delta T_m$) [23]. Normally, these calculations are made considering constant properties in the whole heat exchanger allowing the use of the well-known method: log-mean temperature difference [24]. However, for fluids with high variations of its properties, such as two-phase flows, discretized calculations must be used to obtain accurate results. Another important step is the calculation of the overall heat transfer coefficient, U , where it is considered the convective coefficients of the tube and shell side, tube conduction - and fouling resistances. The pressure drop has a great impact in the operating costs. In addition, shell and tube side pressured drop should be considered to calculate other parts such nozzles, headers, manifolds, etc.

The convective coefficient and pressure drop on shell side are typically calculated using methods Delaware or Kern [25]. In contrast, one of the most utilized commercial software for heat exchanger design (Heat Transfer Research inc. (HTRI) software) is based on the principles of the Stream Analysis method [8].

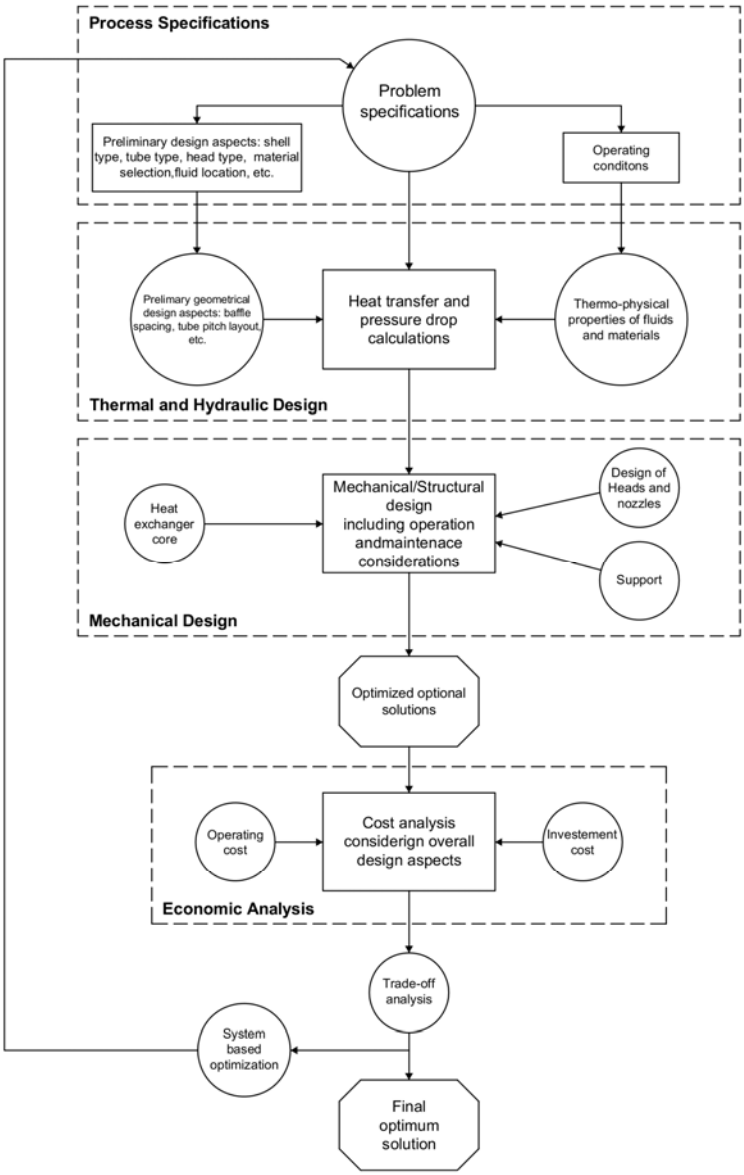

Figure 1.2: Schematic of the main steps of the heat exchanger design process (Adapted from [23]).

1.5.3. Mechanical Design

The aim of the mechanical design is to ensure the integrity of the heat exchanger under design and off-design operating conditions. It should be taken into account that some aspects of the mechanical design affect thermal and hydraulic calculations, therefore the design calculations must be made by an iterative process. The heat exchanger is formed by several elements such as: shell, tubes, tubesheet, head, nozzle, baffle, etc and for each one it is necessary to assure the mechanical/structural integrity. Furthermore, in heat exchangers mechanical and thermal loads are combined, together with complex geometries (especially tubesheet) making sometimes necessary the use of finite element analysis.

Heat exchangers are typically designed following international recognized codes and standards. One of the most important is TEMA standards [26], which provides design guidelines and technical constraints such as: shell types, front head types, rear head types, outside tube diameters, maximum and minimum baffle spacing, clearances, baffle thickness, maximum tube length, fouling factors, tubesheet thickness and others. Most of them are especially useful to set the preliminary mechanical design aspects in order to carry out the thermal and hydraulic design calculations. In addition, the fulfillment of technical constraints is crucial to obtain a good thermal and hydraulic design.

ASME Boiler and Pressure Vessel code [27] presents design guidelines for several aspect of heat exchanger design. On a first step, the thicknesses of the main parts of the heat exchangers such as: tube, shell, head, nozzle and tubesheet are calculated using ASME Section II and VIII div1. Moreover, additional design guidelines are also presented: material selection and properties, head-tubesheet-shell junction, etc. Once the thicknesses are known, a second step is made where all the heat exchanger components must satisfy the protection against plastic collapse limit considering bending plus membrane stresses (Figure 1.3). The equivalent stresses are calculated considering only mechanical load under design conditions. Most of these stresses can be calculated by analytical methods proposed in ASME code, although some complex loadings or geometries are not considered in ASME code and they must be accomplished by complex analytical methods or finite element analysis [28].

The lifetime estimation of the heat exchangers for standard industrial applications with relatively low temperatures (<427 ºC) is made following ASME Section VIII div2. Here two assessments should be considered for the protection against cycling operation: ratcheting and fatigue. The equivalent stresses are calculated considering operating load cycles. For ratcheting assessment, it is considered membrane stresses, bending and secondary stresses for (Figure 1.3). In case of fatigue assessment the peak stress must be included (Figure 1.3).

Stress Category	Primary			Secondary Membrane plus Bending	Peak
	General Membrane	Local Membrane	Bending		
Description	Average primary stress across solid section. Excludes discontinuitis and concentrations. Produced only by mechanical loads.	Average stress across any solid section. Considers discontinuities but not concentration. Produced only by mechanical loads.	Component of primary stress proportional to distance from centroid of solid section. Excludes discontinuties and concentrations. Produced only by mechanical loads	Self-equilibrating stress neccesary to satisfy continuity of structure. Occurs at structural discontinuities. Can be caused by mechanical load or by differential thermal expansion. Excludes local stress concentrations.	1. Increment added to primary or secondary stress by a concentration (notch). 2. Certain thermal stresses which may cause fatigue but not distortion of vessel shape.
Symbol	P_m	P_L	P_b	Q	F

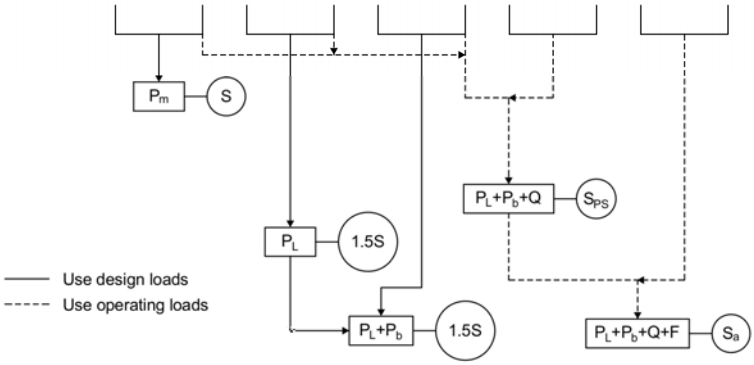

Figure 1.3: Stress categories and limits of equivalent stress [27].

The lifetime estimation for heat exchanger operating at high temperatures (>427 ºC) is made following ASME Section III Div 1 Subsection NH: *Rules for Construction of Nuclear Facility Components*. When the pressure vessel is operated at high temperature the creep damage should be considered [29]. The fatigue damage is related to the magnitude of the stress cyclic variations and the number of cycles to failure is computed as a function of the equivalent strain range. The creep damage is function of the stress level and the temperature [30]. The total damage is calculated by linear summation method using Palmgren-Miner equation [31], which combines fatigue and creep.

Another important factor of the mechanical design is the failure due to vibrations. The high flow velocities lead to high heat transfer coefficients, obtaining in this way

lower surface areas. If the flow velocity overpasses the critical value, it can produce vibration instabilities, which may cause the material erosion or even fatigue failure due to damage in tubes, baffles supports and tube-to-tubesheet joints.

1.5.4. Cost estimation

An economic analysis is required to obtain feasible heat exchanger designs with standard criteria. Therefore, the economic analysis requires the use of cost estimation models. The cost involved in the heat exchanger design can be classified as: capital, installation, operating and maintenance. The capital cost includes the costs associated with design, materials and manufacturing. The capital cost estimation are usually made by using models of economies of scale or cost versus capacity charts [32]. The operating cost includes the costs associated with fluid pumping power, insurance, maintenance, repair, cleaning, lost production/downtime due to failure and energy cost associated with the utility (steam, fuel, water) [23].

1.5.5. Optimization

In a heat exchanger design a high number of variables and constraints are involved. Traditional methods based on trial-and-error calculations may lead to large computational costs in terms of time and low probability to obtain successful results. Therefore, an optimization algorithm is strongly recommended to reduce the computational cost and increase the probability to find the best design. Several optimization techniques have been employed in heat exchanger design: genetic algorithms [33], particle swarm optimization [34], harmony search algorithms [35] and others. Furthermore, the use of suitable objective and constraints functions is also important to obtain successful results.

1.6. Objectives of the thesis

As stated above, the SG has a critical relevance on the plant performance. To optimize the SG operation, it is necessary to develop models that can estimate the stresses and lifetime of the SG components. The main objectives of the PhD thesis are summarized below:

- Design and optimization of the heat exchangers of PTPP using thermal oil as heat transfer fluid.

- Design and optimization of the heat exchangers of the SG of SPTP using molten salt as heat transfer fluid.

- Development of stress and dynamic models of the main parts of the molten-salt SG of SPTP to study its dynamic performance. This allows the study of the daily start-up strategies of the molten-salt SG.

- Development of stress and dynamic models of the main parts of the thermal oil SG of PTPP to study its dynamic performance. This allows the study of the daily start-up of the thermal oil SG.

- Fatigue assessment of the start-up, shutdown and load change operations of the SG following ASME code.

1.7. Structure of this thesis

This PhD thesis is organized in six chapters. Chapters 2 to 5 have been written as independent articles that include abstract, introduction, notation and bibliography.

In Chapter 2, the optimization of the performance for the SG of a PTPP and the heat exchanger design is presented. Also, a recirculation evaporator design is proposed to improve the dynamic performance of the SG. Lastly, the optimization of the molten-salt thermal storage system is performed considering the oil-to-salt heat exchangers cost.

In Chapter 3, a methodology to optimize of the performance of the SG of a SPTP considering the pinch point of the SG as the main variable is presented. Two SG designs are proposed: the first consists of one train, and the other consists of two trains. A comparative study between natural circulation and forced circulation evaporator designs is also presented.

In Chapter 4, different dynamic and stress models of the main parts of the molten-salt SG of a SPTP is presented. A SG daily start-up stress analysis is carried out based on the SG design proposed in Chapter 3. Two start-up initial conditions are analyzed, obtaining the main input variables to operate the steam generator within the allowable stress limits.

In Chapter 5, the stress analysis of the SG start-up of a PTPP based on the SG design proposed in Chapter 2 is presented. Different dynamic and stress models of the main parts of the SG are developed. A finite element analysis is developed to validate the stress models. Lastly, a comparison study between the dynamic behavior between kettle and recirculation evaporator is performed.

In Chapter 6, the fatigue analysis of the SG of a PTPP based on the SG design and stress analysis performed in Chapter 2 and Chapter 5, respectively is presented. Two operations of the start-up of the SG are studied: the evaporator temperature ramp and the heat transfer fluid inlet temperature ramp. Furthermore, the fatigue analysis of the load change operation of SG is also performed.

Finally, Chapter 7 summarizes conclusions of the thesis.

1.8. References

[1] IEA. Renewable power generation costs in 2014 2015:1–52. doi:10.1007/SpringerReference_7300.

[2] Medrano M, Gil A, Martorell I, Potau X, Cabeza LF, Medrano M, et al. State of the art on high-temperature thermal energy storage for power generation. Part 2—Case studies. Renew Sustain Energy Rev 2010;14:56–72. doi:10.1016/j.rser.2009.07.036.

[3] Report S, Pacheco JE, Wolf T, Muley N. Incorporating Supercritical Steam Turbines into Advanced Molten-Salt Power Tower Plants : Feasibility and Performance 2013.

[4] Mehos M, Turchi C, Vidal J, Wagner M, Ma Z, Ho C, et al. Concentrating Solar Power Gen3 Demonstration Roadmap 2017.

[5] IEA. Technology Roadmap Solar Thermal Electricity. Int Energy Agency 2014:52. doi:10.1007/SpringerReference_7300.

[6] SolarConcentra, Plataforma Tecnológica de la Energia Solar Térmica de Concentración. https://www.solarconcentra.org

[7] Henrion T, Ponweiser K, Band D, Telgen T. Dynamic simulation of a solar power plant steam generation system. Simul Model Pract Theory 2013;33:2–17. doi:10.1016/j.simpat.2011.12.009.

[8] Serth RW, Lestina TG. Process Heat Transfer: Principles, Applications and Rules, 2014.

[9] Collier JG, Thome JR. Convective Boiling and Condensation, Clarendon Press, 1994.

[10] Warrier GR, Dhir VK. Heat Transfer and Wall Heat Flux Partitioning During Subcooled Flow Nucleate Boiling--A Review. J Heat Transfer 2006;128:1. doi:10.1115/1.2349510.

[11] Ganapathy V. Steam Generators and Waste Heat Boilers: For Process and Plant Engineers 2015.

[12] European Standard EN12952-3. Water-tube Boiler and Auxiliary Installations - Part 3: Design and Calculation for Pressure Parts 2001.

[13] Alobaid F, Mertens N, Starkloff R, Lanz T, Heinze C, Epple B. Progress in dynamic simulation of thermal power plants. Prog Energy Combust Sci 2017;59:79–162. doi:10.1016/j.pecs.2016.11.001.

[14] Kolb GJ. An Evaluation of Possible Next-Generation High-Temperature Molten-Salt Power Towers, Sandia Natl. Lab. Report, SAND2011-9320, 2011.

[15] Nixon JD, Davies PA. Cost-exergy optimisation of linear Fresnel reflectors. Sol Energy 2012;86:147–56. doi:10.1016/j.solener.2011.09.024.

[16] National Renewable Energy Laboratory (NREL) 2016. http://www.nrel.gov/csp/solarpaces/by_project.cfm.

[17] Vogel AK, Reiling H, Fluri TP, Platzer WJ. High Temperatures in Line Focusing Systems: Dual Loop Cycle Efficiency and Heat Losses. Energy Procedia 2015;69:1461–70. doi:10.1016/j.egypro.2015.03.095.

[18] Laumert B. Csp Roadmap Wp1 2012:1–9.

[19] Usaola J. Participation of CSP plants in the reserve markets: A new challenge for regulators. Energy Policy 2012;49:562–71. doi:10.1016/j.enpol.2012.06.060.

[20] Ferruzza D, Topel M, Basaran I, Laumert B. Start-Up Performance of Parabolic Trough Concentrating Solar Power Plants. SolarPACES Conf Procedings 2016.

[21] Kelly B, Kearney D. Thermal Storage Commercial Plant Design Study for a 2-Tank Indirect Molten Salt System Final Report 2006.

[22] Kelly B. Advanced Thermal Energy Storage for Central Receivers with supercritical coolants, Abengoa Solar Inc., 2010.

[23] Shah R, Sekulic D. Fundamentals of Heat Exchangers Design, John Wiley & Sons Inc. 2003.

[24] Incropera FP, Lavine AS, DeWitt DP. Fundamentals of heat and mass transfer 2011.

[25] Hewit GF, Shires GL, Bott TR. Process Heat Transfer. Boca Raton, FL: CRC Press; 1994.

[26] TEMA. Standards of the tubular exchangers manufacturers association, 9th ed. Tubular Exchanger Manufactures Association, 2007.

[27] American Society of Mechanical Engineers. ASME boiler and pressure vessel code, Section VIII 2010.

[28] Petrova N, Bouzid A-H. Deflections of A Multipass Shell-and-Tube Heat Exchanger Bolted Joint Subjected to Nonaxisymmetric Thermal Loading. J Press Vessel Technol 2012;134:11207. doi:10.1115/1.4004623.

[29] Taira S. Lifetime of structures subjected to varying load and temperature, Creep in structures 1962.

[30] Mirandola a., Stoppato a., Lo Casto E. Evaluation of the effects of the operation strategy of a steam power plant on the residual life of its devices. Energy 2010;35:1024–32. doi:10.1016/j.energy.2009.06.024.

[31] Oakey JE. Power plant life management and performance improvement. Woodhead Publishing; 2011.

[32] Smith R. Chemical process design and integration. John Wiley & Sons; 2005.

[33] Ponce-Ortega JM, Serna-González M, Jiménez-Gutiérrez A. Use of genetic algorithms for the optimal design of shell-and-tube heat exchangers. Appl Therm Eng 2009;29:203–9. doi:10.1016/j.applthermaleng.2007.06.040.

[34] Sadeghzadeh H, Ehyaei MA, Rosen MA. Techno-economic optimization of a shell and tube heat exchanger by genetic and particle swarm algorithms. Energy Convers Manag 2015;93:84–91. doi:10.1016/j.enconman.2015.01.007.

[35] Fesanghary M, Damangir E, Soleimani I. Design optimization of shell and tube heat exchangers using global sensitivity analysis and harmony search algorithm. Appl Therm Eng 2009;29:1026–31. doi:10.1016/j.applthermaleng.2008.05.018.

CHAPTER

TWO

Cost-based design optimization of the heat exchangers in a parabolic trough power plant

Contents

2.1. Abstract 17
2.2. Introduction 18
2.3. Methodology 20
2.3.1. Calculation of heat transfer and pressure drops 20
2.3.2. Economic analysis 22
2.3.3. Genetic algorithm 24
2.4. Initial design of the parabolic trough plant 25
2.5. Mechanical design and TEMA standards 27
2.6. Cost-based design optimization 30
2.6.1. Optimizing the design of the SG 33
2.6.2. Optimizing the design of the oil-to-salt heat exchanger 37
2.7. Conclusions 41
2.8. References 46

2.1. Abstract

This Chapter addresses two important concerns of the design of steam generators of parabolic trough power plants: cost minimization and component reliability. A thorough economic analysis of the heat exchangers of the steam generator and oil-to-

salt heat exchangers of a 50 MWe parabolic trough power plant is presented. The heat exchanger design is performed following TEMA standards and it is optimized using a genetic algorithm. Two design strategies are compared: the minimization of the total heat transfer area and the minimization of the total annualized cost. It is seen that the second approach provides substantial savings over the lifetime of the plant.

The economic analysis reveals a global optimum with an outlet temperature of the heat transfer fluid of 293 ºC and an evaporator pinch point of 4.85 ºC. The best design of the steam generator consists of a TEMA-H shell superheater and preheater and a TEMA-F shell reheater. The best design of the oil-to-salt heat exchangers includes six TEMA-F shell heat exchangers in series, with a log mean temperature difference of 7ºC and the molten salt on the shell-side. Lastly, a TEMA-X recirculation evaporator is proposed with a considerably reduced wall thickness when compared to a kettle evaporator.

2.2. Introduction

Many efforts have been made to increase the economic competitiveness of CSP plants by improving the thermal storage system or optimizing the steam generator (SG) design [1–3]. In this Chapter, we are focused on the heat exchanger design of a parabolic trough power plant.

The design of a heat exchanger used in energy systems is performed in two steps: a) heat transfer and pressure drop calculation and b) cost analysis and optimization. Heat transfer and pressure drop calculations can be found in several published works in literature. The majority of these publications use the Bell-Delaware method for shell side calculations [4–6]. In contrast, one of the most utilized commercial software for heat exchanger design (Heat Transfer Research Inc. (HTRI) software) is based on the principles of the Stream Analysis method [7]. Simplified economic analyses of heat exchangers are published in numerous studies [8–10]. Purohit [11] proposed a thorough method to estimate the purchase cost of heat exchangers based on the Tubular Exchanger Manufacturers Association (TEMA) standards. Cost minimization of heat exchangers involves the selection of different geometric parameters (e.g., shell and tube diameters, tube layout and pitch, the number of tubes, baffle spacing) subject to different design constraints. To minimize the cost, optimization methods such as genetic algorithms (GA), particle swarm optimization and others can be used. Wildi-Tremblay and Gosselin [12] used a GA to minimize the total annual investment and operational cost of a shell and tube heat exchanger. They showed that the GA found the optimal design of eleven design variables 23 times faster than the time required to evaluate all possible combinations. Ponce et al. [13] developed a penalty function to quantify the violation level of heat exchanger design constraints,

improving the performance of the GA. Fettaka et al. [14] performed a multi-objective optimization using a fast and elitist non-dominated sorting genetic algorithm (NSGA-II) to minimize the area and total pressure drop of heat exchangers. They also studied the impact on the optimal design when selected geometric parameters are used either in a discrete or continuous form.

Until today, several studies that estimate the size of SG and oil-to-salt heat exchangers of parabolic trough power plants have been published. For example, Kelly [15] analyzed the impact of the capacity of a CSP plant on the energy cost and presented the layout, surface areas and cost of the SG heat exchangers of a 250 MWe CSP plant. Kelly and Kearney [16] optimized an indirect molten salt thermal energy storage (TES) and performed a preliminary SG sizing. They presented a SG design based on counter-current heat exchangers and estimated the corresponding surface areas and pressure drops. The TES optimization was performed through the sizing of the oil-to-salt heat exchanger, because it affects the total size of the TES system, as well as the performance of the turbine. Cost calculations were performed for the different parts of the storage system, including the oil-to-salt heat exchanger. Herrmann et al. [17] proposed a conventional shell-and-tube design as an economical solution for oil-to-salt heat exchangers. They calculated different heat exchanger sizes for various storage capacities taking into account the heat duty required during charging and discharging. Zaversky et al. [18] proposed an oil-to-salt heat exchanger design with two tube passes and two shell passes and studied its transient response. Although, some heat exchanger design calculations are available, information about velocities, pressure drops and costs is missing. It is thus seen overall that detailed heat exchanger design calculations of SG and oil-to-salt heat exchangers are still not available in literature. The present Chapter aims to address this issue.

This Chapter presents the design and the economic analysis of the SG and oil-to-salt heat exchangers of a 50 MWe parabolic trough solar power plant. The results presented are based on the Stream Analysis method using Wills and Johnston version [7]. The economic analysis follows the methodology proposed by Purohit [11]. For the SG, different evaporator pinch points and heat transfer fluid (HTF) outlet temperatures are studied, bearing in mind the total operational cost. An alternative recirculation evaporator is modeled and compared with a kettle evaporator. Furthermore, the impact of different oil-to-salt heat exchanger approach temperatures on the performance of the power block is analyzed under TES discharging conditions. The analysis is carried out taking into account the total TES cost and the associated cost power block efficiency penalty. The proposed designs of the SG and oil-to-salt heat exchangers follow TEMA standards. Lastly, a GA, following the model developed by Ponce et al. [13], is used to find the optimal heat exchanger design.

2.3. Methodology

2.3.1. Calculation of heat transfer and pressure drops

The Stream Analysis method was chosen for the shell-side calculations in the single-phase heat exchangers. A qualitative analysis of the Stream Analysis method is presented by Palen and Taborek [19]. Since the values of many empirical parameters and correlations are confidential in the HTRI software, simplified correlations developed by Wills and Johnston [7] were used here to calculate the shell-side flow distribution.

In the Stream Analysis method, the shell side flow is divided into six different sub-streams: the tube-to-baffle leakage (A), the cross flow (B), the bundle-to-shell bypass (C), the shell-to-baffle leakage (E) and the tube-pass-partition bypass (F). The pressure drop of each stream in one baffle can be expressed as:

$$\Delta P_j = \frac{K_j (\dot{m}_j / S_j)^2}{2\rho\phi_v} \qquad j = A, B, C, E, F \tag{2.1}$$

with, $\dot{m}_j$, S_j and K_j the mass flow rate, flow area and resistance coefficient for each j stream, respectively, and ϕ_v the viscosity correction factor equal to $(\mu/\mu_w)^{0.14}$. The system of equations can be solved by means of an iterative process. The system converges when achieving the same pressure drop on the meeting points in an ideal baffle hydraulic network. The different streams have different temperature profiles along the heat exchanger. Thus, it is necessary to correct both the log mean temperature difference (LMTD) and the correction factor for LMTD (F), with a temperature profile distortion factor (δ). In this way, the mean temperature difference is:

$$\Delta T_m = \delta F \, LMTD \tag{2.2}$$

The distortion temperature profile effect can be quantified using an empirical correlation [19]. In this Chapter, all designs have been performed with recommended shell-to-baffle clearances and turbulent flow regime. Under these conditions, δ can be considered to be close to 1.

The heat transfer coefficient on the shell side can be estimated with an empirical correlation function of the Reynolds number based on cross flow stream [20].

The total pressure drop on the shell side can be expressed in terms of the pressure drop in the cross-flow zone, windows zone and the nozzles:

$$\Delta P_s = \Delta P_{cross}(N_b + 1) + \Delta P_{window}(N_b) + \Delta P_{nozzle,in} + \Delta P_{nozzle,out} \tag{2.3}$$

The tube side heat transfer coefficient is determined using the Gnielinski correlation [7], while the Darcy friction factor for pressure drop is calculated using the Colebrook correlation [7].

The shell-side heat transfer coefficient in the kettle evaporator (Equation 2.4) was estimated considering the nucleate boiling heat transfer coefficient ($h_{nb,1}$) for a single tube and corrected with the bundle geometry factor (F_b) and the natural convective coefficient (h_{nc}) [21].

$$h_s = h_{nb,1} F_b + h_{nc} \tag{2.4}$$

For the shell side heat transfer coefficient in a recirculation evaporator, in addition to nucleate boiling and natural convective, it is necessary take into account the forced convection due to high circulation flow rates. The forced convection heat transfer coefficient for a two-phase fluid is determined as follows:

$$h_{fc} = h_l F_{tp} \tag{2.4}$$

where, h_l is the liquid-phase heat transfer coefficient and F_{tp} is the two phase factor. The model proposed by Swanson and Palen [22] for the shell side boiling heat transfer coefficient in shell and tube heat exchangers considers the three previously mentioned mechanisms. Thus, the shell side coefficient becomes:

$$h_s = \alpha h_{nb} + h_{nc} + h_{fc} \tag{2.5}$$

where, α is the nucleate boiling suppression factor, $0 \le \alpha \le 1$.

The driving pressure (Equation 2.6) is produced by the density difference between the two-phase mixture in the riser (r) and downcomer (dc) tubes. An important factor when designing natural circulation boilers is the height of the downcomer and the riser because it affects the available driving pressure.

$$\Delta P_{dp} = g \rho_{dc} H_{dc} - g(\rho_{hx} H_{hx} + \rho_r H_r) \tag{2.6}$$

The frictional and momentum (fm) pressure drop is calculated as the pressure drop in the circulation loop of the downcomer, heat exchangers (hx), riser and nozzles (Equation 2.7).

$$\Delta P_{fm} = \Delta P_{dc} + \Delta P_{hx} + \Delta P_{r} + \Delta P_{nozzles} \tag{2.7}$$

Because the calculation procedure couples fluid dynamics with heat transfer, it is necessary to solve the problem by means of an iterative process. First, the evaporator heat transfer area is estimated based only on the nucleate boiling because at this point the circulation rate is unknown and the nucleate boiling is not a function of the mass flow. The evaporator geometric layout can be estimated afterwards. Second, a trial circulation rate is selected to solve the fluid dynamics equation system (Equations 2.6 and 2.7). This step is solved when all frictional pressure drops equals the available driving pressure. At this point, the new evaporator heat transfer area and layout is calculated taking into account the convective boiling produced by the circulation rate estimated in the last iteration. The process is repeated until the pressure drop and the heat transfer convergence is achieved.

2.3.2. Economic analysis

The design feasibility of the heat exchangers is evaluated with an economic analysis. In this Chapter, the total annualized cost (TAC) was used as the objective function of the optimization process [4,13,23]. The expression for total annual cost is:

$$TAC = frc\ C_{capital} + C_{operation} \tag{2.8}$$

$$C_{capital} = C_{hx} + C_{pump} \tag{2.9}$$

$$C_{operation} = C_{power} \frac{H_y}{\eta_{pump}} \left(\frac{\dot{m}_t \Delta P_t}{\rho_t} + \frac{\dot{m}_s \Delta P_s}{\rho_s} \right) \tag{2.10}$$

where, frc is the annuity factor, C_{hx} and C_{pump} are the investment costs of the heat exchangers and pumps, respectively, and $C_{operation}$ is the cost of the power that drives the pumps. To calculate this cost the annual operating hours (H_y) must be known. When the operating hours are not known, a reasonable approximation is made multiplying 8760 with the solar plant capacity factor (CF). The solar capacity factor is

defined as the ratio between the net energy produced in one year and the energy that could have been produced at full-load conditions [24].

According to Hall et al. [8], the investment cost of a heat exchanger can be estimated using Equation 2.11. c_1, c_2 and c_3 are the cost law coefficients and A is the surface area of the heat exchanger. This model reflects economies of a scale typically found in chemical process plants.

$$C_{hx} = c_1 + c_2 A^{c_3} \tag{2.11}$$

A more detailed method proposed by Purohit [11] was used here to calculate the investment cost of heat exchangers. This method is relatively complex because it takes into account many input parameters:

$$C_{hx} = \frac{CE_{index}}{CE_{index,ref}} \left(b \cdot \left(1 + \sum_{i=1}^{N_{inputs}} c_i \right) \cdot A \cdot N_s \right) \tag{2.12}$$

where, CE_{index} is the Chemical Engineering Plant Cost Index, c_i is a correction factor for input i (e.g., tube/shell material, pressure work, etc.), N_s is the number of shells and b is the base cost. The base cost can be expressed as:

$$b = \left(\frac{6.6}{1 - e^{\left(\frac{(7 - D_s)}{27} \right)}} \right) p\, f\, r \tag{2.13}$$

where, D_s is the internal diameter of the shell, p is the cost multiplier of the tube outside diameter, pitch and layout angle, f is the cost multiplier of the TEMA front head type and r is the cost multiplier of the TEMA rear head type.

The cost of the steam drum of the recirculation evaporator can be estimated as a function of the drum metal mass [9].

It should be mentioned that an economic evaluation based on TAC does not take into account all of the costs that may influence the optimum design. For example, each outlet temperature of the power block results in a different thermal oil mass flow in the solar field, and consequently to different pressure drops and pump consumptions. In order to take into account all of the former mentioned costs using standard criteria, the calculation of the levelized cost of energy (LCOE) is required.

$$LCOE = \frac{fcr\ C_{invest} + C_{om} + C_{fuel}}{E_{net}} \tag{2.14}$$

where, C_{invest} is the total investment cost of the plant, C_{om} the annual operational and maintenance costs and C_{fuel} is the cost of the annual use of fuel. These costs have been estimated using data provided by Montes et al. [25]. Since in this Chapter, the considered CSP plant does not include a fossil fuel back-up system, the annual fuel costs are zero. The annual net electric energy produced, E_{net}, was calculated subtracting the annual parasitic losses:

$$E_{net} = E_{gross} - E_{start,SG} - E_{pump,SF} - E_{pump,SG} \tag{2.15}$$

where $E_{start,SG}$ is the annual start-up energy consumption required to warm-up the metal mass of the heat exchangers and $E_{pump,SF}$ and $E_{pump,SG}$ are the annual pump consumptions of the solar field and the SG, respectively.

The investment cost of the TES system was estimated using literature data [3,16]. The cost of the hot and cold tanks, the quantity of the molten nitrate salt and the balance of the storage system were extrapolated as functions of the storage equivalent hours to full load capacity hours. The cost of the nitrate salt pumps was calculated according to the correlation proposed by Kelly and Kearney [16]. The investment cost of the oil-to-salt heat exchanger was estimated using the Purohit method.

2.3.3. Genetic algorithm

The large number of variables and constraints involved in the design of the heat exchangers of the SG cannot be handled by a traditional trial-and-error design method. To obtain improved designs, optimization tools must be used. Commonly used optimization methods for shell and tube heat exchangers are genetic algorithms (GA). The procedure consists of generating an initial population from random variables. Then, crossover and chromosome mutation factors are used to generate a new generation, evaluated by the objective function. This process is repeated until the GA achieves specified criteria.

The fitness function includes the TAC and the penalty function and it is expressed as:

$$fitness(\mathbf{x}) = TAC(\mathbf{x}) + penalty(\mathbf{x}) \tag{2.16}$$

where, $\mathbf{x}$ is the vector of design variables used to minimize the fitness function. The penalty function, defined to provide an efficient performance is expressed as [13]:

$$penalty(\mathbf{x}) = \begin{cases} 0 & if\ \mathbf{x}\ is\ feasible \\ \sum_{i=1}^{N} pc_i\ y_i^2(\mathbf{x}) & otherwise \end{cases} \tag{2.17}$$

where, pc_i is a penalty coefficient that varies with each generation and y_i corresponds to the level of constraint violation. The heat exchanger design variables are shown in Table 2.1.

Table 2.1: Design variables.

Variable	Single-phase heat exchanger	Evaporator
x_1	Shell diameter	Shell diameter
x_2	Tube diameter	Tube diameter
x_3	Tube layout (triangular, square or rotated square)	Tube layout (triangular, square or rotated square)
x_4	Tube pitch	Tube pitch
x_5	Number of shells	Number of shells
x_6	TEMA shell (E, F or H)	Recirculation ratio (for Kettle=0)
x_7	Shell side velocity	Tube side velocity
x_8	Tube side velocity	-
x_9	Baffle cut	-

The optimization parameters of the GA were the following: population size of 100 individuals with an elite count of three individuals, crossover fraction of 0.7 and mutation rate of 0.1. Two stopping criteria were used: the stall generation limit (when no further improvements are observed), which was set to 20; and the maximum number of generations, which was set to 300.

2.4. Initial design of the parabolic trough plant

In this Chapter, a parabolic trough power plant with 7.5 storage hours and a solar multiple of 2 is assumed. A schematic of the parabolic trough CSP plant is shown in Figure 2.1. The plant can be divided into four subsystems: the solar field, the SG, the power block and the TES system. The solar field is composed of parabolic collector sets in parallel loops that concentrate the solar irradiation for heating the thermal oil as heat transfer fluid. Normally, the thermal oil works at temperatures below 400 ºC in order to prevent fluid degradation. Here, the thermal oil is heated in the solar field to a temperature of 393 ºC ($T_{SF,OUT}$). The SG includes the generation train: superheater (SH), evaporator (EV) and preheater (PH) connected in parallel with the reheat train (reheater, RH). Thermal oil flows through the SG to supply the thermal energy to

increase the temperature from the exit water of the last feedwater heater to the high-pressure turbine inlet steam. The power block of the plant is based on a regenerative Rankine cycle with single reheat and extractions to the feedwater heaters. The working fluid of the cycle is water, the live steam pressure and temperature are 106 bar and 377 ºC ($T_{HP,IN}$) and the reheat steam temperature is 378 ºC ($T_{LP,IN}$). The gross power output of the turbine is 55 MWe and the nominal efficiency of the power block is 37.5%. The excess of thermal energy produced in the solar field is sent to the thermal energy storage (TES) unit of the facility. The TES system consists of two molten salt tanks (one cold and one hot), where the hot and cold molten salt is stored in the hot and cold tanks, respectively. Thermal energy is transferred from the thermal oil to the molten salt (charging) and the opposite (discharging) in the oil-to-salt heat exchanger.

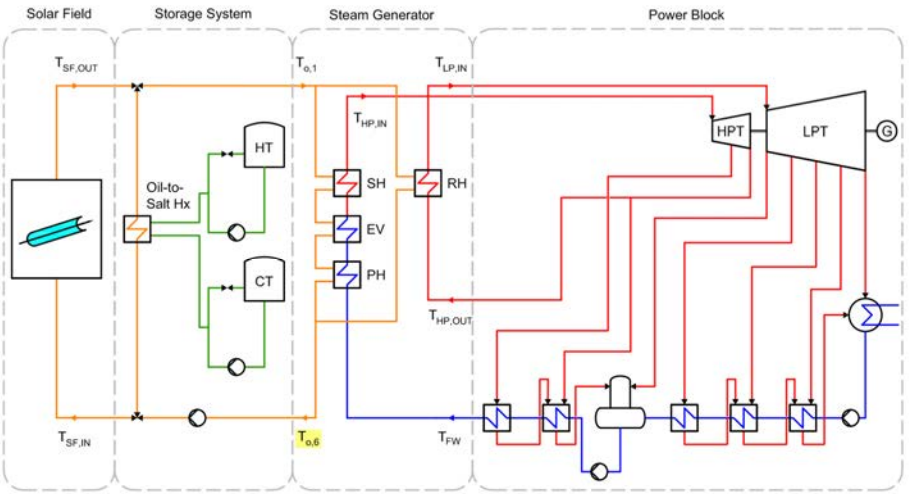

Figure 2.1: Schematic of the parabolic trough solar power plant.

The System Advisor Model (SAM) [26] was used to estimate the annual gross energy E_{gross} and the power pump consumption of the solar field $E_{pump,SF}$. The annual start-up energy was estimated as:

$$E_{start,SG} = W_{hx}\, Cp_w (N_{hot}\Delta T_{hot} + N_{cold}\Delta T_{cold})\eta_{PB} \tag{2.18}$$

where, W_{hx} is the weight of the heat exchangers, Cp_w is the specific heat capacity, η_{PB} is the efficiency of the power block and N_{hot} and N_{cold} are the number of the

annual hot and cold start-ups, respectively. A start-up is considered hot when the metal temperature (measured in the turbine unit before the start-up) is at 80 percent the nominal temperature. In cold start-ups, the metal temperature falls below 60 percent of the nominal temperature. According to Guédez et al. [27], the number of start-ups for a standard parabolic trough plant is 365 per year. Approximately 70 percent of those are hot starts. In this Chapter, it is considered the same cooling evolution for the SG heat exchangers as that considered by Guédez et al. [27].

Nominal values of the Rankine cycle are shown in Table 2.2. Thermodynamic properties of the water and steam streams are calculated based on analytical formulas for absolute and derivative values [28]. Thermal oil properties are selected based on data presented in Ref. [26].

Table 2.2: Nominal values of the 55 MWe (gross) steam power cycle.

Turbine point	Pressure (bar) (T. sat, ºC)	Temperature (ºC)	Mass Flow (kg/s)	Steam condition
HP inlet	106	377	61.91	One phase
Extraction 1	41.33 (252.30)	260.4	6.78	One phase
HP exhaust	20.73	214.2	55.13	Two phase
Extraction 2	20.73	214.2	3.814	Two phase
Condensate Separator	-	-	1.718	-
LP inlet	18.3	378	49.69	One phase
Extraction 3	10.5 (182.01)	310.6	3.114	One phase
Extraction 4	4 (143.61)	202.4	3.09	Two phase
Extraction 5	1.3	107.1	2.096	Two phase
Extraction 6	0.536	83	2.636	Two phase
LP exhaust	0.078	41.03	39.39	Two phase

2.5. Mechanical design and TEMA standards

TEMA standards provide guidelines for shell and tube heat exchanger components, such as: shell type, front head type, rear head type, outside tube diameters, maximum and minimum baffle spacing, clearances, baffle thickness, maximum tube length, fouling factors, tubesheet thickness and others [29]. In this Chapter, the mechanical design was carried out for selected elements of the heat exchangers. Shell and tube thicknesses were calculated according to the ASME code (section VIII and II, respectively) and compared to the minimum thicknesses recommended by TEMA. Baffle thicknesses, tube sheet thicknesses and clearances (shell-baffle, tube-baffle and bundle-shell) were calculated according to TEMA. In addition, the material selected for the shell and plates was ASTM A516 Grade 70 carbon steel. For the tubes ASTM A192 carbon steel was selected [30].

Conventional shell and tube heat exchangers were selected for the oil-to-salt and SG heat exchangers. Different TEMA shell types were modeled in order to enhance the performance of the heat exchanger. TEMA-E type is the most common and economical shell type used in chemical industries. However, this shell type does not always satisfy specific process requirements. In order to improve the thermal effectiveness, a TEMA-F shell type with two tube passes is usually preferred. In this type, a longitudinal baffle divides the flow path, making it a counter-current heat exchanger and avoiding in this way temperature crossings. When a low-pressure drop is required in the shell side, different TEMA shell types may be proposed. For example, TEMA-H and G shell types reduce the pressure drop drastically when compared to F shells. However, G shells are not recommended when larger tube lengths are required [31].

Figure 2.2 illustrates the TEMA shell types developed in this Chapter for single-phase heat exchangers. To estimate the heat transfer and pressure drop in the TEMA-F and H shell types, the geometries have been adapted reducing all stream flow areas by half, compared to the TEMA-E shell [32]. Furthermore, it is assumed that the flow leakage and conduction across the longitudinal baffle are minimized in both cases. This assumption can be made by limiting the maximum shell side pressure drop [33].

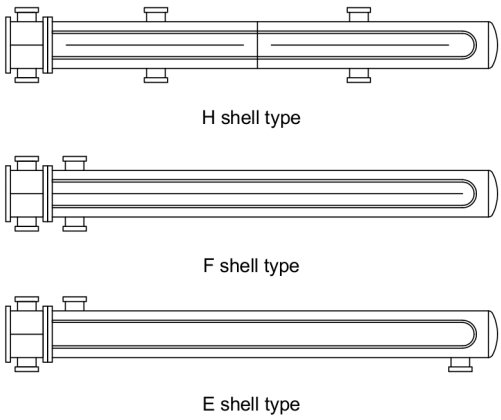

Figure 2.2: TEMA shell types developed for single-phase heat exchangers.

In numerous studies of CSP plants, a kettle evaporator is selected for the SG [15,16,34]. Other references propose a recirculation evaporator as a better option [35,36]. Here, both a recirculation and kettle-type evaporators have been modeled and compared.

A kettle evaporator consists of a horizontal TEMA-K shell with tube bundle (Figure 2.3). The boiling takes place on the shell side and the vapor is separated from

the liquid above the tube bundle. The main advantage of the kettle type is that it is composed of a single unit and thus associated with lower cost, when compared to other types. However, the larger diameter leads to a thicker shell and consequently, to worse performance under thermal stress. In addition, the low velocity on the shell side makes the kettle susceptible to fouling.

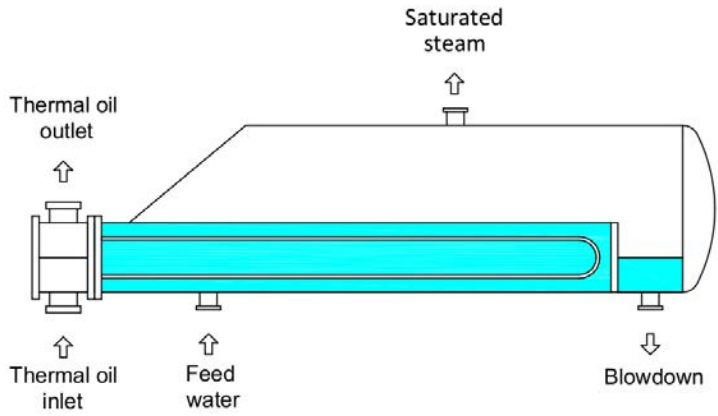

Figure 2.3: Kettle type evaporator.

Recirculation evaporators, also called thermosiphon reboilers, usually have TEMA-G, H or X shells [21]. The latter provides lower investment costs and pressure drops. The boiling occurs outside the tubes on the shell side fed with the two-phase fluid from the steam drum. The density difference between the downcomer and the riser induces a high natural circulation ratio (around 10 times that of the steam exiting). This leads to a higher shell side heat transfer coefficient and a small surface area when compared to the kettle type. Moreover, high circulation tends to decrease the potential fouling. The main advantage of a recirculation evaporator is its smaller shell diameter, compared to other designs. The smaller diameter reduces the shell and tubesheet wall thicknesses and improves the thermal stress behavior. The main disadvantage of this type of evaporator is the higher cost compared to the kettle type. Figure 2.4 illustrates a schematic of a TEMA-X shell recirculation evaporator.

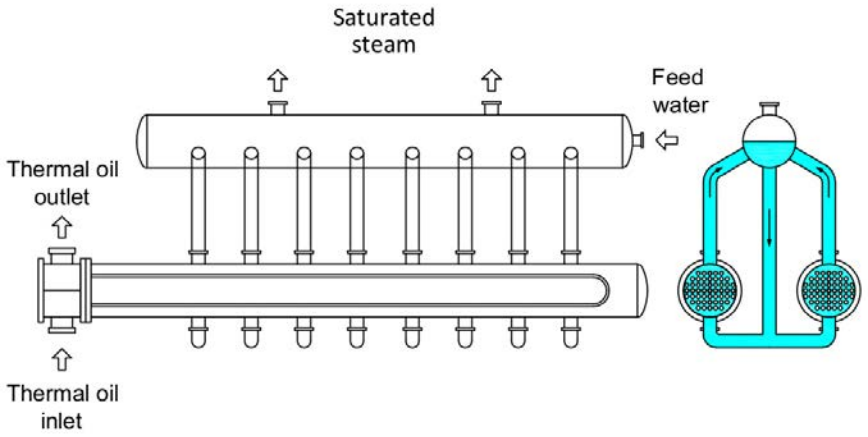

Figure 2.4: TEMA-X shell recirculation evaporator.

A U-tube bundle was selected mainly because it can expand or contract in response to stress differentials. In addition, the tube bundle can be removed, allowing the easy cleaning of the outer side of the tubes [37]. The U-tube bundle is mounted with a fixed tubesheet on the front end and a welded shell cover on the U-bend end [38].

In order to improve the reliability of the heat exchanger a channel integral with tubesheet TEMA-C and -N heads was selected [38]. Both head types have the channel welded to the tubesheet, while the TEMA-N head has the channel welded to the shell as well. The principal advantages of the TEMA-N head are the relatively low cost and the minimum leakage of the shell-side fluid since there are no flanged joints. Thus, it may be used with hazardous or high-pressure fluids on the shell side. The TEMA-C head allows mechanical cleaning because the shell is removable and it is thus chosen with dirty fluid flows on the shell side. In the case of high pressure on the tube side (up to 100 bar), the TEMA-D head is selected [39].

2.6. Cost-based design optimization

To allow the optimization algorithm to obtain feasible designs, selected constraints based on TEMA standards and recommended good practice are used. The general heat exchanger constraints are:

- The shell side velocity is limited between 0.2 m/s and 1.5 m/s [40].
- The minimum tube side velocity is set to 0.5 m/s in order to reduce the fouling resistance, while the maximum is set to 4 m/s to avoid excessive erosion [40]. The maximum steam velocities are set according to the steam velocity diagram of the operational pressure, tube diameter and process type presented by Merritt [41].

- The maximum pressure drop on the thermal oil side of the heat exchangers is set to 1.4 bar [16]. In order to prevent thermal leakage, the maximum shell-side pressure drop in H and F shells is set to 0.5 bar [33].

- The maximum pressure drop on the water side of the heat exchangers is set to 1 bar.

- The maximum straight tube length is set to 24 meters [16]. The length for the U-tube heat exchanger is around half the straight tube length because the tubes are bent in the shape of a U.

- The minimum baffle spacing is limited for good flow distribution and is set to the highest value between $D_s / 5$ and 50 mm. The maximum baffle spacing is limited for two reasons: for proper flow distribution and to prevent sagging and possible tube vibrations.

- The tube length to shell diameter ratio is limited between 8 and 12. Generally longer tubes with smaller diameter and thickness in shell and tubesheet are preferred [42].

- The baffle cut limits are set as a function of the baffle spacing to shell diameter ratio [42].

- The allowed shell-tube diameter combinations are set based on recommended practice [42]. Moreover, the minimum outside tube diameter is limited to be bigger than 14 mm, since diameters smaller than that cannot be cleaned mechanically [40].

- Square and rotated square tube layout is preferred for thermal oil on the shell side, because a triangle layout does not allow mechanical cleaning [40].

- In order to avoid undesirable temperature crosses [38], $F_{\min}$ is set to 0.8 in TEMA-E shells and 0.95 in TEMA-H shell designs.

- The maximum shell side nozzle momentum is limited to 2250 kg/(s²·m). With large mass flows, an impingement plate is added to increase the momentum to 4500 kg/(s²·m) in an effort to decrease the diameter of the nozzle.

The design constraints applied specifically to evaporators and two-phase flows are:

- The maximum heat flux for tube bundle is limited in order to avoid film boiling [21].

- The critical flow (when the flow reaches the velocity of the propagation of pressure waves [43]) in water-steam mixtures is estimated using Equation 2.19 [44]:

$$G_c = \sqrt{2\left[P_{ref} - c_f P_{sat}(T_{ref})\right]\rho_{l,ref}} \tag{2.19}$$

  where, G_c is the critical mass flux, P_{ref}, T_{ref} and $\rho_{l,ref}$ are the pressure, temperature and liquid density in upstream stagnation (i.e., steam drum), respectively, and c_f is a choking correction factor.

- As suggested for high-pressure boilers (> 40 bar) [45], the circulation ratio is limited between 8 and 15.

- The maximum shell side nozzle momentum for the two-phase flow is limited to 1500 kg/(s²·m), in order to prevent unstable operation [42].

- The kettle and drum diameters are chosen in order to not exceed the maximum vapor velocity that allows gravitational settling of entrained liquid droplets. The vapor load is calculated as [21]:

$$VL = 0.064\,\rho_V \left(\frac{\sigma}{\rho_l - \rho_V}\right)^{0.5} \tag{2.20}$$

The required dome segment area (Equation 2.21) is expressed as a function of the steam mass flow ($\dot{m}_v$) and the length of the horizontal drum o kettle (L_d). Then, for a given percentage of water level ($Level$) the minimum drum or kettle diameter is given by Equation 2.22.

$$SA = \frac{\dot{m}_v}{L_d \, VL} \tag{2.21}$$

$$D_{d,\min} = \sqrt{\frac{8\,SA}{\left[2\cos^{-1}\left(\frac{2\,Level}{100}-1\right)-\sin\left(2\cos^{-1}\left(\frac{2\,Level}{100}-1\right)\right)\right]}} \tag{2.22}$$

- A minimum number of exit nozzles is set for improving the longitudinal flow distribution along a drum or a kettle [21].

2.6.1. Optimizing the design of the SG

The configuration of the SG is shown in Figure 2.5 .The design process of the SG requires the definition of the optimal evaporator pinch point (pp_{EV}) and thermal oil outlet temperature ($T_{o,6}$). Different pp_{EV} can be obtained varying the mass flow led to the reheater train. As seen in Figure 2.6, higher pp_{EV} leads to higher temperature differences in the generation train (superheater, evaporator and preheater). Consequently, the surface area of the heat exchangers decreases, reducing the associated investment cost. On the contrary, smaller temperature differences obtained in the reheat train, lead to larger heat transfer areas and higher costs. As a result, a trade-off between the costs of the generation train and the reheater is obtained (Figure 2.7 a). The optimal pp_{EV} is achieved when the total cost of the generation and reheat trains is minimized.

Since the heat duty of the SG is proportional to the thermal oil flow rate and the difference between the inlet and outlet temperatures ($T_{o,1}$ and, $T_{o,6}$ respectively), if $T_{o,1}$ is kept constant, the thermal oil flow rate increases with increasing $T_{o,6}$. On the one hand, higher $T_{o,6}$ increases the power requirement of the pumps and, thus, the operational cost of the SG and the solar field. On the other hand, lower, $T_{o,6}$ leads to lower temperature differences in the SG and greater heat transfer area and higher cost. In this way, a trade-off between the operational and investment costs is obtained (see Figure 2.7 b).

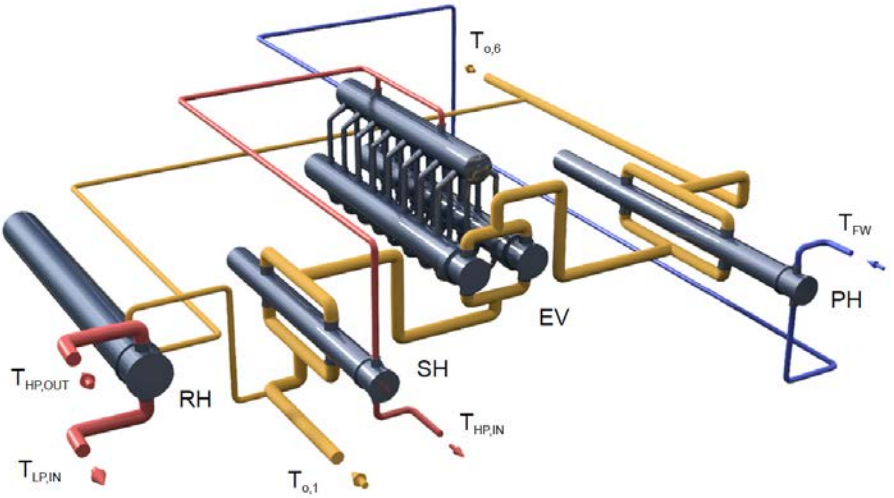

Figue 2.5: SG configuration.

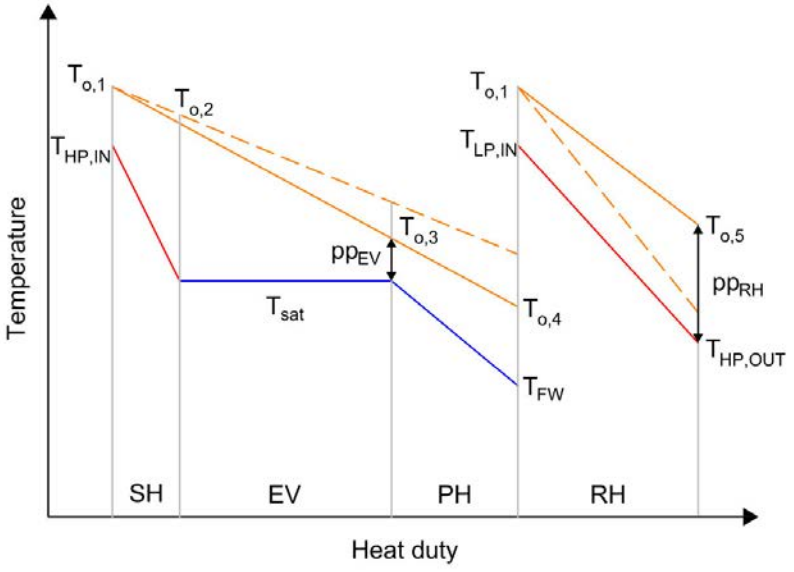

Figure 2.6: SG temperatures versus heat duty.

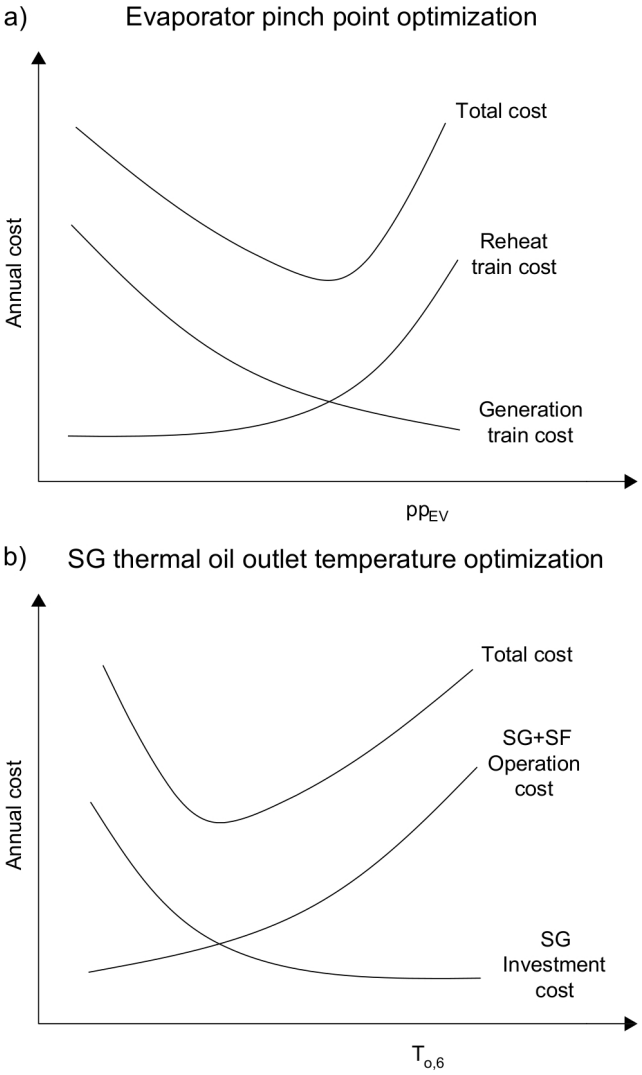

Figure 2.7: SG design optimization: a) evaporator pinch point and b) thermal oil outlet temperature.

The thermal oil mass flow rate is calculated in order to supply the required heat exchanger duties at different $T_{o,6}$ ($T_{o,1}$ is kept constant at 393 ºC). $T_{o,6}$ is varied from 289 to 300 ºC. In all cases, the different reheater mass flows bypassed should not result in pinch points lower than 1 ºC and 3 ºC in the evaporator (pp_{EV}) and reheater (pp_{RH}), respectively. Then, the optimization of the SG heat exchangers was carried out individually for all combinations of pp_{EV} and $T_{o,6}$. Moreover, two optimization

strategies were compared: the TAC minimization and the heat transfer area minimization.

The results of the analysis for the SG are shown Figure 2.8. It can be seen that the LCOE has a higher rate of increase for higher values of pp_{EV}, due to the higher costs of the reheat train. A moderate rate of increase is obtained for lower values of pp_{EV}. The blank region in Figure 2.8 corresponds to reheater pinch points lower than the minimum (infeasible cases). The optimum design corresponds to $T_{o,6}$ equal to 293 ºC and pp_{EV} equal to 4.85 ºC.

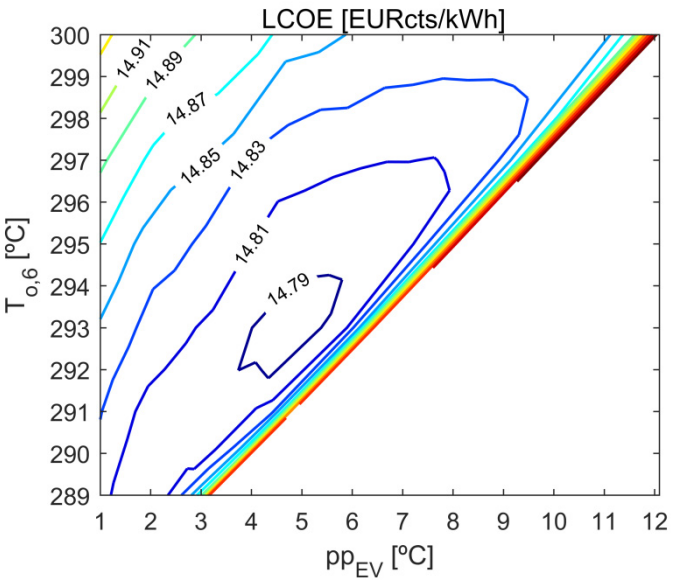

Figure 2.8: Economic analysis of the SG.

Based on common practice in commercial parabolic trough plants [46,47], the SG design is optimized to include two parallel trains, each with a preheater, an evaporator, a superheater and a reheater. Initially, an SG design with one train was carried out. Although this design had lower investment cost, it led to higher wall thicknesses in the heat exchangers. Since only one train is used in this design, the complete SG system must be warmed up. This results in an increased metal mass to be heated-up and may also increase the start-up time considerably. Moreover, this design has smaller heat transfer efficiency when working at part load conditions, compared to the SG design with two parallel trains. These features may decrease the annual energy production and plant operability.

The final design characteristics of the optimized SG heat exchangers are presented in Table 2.3. In the superheater, the reheater and the preheater, the thermal oil is

placed on the shell side and the steam or the high-pressure water on the tube side. In the evaporator, the thermal oil is placed on the tube side and the steam/water mixture on the shell side. The heat exchangers are designed with large length to diameter ratios and small wall thicknesses that can sustain the pressure. Specifically, the design of the recirculation evaporator, made with three units (two TEMA-X shell heat exchangers and one steam drum), leads to a meaningful reduction in the shell diameter, i.e., smaller shell and tubesheet thicknesses, in comparison to a kettle. Since solar plants are subject to daily start-ups, stops and load changes, the reduction of wall thicknesses means lower thermal stress and fatigue damage. Moreover, smaller wall thicknesses allow high temperature gradients and smaller start-up time. The latter is very important for CSP plants because it leads to reduced start-up costs and increases the efficiency [48]. Furthermore, smaller wall thicknesses involve a considerable reduction in metal mass and save energy during the warm-up process.

When TAC minimization strategy is used, the algorithm solution tends to lower velocities on the thermal oil side in order to decrease the operational cost from the pressure drop in the SG. Some studies found in literature assumed high-pressure drops on the thermal oil side, minimizing, in this way, the heat exchanger area. A second optimization of the SG was carried out using as strategy the minimization of the heat exchanger area. It is found that the TAC minimization strategy results in savings of around 3.5 M€ throughout the plant lifetime.

2.6.2. Optimizing the design of the oil-to-salt heat exchanger

The operation of the oil-to-salt heat exchanger determines the temperature drop of the molten salt in the hot tank during charging operation. In addition, it also determines the temperature drop of the thermal oil inlet of the SG during discharging operation. The thermal oil inlet temperature is lower than the nominal conditions, hence it decreases the power block efficiency, and the turbine is operated under part-load conditions. In order to reduce the power block efficiency penalty, the oil-to-salt heat exchanger is designed with very small approach temperatures, in the range of 3-10 ºC [17]. Due to the high heat duty and thermal efficiency required, an oil-to-salt heat exchanger design with TEMA-F shells in series is proposed (see Figure 2.9).

The cycle performance during discharging was calculated through an iterative process. First, an energy balance for each heat exchanger of the SG is defined with an initial thermal oil inlet temperature. The thermal oil mass flow is determined by the nominal conditions.

Table 2.3: Proposed designs of heat exchangers.

Parameter	Superheater	Reheater	Preheater	Evap. Kettle	Evap. Rec. + Drum
Shell diameter, (mm)	880	1130	825	2240/1370a	860/1000b
Baffle cut, (%)	35	30	34	-	-
Baffle spacing, (mm)	762	606	654	-	-
Tubes ext. diameter, (mm)	19.1	15.9	15.9	15.9	15.9
Tubes int. diameter, (mm)	13.6	12.6	11.7	12.6	12.6
Tube pitch, (mm)	24.8	19.9	20.7	19.9	19.9
Tube layout, (º)	90	90	90	30	30
Tube passes, (-)	2	2	2	2	2
Tubes number, (-)	419-U	1149-U	527-U	1997-U	754-U
Tube length, (m)	7.51	10.31	11.44	9.18	10.97
Shell thickness, (mm)	16	16	13	135	64
Tubesheet thickness, (mm)	134	75	126	210	131
Mass flow (tube-side), (kg/s)	30.9	24.8	30.9	263.5	131.75
Mass flow (shell-side)), (kg/s)	263.5	35.1	263.5	- /30.9c	163.78/15.47c
Flow velocity (tube side), (m/s)	11.13	24.03	0.72	1.38	1.83
Flow velocity (shell side), (m/s)	0.80	0.37	0.91	-	0.16
Convective heat transfer coefficient (tube-side), (W/m2 ºC)	3607.1	992.3	7474.8	2738.1	3484.0
Convective heat transfer coefficient (shell-side), (W/m2 ºC)	1757.3	1303.4	2215.7	17929.0	20326.0
Fouling resistance (tube-side), (ºC m2/W)	8.825e-5	3.53e-4	8.82e-5	2.64e-4	2.64e-4
Fouling resistance (shell-side),(ºC m2/W)	2.64e-4	2.64e-4	2.64e-4	1.76e-4	1.76e-4
Overall heat transfer coefficient, (W/m2 ºC)	703.5	358	1014.7	929.3	1030.1
Heat exchange area (per shell), (m2)	377.4	1183.2	602.35	1832.0	826.4
Pressure drop (shell-side), (kPa)	27.7	41.20	51.10	-	9.5/26.94d
Pressure drop (tube-side), (kPa)	75.41	87.08	14.02	31.95	59.28
TEMA designation	DHU	CFU	DHU	NKU	NXU
Total number of shells, (-)	2	2	2	2	4/2e
Total investment cost, (k €)	247	337	428	773	897

[a] Tube bundle diameter.

[b] Steam drum diameter.

[c] Outlet steam mass flow.

[d] Total pressure drop in recirculation loop.

[e] Number of drums.

The inlet pressure of the turbine is calculated until the live steam mass flow and the heat duties in the water/steam side are balanced. The power of the turbine, the power block efficiency and the outlet temperature of last feedwater heater are calculated in each iteration. At this point, the thermal oil outlet temperature of the SG is also calculated. Then, an energy balance in the TES is made and a new thermal oil inlet temperature to the SG is obtained. The process is repeated until convergence of heat duties and temperatures is reached in the SG and TES. The turbine efficiency was modeled as a function of the inlet mass flow rate, which was calculated using the Stodola correlation [49]. In each heat exchanger, the overall heat transfer coefficient

reduction was estimated by raising the tube mass flow reduction ratio to the power of 0.8.

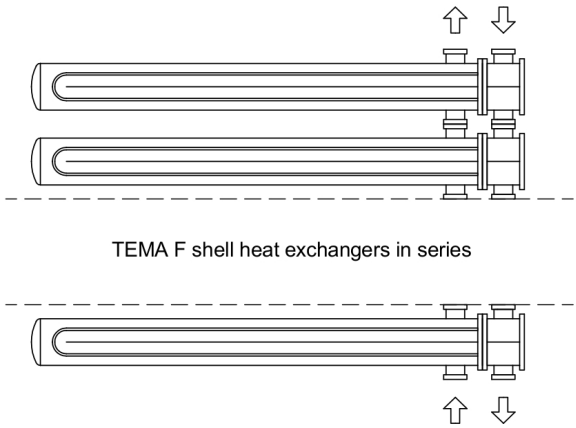

Figure 2.9: Proposed design of oil-to-salt heat exchanger with TEMA F shell in series.

The initial convergence of the system of equations shows an excess of energy in the preheater of the SG that may lead to steaming. This may induce vibrations, which may trigger tube failure due to two-phase flow through the tubes. Although that may occur in practice, steaming is not allowed in the preheater from an economic point of view [50]. In order to avoid steaming, additional water mass flow is assumed to achieve saturation conditions in the exhaust of the water preheater. In order for the evaporator water level to remain constant, the water excess is circulated to the deaerator.

The LCOE of the heat exchanger is calculated for varying LMTD between 2 ºC and 15 ºC. As seen in Figure 2.10, higher values of the LMTD lead to lower power outputs ($W_{turbine}$) and efficiencies (η_{PB}). This is due to the reduced live-steam temperature ($T_{HP,IN}$), inlet pressure ($P_{HP,IN}$) and flow rate ($\dot{m}_{HP,IN}$). As expected, if the outlet temperature of the solar field is kept constant, the hot tank temperature (T_{HT}) decreases with increasing LMTD. On the contrary, the cold tank temperature (T_{CT}) increases with increasing LMTD. This happens because less thermal energy is required in the SG and the decreasing rate of $T_{o,6}$ is smaller than that of $T_{o,1}$.

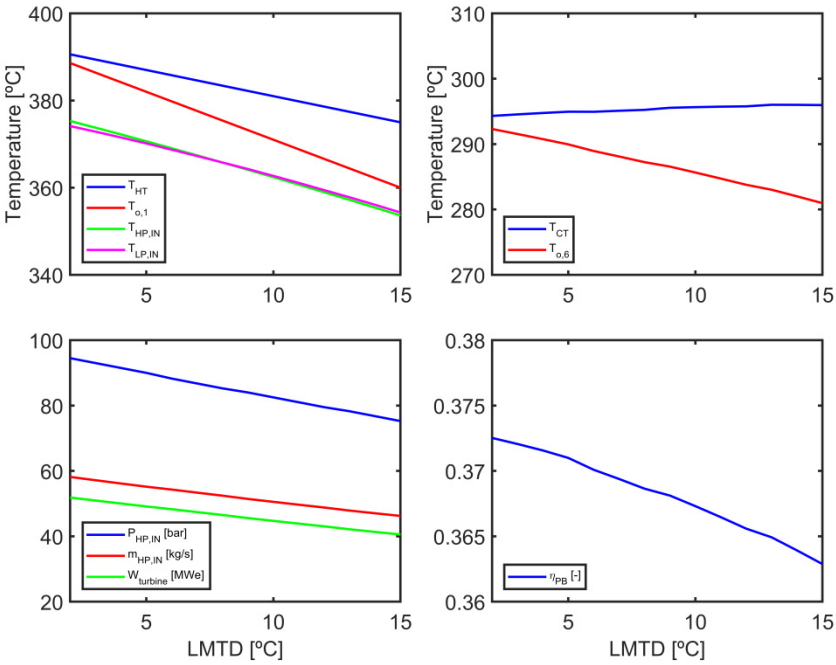

Figure 2.10: Power block performance under part load conditions.

The results of the economic analysis of the TES of the plant, reveal an optimum LMTD equal to 7 ºC (Figure 2.11). This agrees well with published work [16]. A small difference is noted because the cost of the oil-to-salt heat exchanger in [16] was assumed to be approximately 50% lower than in our case. Because, it was not clear from the beginning which fluid should be placed on the tube side and which on the shell side, two TEMA-F shell designs are analyzed for the oil-to-salt heat exchanger. These designs are presented in Table 2.4. The pressure on the thermal oil side was set to 20 bar because the vapor pressure of the oil is around 10 bar at 390 ºC and the total pressure drop in the SG and the oil-to-salt heat exchanger is approximately 10 bar

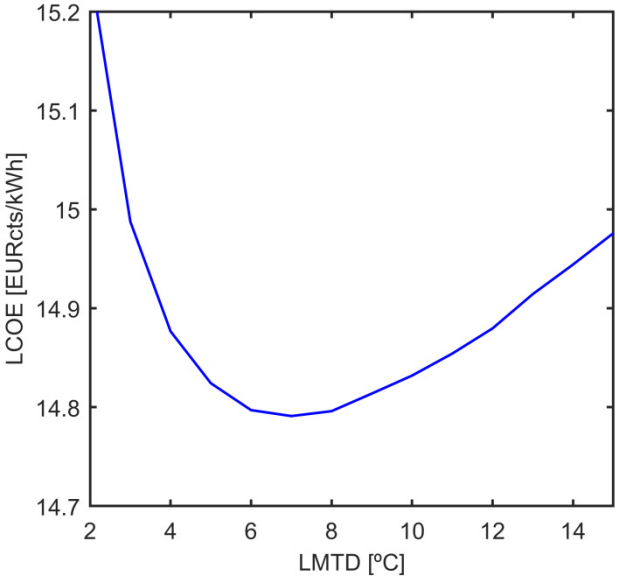

Figure 2.11: Economic analysis of the TES.

In Design 1 the molten salt is placed on the shell side and the thermal oil on the tube side. The opposite is made in Design 2. Design 1 provides a higher overall heat transfer coefficient than Design 2 that leads to lower heat exchange area and cost. On the other hand, Design 2 may lead to a better drainage operation, since the thermal oil (during charging operation) can melt the molten salt inside the tubes easier.

The heat exchanger designs were evaluated during discharging operation. The first calculations may violate the maximum allowed tube spacing, because a large baffle space is required to fulfill the maximum shell side pressure drop. To avoid vibration problems, a rod type baffle is mounted on the tubes [38]. None of the proposed designs satisfied the maximum shell side pressure drop constraint for TEMA-F shells to prevent thermal leakage. This is because standard single segmental baffle leads to high pressure drops on the shell side. Double or triple segmental baffles can be used as a possible solution to reduce the pressure drop on the shell-side.

2.7. Conclusions

In this Chapter, the design of the steam generator heat exchangers and the oil-to-salt heat exchanger of a 50 MWe parabolic trough solar power plant was presented and optimized. The optimized design was based on total costs and was obtained

using a genetic algorithm with design constraints based on recommended good practice and TEMA standards.

The results show a global optimum for outlet temperature of the thermal oil equal to 293 ºC and an evaporator pinch point of 4.85ºC. TEMA-H shells are proposed for the superheater and the preheater, and a TEMA-F shell for the reheater. The reduction of the pressure drop within the steam generator proposed leads to higher savings in the operational cost of the pump of the heat transfer fluid, when compared to other designs reported in literature. Furthermore, a TEMA-X shell recirculation evaporator is proposed, which leads to an important reduction in the shell and tubesheet thicknesses compared with a kettle evaporator. This allows higher temperature gradients in transient regimes.

Table 2.4: Proposed designs for the oil-to-salt heat exchanger.

Parameter	Design 1	Design 2
Shell diameter, (mm)	2.56	2.56
Baffle cut, (%)	31	32
Baffle spacing, (mm)	1574	1557
Tubes ext. diameter, (mm)	19.1	19.1
Tubes int. diameter, (mm)	14.9	14.9
Tube pitch, (mm)	28.7	28. 7
Tube layout, (º)	45	45
Tube passes, (-)	2	2
Tubes number, (-)	2911-U	2914-U
Tube length, (m)	10	9.5
Number of shells (in series), (-)	6	7
Shell thickness, (mm)	41	41
Tubesheet thickness, (mm)	191	195
Mass flow (tube-side), (kg/s)	593	954
Mass flow (shell-side)), (kg/s)	954	593
Flow velocity (tube-side), (m/s)	1.50	1.00
Flow velocity (shell-side), (m/s)	0.55	0.81
Convective heat transfer coefficient (tube-side), (W/m² ºC)	2892	3073
Convective heat transfer coefficient (shell-side), (W/m² ºC)	4318	2374
Fouling resistance (tube-side), (ºC m²/W)	2.6e-4	8.8e-5
Fouling resistance (shell-side), (ºC m²/W)	8.8e-5	2.6e-4
Overall heat transfer coefficient, (W/m² ºC)	827.76	755.59
Heat exchange area (per shell), (m2)	3862	3465
Pressure drop (shell-side), (kPa)	612	513
Pressure drop (tube-side), (kPa)	231	373
TEMA designation	NFU	CFU
Total investment cost, (M€)	5.2	5.8

Lastly, the analysis of the thermal energy storage system revealed an optimum for a logarithmic mean temperature difference of the oil-to-salt heat exchanger of 7 ºC.

With this temperature difference, two designs were proposed. In the first design the molten salt was placed on the shell side and the thermal oil on the tube side. The opposite was made in the second design. The first design is considered the best option, since it was found to have a lower investment cost.

Nomenclature

Abbreviations

CF : capacity factor.
CT : cold tank.
EV : evaporator.
FW : feed water.
HP : high pressure.
HTF : heat transfer fluid.
HT : hot tank.
LP : low pressure.
$LCOE$: levelized cost of electricity (€/kWh).
$LMTD$: log mean temperature difference (ºC).
PB : power block.
PH : preheater.
RH : reheater.
SF : solar field.
SG : steam generator.
SH : superheater.
TAC : total annualized cost (€/year).
TES : thermal energy storage.

Symbols

A : heat transfer area (m^2).
B_c : baffle cut (-).
C : cost (€).
CE_{index} : Chemical Engineering Plant Cost Index (-).
C_p : specific heat capacity (J/kg ºC).
D : diameter (m).

E : energy (kWh/year).

F : log mean temperature difference correction factor (-).

F_b : bundle heat transfer correction factor (-).

F_{tp} : Two phase heat transfer correction factor (-).

G_c : critical mass flux (kg/m^2 s).

H : height (m).

H_y annual plant operation time (h/year).

K : resistance coefficient (-).

L : length (m).

L_{bc} : baffle spacing (m).

N_{cold} : number of cold starts.

N_{hot} : number of hot starts.

N_{tp} : number of tube passes (-).

N_{tt} : number of tubes (-).

N_s : number of shells (-).

P : pressure (Pa).

R : fouling resistance (ºC m^2/W).

S : stream flow area (m^2).

SA : dome segment area (m^2).

T : temperature (ºC).

U : global heat transfer coefficient (W/m^2 ºC).

VL : vapour load parameter (kg/s m^3).

W : weight (kg).

$W_{turbine}$: turbine power (MWe).

b : cost of baseline heat exchanger (EUR/m^2).

c_1 to c_3 : cost law coefficients.

c_f : chocking correction factor (-).

f : cost multiplier for TEMA-type front head (-).

g : gravity acceleration (m/s^2).

h : convective coefficient (W/ m^2 ºC).

l_{ts} : tubesheet thickness (mm).

$\dot{m}$: mass flow rate (kg/s).

p : cost multiplier for tube outside diameter, pitch and layout (-).

pc : penalty coefficient (-).

pp : pinch point (ºC).

r : cost multiplier for TEMA-type rear head (-).

t_s : shell thickness (m).

v : velocity (m/s).

$\mathbf{x}$: vector of optimization variables (-).

$\mathbf{y}$: vector of feasible constraints (-).

Greek Symbols

α : suppression factor (-).

δ : temperature profile distortion factor (-).

η_{PB} : power block efficiency (-).

θ_{tp} tube layout (º).

ρ : density (kg/m^3).

ϕ_v : viscosity correction factor (-).

Subscripts

d : drum.

dc : downcomer.

dp : driving pressure.

fm : frictional and momentum.

fc : forced convection.

hx : heat exchanger.

$invest$: investment.

nb : nucleate boiling.

nc : natural convection.

l : liquid phase.

o : thermal oil.

om : operation and maintenance.

out : outlet.

pl : platforms.

r : riser.

ref : reference condition.

s : shell.

t : outside of tube.

ti : inside of tube.

tp : two phase.

2.8. References

[1] Usaola J. Participation of CSP plants in the reserve markets: A new challenge for regulators. Energy Policy 2012;49:562–71. doi:10.1016/j.enpol.2012.06.060.

[2] National Renewable Energy Laboratory (NREL) 2016. http://www.nrel.gov/csp/solarpaces/by_project.cfm.

[3] Iea. Technology Roadmap-Solar Thermal Electricity 2014:1–52. doi:10.1007/SpringerReference_7300.

[4] Serna M, Jiménez A. A Compact Formulation of the Bell–Delaware Method for Heat Exchanger Design and Optimization. Chem Eng Res Des 2005;83:539–50. doi:10.1205/cherd.03192.

[5] Ravagnani M a. SS, Silva AP, Biscaia EC, Caballero J a. Optimal Design of Shell-and-Tube Heat Exchangers Using Particle Swarm Optimization. Ind Eng Chem Res 2009;48:2927–35. doi:10.1021/ie800728n.

[6] Mizutani FT, Pessoa FLP, Queiroz EM, Hauan S, Grossmann IE. Mathematical Programming Model for Heat-Exchanger Network Synthesis Including Detailed Heat-Exchanger Designs. 2. Network Synthesis. Ind Eng Chem Res 2003;42:4019–27. doi:10.1021/ie020965m.

[7] Serth RW, Lestina TG. Process Heat Transfer: Principles , Applications and Rules. 2014. doi:http://dx.doi.org/10.1016/B978-0-12-397195-1.00005-4.

[8] Hall SG, Ahmad S, Smith R. Capital cost targets for heat exchanger networks comprising mixed material of construction, pressure ratings and exchanger types. Comput Chem Eng 1990;14:319–35.

[9] Seider WD, Seader JD, Lewin DR, Widagdo S. Product and process design principles: synthesis, analysis, and evaluation. 2010.

[10] Taal M. Cost estimation and energy price forecasts for economic evaluation of retrofit projects. Appl Therm Eng 2003;23:1819–35. doi:10.1016/S1359-4311(03)00136-4.

[11] Purohit GP. Estimating Cost of Shell and Tube Heat Exchangers. Chem Eng Res Des 1983.

[12] Willdi PT. Minimizing shell-and-tube heat exchanger cost with genetic algorithms and considering maintenance. Int J Energy Res 2007;31:867–85. doi:10.1002/er.

[13] Ponce-Ortega JM, Serna-González M, Jiménez-Gutiérrez A. Use of genetic algorithms for the optimal design of shell-and-tube heat exchangers. Appl Therm Eng 2009;29:203–9. doi:10.1016/j.applthermaleng.2007.06.040.

[14] Fettaka S, Thibault J, Gupta Y. Design of shell-and-tube heat exchangers using multiobjective optimization. Int J Heat Mass Transf 2013;60:343–54. doi:10.1016/j.ijheatmasstransfer.2012.12.047.

[15] Kelly B. Nexant Parabolic Trough Solar Power Plant Systems Analysis Task 1 : Preferred Plant Size. Contract 2006.

[16] Kelly B, Kearney D. Thermal Storage Commercial Plant Design Study for a 2-Tank Indirect Molten Salt System Final Report 2006.

[17] Herrmann U, Kelly B, Price H. Two-tank molten salt storage for parabolic trough solar power plants. Energy 2004;29:883–93. doi:10.1016/S0360-5442(03)00193-2.

[18] Zaversky F, Sánchez M, Astrain D. Object-oriented modeling for the transient response simulation of multi-pass shell-and-tube heat exchangers as applied in active indirect thermal energy storage systems for concentrated solar power. Energy 2014;65:647–64. doi:10.1016/j.energy.2013.11.070.

[19] Taborek JWP and J. J.W. Palen and J. Taborek, Solution of shell side flow pressure drop and heat transfer by stream analysis method. n.d.

[20] ESDU. Baffled Shell-and-Tube Heat Exchangers: Flow Distribution, Pressure Drop and Heat Transfer Coefficient on the Shellside. ESDU Int Ltd n.d.;No. 83038.

[21] Palen JW. Shell and Tube Reboilers. In Heat Exchanger Design Handbook. New York: Hemisphere Publishing Corp.; 1988.

[22] Swanson LW, Palen JW. Convective Boiling Applications in Shell-and-Tube Heat Exchangers. Heat Transf Res Inc n.d.:45–56.

[23] Smith R. Chemical process design and integration. John Wiley & Sons; 2005.

[24] Wagner SJ, Rubin ES. Economic implications of thermal energy storage for concentrated solar thermal power. Renew Energy 2014;61:81–95. doi:10.1016/j.renene.2012.08.013.

[25] Montes MJJ, Abánades a., Martínez-Val JMM, Valdés M. Solar multiple optimization for a solar-only thermal power plant, using oil as heat transfer fluid in the parabolic trough collectors. Sol Energy 2009;83:2165–76. doi:10.1016/j.solener.2009.08.010.

[26] Version S a M. Solar Advisor Model Reference Manual for CSP Trough Systems 2009.

[27] Guédez R, Spelling J, Laumert B. Reducing the Number of Turbine Starts in Concentrating Solar Power Plants Through the Integration of Thermal Energy Storage. J Sol Energy Eng 2014;137:11003. doi:10.1115/1.4028004.

[28] Garland WJ, Hand BJ. Simple Functions for the Fast Approximation of Light Water Thermodynamic Properties. Nucl Eng Des 1989;113:21--34. doi:http://dx.doi.org/10.1016/0029-5493(89)90293-8.

[29] Byrne RC, Tema, York N, Byrne RC. Standards of the Tubular Exchangers Manufacturers Association. Main 2007.

[30] Zavoico AB. Solar Power Tower - Design Basis Document. Sandia Natl Lab 2001:148. doi:10.2172/786629.

[31] Mukherjee R, Objectives B, Thermal Design and Optimization of Single-Phase Heat Exchangers n.d.:19–50.

[32] Thulukkanam K. Heat Exchanger Design Handbook, Second Edition. 2013. doi:10.1201/b14877.

[33] Mukherjee R. Does Your Application Call for an F-Shell Heat Exchanger? CEP Mag 2004:40–5.

[34] Bradshaw RW, Dawson DB, De la Rosa W, Gilbert R, Goods SH, Hale MJ, et al. Final Test and Evaluation Results from the Solar Two Project. Sandia Natl Lab 2002:294. doi:10.2172/793226.

[35] Aalborg CSP. Aalborg CSP Concentrated Solar Power steam generators 2016. http://www.aalborgcsp.com.

[36] Kolb GJ. An Evaluation of Possible Next-Generation High-Temperature Molten-Salt Power Towers 2011:1–120. doi:SAND20011-9320.

[37] Mukherjee R. Effectively Design Shell-and-Tube Heat Exchanger. Chem Eng Prog 1998:17.

[38] Shah R, Sekulic D. Fundamentals of Heat Exchangers Design. 2003.

[39] Kreith F. The CRC Handbook of Thermal Engineering. Boca Raton: LLC CRC Press; 2000.

[40] Caputo AC, Pelagagge PM, Salini P. Joint economic optimization of heat exchanger design and maintenance policy. Appl Therm Eng 2011;31:1381–92. doi:10.1016/j.applthermaleng.2010.12.033.

[41] Merritt C. Process Steam Systems: A Practical Guide for Operator, Maintainer and Designers. Hoboken, New Jersey: John Wiley & Sons; 2015.

[42] Taborek J. Shell and Tube Heat Exchangers: single phase flow, in Heat Exchanger Design Handbook. New York: Hemisphere Publishing Corp.; 1983.

[43] Fauske HK. Contribution to the theory of two-phase one-component critical flow. Argonne Natl Lab Rep 1962;ANL-6333. doi:Report ANL-6633.

[44] Kim Y-S. A proposed correlation for critical flow rate of water flow. Nucl Eng Technol 2015;47:135–8. doi:10.1016/j.net.2014.11.004.

[45] Ganapathy V. Understanding Boiler Circulation. Chem Eng 2013:52–6.

[46] C. A. d. Andalucía. 43.321/05. Solicitud de aprobación del proyecto de ejecución, y declaración en concreto de la utilidad pública del proyecto Andasol-1,. Boletin oficial del Estado. Gobierno de España; n.d.

[47] Lebrija 1 : International solar thermal reference. Energ Int 2012;123:36–44.

[48] Yang Y, Wang Z, Xu E, Ma G, An Q. Analysis and Optimization of the Start-up Process based on Badaling Solar Power Tower Plant. Energy Procedia 2015;69:1688–95. doi:10.1016/j.egypro.2015.03.130.

[49] Stodola A, Lowenstein LC. Steam and Gas Turbines, vol. I. New York: McGraw-Hill Book Company; 1945.

[50] Sarkar D. Thermal Power Plant: Design and Operation. Elsevier Inc.; 2013.

CHAPTER

THREE

Thermo-economic optimization of molten salt steam generators

Contents

3.1. Abstract....52
3.2. Introduction. 52
3.3. Initial design of SPTP. 54
3.4. Methodology 55
3.4.1. SG design selection. 56
3.4.2. Material Selection....61
3.4.3. Thermal-Hydraulic Design. 62
3.4.4. Mechanical Design. 62
3.4.5. Estimating Cost Models. 68
3.4.6. Heat exchanger Optimization using genetic algorithms. 70
3.5. Optimization. 71
3.5.1. Optimization of the approach point of the SG. 71
3.5.2. Results of the approach point optimization. 71
3.5.3. Optimization of the pinch point of the SG....72
3.5.4. Global optimization procedure. 73
3.5.5. Results of the pinch point optimization. 75
3.5.6. SG proposed design....76
3.6. Conclusions 79
3.7. References....83

3.1. Abstract

This Chapter presents a methodology to guide the design of heat exchangers for a steam generator in a solar power tower plant. The low terminal temperature difference, the high fluid temperatures and the high heat duty, compared to other typical shell and tube heat exchanger applications, made the design of the steam generator for molten-salt solar power towers a challenge from the thermo-mechanical point of view. Both the heat transfer and the thermal stress problems are considered to size the preheater, evaporator, superheater and reheater according to the TEMA standards and ASME Pressure Vessel code. An integral cost analysis on the steam generator design effects on the power plant performance reveals an extremely low value for the optimum evaporator pinch point temperature difference. Furthermore, an optimization using genetic algorithms is performed for each heat exchanger, which leads to economical and feasible designs.

A 110 MWe solar power tower plant is studied. Two configurations of the steam generator are proposed: with one or two trains of heat exchangers. The results show that the optimum pinch point temperature differences are very close to 2.6 ºC and 3 ºC for the steam generator with one and two trains, respectively. The proposed design of the steam generator consists of a U-shell type for superheater and reheater, a TEMA E shell forced circulation evaporator and a TEMA-F shell preheater. Also, the approach point temperature difference analysis is performed to avoid sub-cooled flow boiling in the preheater. An economic study to compare forced and natural circulation evaporator designs is carried out.

3.2. Introduction

Different studies for the design of molten-salt steam generators (SGs) of solar power tower plants (SPTPs) are available in the literature. The design requirements consider the material selection, geometric parameters and overall performance [1]. Other design guidelines also include the economical evaluation of the SG [2]. In both cases, these design recommendations analyze the SG design for a 100 MWe commercial SPTP. In spite of Foster Wheeler recommendations [1], a different approach is accomplished for the SG design of the experimental facility Solar Two [3] and Molten Salt Electric Experiment (MSEE) [4], showing that the SG design is a wide open research field.

The SG design depends also on the manufacturer. In this sense, several SG solutions proposed by different manufacturers were analyzed for a 100MWe commercial solar power plant in [2]. For instance, ABB Lummus [2] design includes a

kettle evaporator and U-tube/straight shell heat exchangers. The salt is placed on the shell side in the superheater and preheater, whereas in the reheater the salt is placed on the tube-side. The superheater design is divided into two shells in series in order to decrease the thermal stress in the tubesheet. The SG design proposed by ABB Lummus presents the lowest cost compared to other manufactures. Struthers Wells [2] uses the same concept as ABB Lummus employing a kettle evaporator and U-tube/straight shell heat exchangers. The principal feature of this design is that the high-pressure water is placed on the shell side in all heat exchangers. This leads to high thicknesses, and thus, high thermal inertia. On the other hand, Foster Wheeler [1,2] proposes a straight tube/straight shell design with the molten salt placed on the shell side. In this design, the inlet and outlet streams pass through different tubesheets, avoiding the potential temperature gradients in the no-tube passes zone. The differential thermal expansion is accommodated by floating tubesheets. Furthermore, a natural circulation design is selected for the evaporator. The design proposed by Babcock and Wilcox (B&W) [2] consists of U-tube/U-shell heat exchangers with the molten salt placed on the shell side. Similarly to the straight tube/straight shell design, the U-shell design also avoids temperature gradients produced by inlet and outlet streams. In addition, the U-shaped tubes can expand or contract in response to the thermal expansion between tubes and shell without the need of floating tubesheets. The main disadvantage is that the U-shell design presents relative high costs. A forced circulation evaporator is selected instead of natural circulation evaporator.

In spite of these useful recommendations shown in [2], several design parameters such as velocities, pressure drops or tube diameters of the heat exchangers are missing. Nevertheless, these recommendations were used for the SG design of the experimental facility Solar Two [3]. Some problems appeared in Solar Two. On the one hand, problems related to the stress corrosion materials appeared in such facility. For this reason, higher corrosion resistance materials for SG have been recommend by different authors [5,6]. On the other hand, further problems related to the salt freeze inside of the tubes of the kettle evaporator occurred in Solar Two [7], pointing out the difficulties found in the industry to design and operate SG systems.

Most recent studies have been made for higher SPTPs capacities where a preliminary SG design can be found. Kolb [8] carried out a study to increase the efficiency of these plants. The SG sizing for 160 MWe subcritical and supercritical steam-cycles was calculated including the associated heat transfer areas and pressure drops. Kelly [9] proposed different strategies to reduce the levelized cost of electricity using supercritical heat transport fluids for central receiver power plants. The sizing and cost analysis of subcritical and supercritical SGs for 400 MWe plants were also studied.

Recently, genetic algorithms (GA) have been used extensively as an optimization method in the heat exchanger design. For instance, Caputo et al. [10] and Sadeghzadehet et al. [11] performed a cost design optimization of shell and tube heat exchanger using GA. Their results show significant cost reductions over heat exchangers designed using traditional methods. Hajabdollahi et al. [12] used both GA and particle swarm method to optimize the cost of a shell and tube heat exchanger condenser. They claim that GA provides lower CPU time compared to particle swarm method.

In the previous Chapter was carried out the optimization of heat exchangers of parabolic trough solar power plant [13]. Two optimization strategies were compared: minimize the heat transfer area and minimize the total annualized cost, considering capital and operation costs. The results show that the minimization of the total annualized cost may lead to lower costs.

In this Chapter, a complete methodology for the design of SG for a SPTP is proposed. This approach considers the general requirements of the SG heat exchangers (superheater, reheater, evaporator, preheater and drum), the materials selection, the thermal-hydraulic and the mechanical designs together with the cost models and an optimization procedure. To accomplish such work, once the general requirements are satisfied, the approach consists of finding the optimum value of the pinch point temperature difference of the SG. An approach point temperature analysis is made to avoid subcooled flow boiling in the preheater in order to use low cost materials. The optimization of each heat exchanger is carried out employing a genetic algorithm, while the overall cost is optimized studying the whole SG.

3.3. Initial design of SPTP

The SPTP analyzed for the SG optimization is Crescent Dunes [14], which consists in a 110 MWe plant with 3.8 solar multiple and 10 storage hours. These features allow obtaining a 52% capacity factor. A simplified schematic of the different subsystems of the plant is shown Figure 3.1. The solar field is composed by heliostats following a radial staggered arrangement, which reflect the solar radiation into a receiver. The heat transfer fluid employed is molten-salt, which is heated from around 290 to 565ºC in the receiver. The thermal energy storage (TES) system is formed by two tanks (one hot and one cold) allowing the controlled release of the thermal energy captured from the solar field. The SG system includes a superheater (SH), reheater (RH), evaporator (EV) and preheater (PH). The hot salt is sent to SG where the thermal energy is transferred to produce main and reheated steam. The power block consists of a subcritical Rankine-cycle with a regenerative system. The main steam pressure and

temperature are 12.6 MPa and 550ºC, respectively; and its efficiency is 44%. The main design values of the power block are summarized in Table 3.1. The water and steam properties are calculated using the correlations published in [15]. The molten-salt properties are obtained from [16].

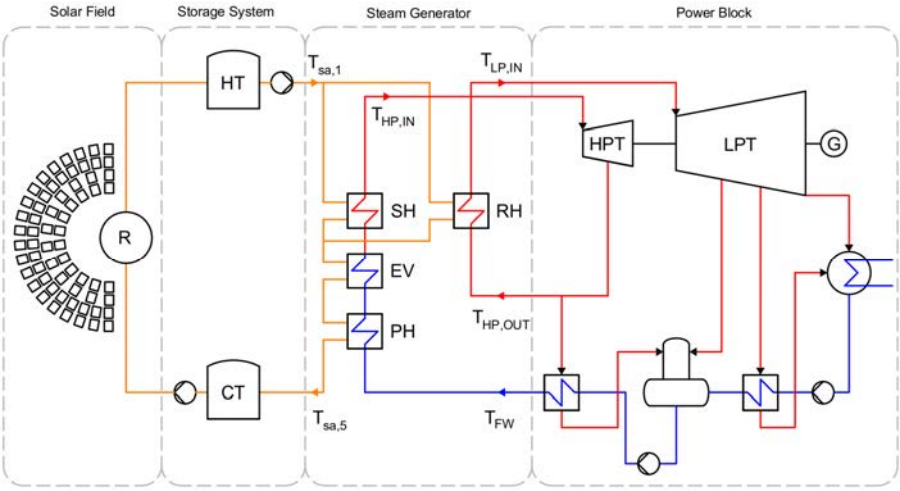

Figure 3.1: Schematic of a SPTP.

Table 3.1: Nominal values of the 110 MWe steam power cycle.

Turbine point	Pressure (MPa)	Temperature (ºC)	Mass Flow (kg/s)
HP in	12.6	550	86.92
HP out	3.4	371	78.70
LP in	*	550	78.70
Feed-Water	*	245	86.92

*These parameters are subjected to SG design calculations.

3.4. Methodology

This section describes the procedure followed to design individually each heat exchanger of the SG. First, an initial design that follows the technical requirements and recommendations is proposed. After that, the materials, the thermal-hydraulic conditions and the mechanical design are analyzed. Figure 3.2 shows a simplified

scheme of the approach, which is further detailed in this section. Later, a global economic optimization of the SG is carried out using GA and costs models.

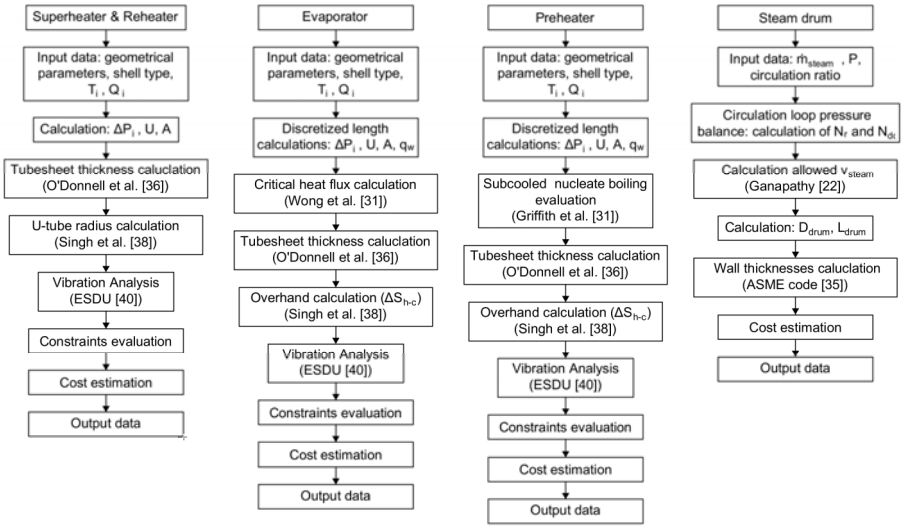

Figure 3.2: Schematic of the main heat exchanger calculations.

3.4.1. SG design selection

A general problem in the heat exchangers of the SG is the differential thermal expansion between the shell and the tubes. This is caused by the high temperature differences between the inlet and the outlet of the working fluids. Then, the different temperature profile of the working fluids leads to different thermal expansion in the shell and the tubes. To solve that, two designs are normally used: U-tube or floating head. The floating head design presents higher costs than U-tube mainly for two reasons: i) higher capital cost [17]; ii) higher cost associated to maintenance [2]. Therefore, in this Chapter a U-tube design is selected for all heat exchangers of the SG.

Since solar plants are subjected to daily transient operations, the reduction of the thicknesses of the heat exchangers may improve dynamic behavior of the SG against thermal stresses. Therefore, low-pressure salt is placed on the shell-side and the high-pressure water/steam on the tube-side.

- **Superheater and reheater requirements**

The main technical problem of the superheater is the high temperature differences between the inlet and outlet of the steam (~200ºC). This may lead to high temperature gradients in a single-tubesheet design, especially in the no-tube-lane zone. Furthermore, the temperature profile in the superheater produces a high differential thermal expansion of the hot leg over the cold leg of the tube bundle. This may involve a high curvature radius in the U-bend and thus an increase in the associated shell diameter. The U-shell design provides a good solution to solve the aforementioned problems since it has two tubesheets, and then, the thermal stresses produced in the no-tube-lane zone are eliminated. Moreover, in this design, a high U-bend radius does not lead to a high shell diameter. This design was employed successfully in the experimental facility MSEE [4].

The technical problems described in the superheater also occur in the reheater, although the working pressure in the reheater is considerably lower. Finally, an U-shell design is selected for the superheater and the reheater.

- **Evaporator requirements**

Several studies of parabolic trough plants include a kettle evaporator for the SG due to its relatively low capital cost and its successful operation in the pioneering CSP plants, such as in Luz Solar Electric Generating Stations (80 MWe) [2]. Nevertheless, the breakage of tubes in a kettle evaporator in Solar Two experimental facility due to the salt freeze-thaw cycling warns against its application [7]. For this reason, in this work a circulation evaporator type with steam drum was selected for the SG.

Mainly two designs are possible for circulation evaporators: forced or natural. According to Pasha [18], heat recovery steam generators (HRSGs) with forced circulation systems have shorter start-up times than natural circulation systems. This is because the natural circulation systems need enough driving pressure to assure natural circulation, which may lead to a high thermal inertia. In addition, in forced circulation evaporators the circulation ratio (total mass flow circulated per unit of steam flow generated) is not dependent on the heat abortion. Thus a lower time is required to achieve the optimal circulation. For these reasons, forced circulation evaporators may provide advantages for plant operability. Normally, in HRSGs with forced circulation systems the circulation ratio is ranged between 3 and 8 [19], whereas in natural circulation systems is ranged between 8 and 25 [18].

In spite of the aforementioned advantages of the forced circulation design, it is not clear what design provides lower costs, in terms of capital investment and operation. Therefore, in this Chapter a cost analysis is carried out to help in the selection of the

best design. The pump operating costs on tube-side and shell-side, the capital cost associated to the heat exchangers and the start-up energy cost are considered. The proposed designs for forced and natural circulation evaporators are illustrated in Figure 3.3-a and Figure 3.3-b, respectively.

Different assumptions are made for the calculations. The number of downcomers and risers is calculated to fulfill the maximum momentum according to [1]. The maximum diameters are set to 450 mm and 150 mm, respectively. In the natural circulation design, the downcomer height is adjusted to provide the specified circulation ratio. In both designs, the tube length is discretized at least to the baffle spacing, to obtain accurate values for the two phase flow calculations (heat transfer coefficient, pressure drop, heat flux, etc.). Details of the evaporator calculations are described in Appendix A.

As can be seen in Figure 3.3-c and Figure 3.3-d forced circulation evaporator provides lower costs. Although both options include an economical straight shell design, the forced circulation design also allows a horizontal orientation to use a U-tube rear-end type and then reduce the heat exchanger costs. In contrast, natural circulation design requires a floating head type increasing the heat exchanger cost.

Different TEMA shell types such H or F are possible solutions as heat exchanger in a horizontal circulation evaporators [20], but finally a TEMA E shell is selected for different reasons. Firstly, TEMA E shell type is one of the most economical and the most common shell designs. Secondly, the inlet salt nozzle can be moved at the bottom of the heat exchanger, reducing the potential thermal stress in the tubesheet. In addition, the thermal stress in the U-tube rear-end type is also reduced since the differential thermal expansion between cold and hot legs is minimized.

- **Preheater requirements**

The preheater do not have a high temperature differences between inlet/outlet on the salt and water sides (around 50ºC and 70 ºC, respectively), therefore a single-tubesheet design is a feasible and economical option. This solution was used in the experimental facility Solar Two without technical issues [3]. Moreover, the pinch point and the approach point temperature differences (Figure 3.4) reported in the literature are typically low, and then, high thermal effectiveness will be required. For these reasons, a TEMA F shell is selected for the preheater.

Typically, in conventional fossil-fired plants and HRSGs, an approach point temperature difference between exit water of the economizer and the saturated water of the steam drum is imposed to prevent generation of steam in last zone of the economizer; this phenomenon is called steaming or subcooled flow boiling. The steaming may lead to vibrations and mechanical damage by water hammer [21],

which can produce a fast deterioration of the economizer, unless a steaming economizer is used. The approach point temperature difference depends on the manufacturers and technologies. For instance, in conventional fossil-fired this temperature difference shows values of 15-25 ºC and in HRSGs ranges from 5 to 35 ºC [22]. For molten salt steam generators, the approach point used by ABB Lummus, Struthers Wells and Foster Wheeler was 0 ºC, in contrast, B&W chose 1.5 ºC [2].

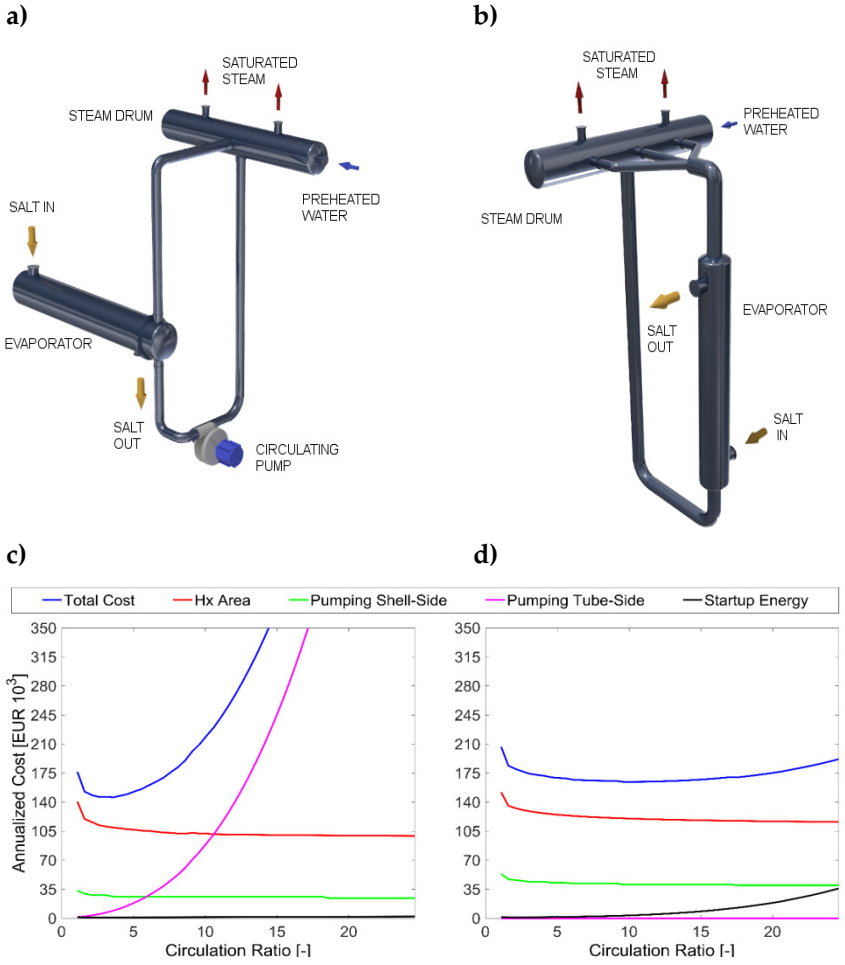

Figure 3.3: Evaporator design: a) Forced circulation evaporator. b) Natural circulation evaporator. The annualized cost against the circulation ratio: c) Forced circulation evaporator; d) Natural circulation evaporator.

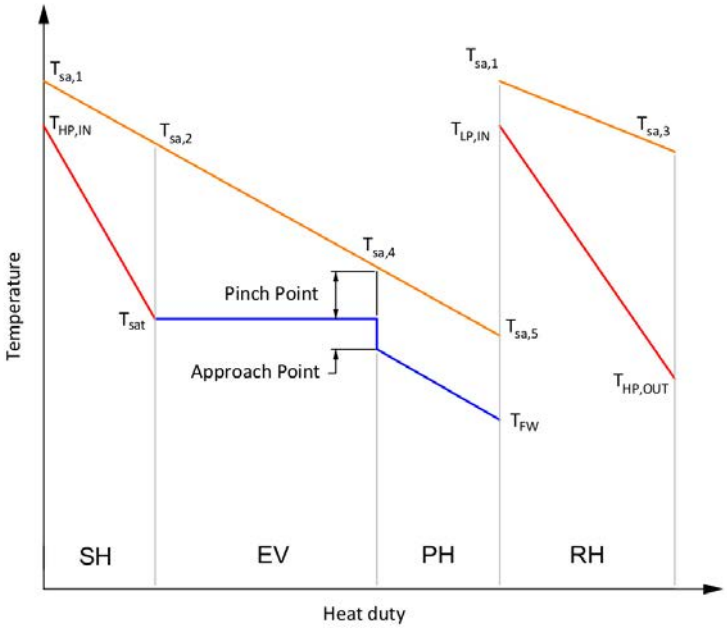

Figure 3.4: Typical temperature profile for the SG.

- **Drum Requirements**

The steam drum size is estimated assuring that the vertical and horizontal steam velocities are below the values recommended by Ganapathy [23]. This is important to achieve a proper operation of the chevron ensuring that the water droplets are not dragged by the steam flow.

Finally, Figure 3.5 shows the heat exchanger configuration selected for the SG.

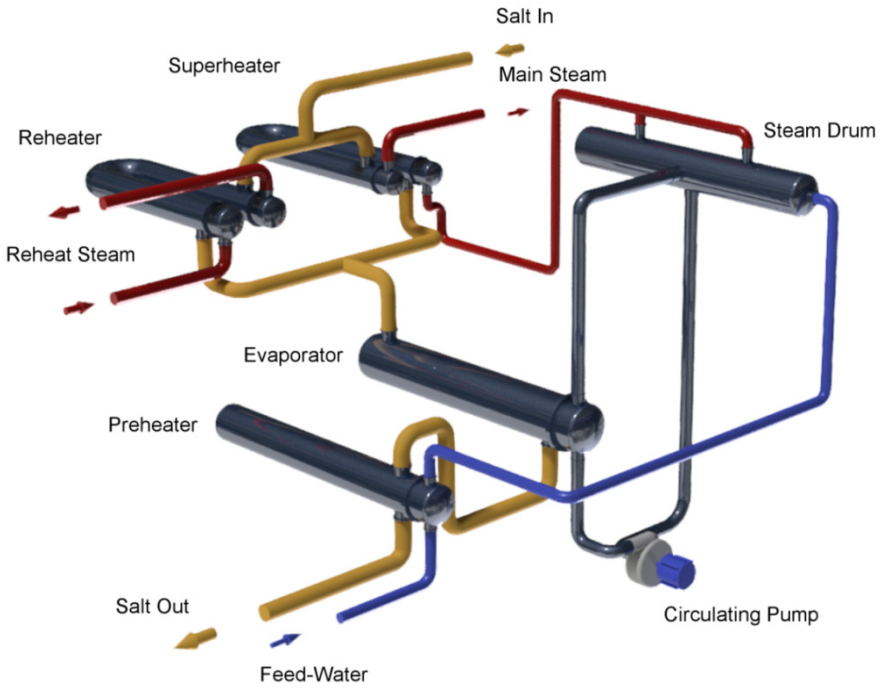

Figure 3.5: Heat exchanger configuration selected for the SG.

3.4.2. Material Selection

Zavoico [5] recommends the materials for different parts of the SG: Gr 347 or 321 stainless steel for the superheater, 9Cr-1Mo alloy steel for evaporator and carbon steel for preheater. For the superheater and the reheater, a lower cost stainless steel such as 304 or 316 are recommended by several manufacturers [2]. In contrast, according to Kelly [7], 304 or 316 stainless steel may be susceptible to stress corrosion cracking because of the potential impurities in the industrial-grade molten-salt used. For the preheater and the evaporator, in a first step, Zavoico [5] recommended materials were selected. Finally, in order to decrease the thermal stress on the U-bend zone, the selected tube materials are ASTM A210, Gr. A1 for preheater and ASTM A213, Gr. 347 for evaporator. The materials selected for the SG are shown in Table 3.2.

Table 3.2: Selected Materials for the main SG components.

Component	Shell and Tubesheet Material	Tube Material
Preheater	A516, Gr. 70	A210, Gr. A1
Evaporator	A387, Gr. 91	A213, Gr. 347
Superheater	A240, Gr. 347	A213, Gr. 347
Reheater	A240, Gr. 347	A213, Gr. 347
Steam Drum	A516, Gr. 70	-

3.4.3. Thermal-Hydraulic Design

The sizing of the SG heat exchangers is carried to fulfill the heat duty requirements, which are specified by the power block. A computer code is performed to calculate several geometric parameters of the heat exchangers.

The shell-side pressure drop is calculated based on the stream analysis method using the Wills-Johnston version [24]. This method consists in a hydraulic network, where the shell-side flow is divided into six different streams: the tube-to-baffle leakage (A), the cross-flow (B), the bundle-to-shell bypass (C), the shell-to-baffle leakage (E) and the tube-pass-partition by-pass (F). The pressure drop per baffle is calculated using Equation 3.1. This equation is solved by an iterative process where the convergence is achieved when the same pressure drop is obtained in the meeting points of the different paths.

$$\Delta P_j = \frac{K_j (\dot{m}_j / S_j)^2}{2 \rho \phi_v} \qquad j = A, B, C, E, F \tag{3.1}$$

At this point, the percentage of the different stream flows respect to the total flow is known, then the heat transfer coefficient on the shell-side can be estimated using the correlation proposed by Engineering Science Data Unit (ESDU) [25], which is expressed in terms of the heat transfer coefficients on cross-flow zone.

- **Double segmental baffle calculations**

In a first step, the heat exchanger design is carried out using single-segmental baffle, obtaining high shell side pressure drops. These optimized designs obtained in the first step tend to minimize the shell-side velocity to reduce the operational cost, in spite of the increment in the heat exchange area and the associated increment in the capital cost. For these reasons, a double-segmental baffle (Figure 3.6) is selected

providing a good option to reduce the pressure drop. In addition, double-segmental baffles may reduce the tube vibration, especially when larger mass flow rates are involved [26].

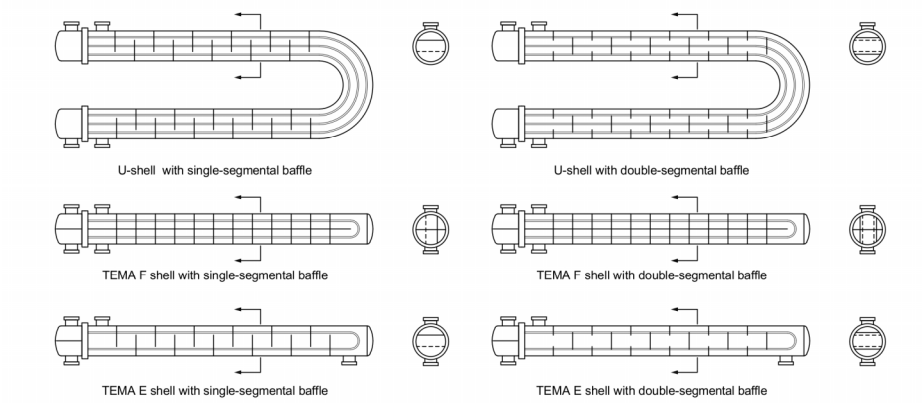

Figure 3.6: Shell and baffle types.

The heat exchanger is divided in two symmetrical main streams to obtain the shell-side pressure drop in double-segmental baffles. Each one has their corresponding sub-streams mentioned before. Now, the ideal hydraulic network is solved adapting conveniently the flow areas of each sub-stream. A similar concept is used in the method proposed by K. P. Singh et al. [27] for triple-segmental baffles calculations. To validate this approximation, different designs reported in the literature were consulted [1,24]. The nozzle pressure drops are also considered in shell-side calculations.

According to ESDU [25] the heat transfer coefficient on the shell side can be estimated considering only the cross-flow in single-segmental baffles. In contrast, this consideration is not valid for double-segmental baffles since the percentage of parallel flow respect to the total flow may increase using double-segmental baffles, and it may lead to a reduction in the overall heat transfer. Then, the heat transfer coefficient on the shell-side is calculated using the Equation 3.2 proposed by Emerson [28]. This equation takes into account the heat transfer coefficients in the cross-flow and window zone, which are weighted by their respective heat transfer areas. The heat transfer coefficient in the cross-flow zone is calculated using the Colburn correlations [24]. The heat transfer coefficient on the window zone is calculated using the correlation proposed by Singh et al. [27].

$$h_s = \frac{A_x h_x + A_w h_w}{A_x + A_w} \tag{3.2}$$

- **Heat transfer and pressure drop inside tubes**

For single-phase flows, the heat transfer on the tube-side is estimated using Gnielinski correlation [24]. Since the heat exchangers are arranged horizontally, the pressure drops on the tube-side by static head losses are neglected. The friction factor is calculated using the Colebrook correlation [24]. The pressure drop for tube pass and the momentum change in nozzles are also taken into account.

For two-phase flows, the heat transfer coefficient is calculated according to Chen's correlation [29]. This correlation considers two heat transfer mechanisms: the nucleate boiling and the two-phase forced convection. The pressure drop for two-phase flows is calculated using the method proposed by Lockhart and Martinelli [24]. Two-phase effect in geometries such as bends and nozzles have been also considered.

- **Critical heat flux calculation**

The critical heat flux is defined as the point which above the two-phase heat-transfer coefficient drops and takes place the departure of nucleate boiling phenomenon. Normally, the evaporators are not designed to operate near of the critical heat flux, not only for the decrease in the heat transfer coefficients but also to prevent the tube wall overheating. This problem appears when a zone in the evaporator exceeds the critical heat flux, showing an alternating process of dryout and wetting in the internal wall [30]. Therefore, cyclic thermal variations in the tube wall may lead to deposit-corrosion and fatigue damage. Moreover, this effect is related to flow instabilities that may reduce the performance.

The critical heat flux point mainly depends on the operating pressure, the mass velocity and the steam quality, the tube orientation, etc. To calculate the critical heat flux in horizontal tubes, the correlation proposed by Wong et al. [31] is used. Moreover, Collier et al. [30] recommends for boiling flows in horizontal tubes a minimum fluid velocity of 2.5 m/s in order to avoid steam water stratification problems.

Forced circulation evaporators require a careful economic study. As shown in Figure 3.3 the optimal value of the circulation ratio is obtained around 2.5. However, the operation at the optimal circulation ratio exceeds the maximum heat flux allowed in the rear-end zone of the U-bend. Then, to operate the evaporator safely, a minimum circulation ratio of 5 is required. Other design employs multi-lead ribbed tubes in the evaporator which increases the steam quality working below of the

critical heat flux conditions [4]. This means that the circulation ratio decreases, and then, the evaporator could be operated in the optimal economic performance. However, no correlations or experimental data about the critical heat flux using multi-lead ribbed tubes were found, and thus, this design option has not been considered in our analysis.

- **Subcooled flow nucleate boiling**

Although, the preheater is designed to not overpass the saturation temperature of the steam drum, subcooled flow nucleate boiling may occur at local conditions. A correlation proposed by Griffith et al. [32], Equation 3..3, is used to estimate the local temperature difference at which starts the Onset of Significant Voids (OSV). Downstream of this point, the void fraction increases rapidly. Therefore, it has been considered steaming conditions when the tube bulk temperature fulfills this condition: $T_{t,bulk} \geq T_{sat} - \Delta T_{sub,OSV}$.

$$\Delta T_{sub,OSV} = q_w \frac{(14 + 0.1P_t)}{v_t} \tag{3.3}$$

A numerical model is performed to calculate the preheater local conditions (heat flux, wall temperature,…) following the method proposed by Hussaini et al. [33].

3.4.4. Mechanical Design

Normally, a feasible heat exchanger is designed considering a high number of constraints. The standards of the Tubular Exchanger Manufactures Association (TEMA) [34] provide many geometrical constraints and design parameters such as: outside tube diameters, maximum and minimum baffle spacing, fouling resistances, clearances, etc. In this Chapter, all heat exchangers are designed to fulfill these requirements. The thicknesses of heads, shells and tubes are calculated according to the ASME Boiler and Pressure Vessel code Sections VIII and II [35]. Other design constraints, which are based on good practice recommendations, are also used [13].

In order to reduce the cost associated to the tube-to-tubesheet welding and tube-support-plate drilling, the number of tubes is minimized [1]. In this way, the optimization algorithm penalizes solutions when the tube length is far from its maximum value.

- **Tubesheet thickness calculation**

Typically, the tubesheet thickness calculation in heat exchangers for standard industrial applications is carried out using ASME Section VIII-Division 1 or/and TEMA standards methods. However, these methods do not consider the thermal stress effects in the U-tube tubesheet design. For this reason, more sophisticated methods were sought. The method proposed by O'Donnell et al. [36], considers the thermal stress and the stress produced by pressure. The thermal stresses are caused by temperature difference in the primary and secondary sides of the tubesheet, and in the no-tube-lane zone. Although in the standard industrial applications these effects are one or two orders of magnitude lower than the pressure stress, thermal stresses may become important when operating at high temperature differences, and thus, they should be combined with the pressure stress [37]. Then, to verify the heat exchanger designs on the safety-side, the O'Donnell method is used to calculate the tubesheet thickness. Figure 3.7 illustrates the operating temperatures in the superheater tubesheet for different shell types. Details of the tubesheet stress calculations according to O'Donnell et al. [36] are described in Appendix B.

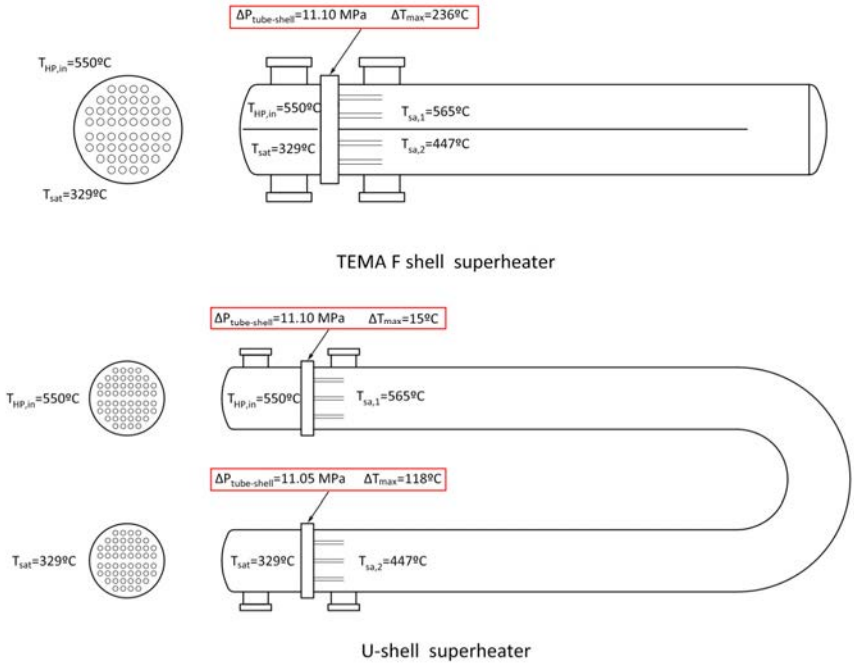

Figure 3.7: Tubesheet temperatures for different superheater shell types.

- **Minimal U-tube radius calculation**

It is well known that the U-tube design avoids the thermal stress problem related to the differential thermal expansion between tubes and shell. Nevertheless, the thermal stress problem related to the differential thermal expansion between the hot leg and the cold leg is still present. The U-bend radius has a great influence on the thermal stress generated. Furthermore, since the tubes are supported by segmental baffles, the thermal expansion of the tubes is not free. Then, the tubes try to lose their straight shape and produce contacts at tubes and baffles located at the end of the U-bends, Figure 3.8. Therefore, the location and the clearances of the last baffles play a key role on the generated stresses. In this Chapter, the minimal radius of the U-bend is calculated using the analytical method proposed by Singh et al. [38]. Figure 3.9 shows the minimal radius against the temperature difference between the hot and the cold legs. The U-tube stress calculation according to Singh et al. [38] is described in Appendix C.

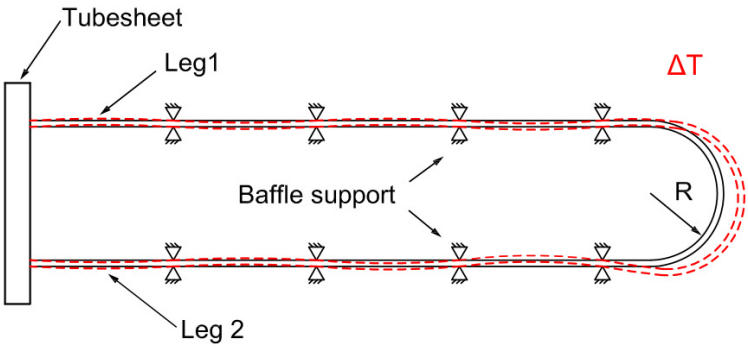

Figure 3.8: U-tube deformation by thermal expansion.

The minimal radius of the U-tube for the superheater and the reheater is calculated using a hot and cold leg overhand difference value of $\Delta S_{h-c} = 0$ in order to minimize the potential tube vibrations problems at the U-bend region. The U-tube radius for the evaporator and the preheater is selected according to the no-tube-lane distances reported in [39]. Then, the hot and cold leg overhand difference is adjusted below the maximum stress limit.

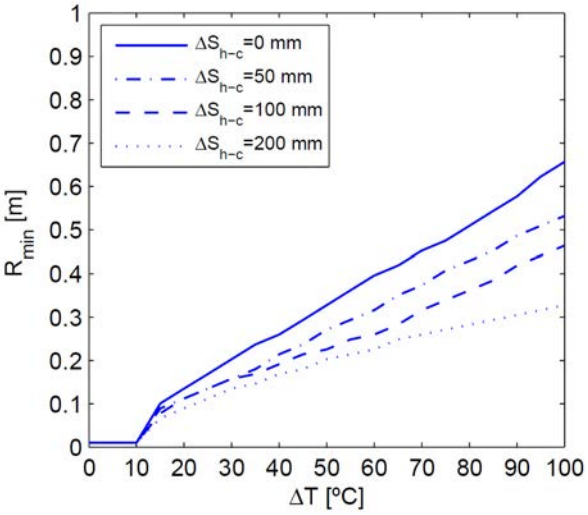

Figure 3.9: Minimal radius against temperature difference between different hot and cold leg overhand differences (ΔS_{h-c}).

- **Vibration Analysis**

In the heat exchanger design high flow velocities lead to high heat transfer coefficients, obtaining in this way benefits such as low surface areas, cost, fouling tendency, etc. However, flow velocities above a critical value can produce vibration problems, which cause the material erosion or even fatigue failure due to damage in tubes, baffles supports and tube-to-tubesheet joints.

A vibration analysis is performed for all heat exchangers using the method proposed by ESDU [40]. This method consists, in a first step, on finding the natural frequency of the tubes, which basically depends of the span length, the second moment of area of the tube and the densities of the shell and tube fluids. On second step, the critical velocity is calculated for a given tube layout.

3.4.5. Estimating Cost Models

In general, the optimization of heat exchanger networks is considered as an isolated system. However, the operation of the SG in a SPTP affects the performance of the whole system. Therefore, it is convenient to evaluate the economic influence of each system.

The costs considered to evaluate SG are, on the one hand, the capital cost of the heat exchangers, the hot pump and the tank size of the TES system. On the other

hand, the operational pump cost of the SG and the receiver. In addition, it is also considered the start-up energy cost. Finally, the total annualized cost (TAC) can be defined as:

$$TAC_1 = frc\ C_{capital} + C_{operation} \tag{3.4}$$

$$C_{capital} = C_{Hx} + C_{Pump} + C_{Tank} \tag{3.5}$$

$$C_{operation} = C_{pumping,REC} + C_{pumping,SG} + C_{start,SG} \tag{3.6}$$

The capital return factor (frc) is calculated considering an interest of 8%, a plant lifetime of 25 years and an annual insurance cost of 1%. The capital cost of the heat exchangers were estimated using the Purohit method [17]. This method takes into account many constructive parameters of the heat exchangers: front/shell and rear TEMA types, heat transfer area, tube layout, tube and shell side pressure, etc. Even cost factors for a wide variety of tube, shell, channel and tubesheet materials are also considered. However, the U-shell type cost factor is not available in this method. For this reason, an extrapolation is made according to the cost data from Foster Wheeler [1]. Since this method was developed in 1982, the heat exchanger costs must be escalated to the present value. According to Vengateson [41], the Chemical Engineering Plant Cost index can be applied for heat exchangers. The steam drum cost is calculated according Seider et al. [42].

The capital cost of the molten-salt pumps and tanks is estimated following the data provided by Kelly and Kearney [43]. The tank size can be calculated considering the storage hours and the molten-salt mass flow rate for the SG at nominal conditions. The costs of the molten-salt pumps, hot and cold, cost are calculated as a function of their required electrical power. The operational pump cost of the SG and the receiver is calculated using the Equation 3.7. The pump efficiency (η_{pump}) is considered to be 70%. The energy electricity cost (C_{power}) is assumed as 0.13 €/kWhe. Since the annual operating time of the SG ($H_{y,SG}$) is not known, it can be estimated by means of the solar plant capacity factor, obtaining 4550 hours.

$$C_{pumping,i} = C_{power} \frac{H_{y,i}}{\eta_{pump}} \left(\frac{\dot{m}_i \Delta P_i}{\rho_i} \right) \tag{3.7}$$

The annual operating time of the receiver ($H_{y,REC}$) is estimated using System Advisor Model (SAM) [16], obtaining 2970 hours. For simplification, it is assumed

that the receiver operates at nominal conditions with an equivalent annual operating time of 2160 hours. The pressure drop in the receiver is estimated using the receiver modeling proposed by Rodríguez-Sánchez et al. [44].

The start-up energy is calculated using Equation 3.8. According to Foster Wheeler [1], the number of hot start-ups (N_{hot}) and warm start-ups (N_{warm}) are 300 and 10, respectively; the proposed cold-down rates of each heat exchanger are also used.

$$C_{start,SG} = C_{power}\left[\sum_{j=1}^{M} V_j \rho_j (N_{hot}\Delta i_{j,hot} + N_{warm}\Delta i_{j,warm}) + W_{htx} Cp_w (N_{hot}\Delta T_{hot} + N_{warm}\Delta T_{warm})\right]\eta_{PE} \quad (3.8)$$

3.4.6. Heat exchanger Optimization using genetic algorithms

Due to the high number of variables and constraints that involve the heat exchanger design, an optimization algorithm is employed to obtain a feasible and an economical design. Genetic algorithms are widely used because of their advantages, which are a relatively easy implementation and low computational cost. Moreover, the possibility of adding constraints and discrete and continuous variables makes these algorithms very attractive for the heat exchanger design. Further details of the GAs performance can be found in [11,45]. Here, the objective function is a combination of TAC and the penalty function, which are shown in Equations 3.9 and 3.10. The penalty function, Equation 3.11, is defined according to Ponce et al. [46] to improve the performance of the algorithm. The main parameters for the GA implementation are the population size of 300 individuals, the crossover fraction of 0.8 and the mutation rate of 0.1. The maximum number of generations and the stall generation limit are set to 200 and 50, respectively. The search variables selected for the heat exchanger design are presented in Table 3.3.

Table 3.3: Search variables selected for the heat exchanger design.

Variable	Single-phase heat exchanger	Evaporator
x_1	Shell diameter	Shell diameter
x_2	Tube diameter	Tube diameter
x_3	Tube layout (triangular, square or rotated square)	Tube layout (triangular, square or rotated square)
x_4	Tube pitch	Tube pitch
x_5	Number of shells	Number of shells
x_6	Shell-side velocity	Shell-side velocity
x_7	Tube-side velocity	Tube-side velocity
x_8	Baffle cut	Baffle cut
x_9	Segmental baffle (single or double)	Circulation ratio

$$TAC_2 = frc\ C_{Hx} + C_{pumping,Hx} \tag{3.9}$$

$$fitness(\mathbf{x}) = TAC_2(\mathbf{x}) + penalty(\mathbf{x}) \tag{3.10}$$

$$penalty(\mathbf{x}) = \begin{cases} 0 & if\ \mathbf{x}\ is\ feasible \\ \sum_{i=1}^{N} pc_i\ y_i^2(\mathbf{x}) & otherwise \end{cases} \tag{3.11}$$

3.5. Optimization

3.5.1. Optimization of the approach point of the SG

In this Chapter, an economic analysis is performed to compare the use of a steaming preheater and a non-steaming preheater. On the one hand, non-steaming preheaters show high approach point values that increase the log mean temperature, and therefore, the heat transfer areas and associated capital costs decrease. In addition, lower quality materials can be used. On the other hand, the heat transfer area of the evaporator increases since more steam must be generated to compensate the subcooled water temperature difference inlet at the steam drum.

In order to calculate the steaming conditions in the preheater, a finite difference scheme is performed using a tube length step of 0.1 m. The heat flux, the velocity and pressure are calculated at local conditions. Then, the Equation 3.3 is used to check if the steaming condition is achieved. If the steaming condition is achieved at any point of the preheater, a steaming preheater is selected; otherwise a non-steaming preheater is selected.

3.5.2. Results of the approach point optimization

The results of the approach point temperature difference analysis are shown in Figure 3.10. A conventional salt temperature difference between inlet and outlet of the SG was selected (565 and 290 ºC, respectively) for this analysis. This means that the pinch point temperature difference is around 6.5 ºC for an approach point of 0 ºC. The results show that the steaming condition should not be achieved for approach points greater than 2.5 ºC. The abrupt change in the TAC is due to the higher cost materials used in the steaming preheater, which has been designed considering the same materials that has been used in the evaporator, Table 3.2. Furthermore, TAC shows a high growth rate for large approach point temperature differences. This means that

the cost reduction due to the preheater area decrease does not compensate the cost increase in the evaporator using larger approach points.

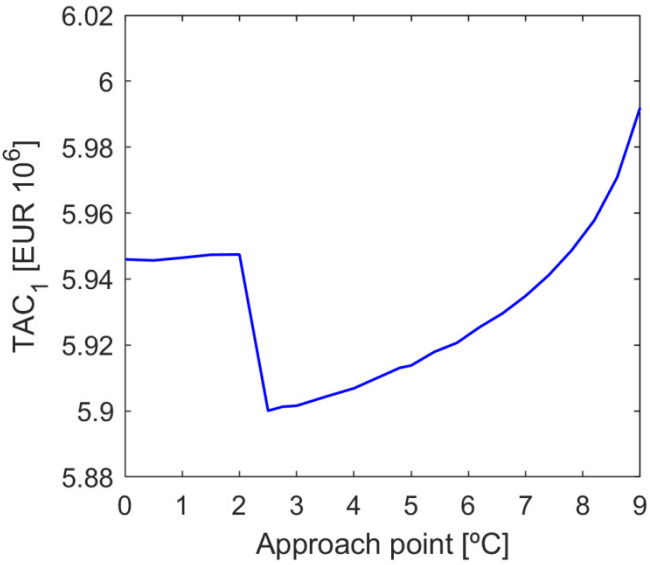

Figure 3.10: Total annualized cost against approach point**.**

Regarding a different salt outlet temperature while keeping constant the inlet salt temperature to 565 ºC, different pinch points will be obtained, Figure 3.4. Figure 3.11 shows the minimum approach points for different pinch points at which the steaming conditions are not achieved, and then, non-steaming preheaters can be used. As can be seen in Figure 3.11, the approach point increases with the pinch point. Large values of the pinch point reduce the heat transfer area needed due to the increase of the heat flux, and thus, the subcooled temperature difference increases too, Equation 3.3

3.5.3. Optimization of the pinch point of the SG

The pinch point optimization is a typical methodology used to evaluate the performance in systems such as HRSGs and heat exchanger networks (HENs) [47,48]. In this Chapter, this methodology is used but a different approach is proposed for the SG design of SPTPs.

The pinch point is defined as the temperature difference between the inlet water evaporator temperature and the outlet salt evaporator temperature. The pinch point temperature difference has a high impact on the heat transfer areas of the SG, especially in the evaporator and the preheater. The pinch point also determines the

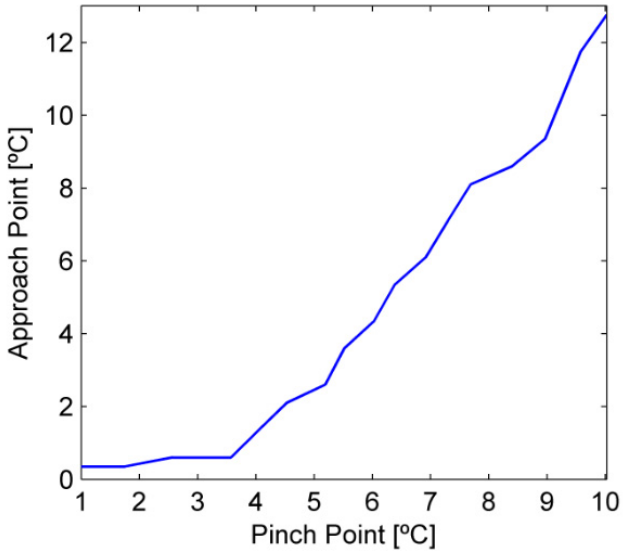

Figure 3.11: Approach point against pinch point.

salt mass flow rate and the outlet salt temperature of the SG. Then, low pinch point values may lead to large heat transfer areas, and therefore, high capital costs of the heat exchangers. Moreover, large heat transfer areas may also cause a high start-up energy consumption.

On the other hand, high pinch point values may increase the operational pump costs since high mass flow rate must circulate. This is very important because it affects: i) the SG pump energy consumption, ii) the receiver pump energy consumption, and iii) the storage tank size and its capital costs associated.

In this way, a trade-off between the mentioned costs may be obtained for a pinch point value that minimizes TAC. Figure 3.12 shows a schematic of the evolution of the mentioned costs against the pinch point.

3.5.4. Global optimization procedure

The high number of possible combinations of the design variables of the four heat exchangers optimized simultaneously leads to a huge computational cost for the global optimization (around 10^{24} possible combinations). Therefore, an alternative method is proposed to reduce the number of the design variables and the computational cost. The salt-side velocity has a very important effect in the total cost for different reasons. On the one hand, the thermal conductivity of the molten salt is lower than the water/steam. On the other hand, the shell-side velocities are normally

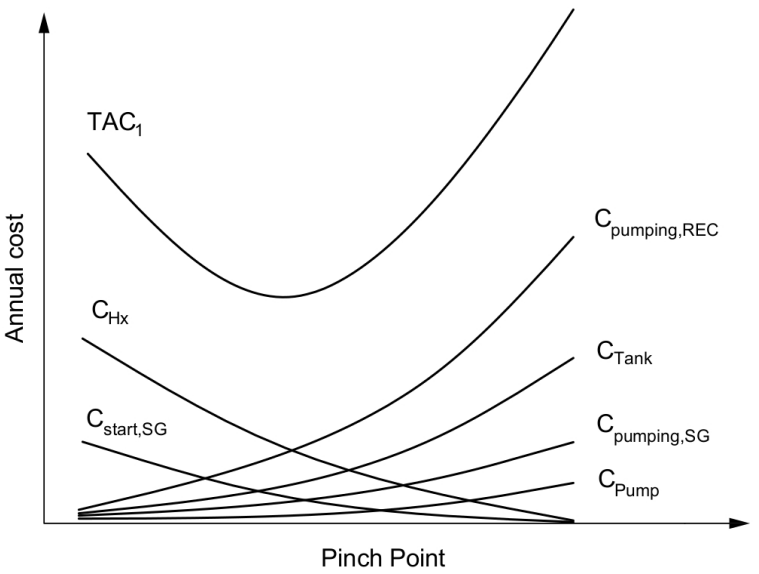

Figure 3.12: Evolution of different costs against the pinch point.

lower than in the tube-side. Therefore, the overall heat transfer coefficient is dominated by the heat transfer on the salt side. This means that a high salt-side velocity reduces the heat transfer area, and then, decreases the capital cost. However, a high salt-side velocity increases the pressure drop and the associated operational costs. For these reasons, the salt-side velocity is selected as the main global design variable.

Bearing in mind that the heat exchanger optimization is made in a first step individually, this means that the GA minimizes TAC without considering the cost of other heat exchangers. In the second step, the whole system is considered in the global optimization algorithm. This algorithm can increase the salt-side velocity in the heat exchangers with higher capital costs (combination of the cost associated to the heat transfer area, material, shell type, …) or operate in the opposite form, changing the operating conditions of the cheapest heat exchangers. Then, the SH, RH, EV and PH are optimized simultaneously by means of TAC_1, where the design variables are only the shell side velocities of each heat exchanger. A simplified scheme of the optimization algorithm is shown in Figure 3.13.

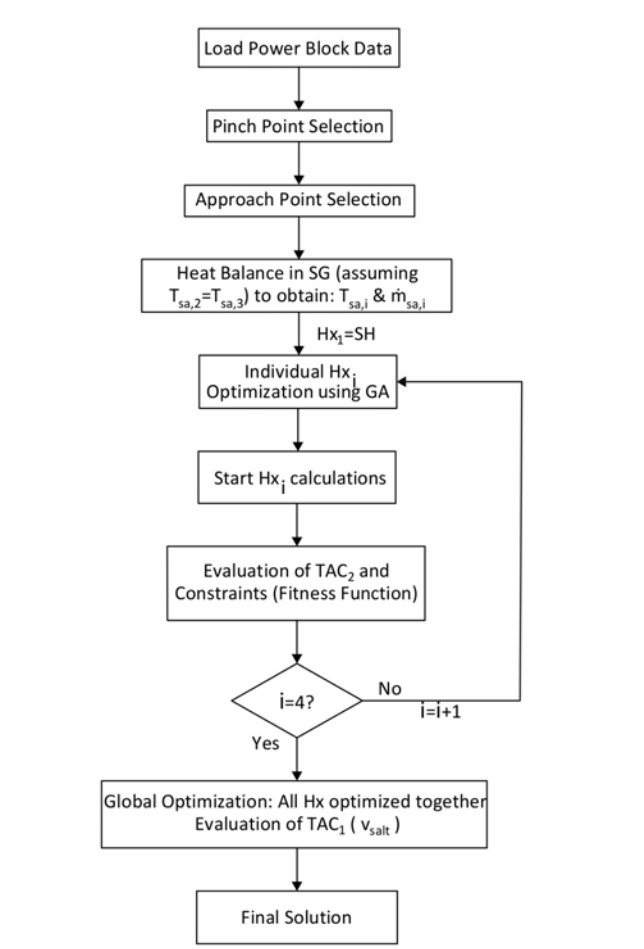

Figure 3.13: Schematic of the optimization algorithm.

3.5.5. Results of the pinch point optimization

In commercial solar power plants the SG is divided in two parallel trains [49,50]. This practice may reduce the stop time of the plant due to the potential failure risk of the SG. Although, initially it is not clear the advantages of a SG with two parallel trains, in this Chapter a cost analysis is carried out for two different SG layouts: i) with only one train; ii) with two trains in parallel. A schematic of the SG layout with two trains is shown in Figure 3.14. Each train is formed by superheater, reheater, evaporator and preheater.

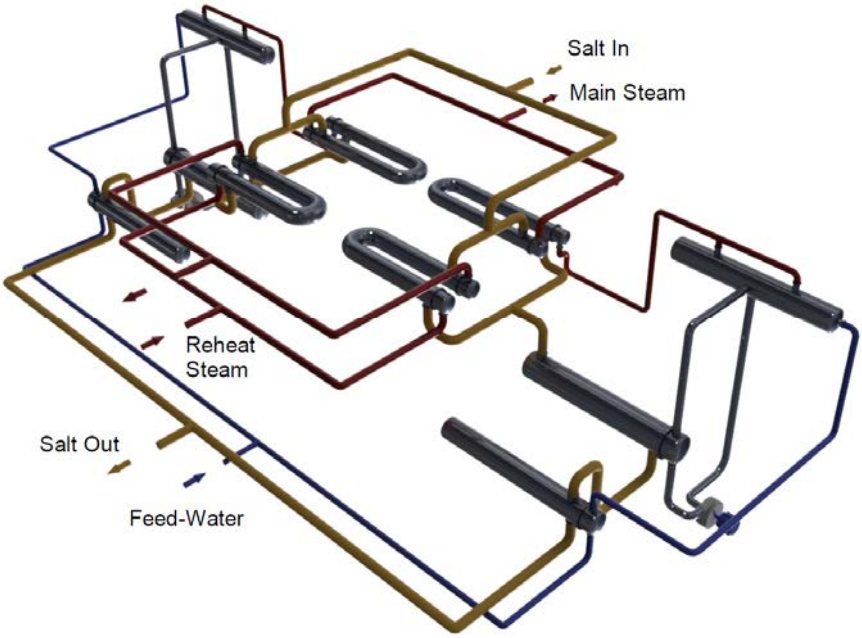

Figure 3.14: SG layout with two trains in parallel**.**

The pinch point optimization results for both SG layouts are illustrated Figure 3.15. It can be seen that the minimum values of TAC corresponds to the optimum pinch points, which are 2.6 ºC and 3 ºC for the SG layouts with one and two trains, respectively. The SG with two trains has a higher TAC than the SG with one train due to the greater number of units used, i.e., heat exchangers, drums and pumps.

The optimal pinch points obtained are lower than the values suggested by the manufacturers, which range from 4.5 to 10 ºC [2]. This result can be explained due to the consideration in our model of the receiver pump operating costs, which are quite high. The results show that the optimal pinch points produces substantial savings compared to a value of 10 ºC (around 0.4 M€/year). In terms of temperature, a pinch point of 2.6 ºC causes a SG salt outlet temperature of 286 ºC, whereas a pinch point of 3 ºC produces a salt outlet temperature of 286.5 ºC.

3.5.6. SG proposed design

The proposed designs of heat exchangers for the SG layouts with one and two trains are presented in Tables 3.4 and 3.5, respectively. These results are based on the pinch point optimization presented before. Several design parameters are included in

the heat exchanger calculations. Also, the steam drum data of each SG layout is shown in Table 3.6.

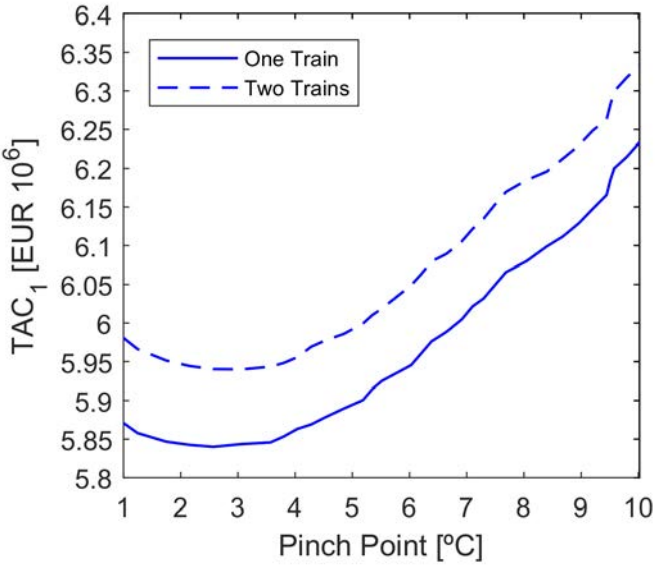

Figure 3.15: Total annualized cost against pinch point.

The results show that the SG with one train has lower capital cost than with two trains. Moreover, the start-up energy cost is around 50% lower for the SG with one train. This seems logical since the SG with two trains a larger mass of metal and fluid to be warmed-up. The SG pump operating costs are practically the same for both SG layouts.

Table 3.4 shows that higher thicknesses are obtained in shells and tubesheets for the SG layout with one train. Since SPTPs are subjected to daily start-ups, it is expected that the SG layout with two trains shows a better behavior against thermal stresses. Furthermore, this may lead to lower start-up times when using only one of the two parallel trains due to its lower thermal inertia compared to the SG with one train. This feature might be interesting to increase the plant operability.

Table 3.4: Proposed design of the heat exchangers for the SG layout with one train.

Parameter	Superheater	Reheater	Evaporator	Preheater
Shell diameter, (mm)	884	1010	1796	1600
Baffle cut, (%)	28	22	23	24

Baffle spacing, (mm)	612	317	569	658
Tubes ext. diameter, (mm)	15.9	25.4	15.9	15.9
Tubes int. diameter, (mm)	12.2	21.2	12.2	12.2
Tube pitch, (mm)	20.7	31.8	20.7	23.9
Tube layout, (º)	45	30	90	45
Tube passes, (-)	1	1	2	2
Tubes number, (-)	1219	815	2737-U	1615-U
Tube length, (m)	20.81	22.09	9.43	11.04
Shell thickness, (mm)	12.7	12.7	15.9	15.9
Tubesheet thickness, (mm)	254	193	400	312
U-tube minimal radius, (mm)	395	713	42	48
Mass flow (tube-side), (kg/s)	86.92	78.70	567.13	86.92
Mass flow (shell-side)), (kg/s)	390.44	183.30	573.75	573.75
Flow velocity (tube-side), (m/s)	13.21	23.96	2.53	0.61
Flow velocity (shell-side), (m/s)	0.65	0.50	0.60	0.70
Convective heat transfer coefficient (tube-side), (W/m2 ºC)	3649	1227	27688	6598
Convective heat transfer coefficient (shell-side), (W/m2 ºC)	5213	3656	4200	4234
Fouling resistance (tube-side), (ºC m2/W)	8.825e-5	8.825e-5	2.647e-04	8.825e-5
Fouling resistance (shell-side), (ºC m2/W)	8.825e-5	8.825e-5	8.825e-5	8.825e-5
Overall heat transfer coefficient, (W/m2 ºC)	1241	664	1295	1448
Heat exchange area (per shell), (m2)	1133	1294	2597	1857
Pressure drop (shell-side), (kPa)	148	149	172	205
Pressure drop (tube-side), (kPa)	105	70	122	13
Shell type	U-shell	U-shell	TEMA E	TEMA F
Baffle type	double-segmental	double-segmental	single-segmental	double-segmental
Total number of shells, (-)	1	1	1	1
Heat exchanger cost, (k €)	1019	1267	1437	568

Table 3.5: Proposed design of the heat exchangers for the SG layout with two train.

Parameter	Superheater	Reheater	Evaporator	Preheater
Shell diameter, (mm)	600	731	1169	1066
Baffle cut, (%)	28	22	28	26
Baffle spacing, (mm)	443	228	470	515
Tubes ext. diameter, (mm)	12.7	25.4	15.9	12.7
Tubes int. diameter, (mm)	9.4	21.2	12.2	9.4
Tube pitch, (mm)	19.0	31.8	19.9	19
Tube layout, (º)	30	30	30	45
Tube passes, (-)	1	1	2	2
Tubes number, (-)	731	412	1396-U	1088-U
Tube length, (m)	20.19	22.35	9.32	9.71
Shell thickness, (mm)	9.5	12.7	12.7	15.9
Tubesheet thickness, (mm)	146	134	271	207
U-tube minimal radius, (mm)	441	849	40	38
Mass flow (tube-side), (kg/s)	43.46	39.35	305.37	43.46
Mass flow (shell-side)), (kg/s)	195.22	91.65	286.87	286.87

Flow velocity (tube-side), (m/s)	18.70	23.70	2.68	0.76
Flow velocity (shell-side), (m/s)	0.47	0.44	0.50	0.66
Convective heat transfer coefficient (tube-side), (W/m2 ºC)	5088	1216	28370	8368
Convective heat transfer coefficient (shell-side), (W/m2 ºC)	4499	3324	3716	4382
Fouling resistance (tube-side), (ºC m2/W)	8.825e-5	8.825e-5	2.647e-04	8.825e-5
Fouling resistance (shell-side), (ºC m2/W)	8.825e-5	8.825e-5	8.825e-5	8.825e-5
Overall heat transfer coefficient, (W/m2 ºC)	1341	648	1247	1544
Heat exchange area (per shell), (m2)	524	662	1347	871
Pressure drop (shell-side), (kPa)	146	149	119	199
Pressure drop (tube-side), (kPa)	253	70	133	18
Shell type	U-shell	U-shell	TEMA E	TEMA F
Baffle type	double-segmental	double-segmental	single-segmental	double-segmental
Total number of shells, (-)	2	2	2	2
Heat exchanger cost, (k €)	1355	1886	1534	509

Table 3.6: Proposed design of the steam drums.

Parameter	One Train	Two Trains
Drum cost, (k€)	201	193
Drum diameter, (mm)	1799	1272
Drum wall thickness, (mm)	111	79.4
Drum length (m)	9.00	6.36
Number of drums, (-)	1	2
Riser diameter, (mm)	150	147
Riser wall thickness, (mm)	6.4	6.4
Number of risers (per drum), (-)	24	13
Downcomers diameter, (mm)	428	445
Downcomers wall thickness, (mm)	6.4	6.4
Number of downcomers (per drum), (-)	2	1

3.6. Conclusions

In this Chapter, the design of the heat exchangers of the steam generator for a 110MWe solar power tower plant is presented. A methodology to optimize the evaporator pinch point temperature difference is proposed considering several costs associated with the performance of the whole system.

An optimization method based on genetic algorithms is also proposed to find economic and feasible heat exchanger designs. This is made following TEMA standards, ASME Pressure Vessel code and the good practice recommendations of several references. A thorough mechanical design is performed considering thermal

stresses on tubesheets and U-bends. Furthermore, a vibration analysis is carried out to assure the safe operation.

The cost analysis shows lower annual costs (capital and operation) for the forced circulation evaporator comparing to the natural circulation design. The forced circulation evaporator is also preferred because this design may lead to shorter start-up times. An approach point temperature difference analysis is carried out in order to avoid subcooled flow boiling in the preheater. Then, lower cost materials could be used in the preheater reducing in this way the capital cost.

The final steam generator design consists of: U-shell design for superheater and reheater, TEMA E shell for evaporator and TEMA F shell for preheater. The TEMA E shell in the evaporator provides a good solution to reduce the thermal stresses in tubesheet and U-tube. Two steam generator layouts are studied: with one or two trains of heat exchangers. The results show that the global optimum of the evaporator pinch points are 2.6 ºC and 3ºC for the steam generator with one and two trains, respectively, while their respective capital cost are 4.3 M€ and 5.3 M€.

Nomenclature

Abbreviations

B & W : Babcock and Wilcox.
CT : cold tank.
CSP : concentrating solar plants.
ESDU : engineering science data unit.
EV : evaporator.
FW : feed water.
GA : genetic algorithm.
HEN : heat exchanger network.
HP: high pressure.
HPT : high pressure turbine.
HRSG : heat recovery steam generator.
HTF : heat transfer fluid.
HT : hot tank.
Hx : heat exchanger.
LP : low pressure.
LPT : low pressure turbine.

$MSEE$: molten salt electric experiment.
OSV : onset of significant voids.
PH : preheater.
REC : receiver.
RH : reheater.
SAM : system advisor model.
SG : steam generator.
SH : superheater.
$SPTP$: solar power tower plant.
TAC : total annualized cost (€/year).
TES : thermal energy storage.

Symbols

A : heat transfer area (m^2).
B_c : baffle cut (-).
C : cost (€).
Cp : specific heat capacity (J/kg ºC).
D : diameter (m).
H_y : annual plant operation time (h/year).
K : resistance coefficient (-).
L : length (m).
L_{bc} : baffle spacing (m).
L_{tp} : tube pitch (mm).
N_b : number of baffles (-).
N_{hot} : number of hot starts.
N_{warm} : number of warm starts.
N_{tp} : number of tube passes (-).
N_{tt} : number of tubes (-).
N_s : number of shells (-).
P : pressure (Pa).
Q : heat (W).
R : fouling resistance (ºC m^2/W).
$R_{\min}$: U-tube minimal radius (mm).

S : stream flow area (m^2).
T : temperature (ºC).
U : global heat transfer coefficient (W/m^2 ºC).
W : weight (kg).
h : convective coefficient (W/m^2 ºC) or .
i : specific enthalpy (J/kg).
l_{ts} : tubesheet thickness (mm).
$\dot{m}$: mass flow rate (kg/s).
pc : penalty coefficient (-).
q_w : local heat flux (W/m^2).
t_s : shell thickness (m).
v : velocity (m/s).
$\mathbf{x}$: vector of optimization variables (-).
$\mathbf{y}$: vector of feasible constraints (-).

Greek Symbols

ΔS_{h-c} : hot and cold leg overhand difference (mm).
η : efficiency (-).
θ_{tp} : tube layout (º).
ρ : density (kg/m^3).
ϕ_v : viscosity correction factor (-).

Subscripts

dc : downcomer.
r : riser.
s : shell.
sa : salt.
sat : saturated.
sub : subcooled.
t : tube.
ti : inside of tube.
w : window zone
x : cross-flow zone.

3.7. References

[1] Sandia Natl. Lab., Molten Salt Receiver Subsystem Research Experiment Phase 1 - Final Report, Volume 1. Foster Wheeler Solar Development Corporation, Sandia Natl. Lab. Report SAND82-8179, (1984).

[2] Sandia .Natl. Lab., Betchel. Corporation, Investigation of Thermal Storage and Steam Generator Issues, Sandia Natl. Lab. Report SAND 93-7084, (1993).

[3] J.E. Pacheco, Final Test and Evaluation Results from the Solar Two Project, Sandia Natl. Lab. Report, SAND2002-0120, (2002).

[4] W. a. Allman, D.C. Smith, C.R. Kakarala, The Design and Testing of a Molten Salt Steam Generator for Solar Application, J. Sol. Energy Eng. 110 (1988) 38–44. doi:10.1115/1.3268235.

[5] A.B. Zavoico, Solar Power Tower - Design Basis Document, Sandia Natl. Lab. Report, SAND2001-2100, (2001).

[6] B. Kelly, Lessons Learned, Project History, and Operating Experience of the Solar Two Project, Sandia Natl. Lab. Report SAND2000-2598, 1 (2000).

[7] R. Moore, M. Vernon, C.K. Ho, N.P. Siegel, G.J. Kolb, Design considerations for concentrating solar power tower systems employing molten salt, Sandia Natl. Lab. Report, SAND2010-6978, (2010).

[8] G.J. Kolb, An Evaluation of Possible Next-Generation High-Temperature Molten-Salt Power Towers, Sandia Natl. Lab. Report, SAND2011-9320, (2011).

[9] B. Kelly, Advanced Thermal Energy Storage for Central Receivers with supercritical coolants, Abengoa Solar Inc., (2010).

[10] A.C. Caputo, P.M. Pelagagge, P. Salini, Heat exchanger design based on economic optimisation, Appl. Therm. Eng. 28 (2008) 1151–1159. doi:10.1016/j.applthermaleng.2007.08.010.

[11] H. Sadeghzadeh, M.A. Ehyaei, M.A. Rosen, Techno-economic optimization of a shell and tube heat exchanger by genetic and particle swarm algorithms, Energy Convers. Manag. 93 (2015) 84–91. doi:10.1016/j.enconman.2015.01.007.

[12] H. Hajabdollahi, P. Ahmadi, I. Dincer, Thermoeconomic optimization of a shell and tube condenser using both genetic algorithm and particle swarm, Int. J. Refrig. 34 (2011) 1066–1076. doi:10.1016/j.ijrefrig.2011.02.014.

[13] P.A. González-Gómez, F. Petrakopoulou, J.V. Briongos, D. Santana, Cost-based design optimization of the heat exchangers in a parabolic trough power plant, Energy. 123 (2017) 314–325.

[14] National Renewable Energy Laboratory (NREL), (2016). http://www.nrel.gov/csp/solarpaces/by_project.cfm.

[15] W.J. Garland, B.J. Hand, Simple Functions for the Fast Approximation of Light Water Thermodynamic Properties, Nucl. Eng. Des. 113 (1989) 21--34. doi:http://dx.doi.org/10.1016/0029-5493(89)90293-8.

[16] National Renewable Energy Laboratory (NREL), Solar Advisor Model Reference Manual for CSP Trough Systems, (2009).

[17] G.P. Purohit, Estimating costs of shell-and-tube heat exchangers, Chem. Eng. (1983) 56–67.

[18] A. Pasha, Gas Turbine Heat Recovery Steam Generators for Combined Cycles Natural or Forced Circulation Considerations, ASME 1988 International Gas Turbine and Aeroengine Congress and Exposition, Volume 4: Heat Transfer; Electric Power; Industrial and Cogeneration, , (1988).

[19] V. Ganapathy, Understanding Boiler Circulation, Chem. Eng. (2013) 52–56.

[20] J.W. Palen, Shell and Tube Reboilers. In Heat Exchanger Design Handbook, Hemisph. Publ. Corp. (1983).

[21] W. Francis, M.C. Peters, Fuels and Fuel Technology, Reg. Oceanogr. (1980).

[22] V. Ganapathy, Heat-recovery steam generators: Understand the basics, Chem. Eng. Prog. 92 (1996) 32–45.

[23] V. Ganapathy, Steam Generators and Waste Heat Boilers: For Process and Plant Engineers, (2015).

[24] R.W. Serth, T.G. Lestina, Process Heat Transfer: Principles, Applications and Rules, (2014).

[25] ESDU, Engineering Science Data Unit (ESDU), Baffled Shell-and-Tube Heat Exchangers: Flow Distribution, Pressure Drop and Heat Transfer Coefficient on the Shellside, Item No. 83038, (1984).

[26] R. Shah, D. Sekulic, Fundamentals of Heat Exchangers Design, John Wiley & Sons Inc., (2003).

[27] K.P. Singh, M. Holtz, A Method to Design Shell-Side Pressure Drop Constrained Tubular Heat Exchangers, Eng. Power. (1977) 441–448.

[28] W.H. Emerson, Shell-side pressure drop and heat transfer with turbulent flow in segmentally baffled shell-and-tube heat exchangers, Int. J. Heat Mass Transf. 6 (1963) 649–668. doi:10.1016/0017-9310(63)90037-1.

[29] J.C. Chen, Correlation for boiling heat transfer to saturated fluids in convective flow, Ind. Eng. Chem. Process Des. Dev. 5 (1966) 322–329. doi:10.1021/i260019a023.

[30] J.G. Collier, J.R. Thome, Convective Boiling and Condensation, Clarendon Press, (1994).

[31] Y.L. Wong, D.C. Groeneveld, S.C. Cheng, Chf prediction for horizontal tubes, Int. J. Multiph. Flow. 16 (1990) 123–138. doi:10.1016/0301-9322(90)90043-I.

[32] G.R. Warrier, V.K. Dhir, Heat Transfer and Wall Heat Flux Partitioning During Subcooled Flow Nucleate Boiling--A Review, J. Heat Transfer. 128 (2006) 1. doi:10.1115/1.2349510.

[33] I.S. Hussaini, S.M. Zubair, M.A. Antar, Area allocation in multi-zone feedwater heaters, Energy Convers. Manag. 48 (2007) 568–575. doi:10.1016/j.enconman.2006.06.003.

[34] TEMA Report, Standards of the Tubular Exchangers Manufacturers Association, (2007).

[35] American Society of Mechanical Engineers. ASME boiler and pressure vessel code, Section VIII, (2010).

[36] W.J. O'Donnell, B.F. Langer, Design of perforated plates, J. Eng. Ind. 84 (1962) 307–319. doi:10.1115/1.3667483.

[37] J. Busuttil, Detailed stress analysis of SM-1 steam generator tube sheet, ALCO Products Inc., (1962).

[38] K.P. Singh, M. Holtz, On Thermal Expansion Induced Stresses in in U-Bends of Shell-and- Tube Heat Exchangers, Eng. Power. 101 (1979) 634–639.

[39] J. Taborek, Shell and Tube Heat Exchangers: single phase flow. In Heat Exchanger Design Handbook, Hemisph. Publ. Corp. (1983).

[40] ESDU, Engineering Science Data Unit (ESDU), Flow induced vibration in tube bundles with particular reference to shell and tube heat exchangers, Item No. 87019, (1987).

[41] U. Vengateson, Design of multiple shell and tube heat exchangers in series: E shell and F shell, Chem. Eng. Res. Des. 88 (2010) 725–736. doi:10.1016/j.cherd.2009.10.005.

[42] W.D. Seider, J.D. Seader, D.R. Lewin, S. Widagdo, Product and process design principles: synthesis, analysis, and evaluation, (2010).

[43] B. Kelly, D. Kearney, Thermal Storage Commercial Plant Design Study for a 2-Tank Indirect Molten Salt System Final Report, (2006).

[44] M.R. Rodriguez-Sanchez, A. Sanchez-Gonzalez, C. Marugan-Cruz, D. Santana, Saving assessment using the PERS in solar power towers, Energy Convers. Manag. 87 (2014) 810–819. doi:10.1016/j.enconman.2014.07.076.

[45] J. Yang, A. Fan, W. Liu, A.M. Jacobi, S.-R.R. Oh, W. Liu, Optimization of shell-and-tube heat exchangers conforming to TEMA standards with designs motivated by constructal theory, Energy Convers. Manag. 77 (2014) 468–476. doi:10.1016/j.ijheatmasstransfer.2014.06.046.

[46] J.M. Ponce-Ortega, M. Serna-González, A. Jiménez-Gutiérrez, Use of genetic algorithms for the optimal design of shell-and-tube heat exchangers, Appl. Therm. Eng. 29 (2009) 203–209. doi:10.1016/j.applthermaleng.2007.06.040.

[47] M. Ghazi, P. Ahmadi, A.F. Sotoodeh, A. Taherkhani, Modeling and thermo-economic optimization of heat recovery heat exchangers using a multimodal genetic algorithm, Energy Convers. Manag. 58 (2012) 149–156. doi:10.1016/j.enconman.2012.01.008.

[48] M. Čehil, S. Katulić, D.R. Schneider, Novel method for determining optimal heat-exchanger layout for heat recovery steam generators, Energy Convers. Manag. (2017). doi:10.1016/j.enconman.2017.03.033.

[49] Energetica Int., Lebrija 1 : International solar thermal reference, (2012).

[50] C. A. D. Andalucía, 43.321/05. Solicitud de aprobación del proyecto de ejecución, y declaración en concreto de la utilidad pública del proyecto Andasol-1, (2005).

CHAPTER

FOUR

Steam generator daily start-up for solar power tower plants

Contents

4.1. Abstract 88

4.2. Introduction 88

4.3. System description 90

4.3.1. Turbine operation modes 92

4.3.2. Control system 92

4.3.3. Start-up initial conditions 94

4.4. Modeling and validation 96

4.4.1. Single phase flow heat exchangers 96

4.4.2. Two phase flow model for evaporator and steam drum 98

4.4.3. Stresses on steam drum and SH header 100

4.4.4. Stresses on tubesheet 101

4.4.5. Stresses on U-tubes 108

4.5. Results 109

4.5.1. Feedwater temperature 110

4.5.2. Daily start-up with non-isothermal initial conditions 111

4.5.3. Daily start-up with isothermal initial conditions 114

4.6. Conclusions 118

4.7. References 123

4.1. Abstract

In solar power tower plants, high operating temperatures of the working fluids are combined with daily start-ups and shutdowns. An important challenge for concentrating solar plants comes from the increasing of the flexibility by means of faster start-up and/or load changes. These operating conditions may lead to high stress in thick-walled components and may also lead to eventual material failure. For these reasons, a dynamic analysis is mandatory to assure the life-time of the steam generator.

In this Chapter, different transient models are developed to analyze the dynamic behavior of a steam generator based on conventional shell and tube heat exchangers. The transient stress models are specially focused on the most critical parts of the shell and tube heat exchangers: tubesheet and tubesheet junction. Two start-up initial conditions are analyzed, obtaining the main input variables to operate the steam generator within the allowable stress limits. The first initial condition assumes a non-isothermal temperature profile of the heat exchangers at the beginning of the start-up, whereas the second initial condition assumes an isothermal temperature profile of 290 ºC. The first condition takes around 50 min to reach nominal conditions requiring 600 tons of hot salt, whereas the second condition takes around 110 min requiring 716 tons.

4.2. Introduction

Concentrating solar power (CSP) plants with thermal energy storage (TES) system enhances the possibility to participate in grid balancing services [1]. In this way, these plants may be considered as dispatchable and therefore, an improvement of the flexibility by means of fast start-ups and/or load changes may lead to additional revenues [2]. Moreover, fast start-ups are specially interesting for CSP plants due to the increase of the annual electricity production [3,4]. However, the start-up and/or load changes ramps are limited by the thermal stresses in thick-walled parts of the steam generator (SG) and/or the steam turbine. These thermal changes may produce fatigue and/or creep damage in the SG [5]. For this reason, a considerable effort should be made to develop dynamic models that consider their operational life-time of the materials. These models allow the study of different strategies to operate the plant on the safety-side while saving energy during the start-up and shutdown processes.

One of the main features of the solar power tower plants (SPTPs) is the higher operating temperatures compared to parabolic trough and linear Fresnel plants [2].

This leads to an increment in the thermal efficiency of the power block, which also reduce the specific costs. Examples of the feasibility of SPTPs technology are Gemasolar or Crescent Dunes. However, other technologies, such as fire-boilers or combined-cycle plants (CCPs), work at similar temperatures to SPTPs. The main difference between conventional and SPTPs appears in the SG. The heat exchangers of the SG are based on conventional shell and tube designs. These heat exchangers are sized by means of analytical methods proposed by TEMA standards [6] and/or ASME code Section VIII-Div1 [7] considering continuous operation at nominal conditions [8]. As in SPTPs the SG will be operated with daily start-up, load change and shutdowns, a transient stress analysis is required. Nevertheless, no specific guidelines are showed in TEMA standards [6] and/or ASME Section VIII-Div1 [7] for complex zones, such as the tubesheet, when: transients thermal loadings occur [9], temperature gradients on the junction appear [10] or the tubesheet has a non-standard design [11]. Therefore, these issues must be accomplished by finite element analysis or complex analytical methods to obtain accurate results.

Start-up and shutdown operations become critical for getting operational flexibility. Such adaptability is critical for the necessary adaptation of the power production to the grid demand. In this line CCPs has become an invaluable thermal power plant technology found in conventional power generation mix, providing both the power generation flexibility and the energy security to grid balance services. The reliability of the CCPs lies on the corresponding dynamical response of the heat recovery steam generator (HRSG) system, which exhibits remarkable operational similarities with the SGs found in SPTPs. In recent years, many efforts have been made to develop simulation models focused on the dynamic behavior of the HRSG that can be useful for the development of SGs of SPTPs. This interest is mainly motivated by the liberalization of the electricity market and the introduction of the renewable energies which are driven to the need of improving the operational flexibility of CCPs [5]. For example, Kim et al. [12] developed a HRSG model based on lumped capacitance method. A cold start-up procedure is studied to keep the thermal stress of the steam drum within the permitted limits by means of the exhaust gas turbine bypass. Mertens et al. [13] performed a transient model of HRSG using Apros software tool [14] to compare the dynamic performance of natural circulation drum-type HRSG with once-trough type HRSG. Their results show that the once-trough type achieves nominal pressure conditions slightly faster than drum-type.

Focusing on the CSP plant simulation, the dynamic behavior of the SG has been addressed in different studies. For instance, Heiko et al. [15] presented a parabolic trough CSP plant model using Dymola software tool [16]. They studied hot and warm approaches for the power-block start-up. Although, the main thermodynamic variables are shown, the technical constraints used for SG, such as stresses or

temperatures differences, are missing. Foster Wheeler [17] presented a detailed study about design and performance of molten salt SG for SPTP. Start-up and load-change procedures were described considering several initial conditions. However, in [17] a fixed pressure turbine operation is assumed for all SG operations conditions. While in the recent years sliding pressure turbine operation has been established due to different advantages in control and efficiency under part-load conditions [18]. Pacheco et al. [19] described different procedures for daily start-up and shutdown operations on the SG based on the experience of the SPTP experimental facility "Solar Two". Problems related to salt freeze in evaporator, due to the low inlet temperature in the start-up, lead to add an additional start-up feedwater to assure safe operation of the SG.

In this Chapter, the transient dynamic response of the SG of a STPT is modeled in order to analyze its start-up process. As the temperature and stresses are decoupled, the model first calculates the temperature changes in the heat exchangers and steam drum during the start-up. Then, the model computes the stress values on the critical components of the heat exchangers, such as tubesheet and tubesheet junction, in order to work below the maximum stress limit. European standard EN 12952-3 [20] is used to estimate thermal and pressure stresses on the superheater head and the steam drum. In order to adjust the dynamic response to the start-up requirements, a control loop has been designed. Two different initial conditions are analyzed for the start-up, taking 50 minutes to start-up for non-isothermal conditions and 110 min for isothermal conditions.

4.3. System description

A 110 MWe power block subcritical Rankine-cycle with regeneration is selected to model the SG system of the SPTP. The plant is composed mainly by four sub-systems: solar field, storage system, steam generator and power block. In the solar field thousands of heliostats reflect the Sun on a central receiver. The heat transfer fluid (HTF) is molten-salt, which is heated up from 290 ºC to 565 ºC in the solar tower receiver. A storage system formed by two tanks (one hot and one cold) stores and delivers the energy captured by the solar field in a controlled way. The steam generator system includes a superheater (SH), reheater (RH), evaporator (EV) and preheater (PH). The hot salt is sent to the SG where the thermal energy is transferred to produce main and reheated steam. Additionally, the SG includes, among others, feedwater pumps, hot salt pumps, the steam drum, supporting systems, etc. The heat exchanger design for the SG proposed in Chapter 3 is chosen for the dynamic

analysis [21]. The main subsystems of the SPTP are represented in Figure 4.1, it includes the main design parameters used in the start-up procedures studied.

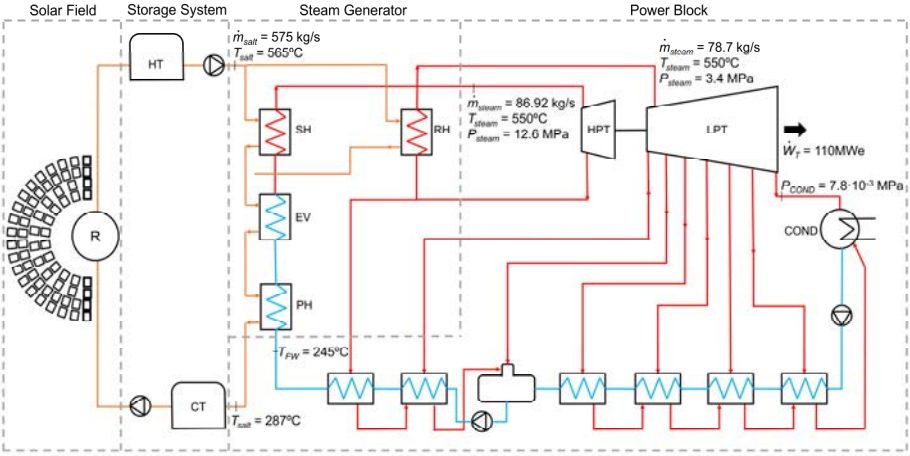

Figure 4.1: Schematic of SPTP.

In the heat exchangers of the SG, the molten salt is placed on the shell side and the steam/water flow is placed on the tube side because of the high steam/water pressure. Firstly, the PH, which consists of a U-tube/TEMA F shell heat exchanger type, heats the feedwater up to saturation conditions. The EV consists of a U-tube/TEMA E shell type where the inlet salt nozzle is put far from the tubesheet to minimize its thermal stress. A forced circulation evaporator system is chosen to increase the operability in the start-up process [22]. The steam drum is arranged horizontally to reduce the steam velocity and improve the water droplets separation through the action of chevrons. Finally, the SH and RH are counter-current U-shell/U-tube heat exchangers.

The intermittent operation of the SG of SPTPs can produce fatigue damage due to the cyclic stress. Furthermore, the high temperatures and the potential impurities of the molten salt in a industrial-grade process may lead to stress corrosion cracking damage. Therefore, the material selection is one of the most critical point to assure the reliability of the heat exchangers. Kelly [23] recommended stainless steel Gr347 or 321 for the hot salt piping according to the Solar Two operating experience. Following this recommendation, the materials selected for the SG are shown in Table 4.1.

Table 4.1: Selected Materials for the main SG components.

Component	Shell, channel and tubesheet	Tube
Preheater	A516, Gr. 70	A210, Gr. A1
Evaporator	A387, Gr. 91	A213, Gr. 347
Superheater	A240, Gr. 347	A213, Gr. 347
Reheater	A240, Gr. 347	A213, Gr. 347
Steam Drum	A516, Gr. 70	-

4.3.1. Turbine operation modes

The efficiency of thermal power plants can be increased changing form fixed to sliding pressure operation mode [18]. The main advantages of the sliding operation mode are the reduction of the power pump consumption and the efficiency increment of the SG because of the increment of the mean temperature difference in the heat exchangers. An additional benefit of the sliding operation mode is the reduction of throttling losses of the turbine, which may lead to a higher turbine power output under part load operation. However, the fixed pressure mode has the advantage of preventing the potential risk of salt freeze in the evaporator, since the minimum temperature assumed is 290 ºC, the minimum pressure is 7.4 MPa. In this Chapter, both fixed and sliding operation models are used for the start-up conditions analyzed. When the steam turbine is operated from 0% to 50% of load, a fixed pressure mode is used. From 50% to 100% load a sliding pressure mode is assumed.

The power block transient operation is modeled as series of steady-state conditions. The model provides the temperature, mass flow rate and pressure of the main inputs of the SG (the feed water and reheat inlet steam) and the turbine power output for design and part-load conditions.

4.3.2. Control system

The control system is aimed to guide a stable simulation of the SG transient response during the daily start-up operation. A schematic of the control system used during the simulations is shown in Figure 4.2. This control scheme is adapted from the control system proposed by [17] .The control valves shown in the diagram identify the flow streams that can be regulated during the start-up operation. The control system is important to solve the proposed transient models applied to the two daily start-up procedures studied. Otherwise, it would not be possible to capture the dynamic behavior of the SG system [24]. A PID control strategy has been chosen to guide the start-up process. As it is shown in Figure 4.2, excepting for the drum level, which is driven by a proportional action (P), most of the manipulated variables are

operated with proportional and integral actions (PI) in accordance with the proposed start-up scenarios. The controlled variables of the SG are the salt and steam temperatures, the steam flow rate, the steam pressure and the steam drum water level. The manipulated variables are the mass flow rate of the salt, the steam flow, the SH and the RH attemperation systems and the variable-speed salt pumps.

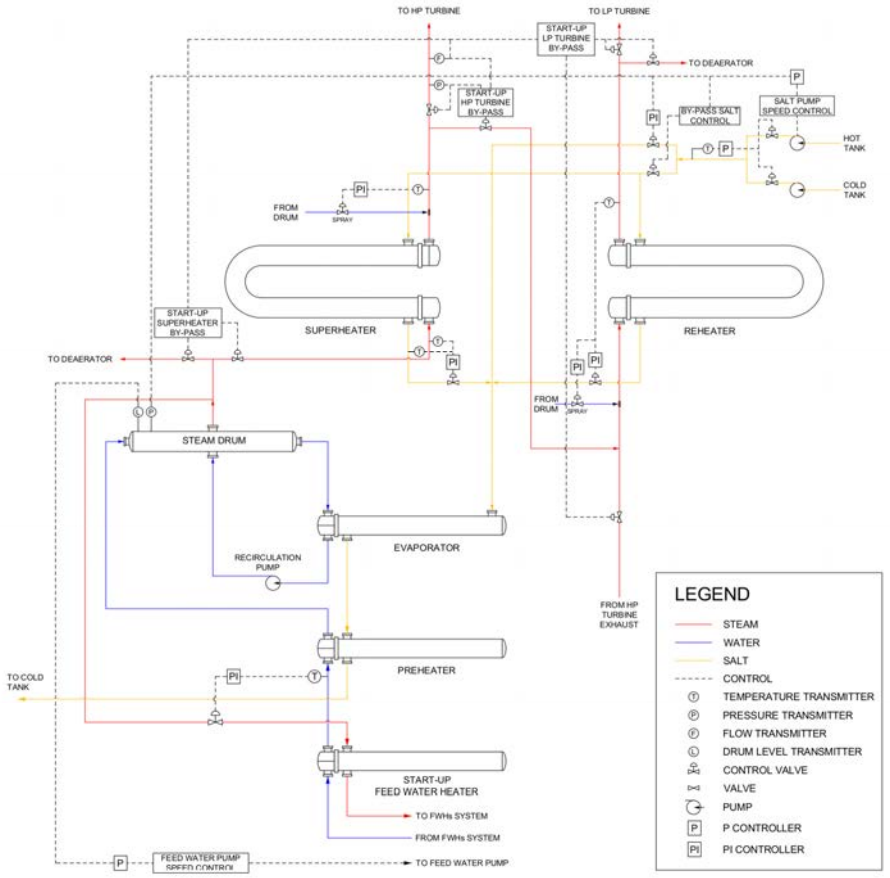

Figure 4.2: Schematic of SG and control system.

The SH and the RH attemperation systems keep constant the inlet temperatures of the high pressure (HP) and low pressure (LP) turbines against transient disturbances. This procedure reduces the fatigue damage of the HP/LP turbines. As can be seen in Figure 4.2, the SH attemperator is placed at the inlet and outlet, whereas the RH attemperator is only placed at the inlet [17]. The attemperator placed at the inlet of the heat exchangers ensures that the steam is free of water droplets and a better control of the thermal shock of the pipe walls [25]. In contrast, the attemperator placed on the

outlet of the heat exchangers provide a direct control with no time lags [26]. Furthermore, the attemperation steam flow is limited to 8% of the total flow [25].

Besides of the attemperation system, the SH and RH outlet temperature is also regulated by salt mass flow valves. The salt flow rate changes under part-load conditions, making necessary a SH-RH salt by-pass line to send the salt excess flow to the EV. This line increases the evaporator heat duty and the pressure in the steam drum, which may produce an increase in the steam flow rate if the throttle valve position does not change.

The proposed system checks the temperature difference between the salt outlet and the steam inlet in the SH and RH, controlling the salt valves. In this way, the lower tubesheet of the SH, which is a potential critical part, works in allowable stress ranges.

The steam drum pressure control depends on the turbine operation mode. For fixed pressure mode, the by-pass salt valve control sends extra salt flow rate to assure the minimal steam drum pressure. When the turbine is operating on sliding pressure mode, the steam drum pressure is automatically regulated by the saturated steam outlet. Furthermore, the steam drum level is kept into suitable ranges by means of the feedwater mass flow rate using a proportional control system.

4.3.3. Start-up initial conditions

Two initial conditions are considered for the heat exchangers of the SG at the beginning of the start-up process, which are: daily non-isothermal initial conditions [17] and daily isothermal initial conditions [19]. The salt temperature profiles of the SG are shown in Figure 4.3 for both starting procedures and for full load conditions of the plant.

- **Daily start-up with non-isothermal conditions**

The heat exchangers of the SG are closed after the night shutdown and thermally isolated to reduce the heat losses [17]. As they are filled with hot salt, each heat exchanger has different temperatures. This procedure was proposed by Foster Wheeler assuming non-isothermal initial conditions on a daily start-up [17]. The initial temperature profiles of the heat exchangers at the beginning of the daily start-up are calculated from the night shutdown condition, which corresponds to fixed

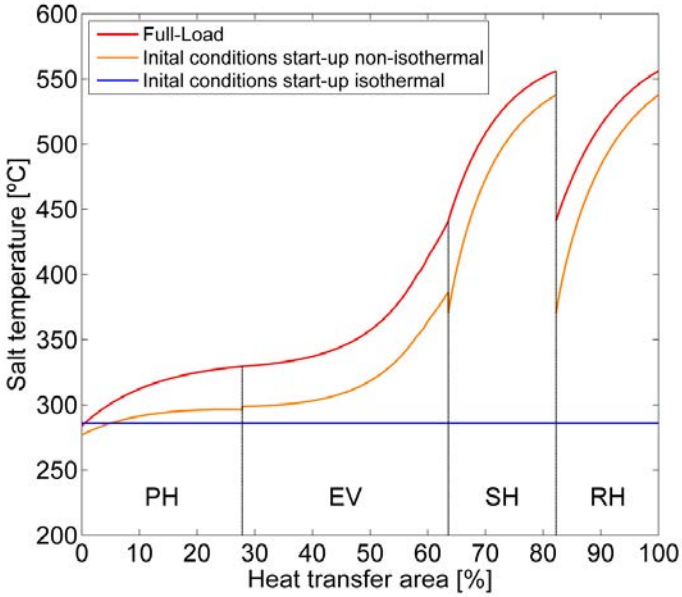

Figure 4.3: Salt temperature profiles in SG.

pressure operation mode at 25% of load with a steam drum pressure of 7,4 MPa and a saturation temperature of 290 ºC. These conditions are set as freeze salt protection point and correspond to the fixed turbine operation mode. A temperature difference is subtracted for each heat exchanger following the cooling rates published in [17] due to the night cooldown period. It is assumed 8 hours of cooldown time and the longitudinal heat conduction of the salt is neglected. The feasibility of this approach is ensured by a salt freeze protection system that consists on an electric heat tracing system in the SG.

- **Daily start-up with isothermal conditions**

A different strategy is followed by the Solar Two for a daily start-up in which the cold salt circulates during the night through the SG [19]. The SG temperature is kept constant to 290 ºC at the beginning of the daily start-up. This procedure compensates the energy losses from the heat exchangers to the ambient and the energy required to heat-up the feedwater. However, more energy is needed to heat-up the feedwater than to compensate the energy losses. On the one hand, the energy losses during the night are small due to the good insulation systems of the heat exchangers. On the other hand, a high energy is needed to keep the water level in the evaporator to

compensate the steam leakage through the pressure relief valves and the water blowdown.

In contrast, considering the Foster Wheeler [17] approach the SG heat exchanger filled with salt achieve the isothermal condition as a result of few days without SG operation. The salt freeze protection system is provided by electric heat tracing to keep the temperature not less than 290 ºC in whole SG system. It should be mentioned that Foster Wheeler approach is considered for a 100 MWe plant, whereas the Solar Two approach is considered for a 12.5 MWe plant.

It is worth to mention that other heat-up systems were considered in Solar Two for heat exchangers and salt pipe lines: electrical heat tracing or intermittent operation of the salt circulating pumps [45]. The first approach results in a higher energy consumption that the second approach. However, the intermittent operation requires a high number of measurements in the flow circuit and even it does not avoid the potential salt freeze due to measurements failure. Moreover, the intermittent operation on the salt circulating pumps may lead to a fatigue failure. Finally, the overnight temperature control of the SG (heat exchangers and pipe lines) is made by continuous operation of both electric heat tracing and cold salt circulating pump.

4.4. Modeling and validation

This section describes the models used to calculate the transient and dynamic response of the SG the start-up. The models either use the theoretical approaches proposed in the literature or are developed to reflect the transient response of the SG. The main goal of the models consists on finding the highest stress values on the SG, identifying which is the critical part of the heat exchangers. As the stress and temperature calculations are decoupled, the first step consists on calculating the temperature profiles of the heat exchangers.

4.4.1. Single phase flow heat exchangers

The SH, RH and PH are modeled as counter-current heat exchangers [27]. Assuming that negligible wall resistance and heat transfer to the outer wall, the heat balance can be expressed as follows:

$$D_{sa}\frac{\partial T_{sa}}{\partial t}+L_{sa}\frac{\partial T_{sa}}{\partial x}+T_{sa}=T_{m} \tag{4.1}$$

$$D_m \frac{\partial T_m}{\partial t} + T_m = \frac{h_{sa} A_{sa} T_{sa} + h_{st} A_{st} T_{st}}{h_{sa} A_{sa} + h_{st} A_{st}} \tag{4.2}$$

$$D_{st} \frac{\partial T_{st}}{\partial t} - L_{st} \frac{\partial T_{st}}{\partial x} + T_{st} = T_m \tag{4.3}$$

where $L = \frac{C \dot{m}}{h A}$ is the characteristic length and $D = \frac{\rho C A_c}{h A}$ is the characteristic time.

The above equation system can be solved numerically using an implicit finite difference scheme. Other option to solve the equation system above can be adopted by means of the method proposed by Ansari and Mortazavi [28]. This method is based on the analytical solution of Equations 4.1 and 4.3 assuming that the wall temperature variation is a first order system for one cell. Then, the analytic solutions are used to obtain the outlet temperatures on each cell. Figure 4.4 shows the comparison of the solutions for different heat capacities of the metal wall by analytical and numerical approaches. The results show that numeral solution presents similar values to the analytical model, and thus, the numerical model is employed in this Chapter. The heat exchangers are discretized along the tube length at least to the baffle spacing (Table 3.4). The time step is calculated to fulfill the Courant condition.

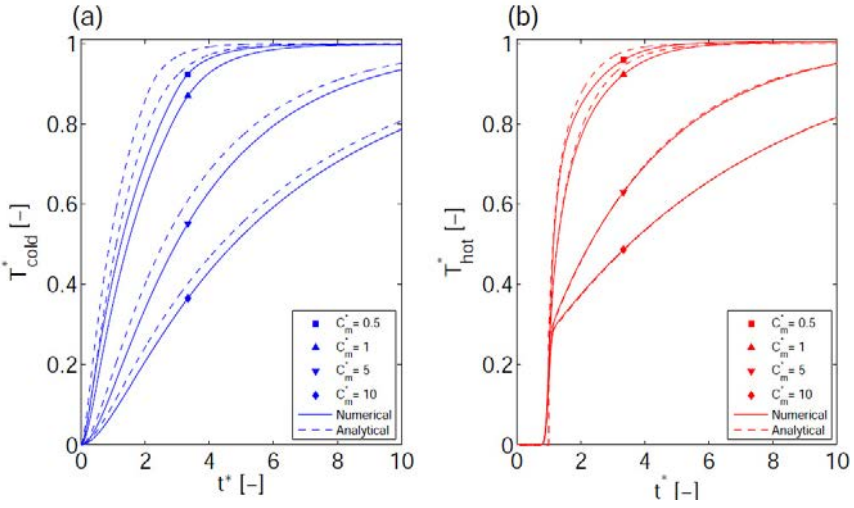

Figure 4.4: Response comparison between numerical and analytical methods for a temperature step change in the hot fluid: a) cold fluid outlet and b) hot fluid outlet.

The fluid properties are calculated in each time step. The heat transfer coefficient on the water/steam side in PH, SH and RH is calculated according to Gnielinski correlation [29]. The heat transfer coefficient on the shell side is calculated using:

$$h_s = h_{s,0}\left(\frac{\dot{m}_{sa}}{\dot{m}_{sa,0}}\right)^{0.6} \tag{4.4}$$

where $h_{s,o}$ is the heat transfer coefficient of the shell at nominal conditions, which is calculated as function of the heat transfer coefficient in the cross-flow zone using the Colburn correlation [30] and heat transfer coefficient in the window zone using the Singh et al. [31] correlation. Both are weighted considering their respective heat transfer areas.

4.4.2. Two phase flow model for evaporator and steam drum

A mathematical model is proposed to estimate the dynamic behavior of the evaporator and the steam drum [12,32]. The thermal inertia of the water/steam mixture and the metal mass are considered. The metal wall temperature of the evaporator and steam drum is assumed to be equal to the steam/water mixture, i.e., the saturation temperature. Similarly, the steam outlet enthalpy is assumed to be equal to the vapor enthalpy. The mass and energy balances in the evaporator-drum control volume leads to the following Equations 4.5, 4.6 and 4.7.

$$\frac{d(\rho_w V_w)}{dt} + \frac{d(\rho_{st} V_{st})}{dt} = \dot{m}_w - \dot{m}_{st} \tag{4.5}$$

$$\frac{d(\rho_w V_w u_w)}{dt} + \frac{d(\rho_{st} V_{st} u_{st})}{dt} + M_{ev} C_m \frac{d\,T_{m,ev}}{dt} = \dot{m}_w i_w - \dot{m}_{st} i_{st} + \dot{m}_{sa} i_{sa,i} - \dot{m}_{sa} i_{sa,o} \tag{4.6}$$

$$\dot{m}_{sa} i_{sa,i} - \dot{m}_{sa} i_{sa,o} = h_{sa,ev} A_{ev} (\overline{T}_{sa,ev} - T_{m,ev}) \tag{4.7}$$

The saturated water and steam properties are calculated using XSteam tool [33]. The equation system presented above is valid to calculate the dynamic behavior of the steam drum pressure. However, in order to calculate the dynamic behavior of the steam drum water level two additional equations are needed [32]. The first equation is obtained from an energy balance in evaporator. In order to avoid the use of partial

differential equations and simplified the calculations, a lumped parameter model is used to describe the dynamic behavior of the tube bundle of the evaporator. The second equation is obtained by a mass balance on the steam under the liquid level of the steam drum. Finally, a non-linear equation system formed by four equations is obtained, which is solved by explicit scheme using Runge-Kutta method. A time step of 1 second is used to ensure the numerical stability. Figure 4.5 shows the model response for different two step disturbances [32]. Figure 4.5 shows the model response for a heat step of 10MWth. As expected, the heat step result in an increase of the steam mass fraction (Figure 4.5c), which lead to a pressure increase (Figure 4.5a). The pressure raise increases the steam condensation leading to an increment on the water volume (see Figure 4.5b). From the drum level control point of view, the complexity of the two-phase problem is illustrated in Figure 4.5d. Initially the drum level slightly increases due to steam condensation produced by pressure increment and later decreases because the reduction of the steam volume.

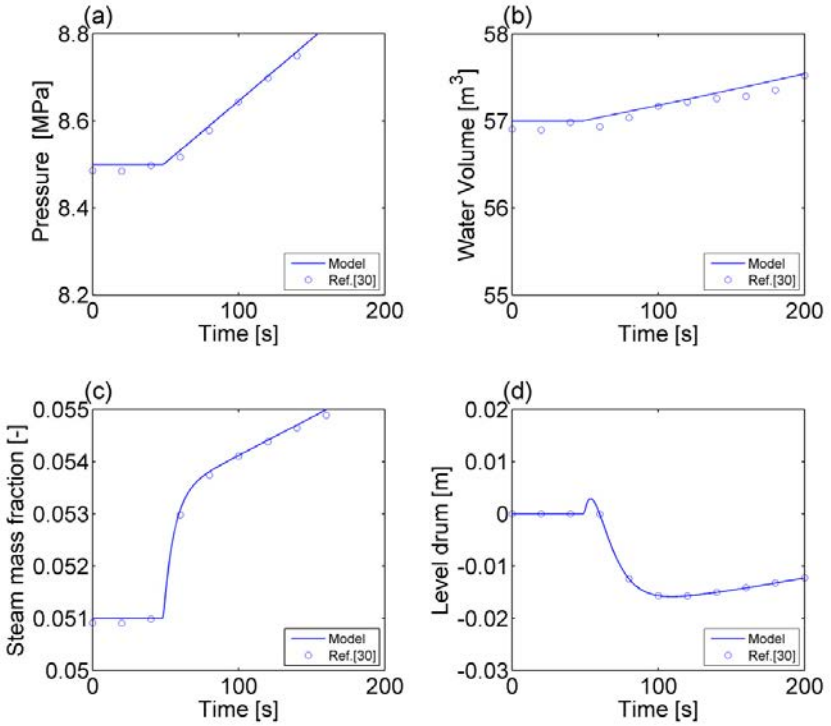

Figure 4.5: Response of the system for a heat step of 10 MWth: a) steam drum pressure; b) total water volume ; c) evaporator outlet steam mass fraction; d) steam drum level.

4.4.3. Stresses on steam drum and SH header

A widely used methodology to estimate the maximum heating rates of thick-walled components is proposed by European standard EN 12952-3 [20], in which several concentration factors for different geometries, connections shapes and loadings can be found. Usually, in conventional boilers the limiting components are the heads of SH and RH, the steam drum, and the T and the Y shaped junctions of steam pipelines [8]. The total tangential stress is calculated combining pressure and thermal stresses using their respective concentration factors:

$$\sigma = \sigma^{P} + \sigma^{T} = \alpha_{m} \frac{D}{2\,t_{j}} P_{j} + \alpha_{t} \frac{\beta_{t} E}{1-v} (T_{ave} - T_{su}) \tag{4.8}$$

where T_{ave} is the metal average temperature and T_{su} is the inner surface temperature. The thermal concentration factor (α_t), is function of the working fluid (steam or water) and the diameter ratio between the main component and the outlet/inlet pipeline. The pressure concentration factor (α_m) mainly depends on the ratio between the diameter and thickness of the main component and the outlet/inlet pipeline. According to Taler et al. [34] two points should be considered in a T-junction connection, as shown in Figure 4.6. This method is used to estimate the stress on the T-junction formed by steam drum-downcomer junction and SH head-nozzle junction.

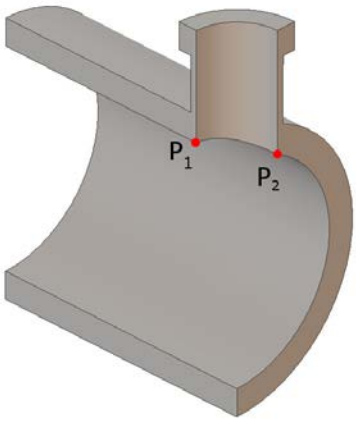

Figure 4.6: T-junction points selected.

A transient temperature model is performed to estimate the average and inner metal wall temperatures for the steam drum and the SH head (Equation 4.9). The model considers that the temperature varies only in the radial direction. A heat transfer boundary condition is used in the inner surface, whereas an insulated boundary condition is considered in the outer surface.

$$\begin{aligned}
&\frac{1}{r}\frac{\partial}{\partial r}\left(r\frac{\partial T}{\partial r}\right)=\frac{1}{a}\frac{\partial T}{\partial t}\\
&T(r,0)=T_0\\
&-k\left.\frac{\partial T}{\partial r}\right|_{r=r_i}=h_j\left(T_j(t)-T(r_i,t)\right)\\
&\left.\frac{\partial T}{\partial r}\right|_{r=r_o}=0
\end{aligned} \tag{4.9}$$

The above equation is solved numerically using the Crank-Nicolson method. The wall thickness is discretized along the radial coordinate to obtain increments not higher than $5{\cdot}10^{-3}$ m. The time step is calculated according to von Neumann stability criterion. The Once the radial temperature distribution of the metal wall is known, the average wall temperature is calculated according Kim et al. [12].

4.4.4. Stresses on tubesheet

One of the most critical parts of the shell and tube heat exchanger is the tubesheet due to its complex geometry [35]. Tubesheet design calculations, for heat exchangers in standard industrial applications, are typically performed according ASME Section VIII-Div 1 or/and TEMA standards [6]. However, no specific guidelines are showed in TEMA standards or/and ASME code for complex loadings such as transients thermal loadings [9] or thermal gradient on the junction behavior [10]. For this reason, the method proposed by O'Donnell et al. [36] is used for the tubesheet stress calculation. A schematic of the main tubesheet zones is illustrated in Appendix B.

The main equations for the stress calculations proposed by O'Donnell et al. [36] are shown in Table 4.2. On a first step, the effective elastic constants, which are function of the ligament efficiency and the tube pitch layout, are calculated. On a second step, the pressure stresses are calculated considering an equivalent solid plate [37]. The ligament stress is calculated combining the pressure stress using Equation 4.10 and the thermal stress using Equation 4.14, considering their stress sign. A

considerable temperature difference in no-tube-lane zone is found in PH, therefore the stress must be calculated using Equations 4.15 and 4.16.

Table 4.2: Main equations for stress calculations proposed by O'Donnell et al. [36].

Load	Stress intensity	Equation
Pressure and thermal	Average across ligament at either surface of plate	$\sigma_{eff} = K\frac{R}{h}\lvert\sigma_1\rvert$ (4.10)
Pressure	Average across ligament and through thickness	$S_{eff} = \frac{R}{h}\left[\left(\frac{\Delta P r}{H}\right)^2 + (\sigma_r)^2\right]$ (4.11)
Pressure and thermal	Peak in ligaments	$\sigma_{\max} = Y\sigma_1 + P$ (4.12)
Pressure and thermal	Peak at perforations adjacent to rim	$\sigma_{\max} = K_r\sigma_{rim} + P$ (4.13)
Thermal (skin effect)	Peak at surface	$\sigma_{\max} = \frac{E\beta_t(T_{ave} - T_{su})}{1-\nu}$ (4.14)
Thermal (temperature difference across no-tube-lane zone)	Peak in ligaments	$\sigma_{\max} = \frac{K_u E^* \beta_t(T_H - T_C)}{2}$ (4.15)
Thermal (temperature difference across no-tube-lane zone)	Peak at holes adjacent to no-tube-lane zone	$\sigma_{\max} = \frac{K_D E \beta_t(T_H - T_C)}{2(1-\nu)}$ (4.16)

- **Thermal tubesheet ligament analysis**

Under start-upstart-up conditions, the Biot number varies from 0.03 to 0.25 in the surface of the tubesheet ligament. When Biot number is higher than 0.05 in cylinders, the transient conduction analysis would be convenient [38]. Assuming an equilateral triangle pitch layout, an isolated cylinder is analyzed as is shown in Figure 4.7. The calculation of the transient temperature field of the simplified tubesheet ligament model is calculated using Equation 4.17. Symmetric boundary conditions are considered for the outer wall of the simplified ligament model. The boundary conditions used on tube, head and shell side are described in Figure 4.7.

The Equation 4.17 is discretized in a grid of nodes where the radial and axial increments are not higher than $5{\cdot}10^{-3}$ m. The Equation 4.17 is solved numerically by time implicit finite difference scheme. An example of the transient temperature field evolution on the tubesheet ligament is shown in Figure 4.8, for a temperature step of 35 ºC on the shell-side fluid. At this point, the surface temperature (T_{su}) and average

wall temperature (T_{ave}) are known, and then, the thermal stresses on the tubesheet ligament can be calculated using Equation 4.14. This approach guarantees a conservative calculation because it is assumed that the tubesheet has perfectly clamped edges.

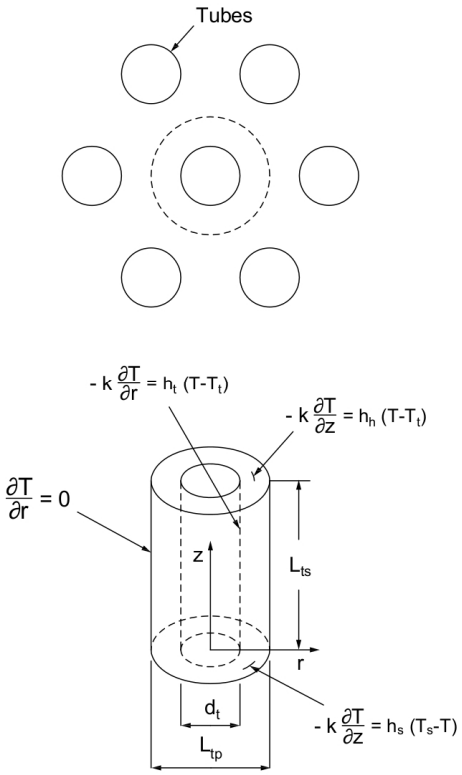

Figure 4.7: Tubesheet ligament boundary conditions.

$$\frac{1}{r}\frac{\partial}{\partial r}\left(r\frac{\partial T}{\partial r}\right)+\frac{\partial^2 T}{\partial z^2}=\frac{1}{a}\frac{\partial T}{\partial t} \tag{4.17}$$

- **Tubesheet junction**

According to Soler et al. [39] three tubesheet junctions types are possible: two side gasketed, two side integral and one side integral with other side gasketed. In this

Chapter, an integral junction type is considered for both head and shell side. The stresses on the junctions of the tubesheet are normally estimated using Finite Element Analysis (FEA) because of the complex geometry of the head [35,40]. FEA is out of the scope of this work since the goal of this analysis is to develop low-time consuming simplified-models. Therefore, an analytical model is proposed to estimate the stresses of the tubesheet junction. A schematic of the head-tubesheet-shell junction forces and moments is shown in Figure 4.9. The displacements and forces can be related as a function of their respective stiffness as: $F_j = K_j x_j$ or $x_j = K_j^{-1} F_j = K'_j F_j$. Then, the problem can be written in matrix form and the displacements of the shell and the head can be calculated using Equation 4.18. The displacements of the tubesheet are calculated using Equation 4.19.

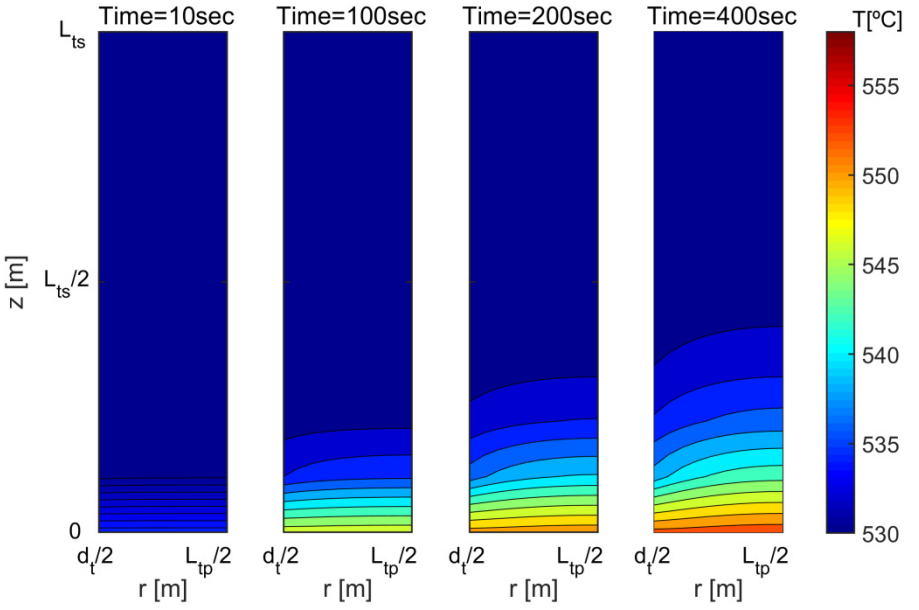

Figure 4.8: Transient temperature field in tubesheet ligament zone.

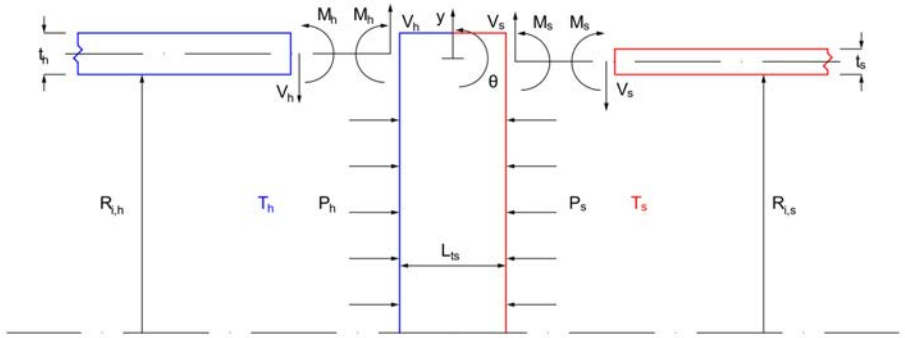

Figure 4.9: Schematic of the head-tubesheet-shell junction forces.

$$\begin{Bmatrix} y_h \\ \theta_h \\ y_s \\ \theta_s \end{Bmatrix} = \begin{bmatrix} K'_{cyl,My} & -K'_{cyl,Vy} & 0 & 0 \\ K'_{cyl,M\theta} & -K'_{cyl,V\theta} & 0 & 0 \\ 0 & 0 & -K'_{cyl,My} & K'_{cyl,Vy} \\ 0 & 0 & K'_{cyl,M\theta} & -K'_{cyl,V\theta} \end{bmatrix} \begin{Bmatrix} M_h \\ V_h \\ M_s \\ V_s \end{Bmatrix} + \begin{bmatrix} K'_{cyl,t,y} & 0 \\ 0 & 0 \\ 0 & K'_{cyl,t,y} \\ 0 & 0 \end{bmatrix} \begin{Bmatrix} T_{ave,h} \\ T_{ave,s} \end{Bmatrix} + \begin{bmatrix} K'_{ciy,p} & 0 \\ 0 & 0 \\ 0 & K'_{cyl,p} \\ 0 & 0 \end{bmatrix} \begin{Bmatrix} P_h \\ P_s \end{Bmatrix} \quad (4.18)$$

$$\begin{Bmatrix} y_{ts,h} \\ \theta_{ts,h} \\ y_{ts,s} \\ \theta_{ts,s} \end{Bmatrix} = \begin{bmatrix} \frac{L_{ts}}{2}K'_{ts,My} & \frac{L_{ts}}{2}K'_{ts,Vy} & \frac{L_{ts}}{2}K'_{ts,My} & \frac{L_{ts}}{2}K'_{ts,Vy} \\ -K'_{ts,M\theta} & -K'_{ts,V\theta} & -K'_{ts,M\theta} & -K'_{ts,V\theta} \\ -\frac{L_{ts}}{2}K'_{ts,My} & -\frac{L_{ts}}{2}K'_{ts,Vy} & -\frac{L_{ts}}{2}K'_{ts,My} & -\frac{L_{ts}}{2}K'_{ts,Vy} \\ -K'_{ts,M\theta} & -K'_{ts,V\theta} & -K'_{ts,M\theta} & -K'_{ts,V\theta} \end{bmatrix} \begin{Bmatrix} M_h \\ V_h \\ M_s \\ V_s \end{Bmatrix} + \begin{bmatrix} K'_{ts,t,y} & 0 \\ K'_{ts,t,\theta} & -K'_{ts,t,\theta} \\ 0 & K'_{ts,t,y} \\ K'_{ts,t,\theta} & -K'_{ts,t,\theta} \end{bmatrix} \begin{Bmatrix} T_{ts,su,h} \\ T_{ts,su,s} \end{Bmatrix} + \begin{bmatrix} -\frac{L_{ts}}{2}K'_{ts,p\theta} \\ K'_{ts,p\theta} \\ \frac{L_{ts}}{2}K'_{ts,p\theta} \\ K'_{ts,p\theta} \end{bmatrix} \{P_h - P_s\} \quad (4.19)$$

The stiffnesses K_i for a cylinder and solid disk for pressure and thermal loads are calculated according to [41-42]. The stiffness of the tubesheet is modified as an equivalent solid plate using the equivalent elastic modulus and poison coefficient as function of the ligament efficiency and pitch layout according to ASME code [7]. In a first step, the free displacements (y_j, θ_j) on the tubesheet, head and shell are calculated only considering the pressure and thermal loads, i.e. without the interaction of the moments and forces. On a second step, the moments and forces are calculated to achieve the compatibility of the displacements.

- **Thermal tubesheet junction analysis**

A numerical model based on Equation 4.17 is also carried out to calculate the transient temperature field on the tubesheet junction. The Equation 4.17 is discretized in a grid of nodes where the radial and axial increments are limited to 10^{-2} m. A schematic of the boundary conditions is shown in Figure 4.10. An example of the transient temperature field evolution on the tubesheet junction is shown in Figure 4.1, for a temperature increment of 150 ºC on shell and tube -side fluids. As can be seen the transient effect or characteristic time is longer for tubesheet junction than tubesheet ligament. This leads to higher variations between peaks and valleys on thermal stresses during the start-up or load change processes.

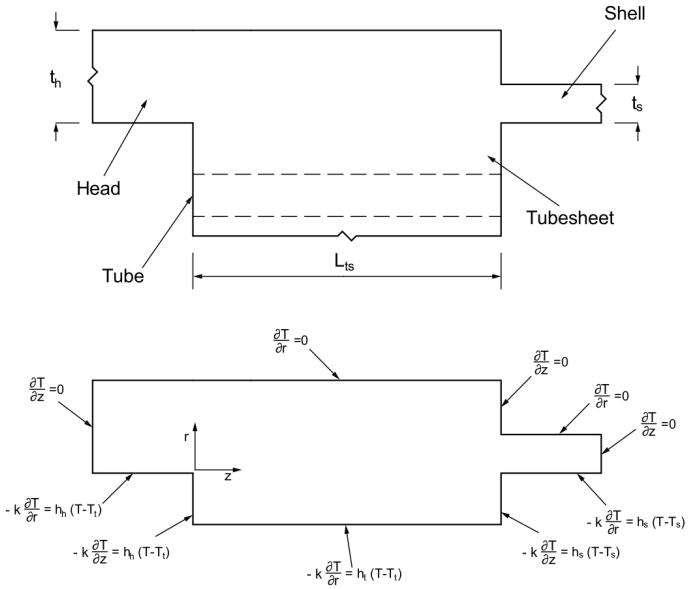

Figure 4.10: Schematic of the tubesheet junction boundary conditions.

The surface wall temperatures depend on the heat transfer coefficient due to the heat transfer boundary conditions used. The complex estimation of the heat transfer coefficients on head and shell side, makes necessary to simplify its calculation. On the one hand, the heat transfer coefficient on the tubesheet of the shell side wall is calculated as one order of magnitude lower than the cross flow on shell side. On the other hand, the heat transfer coefficient on the tubesheet of the head side wall is

considered one order of magnitude lower than the heat transfer coefficient of the tube side.

The membrane stresses of the head and shell at the junction are calculated using the equations presented in [42]. Once the moments are known, the bending stresses of the head and shell can be estimated using Equation 4.20. The stresses at the tubesheet-head junction are calculated using a conservative approach combining the tangential head transient thermal stress with the axial head bending stresses using the von Mises equation [7]. The stresses suffered on the tubesheet-shell junction are calculated considering only the peak thermal stress by using Equation 4.14.

$$\sigma_b = \pm \frac{6M}{t^2} \tag{4.20}$$

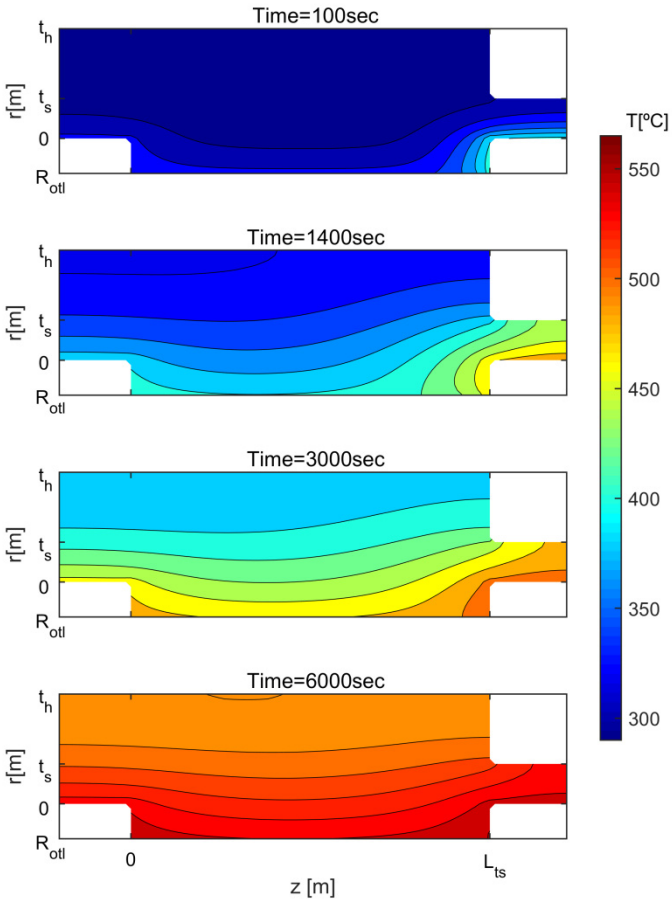

Figure 4.11: Transient temperature field in tubesheet junction.

4.4.5. Stresses on U-tubes

Although U-tube design is used to avoid the differential thermal expansion between shell and tubes, the thermal stresses in U-bend appear since the tubes are supported by segmental baffles. As the tubes are not free to expand, the tubes try to lose their straight shape and produce contacts with the segmental baffles supports, Figure 4.12. The minimal U-bend radius can be calculated to not overpass the maximum stress limit working at design conditions. However, this stress level is strongly dependent of the temperature profiles of the hot and cold fluids along the heat exchanger, which change during the transient operation. For this reason, a transient analysis is required for the U-tubes.

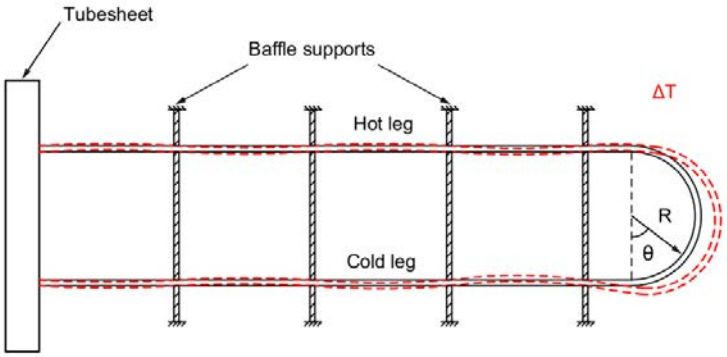

Figure 4.12: U-tube deformation by thermal expansion.

An analytical model proposed by Singh et al. [43] is used to calculate the thermal stress on U-tubes. The model can be written as a matrix form based on the stiffnesses of the U-tubes, which are mainly function of the displacements, baffle spacing, tube length, modulus of elasticity and moment of inertia. The displacement of the hot leg over cold leg can be calculated using Equation 4.21, assuming the axial force $F = 0$. The problem can be solved by an iterative process until the convergence of the displacements, forces and moments are reached.

$$\delta = (\overline{\beta_{hot}\Delta T_{hot}} - \overline{\beta_{cold}\Delta T_{cold}})L - \frac{2F}{AE}L \tag{4.21}$$

Once the forces and moments are known, the moment function ($M(\theta)$) in the U-bend can be calculated. Then, the stress is calculated as follows:

$$\sigma(\theta) = \frac{\psi \; M(\theta) \; r_o}{I} \tag{4.22}$$

where ψ is the stress intensification factor for the U-bend and, r_o is the outer-tube radius. An example of the SH U-bend thermal stress along the angle θ for different temperature differences between hot leg and cold leg is shown in Figure 4.13. As can be seen, the maximum stress on the SH U-bend is obtained for θ = 0º.

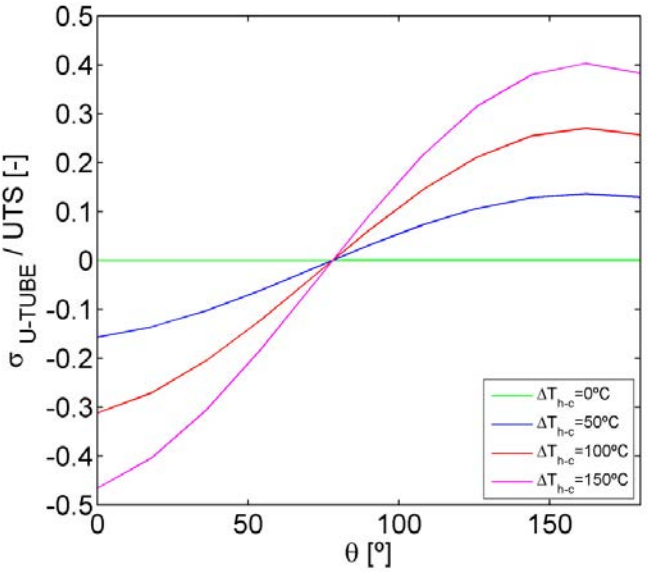

Figure 4.13: SH U-bend stress for different temperature differences between hot leg and cold leg.

4.5. Results

The results of the different start-up conditions considered for the SG are presented in this section. First, an analysis of the SG performance for two different feedwater heat-up systems is carried out: i) with water recirculation from steam drum; ii) with steam recirculation from steam drum using a start-up feedwater heater. Then, the

results of the daily start-up with non-isothermal conditions and isothermal conditions are presented. For both starting-up procedures, an analysis of the stresses of the main components is also presented.

To carry out the dynamic analysis of the SG, all described models are computed together in order to estimate the stress in real time. Since each model uses different time steps, a global time step of 15 seconds is chosen to update the calculations of the different models. A global time step of 30 seconds is set to update the temperature field calculations of tubesheet ligament and junction to improve the calculation process performance.

4.5.1. Feedwater temperature

Under start-up conditions, the feedwater heater system is not able to provide the feedwater at its full-load temperature set point. To solve this issue, a back-up system such as auxiliary heaters may be installed [44]. In a first step, the feedwater heating-up system described in [17] is adopted. This procedure basically consists on heating-up the feedwater at 245ºC before to the preheater inlet by mixing hot water from the drum (290 ºC). As can be seen in Figure 4.14-a/b, high water mass flow rate ($\dot{m}_{w,rec}$) must be circulated from the drum to keep the preheater inlet-temperature set-point. This high mass flow rate reduces excessively the temperature of the preheater salt outlet up to ($T_{PH,sa,o} \approx 250$ ºC), increasing the potential risk of salt freezing. For this reason, a different feedwater heat-up system is needed.

Based on the Solar Two operation experience, Pacheco et al. [19] proposed the use of a start-up feedwater heater (Figure 4.2), in which auxiliary steam is extracted from steam drum to heat-up the feedwater. Furthermore, the preheater inlet temperature set point is increased from 245 ºC to 260 ºC. This alternative mode is implemented and the results are shown in Figure 4.14-c/d. As can be seen in Figure 4.14-c/d, the circulated steam mass flow from the drum ($\dot{m}_{st,rec}$) is considerably lower than the water circulation system ($\dot{m}_{FW}$), although the preheater inlet temperature set point has been increased. Now, the preheater salt outlet temperature is around to ($T_{PH,sa,o} \approx$ 270 ºC, which can be considered as a safe operation.

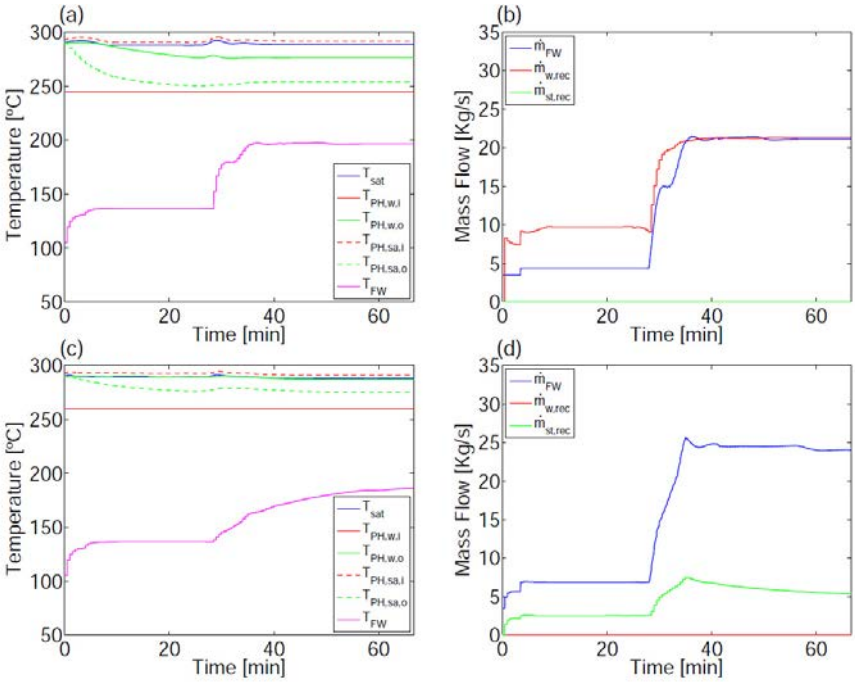

Figure 4.14: Feedwater system performance: a, b) without start-up feedwater heater; c, d) with start-up feedwater heater.

4.5.2. Daily start-up with non-isothermal initial conditions

For daily non-isothermal initial conditions the heat exchangers of the SG are closed after the night shutdown and thermally isolated to reduce the heat losses [17]. As they are filled with hot salt, each heat exchanger has different temperatures, as was described in Figure 4.3.

Figure 4.16 shows the time evolution of the main thermodynamic variables during the start-up and steady state of the SG. In addition, a schematic of the startup procedure, where the main steps are described, is shown in Figure 4.15. Both Figures 4.16 and 4.17 differentiate between the starting-up and nominal conditions by a vertical line. It is assumed that the TES system has enough energy to initialize the start-up of the SG.

In a first step, the hot and cold salt pumps provide a mass flow rate of 4% of nominal flow to SG [17]. The salt is sent to EV at 448 ºC by the bypass-line, which is the design salt inlet temperature. The salt also circulates to the PH. The steam generated is sent to the start-up feedwater heater, in which the feedwater is heated up 260 ºC when enters to the PH. It is assumed that the feedwater available at the

beginning of the start-up is at 100 ºC from deaerator. The steam drum pressure is kept constant to 7.4 MPa until the turbine achieves the sliding pressure conditions (Figure 4.16-c).

After t = 4 min, the salt is sent to SH and RH at 565 ºC (Figure 4.16-a), when the steam generation is established to 4%. At the same time, the saturated steam from the steam drum is sent to the SH and the outlet steam is sent to the RH by the SH-RH by-pass line, where the attemperation system keeps the RH steam inlet temperature at 365 ºC. Moreover, an additional valve is used in the SH-RH by-pass line to reduce the RH inlet pressure in an allowable range. The RH outlet steam is sent to deaerator. During this process, the salt flow rate is increased to 5%.

When the steam generation is set to 5% and the SH and RH outlet steam temperature is kept to 496 ºC (Figure 4.16-b/d), the steam is sent to HP and LP turbines, respectively [17]. Then, the SH to RH steam by-pass line is closed. This process is kept until the turbine synchronization is completed, which takes around 15 minutes [17].

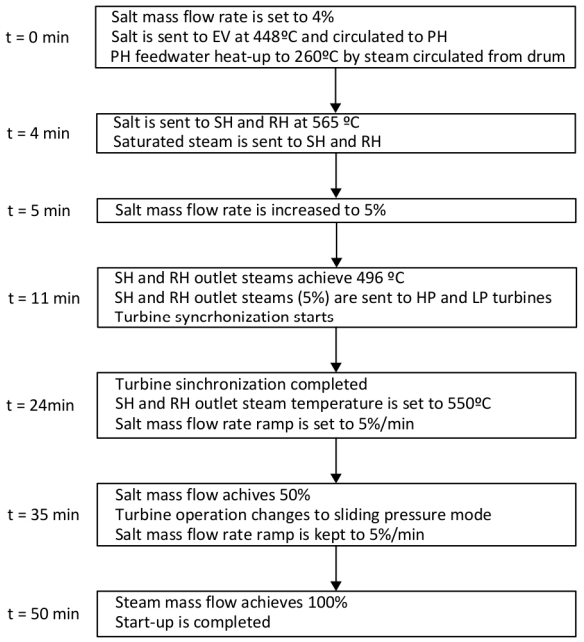

Figure 4.15: Schematic of the procedure of the start-up with non-isothermal initial conditions.

At t = 24 min, the turbine synchronization is completed and the SH and RH steam outlet temperature is increased from 496 ºC to 550 ºC (Figure 4.16-b/d). The salt mass flow rate is increased by a ramp of 5%/min until 50 % of its nominal value (Figure 4.16-a). At this load point, the turbine is switched from fixed pressure mode to sliding pressure mode. Now, the salt flow rate ramp is kept to 5%/min until the salt flow rate reaches its nominal value. At the same time, the pressure on the steam drum start to raise (Figure 4.16-c), as consequence of the sliding pressure mode the steam mass flow rate increases too.

Full load conditions are achieved after 50 min. The energy delivered from TES system and the required mass of hot salt to start-up with non-isothermal initial conditions is around 70 MWth using 600 tons, respectively. The energy consumption of the salt pumps is around 45 kWhe.

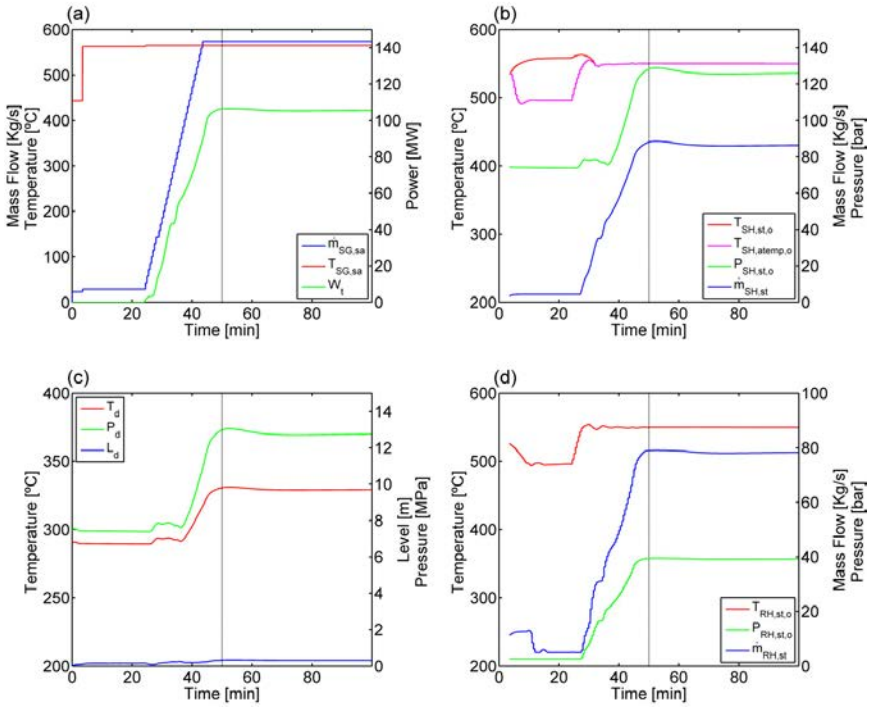

Figure 4.16: Non-isothermal start up simulation: a) salt temperature and mass flow rate, turbine power output; b) SH performance; c) steam drum performance; d) RH performance.

Typically, the stress is limited to avoid the material failure along its lifetime operation. Following ASME code [7], two different mechanisms of damage are calculated: creep and fatigue. The fatigue damage is related with the magnitude of the stress cyclic variations, and the number of cycles to failure is computed as function of the equivalent strain range [7]. The creep damage is function of the stress level and the temperature. A conservative stress limit equal to 40% of the Ultimate Tensile Strength (UTS) is imposed. This stress limit value considers both fatigue and creep damages.

The stress evolution of the SG components is shown Figure 4.17. The stress evolution can be divided in two groups. Group 1 (Figure 4.17-a/b/c/e/f/g) refers to the parts where the thermal inertia is significant and therefore a delay is found between the wall inner surface temperate and the average wall temperature. These stresses are produced in tubesheet ligament, tubesheet-head junction, tubesheet-shell junction, the steam drum and the inlet and outlet SH heads. Group 2 (Figure 4.17-d/h) refers to the parts where that the thermal inertia can be neglected. These stresses are produced in the no-tube-lane tubesheet zone and U-tubes.

For the non-isothermal start-up, the most limiting stresses are marked with a red circle in Figure 4.17. These stresses are obtained in the SH lower tubesheet-shell junction (Figure 4.17-c) when the pressure raises on the steam drum (Figure 4.16-c). Although the highest stresses are obtained in the SH and RH U-tube (Figure 4.17-h), these values do not limit the start-up ramp. Firstly, it should be noted that the highest U-tube stresses correspond to U-tubes with the lowest radius. Secondly, this problem is independent of the temperature change rate, since it is only function of the temperature profile state along the heat exchanger. Then, this issue can be solved by increasing the minimal U-bend radius. However, the most interesting result is that the SH and RH U-tube are more stressed during part-load operation than during full-load operation. This result is caused due to the higher temperature differences between the hot leg and cold leg under part-load conditions.

4.5.3. Daily start-up with isothermal initial conditions

For a daily start-up with isothermal initial condition is considered that, after the plant shutdown, cold salt is pumped through the heat exchangers during the night. In this way, the temperature is kept constant at 290ºC in the whole SG at the beginning of the start-up process. The steam drum pressure is kept constant to 7.4 MPa. During this period the potential condensation of the steam SH and RH should be taken to the deaerator. A schematic of the start-up procedure and the time evolution of the main parameters are shown in Figures 4.18 and 4.19, respectively. The isothermal and non-

isothermal SG conditions have practically the same start-up procedure since both are considered as a daily start-up, and thus, the turbine inlet conditions are the same.

In a first step, salt is sent to the EV through the by-pass line at 350 ºC to start the heat-up process of the EV and PH. When the steam production is established around of 4%, the salt and steam valves are opened in the RH and SH. The salt temperature change rate is set to 150 ºC/hr (Figure 4.19-a).

At t = 67 min the SH and RH steam temperatures achieve 496 ºC, these steam flows are sent to HP and LP turbines stages to start the synchronization. At the end of the turbine synchronization the steam outlet temperatures are increased to 550 ºC (Figure 4.19-b/d). At this point, the salt flow rate is increased by a ramp of 5%/min until the sliding pressure turbine operation condition is achieved. Then, the salt flow rate ramp is increased by 5%/min until achieving full-load conditions.

The start-up process finishes after 110 min when full load conditions are obtained. The energy delivered from TES system to accomplish the start-up with isothermal initial condition is around 85 MWth whereas the hot-salt mass required is 716 tons. The energy consumption of the salt pumps is around 53 kWhe.

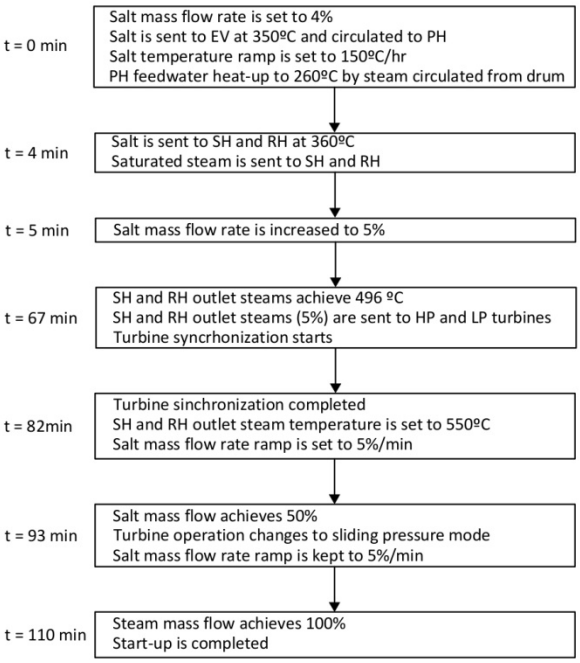

Figure 4.17: Schematic of the procedure of the start-up with non-isothermal initial conditions.

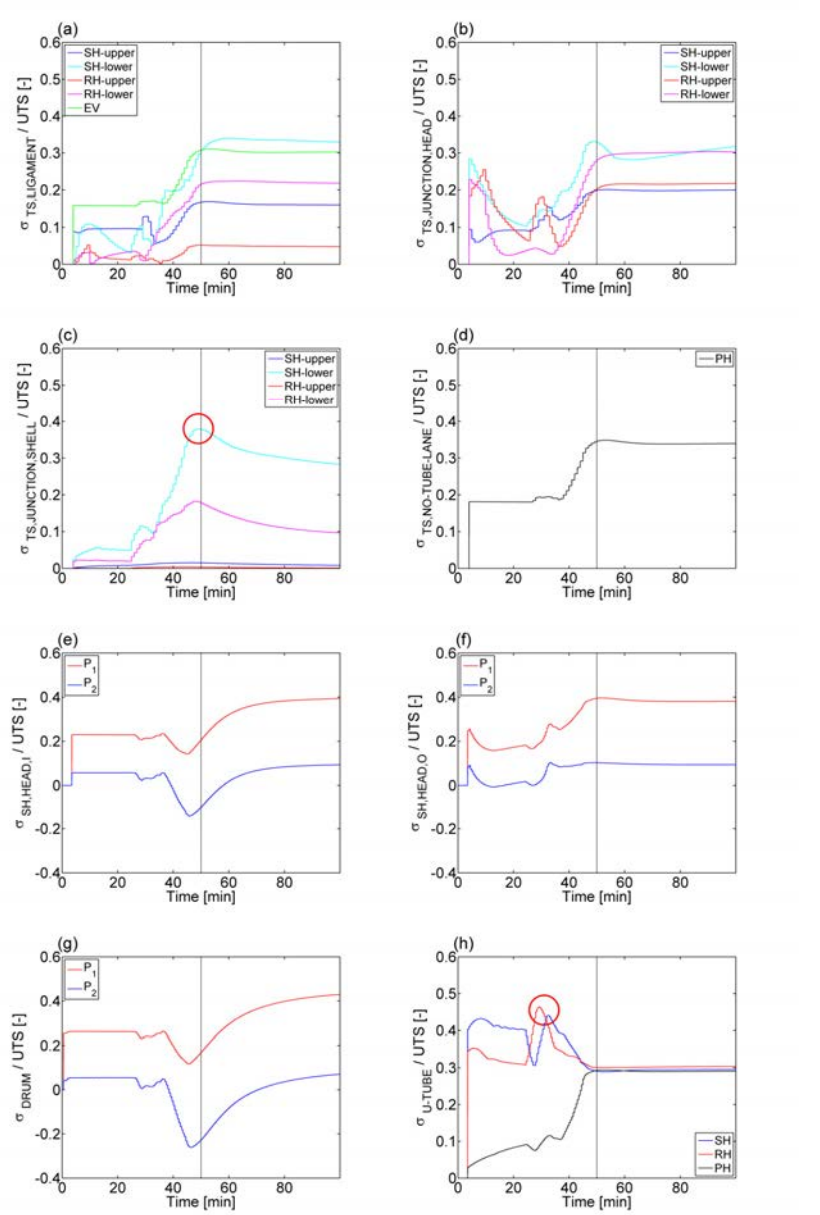

Figure 4.18: Stress evolution of the main components during non-isothermal start-up: a) tubesheet ligament stresses; b) tubesheet head junction stresses ;c) tubesheet shell junction stresses; d) tubesheet no-tube-lane stresses; e) SH inlet head nozzle junction stresses; f) SH outlet head nozzle junction stresses; g) steam drum downcomer junction stresses; h) U-tube stresses.

The stress evolution of the main components of the SG are depicted in Figure 4.20. As can be seen in Figure 4.20, the highest stress values are obtained in the SH upper tubesheet-head junction (Figure 4.20-b), the SH lower tubesheet-shell junction (Figure 4.20-c) and the U-tubes in the SH and the RH (Figure 4.20-h).

At the beginning of the start-up, the limiting stress is found in the SH upper tubesheet-head junction (Figure 4.20-b). Although the salt enters to the RH at high temperature, the higher thickness of the SH leads to higher thermal stresses in the SH than the RH. It should be noted that the stress on the SH tubesheet-head junction are higher than in the ligament. This is caused due to the higher thermal inertia values of the SH tubesheet-head junction, which leads to higher delay between the surface temperature and the average wall temperature.

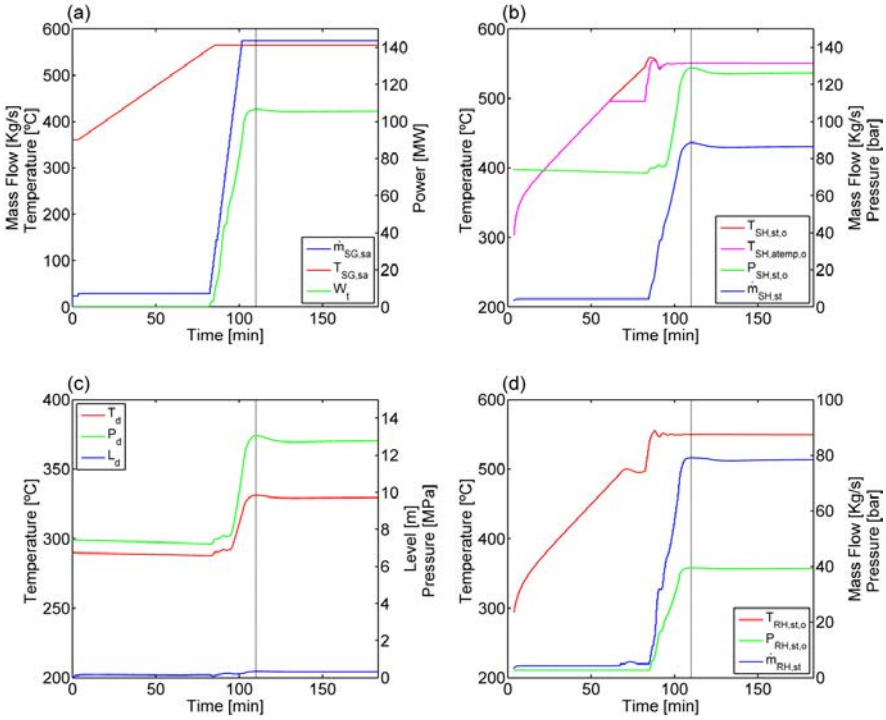

Figure 4.19: Isothermal start-up simulation: a) salt temperature and mass flow rate, turbine power output; b) SH performance; c) steam drum performance; d) RH performance.

When the sliding pressure condition is achieved at t = 93 min, the pressure in the steam drum begins to increase, and as a result, the stresses on the steam drum and SH lower tubesheet grow up (Figure 4.20-c). At this point, the SH lower tubesheet-shell

junction is the most limiting part. Moreover, the transient thermal stresses are higher in the tubesheet junction (Figure 4.20-c) than in the head at the nozzle point (Figure 4.20-e). This is caused by the higher thickness on the head at the tubesheet junction than in the head at the nozzle point, which is made to reduce the bending stress of the heat at the tubesheet junction point. The highest U-tube stress values in the SH and the RH (Figure 4.20-h) are obtained when the highest temperature difference between the salt inlet and the steam inlet appear.

As occurred in the non-isothermal start-up, the maximum allowable stress limit of 40% of UTS is overpassed. However, as mentioned before, the stresses of the U-tube do not limit the start-up ramp, since this problem can be easily solved increasing the U-bend radius. Other possible solution would be an increase of outside tube diameter and then, the tube thickness and their stiffness.

4.6. Conclusions

A steam generator off-design analysis for a solar power tower plant is performed. The steam generator design consists of conventional shell and tube heat exchangers based on TEMA and ASME standards. Different dynamic models of the main components of the steam generator are developed to estimate the temperature field and stresses of the most critical parts of the shell and tube heat exchangers, such as the tubesheet and the tubesheet junction. The European standard EN 12952-3 [20], which is normally used for conventional boilers, is used to calculated stress values of the steam drum and superheater heads. A basic simulation control scheme is applied to obtain the transient response of the system.

Two start-up strategies are studied. The first one is based on Foster Wheeler manufacturer approach [17], in which the heat exchanger valves are closed after the plant shutdown, and thus the initial temperature profile is non-isothermal. The results show that the steam generator start-up takes around 50 minutes to achieve full load conditions. A mass of hot salt of 600 tons (70 MWth) and a consumption of 45 kWhe in the molten salt pumps are needed for this start-up.

The second strategy studied is based on Solar Two operating experience [19]. Here, steam-generator temperature profile is isothermal, 290 ºC at the beginning of the start-up. In this case, cold salt is circulated through the steam generator during the night to reduce the risk of salt freeze. The results show that the steam generator needs around 110 minutes to achieve full load conditions. A mass of hot salt of 716 tons (80 MWth) and a parasitic consumption of 53 kWhe of the molten salt pumps are needed.

The main input variables, such as the mass flow and the temperature change rates, are calculated for both strategies to avoid the overpassing of the stress limits on the

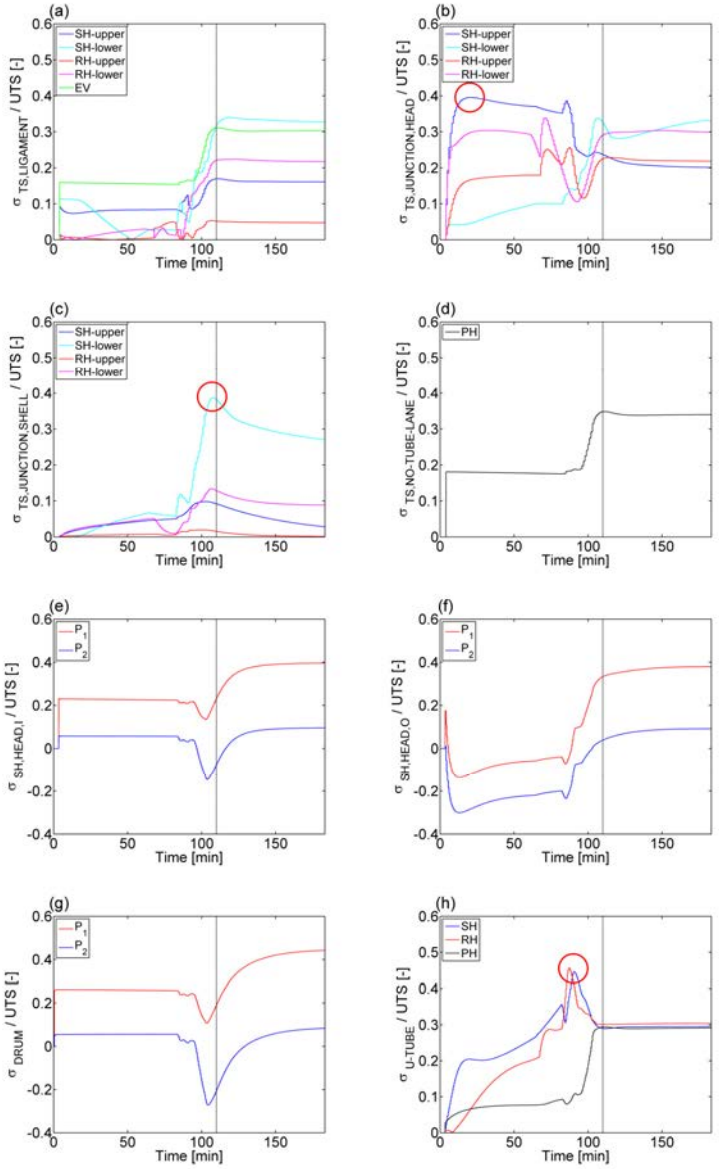

Figure 4.20: Stress evolution of the main components during isothermal start-up: a) tubesheet ligament stresses; b) tubesheet head junction stresses ;c) tubesheet shell junction stresses; d) tubesheet no-tube-lane stresses; e) SH inlet head nozzle junctionstresses; f) SH outlet head nozzle junction stresses; g) steam drum-downcomer junction stresses; h) U-tube stresses.

proposed steam generator. In both start-up strategies is found that the most constrained part of the steam generator is the SH tubesheet junction.

Furthermore, two start-up feedwater heat-up strategies are compared. The first one is based on water drum recirculation and the second in steam recirculation. Although the second one needs an additional start-up feedwater heater, the reduction of the potential salt freeze risk due to the higher outlet preheater salt temperature may compensate the initial investment. Moreover, high mass flow rates of water are required in the drum circulation systems to achieve the SG feedwater inlet temperate, and this may lead to higher operational pump costs.

Nomenclature

Abbreviations

CCPs : combined-cycle plants
CSP : concentrating solar plants.
EV : evaporator.
FW : feed water.
HP : high pressure.
HPT : high pressure turbine.
HRSG : heat recovery steam generator.
HTF : heat transfer fluid.
HT : hot tank.
Hx : heat exchanger.
LP : low pressure.
LPT : low pressure turbine.
PH : preheater.
REC : receiver.
RH : reheater.
SG : steam generator.
SH : superheater.
SPTP : solar power tower plant.
TES : thermal energy storage.
UTS : ultimate tensile strength.

Symbols

A : heat transfer area (m^2).

A_c : cross section area (m^2).

C_m^* : dimensionless thermal capacitance of metal wall (-).

D : diameter (m), characteristic time constant (-).

E : modulus of elasticity (MPa).

F : force (N).

I : moment of inertia (m^4).

K : stiffness (N/m).

K' : inverse of stiffness (m/N).

L : length (m), characteristic length constant (-), level (m).

L_{tp} : tube pitch (mm).

L_{ts} : tubesheet thickness (m).

M : mass (Kg), moment (N m).

P : pressure (Pa).

R : radius (m).

R_{otl} : radius of a circle circumscribed to outermost tube of a bundle (m).

T : temperature (ºC).

T^* : dimensionless temperature (-).

V : volume (m^3), vertical force (N).

W_t : turbine power (MWe).

a : thermal diffusivity (m/s^2).

h : convective coefficient (W/ m^2 ºC)

i : specific enthalpy (J/kg).

l_{ts} : tubesheet thickness (mm).

$\dot{m}$: mass flow rate (kg/s).

t : time(s)

t_j : thickness of component j (m).

t^* : dimensionless time(-).

r : radial coordinate (-).

u : specific internal energy (KJ/kg).

y : vertical displacement (m).

z : axial coordinate (-).

Greek Symbols

α_t : thermal stress concentration factor (-).

α_m : pressure stress concentration factor (-).

β_t : linear thermal expansion coefficient (1/K).

θ : rotation angle (rad), circumferential coordinate (-).

ν : Poisson's ratio (-).

ρ : density (kg/m^3).

α_t : stress (MPa).

ψ : U-tube stress concentration factor (-).

Subscripts

0 : nominal conditions.

ave : average.

atemp : attemperator.

b : bending.

cyl : cylinder.

d : drum.

dc : downcomer.

h : head.

i : inlet, inner

m : metal.

o : outlet, outer.

r : riser.

rec : recirculated.

s : shell.

sa : salt.

sat : saturated.

st : steam.

su : surface

t : tube, thermal.

tp : tube pitch.

ts : tubesheet.

w: water.

4.7. References

[1] Usaola J. Operation of concentrating solar power plants with storage in spot electricity markets. IET Renew Power Gener 2012;6:59. doi:10.1049/iet-rpg.2011.0178.

[2] Mehos M, Turchi C, Vidal J, Wagner M, Ma Z, Ho C, et al. Concentrating Solar Power Gen3 Demonstration Roadmap 2017.

[3] Pelagotti L, Sørensen K, Condra TJ, Franco A. Modelling of a Coil Steam Generator for CSP applications 2014.

[4] Ferruzza D, Topel M, Basaran I, Laumert B. Start-Up Performance of Parabolic Trough Concentrating Solar Power Plants. SolarPACES Conf Procedings 2016.

[5] Benato A, Bracco S, Stoppato A, Mirandola A. LTE: A procedure to predict power plants dynamic behaviour and components lifetime reduction during transient operation. Appl Energy 2016;162:880–91. doi:10.1016/j.apenergy.2015.10.162.

[6] TEMA, Standards of the tubular exchangers manufacturers association, 9th ed. Tubular Exchanger Manufactures Association, 2007.

[7] American Society of Mechanical Engineers. ASME boiler and pressure vessel code, Section VIII 2010.

[8] Dzierwa P, Taler J. Optimum heating of thick wall pressure components of steam 2016:1–9.

[9] Reinhardt W, Kizhatil R, Mcclellan GH. Analysis of a Tubesheet Undergoing Rapid Transient 2016;122:476–81.

[10] Petrova N, Bouzid A-H. Deflections of A Multipass Shell-and-Tube Heat Exchanger Bolted Joint Subjected to Nonaxisymmetric Thermal Loading. J Press Vessel Technol 2012;134:11207. doi:10.1115/1.4004623.

[11] Li G, Zhao J. Design by Finite Element Analysis on Design by Finite Element Analysis on Tubesheet of Heat Exchanger with a Central Hole 2014:1–6.

[12] Kim TS, Lee DK, Ro ST. Analysis of thermal stress evolution in the steam drum during start-up of a heat recovery steam generator. Appl Therm Eng 2000;24:137–49. doi:10.1002/(SICI)1099-114X(200002)24.

[13] Mertens N, Alobaid F, Starkloff R, Epple B, Kim HG. Comparative investigation of drum-type and once-through heat recovery steam generator during start-up. Appl Energy 2015;144:250–60. doi:10.1016/j.apenergy.2015.01.065.

[14] Apros: advanced process simulation software 2017. http://www.apros.fi/en/ [accesed 08/07/2017].

[15] Schenk H, Dersch J, Hirsch T, Polklas T. Transient Simulation of the Power Block in a Parabolic Trough Power Plant. Proceeding 11 Th Int Model Conf 2015:605–14. doi:10.3384/ecp15118605.

[16] DYMOLA Systems Enginering: Multi-Engineering Modeling and Simulation bason on Modelica and FMI 2017. https://www.3ds.com/products-services/catia/products/dymola/ [accesed 08/07/2017].

[17] Sandia Natl. Lab., Molten Salt Receiver Subsystem Research Experiment Phase 1 - Final Report, Volume 1. Foster Wheeler Solar Development Corporation, Sandia Natl. Lab. Report SAND82-8179 1984.

[18] ABB. Power Generation Energy Efficient Design of Auxiliary Systems in Fossil-Fuel Power Plants 2009:358.

[19] Pacheco JE. Final Test and Evaluation Results from the Solar Two Project, Sandia Natl. Lab. Report, SAND2002-0120 2002.

[20] European Standard EN12952-3. Water-tube Boiler and Auxiliary Installations - Part 3: Design and Calculation for Pressure Parts 2001.

[21] González-Gómez PA, Gómez-Hernández J, Briongos JV, Santana D. Thermo-economic optimization of molten salt steam generators. Energy Convers Manag 2017;146:228–43. doi:10.1016/j.enconman.2017.05.027.

[22] González-Gómez PA, Gómez-Hernández J, Briongos JV, Santana D. Evaporator optimization for solar tower power plants. 10º edición del Congr. Int. Ing. Termodin., 2017.

[23] Moore R, Vernon M, Ho CK, Siegel NP, Kolb GJ. Design considerations for concentrating solar power tower systems employing molten salt, Sandia Natl. Lab. Report, SAND2010-6978, 2010.

[24] Alobaid F, Karner K, Belz J, Epple B, Kim H-G. Numerical and experimental study of a heat recovery steam generator during start-up procedure. Energy 2014;64:1057–70. doi:10.1016/j.energy.2013.11.007.

[25] Rayaprolu K. Boilers for Power and Process 2009.

[26] Mishra IB. Training Manual On CFBC Boilers 2012.

[27] González-Gómez PA, Petrakopoulou F, Briongos JV, Santana D. Steam Generator Design for Solar Towers using Solar Salt as Heat Transfer Fluid. SolarPaces Conf 2016.

[28] Ansari MR, Mortazavi V. Simulation of dynamical response of a countercurrent heat exchanger to inlet temperature or mass flow rate change. Appl Therm Eng 2006;26:2401–8. doi:10.1016/j.applthermaleng.2006.02.015.

[29] Serth RW, Lestina TG. Process Heat Transfer: Principles, Applications and Rules, 2014.

[30] Taborek J. Shell and Tube Heat Exchangers: single phase flow. In Heat Exchanger Design Handbook. Hemisph Publ Corp 1983.

[31] Singh KP, Holtz M. A Method to Design Shell-Side Pressure Drop Constrained Tubular Heat Exchangers. Eng Power 1977:441–8.

[32] Astrom KJ, Bell RD. Drum-boiler dynamics. Automatica 2000;36:363–78.

[33] Holmgren M. X steam for Matlab 2006. www.x-eng.com .

[34] Taler J. A new method for optimum heating of steam boiler pressure components. Int J Energy Res 2007;31:135–47. doi:10.1002/er.

[35] Ando M, Hasebe S, Kobayashi S, Kasahara N, Toyoshi A, Ohmae T, et al. Thermal transient test and strength evaluation of a tubesheet structure made of Mod.9Cr-1Mo steel. Part II: Creep-fatigue strength evaluation. Nucl Eng Des 2014;275:422–32. doi:10.1016/j.nucengdes.2014.04.029.

[36] O'Donnell WJ, Langer BF. Design of perforated plates. J Eng Ind 1962;84:307–19. doi:10.1115/1.3667483.

[37] Timoshenko S. Theroy of Plates and Shells, McGraw-Hill Book Co. 1940.

[38] Incropera FP, Lavine AS, DeWitt DP. Fundamentals of heat and mass transfer 2011.

[39] Soler A, Caldwell SM, Singh KP. Tubesheet Analysis—A Proposed ASME Design Procedure. Heat Transf Eng 1987;8:40–9. doi:10.1080/01457638708962801.

[40] Shen J, Tang Y, Xu J, Liu Y. Strength and fatigue analysis of tubesheet subjected to thermal shock. Proc ASME 2016 2016:1–8.

[41] Barron RF, Barron BR. Design for Thermal Stresses 2012.

[42] Young WC, Budynas RG. Roark's Formulas for Stress and Strain. McGraw-Hill Book Company; 2002.

[43] Singh KP, Holtz M. On Thermal Expansion Induced Stresses in in U-Bends of Shell-and- Tube Heat Exchangers. Eng Power 1979;101:634–9.

[44] Zavoico AB. Solar Power Tower - Design Basis Document, Sandia Natl. Lab. Report, SAND2001-2100 2001.

[45] Kelly B. Lessons Learned, Project History, and Operating Experience of the Solar Two Project, Sandia Natl. Lab. Report SAND2000-2598 2000;1.

CHAPTER

FIVE

Dynamic analysis of the steam generator of parabolic trough power plants

Contents

5.1. Abstract 128

5.2. Introduction 128

5.3. Plant description 130

5.3.1. Tubine operation mode 132

5.3.2. SG control system 132

5.3.3. Start-up initial conditions 134

5.4. Methodology 134

5.4.1. Single phase flow heat exchangers 134

5.4.2. Two phase flow model for EV and steam drum 137

5.4.3. Steam drum and SH nozzle stress calculation 138

5.4.4. Tubesheet stress calculation 142

5.4.5. Tubesheet junction stress calculation 145

5.4.6. U-tube stress calculation 150

5.5. Results and discussion 151

5.5.1. SG daily start-up simulation 152

5.5.2. Stress analysis 154

5.5.3. Comparison between kettle and TEMA X evaporators 156

5.6. Conclusions 159

5.7. References 162

5.1. Abstract

The thermal stress on thick-walled components, such as tubesheets and steam drums, limits both the temperature ramp-up rates and the temperature differences between outer and inner walls. In addition, the cyclic operation of concentrating solar power plants leads to fatigue damage. For these reasons, a stress analysis of the steam generator is required to assure its lifetime.

This Chapter investigates the start-up of a steam generator designed for a parabolic trough power plant. For that purpose, three transient models for steam generator heat exchangers and steam drum are developed. The stress analysis is focused on critical parts of the steam generator based on shell-and-tube heat exchangers such: tubesheets, tubesheet junctions, head-nozzle junctions, steam drum-downcomer junction and U-bend regions. Moreover, three finite element simulations are carried out to compute the stress and compare it with the stress calculated by means of simplified analytical models.

The results show that U-tube tubesheets are exposed to high thermal stresses in the no-tube-lane zone, especially in the reheater. The steam generator start-up can be accomplished in around 45 minutes whereas the thermal energy required is 36.4 MWh_{th}. Lastly, the TEMA X recirculation evaporator presents a thermal stress reduction of 35% compared to kettle evaporator.

5.2. Introduction

Concentrating solar power (CSP) plants with thermal storage have become promising alternative to traditional power plants to generate electricity. To further enhance the participation of CSP plants in grid regulation services and increase the annual electricity production, it is necessary to increase their flexibility [1–3]. A critical component is the steam generator (SG), which provides the steam needed in the power block to meet the electricity demand. The steam generator (SG) of concentrating solar power (CSP) plants typically operates in a different way than the SG of conventional base-load power plants. The cyclic nature of the solar energy may lead to a high number of start-ups, shut-downs and load changes. This requires a thorough dynamic analysis to estimate the stresses in order to evaluate the fatigue damage produced by the cyclic operation. In this way, the stress estimation becomes critical to quantify the lifetime reduction on the SG components. As a result, an optimization of the CSP plant operation should take into account the revenues produced by an increment of the annual production and flexibility, and the increment of the costs by the maintenance and/or replacement of SG components.

Several studies can be found about the stress analysis of the start-up of conventional fired-boiler plants [4,5]. In these plants the steam drums and superheater (SH) headers are normally considered the most critical parts. The stresses of these components are typically estimated using EN 12952-3 [6] by means of simplified analytical models due to their relative low complexity of their geometry. For example, Taler et al. [7] developed an innovative method to optimize the start-up of fired-boilers focused on the steam drum stresses. This method consists of the construction of an analytic stress function of the steam drum by means of finite element analysis results. Then, the negative thermal stress, which compensates the positive pressure stresses, can be calculated by using the analytic function. As a result, a meaningful reduction of the start-up time is obtained. Similar studies about the dynamic behavior of heat recovery steam generators (HRSGs) of combined cycled plants (CCPs) are also available [8,9]. However, most of them are focused in the dynamic modeling and control, where the stress analysis are accomplished using simplified models or even omitted. As it occurs with conventional fired-boiler studies, the critical components considered in most of the works about HRSGs are the steam drum and superheater headers [10,11]. On the other hand, Casella et al. [12] performed a dynamic simulation of the start-up of CCP focusing on the stresses of the steam turbine. The results show a significant reduction of the start-up time by increasing the gas turbine load rates without any significant increment of the rotor stresses in the steam turbine.

Normally the SG of CSP plants are based on conventional shell-and-tube heat exchangers as was shown in previous Chapters [13,14]. Widely used methods for the heat exchanger design are TEMA standards [15] or ASME Section VIII div 1 [16], which consider continuous operation and do not include cyclic assessment and fatigue [17]. In addition, these standards do not address specific guidelines for the stress estimation of typical loads of a SG: thermal loads on U-tube tubesheets [14] and temperature gradients on the tubesheet junctions [18]. Therefore, in such cases it is convenient a finite element analysis in order to assure accurate results.

In recent years a significant effort has been made by many authors to study the dynamic modeling of CSP plants. For example, Hirsh et al. [19] analyzed the energy required for the start-up of the parabolic trough power plant (PTPP) focusing on the power block and solar field. Nevertheless, many technical constraints about the power block start-up (heating up evaporator and superheater, turbine synchronization,..) have not been considered yet. Ferruzza et al. [2] studied the impact on the yearly energy production of a PTPP for ramp-up rates on evaporator, superheater and turbine. The results showed that the optimal range evaporator ramp-up rates should be in the range from 7-10 K/min. However, the geometry of the SG components was not considered. Schenk et al. [20] performed a dynamic model of a

PTPP using Dymola/Modelica environment [21]. They optimized the thermal oil mass flow rate to be sent to the power block by minimizing the thermal energy required in the start-up. Although the technical constraints for the SG start-up are not explicitly shown, a detailed procedure explanation together with the time evolution of the main thermodynamic variables is available. Foster Wheeler [22] presented a study about the design and dynamic analysis of molten salt SG for SPTP. Control system details, several start-up and load-change procedures are described considering different scenarios.

In this Chapter a dynamic analysis of the SG start-up of PTPP is carried out. Dynamic models for heat exchangers TEMA F and H, and TEMA X recirculation evaporator with steam drum are developed. In order to reflect the technical constraints of the heat exchangers during the transient response, several analytical models are developed to estimate the stresses on their critical parts: tubesheets, tubesheet junctions, head-nozzle junctions, steam drum-downcomer junction and U-bend regions. The analytic stress models are validated using a finite element analysis software (ABAQUS/CAE software [23]). A PID control system is developed to guide the SG start-up. Finally, a stress analysis of the SG start-up is performed to check that the proposed procedure operates the SG within allowable ranges, comparing TEMA X recirculation and kettle designs for the evaporator.

5.3. Plant description

A PTPP layout similar to the commercial plant Andasol 1 is selected [24]. Figure 5.1 shows the plant layout with the main subsystems: solar field, storage system, steam generator (SG) and power block. In the solar field the parabolic collector concentrates the solar radiation to heat-up the thermal oil at around 393ºC. The solar field is sized to obtain a solar multiple of 2. The storage system is formed by two molten salt tanks (one cold and another hot). The storage system is sized to 7.5 hours of full load operation of the power block. The thermal energy of the thermal oil is transferred to molten salt in the oil-to-salt heat exchangers in charging mode. The flow direction is reversed in discharge mode.

The thermal oil is sent to the SG to produce the high and low pressure steams. The power block consists of a 55 MWe (gross) turbine with five closed feed-water heaters (2 high-pressure, 3 low-pressure) and a deaerator. The low-pressure turbine steam outlet is sent to the condenser where the heat is dissipated providing a pressure reduction. Table 5.1 shows the main design parameters of the SG and the power block.

Table 5.1: Power Block and SG design parameters.

Parameter	Value
Steam turbine power	55 MWe
Thermal oil inlet temperature	393 ºC
Thermal oil mass flow rate	593 kg/s
Thermal oil outlet temperature	293 ºC
Main steam temperature	377 ºC
Main steam mass flow rate	61.91 kg/s
Main steam pressure	10.6 MPa
Reheat steam temperature	377 ºC
Reheat steam mass flow rate	49.69 kg/s
Reheat steam pressure	18.3 MPa
Feed-water temperature	245 ºC
Condenser pressure	0.0078 MPa

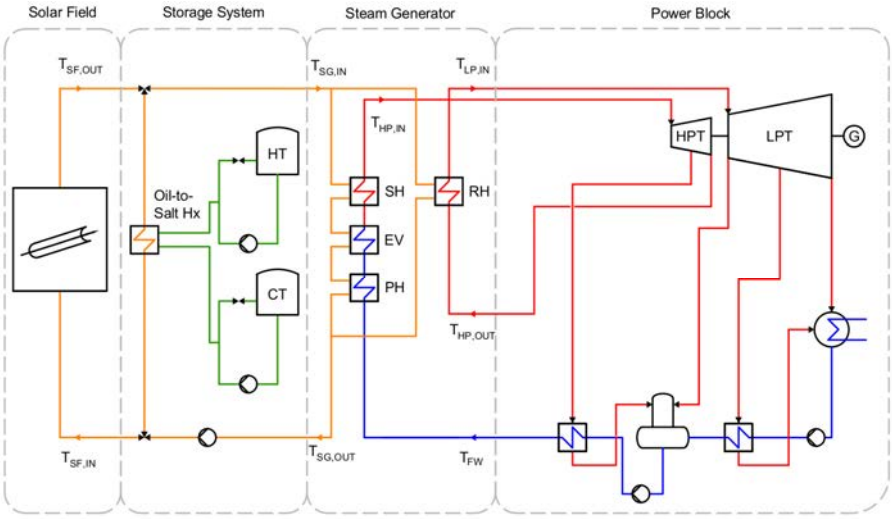

Figure 5.1: Schematic diagram of the PTPP considered.

The methodology presented in Chapter 2 is used to design the heat exchangers of the SG [13]. The SG is divided into two parallel trains each one formed by: SH, RH, EV and PH. The thermal oil is placed on the shell-side in SH, RH and PH whereas the high-pressure water/steam is placed on tube-side. In contrast, the EV flows are set in the opposite way. PH and SH consist of U-tube/TEMA H shell type heat exchangers. The TEMA H shell type is selected to provide very low pressure drops on shell-side,

leading to a considerable reduction in the power pump costs. RH consists of U-tube/TEMA F shell heat exchanger type. TEMA F shell type is selected to provide high thermal efficiency since the flows are set as a counter-current. Finally, a U-tube/TEMA X shell type recirculation evaporator with steam drum is selected for the EV. This design provides different advantages for CSP plants. Since the evaporator is divided in two TEMA X shell heat exchangers in parallel, the shell diameter is reduced decreasing the tubesheet and shell thicknesses considerably. Furthermore, the natural circulation system avoids the operational pump costs on shell-side. TEMA X shell provides very low pressure drops on shell-side due to the pure cross flow configuration. The high recirculation ratio avoids the potential fouling on the shell-side.

As a first option the material selected for the heat exchangers shell, tubesheet and head was SA-285-C [25]. However, the high thicknesses obtained led to selecting other material with higher allowable stress limit. The tube and steam drum materials are selected according to Refs. [14,26]. Finally, the materials selected for the SG are summarized in Table 5.2.

Table 5.2: Selected Materials for the main SG components.

Component	Shell, head and tubesheet	Tube
Preheater	A266, Gr. 2	A210, Gr. A1
Evaporator	A266, Gr. 2	A210, Gr. A1
Superheater	A266, Gr. 2	A210, Gr. A1
Reheater	A266, Gr. 2	A210, Gr. A1
Steam Drum	A516, Gr. 70	-

5.3.1. Power block model

The power block transient performance is modeled as series of steady-state conditions of different loads. The model provides the temperature, mass flow rate and pressure of the main inputs of the SG: the feed water and reheat inlet steam. The model also calculates the turbine power output.

5.3.2. SG control system

A control system is developed to model the dynamic response of the SG during the start-up operation. This control scheme is based on the control system proposed in Chapter 4. In Figure 5.2 a simplified scheme of the control system is illustrated. A PID control is selected to guide the start-up process. It should be taken into account that the control systems have a great relevance on the dynamic response the SG [28],

therefore the controller parameters (proportional and integral) are calculated to obtain realistic response velocities.

The SH and RH outlet steam temperatures are kept under the feasible temperature range by means of the attemperation control loop. This is made to assure the safe operation of the steam turbine. The RH attemperation system is placed at the inlet to avoid wet steam [29]. Moreover, the attemperator flow from the steam drum is limited to 8% of the total flow [29]. A SH and RH thermal oil by-pass control loop works to keep the energy balance and avoid the raising of the outlet steam temperatures. The excess of thermal oil is sent to EV. If the turbine synchronization is not completed, the steam drum pressure increases and must be regulated by the steam by-pass line to deaerator. When the turbine synchronization is completed, the turbine operation is set to sliding pressure mode and the steam drum pressure is regulated by the steam mass flow inlet. Lastly, the steam drum level is regulated by means of a proportional controller that sets the feed-water mass flow inlet into the SG.

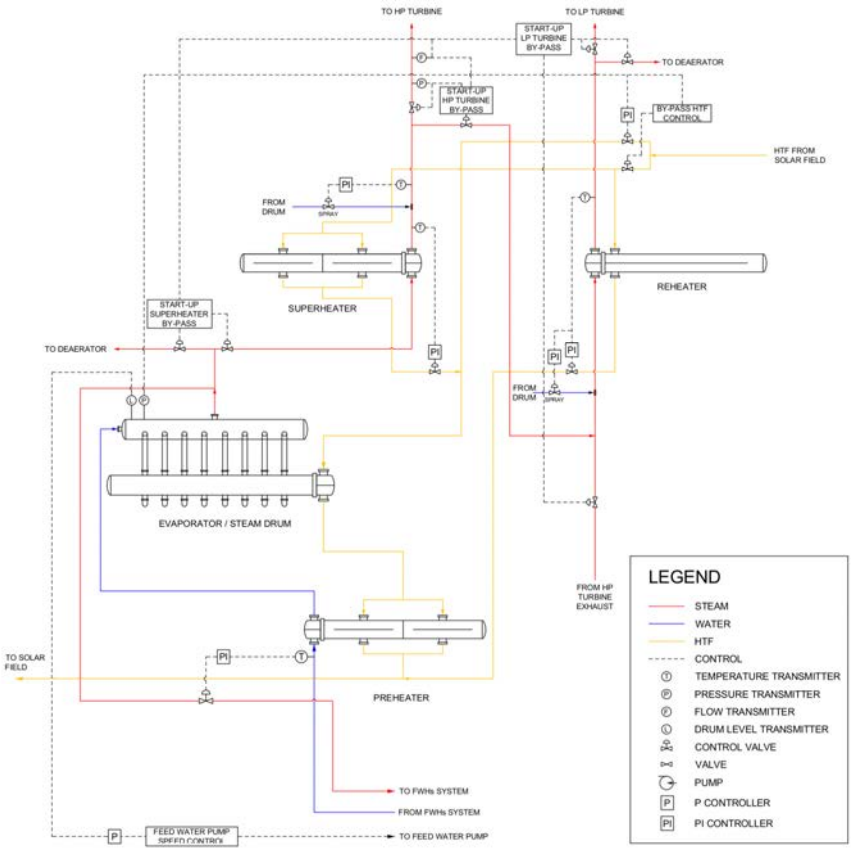

Figure 5.2: Schematic of SG and control system.

5.3.3. Start-up initial conditions

In CSP plants, the heat transfer fluid is typically circulated into the SG during the night shutdown [30]. Among other reasons, this procedure provides the energy required to heat-up the feed-water necessary to keep the steam drum level, which has decreased during the night because of the pressure relief valves and the water blowdown process. In this Chapter, this methodology is also used and it is assumed that the thermal oil circulates during the night. As a result, an isothermal initial condition is assumed for the heat exchangers of SG.

5.4. Methodology

5.4.1. Single phase flow heat exchangers

- **TEMA F transient model for RH**

A TEMA F shell-type heat exchanger is used for RH. An energy balance for one cell is made to evaluate its transient response. The following assumptions are made: the conduction wall resistance is negligible in comparison with the convection resistance, the longitudinal conduction of the tube wall is neglected, the heat losses to the ambient are not considered, there is no leakage of fluid or heat through or around the horizontal baffle and the heat transfer coefficient of both fluids are constant in each cell. As a result, TEMA F shell is modeled as a counter-current heat exchanger. Then, the energy balance can be expressed as follows:

$$D_{HTF}\frac{\partial T_{HTF}}{\partial t}+L_{HTF}\frac{\partial T_{HTF}}{\partial x}+T_{HTF}=T_m \tag{5.1}$$

$$D_m\frac{\partial T_m}{\partial t}+T_m=\frac{\alpha_{HTF}\,A_{HTF}T_{HTF}+\alpha_{st}\,A_{st}\,T_{st}}{\alpha_{HTF}\,A_{HTF}+\alpha_{st}\,A_{st}} \tag{5.2}$$

$$D_{st}\frac{\partial T_{st}}{\partial t}-L_{st}\frac{\partial T_{st}}{\partial x}+T_{st}=T_m \tag{5.3}$$

where $L=\dfrac{C\dot{m}}{\alpha A}$ is the characteristic length and $D=\dfrac{\rho C A_c}{\alpha A}$ is the characteristic time. The equations system is solved numerically by implicit finite difference method. The validation of the finite difference model is carried out by using the analytical

model results proposed by Ansari an Mortazavi [31] (see Figure 4.4). The analytical method consists of the analytical solution of the Equations 5.1 and 5.3 considering a first order model for the metal wall.

- **TEMA H transient model for SH and PH**

A TEMA H shell heat exchanger is used for SH and PH. A schematic of the TEMA H shell can be shown in Figure 5.3-a. It can be seen that the TEMA H shell can be divided into 8 sections, where each one can be classified as counter-current or co-current heat exchanger. A transient model is proposed to describe the heat exchanger following the approach shown for RH for counter-current. Different compatibility temperature equations are added to joint counter-current and co-current parts of TEMA H heat exchanger. A discretization scheme of the TEMA H shell heat exchanger is shown in Figure 5.3-b.

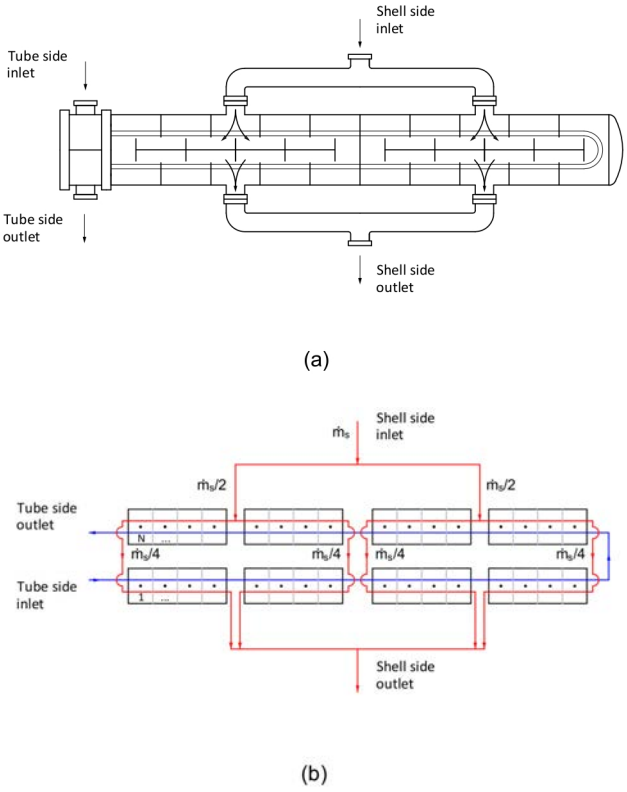

Figure 5.3: Schematic TEMA H shell heat exchanger.

A comparison of the transient responses of the outlet temperatures between the TEMA F and TEMA H shell against an inlet temperature step for different wall capacities is shown in Figure 5.4. As can be seen, the TEMA H shell has a slightly faster response on the outlet temperature of the hot fluid compared to TEMA F shell, whereas the transient response on the cold fluid is slightly slower. A higher difference is obtained on the steady-state outlet temperatures. This makes sense since the thermal efficiency of the TEMA H is lower than the TEMA F. Note that TEMA F shell is considered as a pure counter-current heat exchanger in this Chapter.

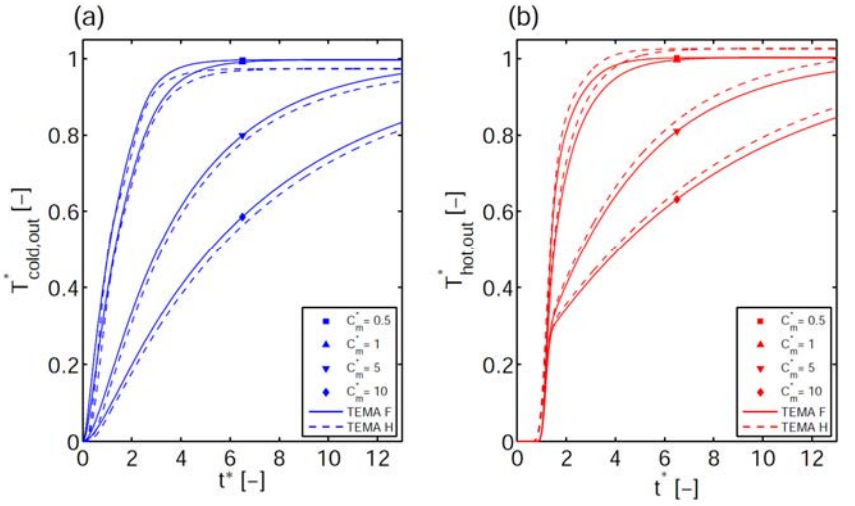

Figure 5.4: Transient responses of the outlet temperatures of the TEMA F and TEMA H shell against an inlet temperature step for different wall capacities.

Note that neither experimental data nor mathematical models have been found to validate the transient response of the TEMA H shell. For this reason, a steady-state heat duty balance between the hot and cold fluids is made to validate the model, obtaining a difference less than 1e-1 W. Moreover, the steady-state temperature has a close fit to the outlet design temperatures. The steady-state temperature profiles of the SH are shown in Figure 5.5, where it can be easily check the counter-current and co-current flow paths formed in the TEMA H shell.

The heat exchangers are discretized along their tube length at least to the baffle spacing (Table 2.3). The time step is calculated to assure that the Courant number is less than 1. The properties of both fluids are calculated on each time step. The heat transfer coefficient on the water/steam side is calculated using Gnielisnki correlation [32]. The heat transfer coefficient on the shell-side is corrected considering the shell mass flow ratio to the power of 0.6 [33]. The heat transfer coefficient in nominal

conditions is calculated taking into account two different zones: (i) cross-flow zone, in which is calculated according to Colburn correlations [34]; (ii) window zone, in which is calculated using the correlation proposed by Singh et al. [35].

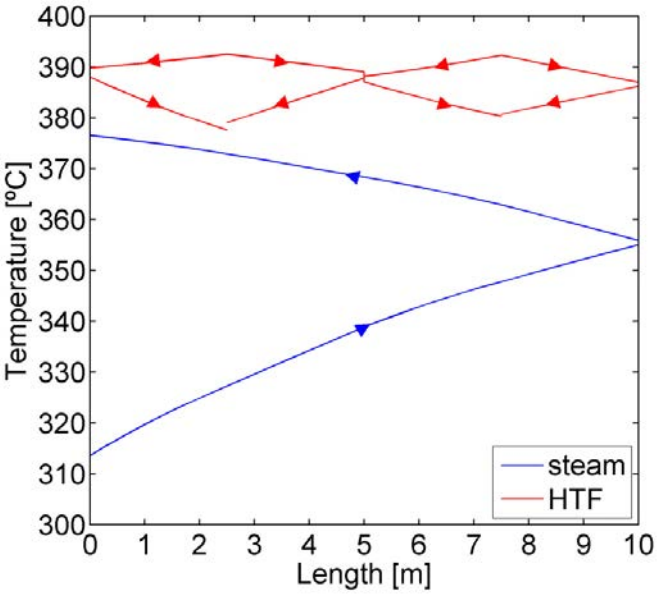

Figure 5.5: Steady-state temperature profiles of the SH.

5.4.2. Two phase flow model for EV and steam drum

EV and steam drum are modeled according to [36,37]. The model considers the inertia of the water/steam mixture and the metal mass. Moreover, the model also assumes that the metal wall temperature of the evaporator and steam drum is equal to the saturation temperature of the steam/water mixture. The mass and energy balances in the control volume on the evaporator-drum lead to Equations 5.4, 5.5 and 5.6. The fluid properties are calculated using XSteam tool [38].

$$\frac{d(\rho_w V_w)}{dt} + \frac{d(\rho_{st} V_{st})}{dt} = \dot{m}_w - \dot{m}_{st} \tag{5.4}$$

$$\frac{d(\rho_w V_w u_w)}{dt} + \frac{d(\rho_{st} V_{st} u_{st})}{dt} + M_{ev} C_m \frac{d T_{m,ev}}{dt} = \dot{m}_w h_w - \dot{m}_{st} h_{st} + \dot{m}_{HTF} h_{HTF,i} - \dot{m}_{HTF} h_{HTF} \tag{5.5}$$

$$\dot{m}_{HTF} h_{HTF,i} - \dot{m}_{HTF} h_{HTF,o} = \alpha_{HTF,ev} A_{ev} (\overline{T}_{HTF,ev} - T_{m,ev}) \tag{5.6}$$

The model presented above allows the calculation of the transient response of the pressure and the total water volume although, in order to estimate the steam drum water level, it is necessary two additional equations [36]. On the one hand, the first equation is obtained by an energy balance in a volume control located in the tube bundle of EV under the assumption of a linear distribution of the steam mass quality along the path of the two-phase flow for the tube bundle. On the other hand, the second equation is obtained from a mass balance for the steam under the liquid level. As a result, the model can be expressed by means of four equations which are solved by using a fourth order Runge-Kutta scheme. A time step of 1 second is used to ensure the numerical stability. An example of open loop response of the evaporator and steam drum model against a step of 10 kg/s on the outlet steam is shown in Figure 5.6. This operation is usually used in the practice when the steam drum valve is slightly opened and set it in a new position. As can be seen in Figure 5.6-a, the pressure starts to drop when valve opening take places. This effect is explained by using the global mass balance equation, from which a pressure drop is obtained by the reduction of the steam mass stored in the steam drum. Nevertheless, a more complex effect is obtained in the transient response of the steam drum level. Firstly, a suddenly increment of the steam drum water level is obtained due to the increase of the volume of the steam dissolved in the saturated water. This increment of the steam volume is produced by the decrease of the density of the saturated steam because of the pressure drop. Secondly, the steam drum level starts to drop due to the loss of the steam dissolved in the saturated water.

5.4.3. Steam drum and SH nozzle stress calculation

Typically, in conventional boilers the most limiting factors are the thick-walled components such as the SH headers, the steam drum and the T-junctions of pipelines [39]. The European standard EN 12952-3 [6] presents a methodology to calculate the thermal and mechanical stresses in the aforementioned components. This standard proposes analytical correlations to calculate thermal and mechanical stress concentration factors for a wide range of geometries of T-junctions, which are very useful to avoid tedious finite element analysis. The stresses are calculated as the sum of thermal and pressure stresses according to Equation 5.7.

$$\sigma = \sigma^{P} + \sigma^{T} = \alpha_{m} \frac{D}{2\,t_{j}} P_{j} + \alpha_{t} \frac{\beta_{t} E}{1-\nu} (T_{ave} - T_{su}) \tag{5.7}$$

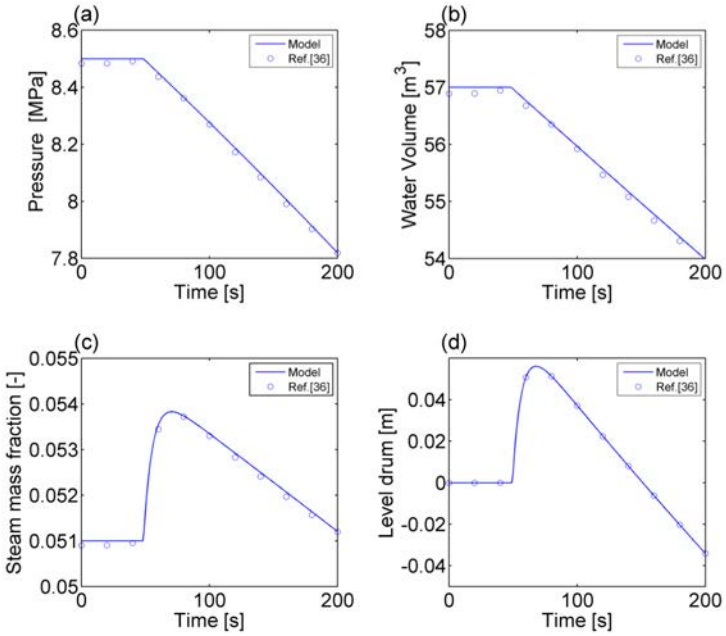

Figure 5.6: Response of the system for a steam mass flow step of 10 kg/s: a) steam drum pressure; b) total water volume; c) evaporator outlet steam mass fraction; d) steam drum level.

where T_{ave} is the metal average temperature and T_{su} is the inner surface temperature. The thermal stress concentration factor α_t, is mainly a function of the working fluid (steam or water) and the diameter ratio between the main component and the outlet/inlet pipeline. The mechanical concentration factor α_m, depends on the ratio between the diameter and thickness of the main component and the outlet/inlet pipeline. Normally, the stress on a T-junction is calculated on the point that presents the greatest stresses, P_1 (Figure 5.7). However, during the start-up, the most limiting stress can be obtained in P_2 (Figure 5.7) [39]. For this reason, in this Chapter the stresses on T-junction are calculated on both points.

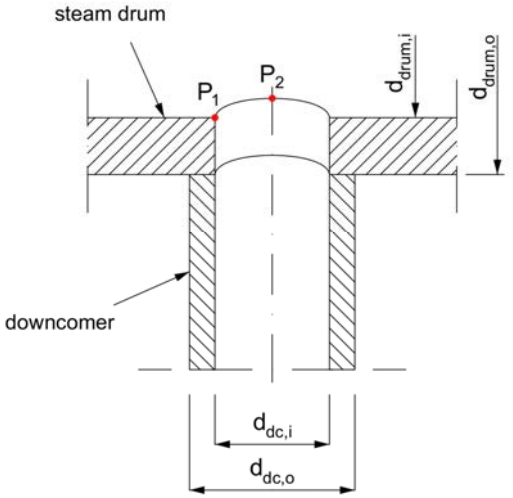

Figure 5.7: Selected points for stresses calculation of the steam drum-downcomer junction.

The temperature field along the radial coordinate is calculated by means of the thermal model described by Equation 5.8, which calculation details are shown in Chapter 4. When the temperature field is known, the average metal temperature, T_{ave} is calculated according to [37]. It is worth to mention that this model takes into account the heat transfer coefficient in the inner wall, which undergoes a great variation during the start-up.

$$\begin{aligned} &\frac{1}{r}\frac{\partial}{\partial r}\left(r\frac{\partial T}{\partial r}\right)=\frac{1}{a}\frac{\partial T}{\partial t} \\ &T(r,0)=T_0 \\ &-k\left.\frac{\partial T}{\partial r}\right|_{r=r_i}=h_j(T_j(t)-T(r_i,t)) \\ &\left.\frac{\partial T}{\partial r}\right|_{r=r_o}=0 \end{aligned} \tag{5.8}$$

Nevertheless, the normative EN 12952-3 [6] may lead to conservative results [40]. For this reason finite element analysis (FEA) using ABAQUS/CAE software [23] is carried out to estimate the stresses with high accuracy. The FEA is built with element type C3D20RT (20-node thermally coupled brick, triquadratic displacement, trilinear

temperature and reduced integration). Figure 5.8 shows the FEA results obtained in SH head-nozzle T-junction for pressure and thermal load under nominal conditions. The boundary conditions used are: i) zy plane symmetry condition (the displacement and rotation are fixed on zy plane, and z and y directions, respectively); ii) xy plane symmetry condition; iii) the displacement on y direction is fixed on the nozzle top; iv) pressure load on the end cap.

Table 5.3 compares the results obtained by FEA and the analytical method. As can be seen, the stresses are slightly overestimated at the P_1 using Equation 5.7. The stress on P_2 is calculated assuming an infinite plate according to [41], since the concentration factors for P_2 are not available in the normative EN 12952-3 [6].

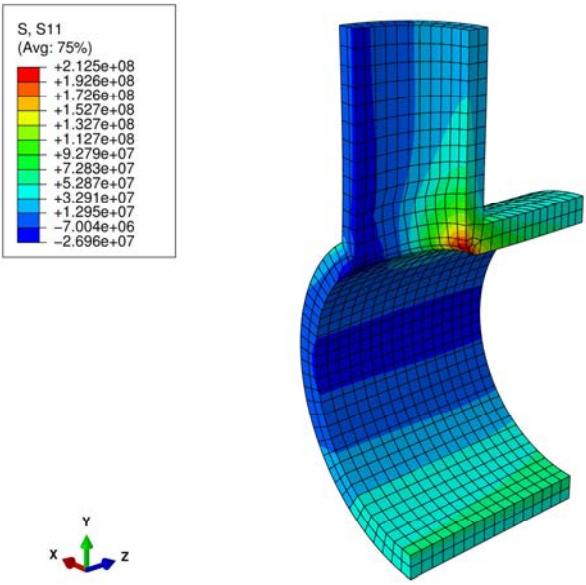

Figure 5.8: FEA results obtained in SH head-nozzle T-junction.

Table 5.3: Comparison between analytical and FEA results obtained in SH head-nozzle T-junction.

Load	Point	Analytical, Maximum stress, (MPa)	FEA, Maximum stress, (MPa)
Pressure and thermal	Point 1, Equation 5.7	230.3	212.5
Pressure and thermal	Point 2, Equation 5.7	-67.1	-26.9

5.4.4. Tubesheet stress calculation

The tubesheet is one of the most challenging components in the design of the conventional shell-and-tube heat exchanger. This is due to its complex geometry with a three-dimensional structure with holes and junctions with shell and head [42]. The tubesheet, as a part of the heat exchanger, is generally subjected to a combination of thermal and pressure loads that generate a complex stress state. Conventional methods to calculate the stress on tubesheet such TEMA standards [15] or ASME Section VIII-Division 1 [16] do not address specific guidelines for complex thermal loadings such as no-tube-lane thermal stresses. Thus, in order to consider the aforementioned effects and others, the method proposed by O'Donnell et al. [43] is used in this Chapter. In this method, the tubesheet stresses are calculated by means of the following steps. Firstly, the equivalent elasticity modulus and the equivalent poison ratio are calculated, which are mainly function of the ligament efficiency and tube pitch layout. Secondly, pressure or thermal stresses are calculated as an equivalent solid plate. Finally, the stress on the ligament is calculated by means of the stress concentration factor which is a function of the tubesheet geometry. The main equations for the tubesheet stress calculations proposed by O'Donnell et al. [43] are summarized in Table 5.4.

Table 5.4: Main equations for stress calculations proposed by O'Donnell et al. [43].

Load	Stress intensity	Equation
Pressure and thermal	Average across ligament at either surface of plate	$\sigma_{eff} = K\frac{R}{h}\lvert\sigma_1\rvert$ (5.9)
Pressure	Average across ligament and through thickness	$S_{eff} = \frac{R}{h}\left[\left(\frac{\Delta P r}{H}\right)^2 + \left(\sigma_r\right)^2\right]$ (5.10)
Pressure and thermal	Peak in ligaments	$\sigma_{\max} = Y\sigma_1 + P$ (5.11)
Pressure and thermal	Peak at perforations adjacent to rim	$\sigma_{\max} = K_r\sigma_{rim} + P$ (5.12)
Thermal (skin effect)	Peak at surface	$\sigma_{\max} = \frac{E\beta_t(T_{ave} - T_{su})}{1-\nu}$ (5.13)
Thermal (temperature difference across no-tube-lane zone)	Peak in ligaments	$\sigma_{\max} = \frac{K_u E^* \beta_t(T_H - T_C)}{2}$ (5.14)
Thermal (temperature difference across no-tube-lane zone)	Peak at holes adjacent to no-tube-lane zone	$\sigma_{\max} = \frac{K_D E \beta_t(T_H - T_C)}{2(1-\nu)}$ (5.15)

A two dimensional transient thermal model of the tubesheet ligament (Equation 5.16) is performed to calculate the surface wall temperate (T_{su}) and the average wall temperature (T_{ave}) necessary for Equation 5.13. The model considers three heat transfer boundary conditions on the ligament surface with a fluid contact and another additional symmetric boundary condition (see Figure 4.7).

$$\frac{1}{r}\frac{\partial}{\partial r}\left(r\frac{\partial T}{\partial r}\right)+\frac{\partial^2 T}{\partial z^2}=\frac{1}{a}\frac{\partial T}{\partial t} \tag{5.16}$$

The thermal stress presented in the no-tube-lane zone of the tubesheet is calculated using Equation 5.14 and Equation 5.15. However, the model proposed by O'Donnell et al. [43] does not take into account plane shears [44]. Therefore, such simplifications may lead to inaccurate results, especially at the interfaces of the perforated and solid regions of the tubesheet. In addition, it is observed that the RH has a great thermal difference in the no-tube-lane zone, which can generate high stresses.

A FEA model is performed for the RH to validate the analytical model developed. Due to the symmetry in geometry and loads only a sector of 180º is modeled including the shell and head junctions. In order to obtain realistic results the perforated holes of the tubesheet are included in the model. Figure 5.9 shows the temperature field of the FEA model considering the thermal and pressure loads at nominal conditions (the shell side temperatures are not considered). The boundary conditions used are: i) yx plane symmetry; ii) zx plane symmetry on the end cap of the head.

The comparison between the FEA and analytical stress results is summarized in Table 5.5. The results are obtained for nominal conditions. As can be seen, the stresses produced in ligaments near of the no-tube-lane zone are underestimated by the Equation 5.14 around 37.7% compared with the results obtained by FEA. In contrast, the stresses obtained in the holes adjacent to the no-tube-lane zone are overestimated for the Equation 5.15 compared with the FEA results. Figure 5.10 shows the FEA stress results in the tubesheet ligaments due to temperature difference across no-tube-lane. For the pressure load cases, the FEA results show that the stresses are overestimated between 30 and 40 % using Equation 5.9. Finally, as a result of the FEA of the RH it is expected that the stresses on tubesheet will be calculated on the safety side.

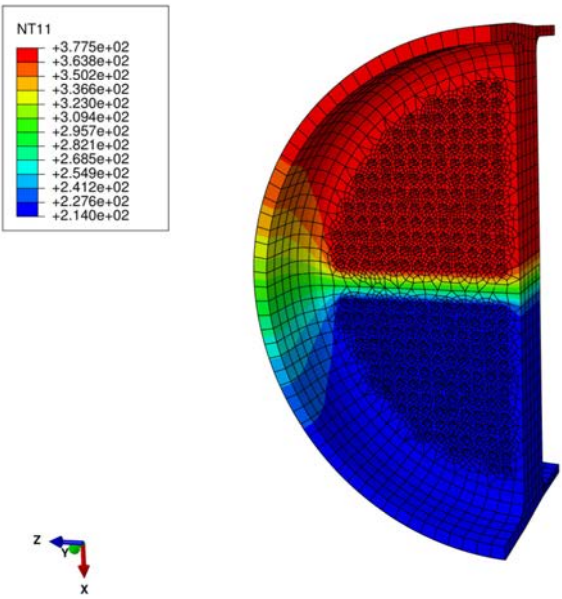

Figure 5.9: RH FEA temperature field results.

Table 5.5: Comparison between analytical and FEA results obtained for RH.

Load	Point	Analytical, Maximum stress, (MPa)	FEA, Maximum stress, (MPa)
Pressure	Ligament, Equation 5.9	57.1	42.7
Pressure	Rim zone, Equation 5.9	28.6	20.1
Thermal (temperature difference across no-tube-lane zone)	Peak in ligaments, Equation 5.14	320.7	263.4
Thermal (temperature difference across no-tube-lane zone)	Peak at holes adjacent to no-tube-lane zone , Equation 5.15	509.5	432.6

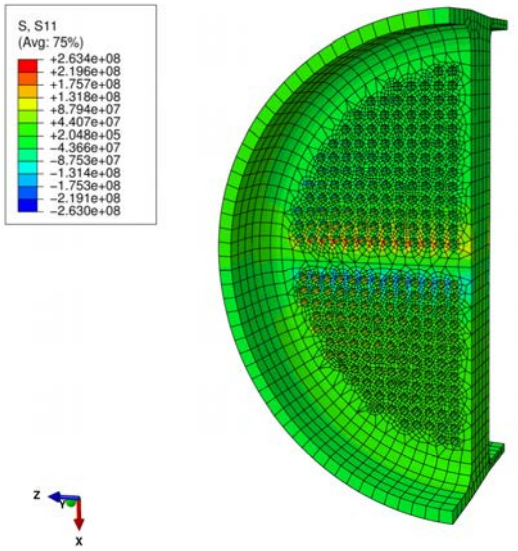

Figure 5.10: RH FEA stress results in ligaments due to temperature difference across no-tube-lane.

5.4.5. Tubesheet junction stress calculation

The ASME Pressure vessel code considers six possible junction configurations for U-tube tubesheets as a combinations of integral, gasketed and gasketed extended as a flange [16]. In this Chapter, an integral junction type is considered for both head and shell side. Although the tubesheet junction has a great relevance in the stress suffered on the tubesheet, TEMA tubesheet design method does not include the mechanical loading from the shell or the head walls [45]. However, ASME VIII div 2 [16] U-tube tubesheet design method takes into account these effects. It should be considered that the calculation procedure is tedious and oriented to design, and thus, another option is sought in order to reduce the calculations for the SG start-up simulation. A viable option consists in the development of a simplified analytical model of the head-tubesheet-shell junction. A schematic of the moment and forces in tubesheet junction is illustrated in Figure 5.11. Considering elastic conditions, the displacements and forces are related by the stiffnesses: $F_j = K_j\, x_j$ or $x_j = K_j^{-1} F_j = K'_j\, F_j$. Neglecting the thermal loads, the displacements of the shell and head, and the displacements of the tubesheet can be calculated using Equations 5.17 and 5.18, respectively.

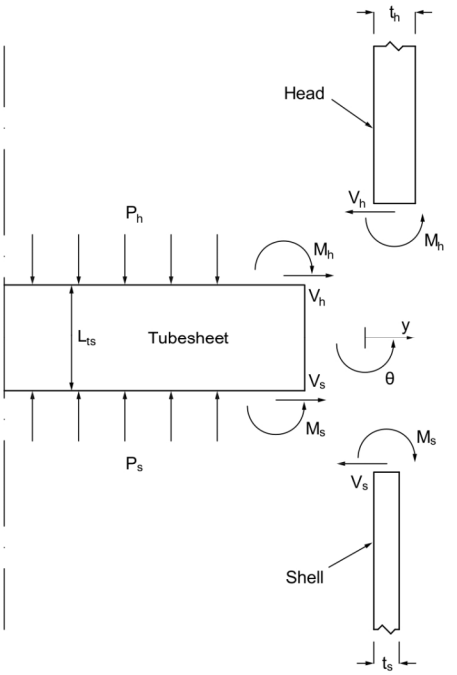

Figure 5.11: Force analysis on the tubesheet junction.

$$\begin{Bmatrix} y_h \\ \theta_h \\ y_s \\ \theta_s \end{Bmatrix} = \begin{bmatrix} K'_{cyl,My} & -K'_{cyl,Vy} & 0 & 0 \\ K'_{cyl,M\theta} & -K'_{cyl,V\theta} & 0 & 0 \\ 0 & 0 & -K'_{cyl,My} & K'_{cyl,Vy} \\ 0 & 0 & K'_{cyl,M\theta} & -K'_{cyl,V\theta} \end{bmatrix} \begin{Bmatrix} M_h \\ V_h \\ M_s \\ V_s \end{Bmatrix} + \begin{bmatrix} K'_{ciy,p} & 0 \\ 0 & 0 \\ 0 & K'_{cyl,p} \\ 0 & 0 \end{bmatrix} \begin{Bmatrix} P_h \\ P_s \end{Bmatrix} \tag{5.17}$$

$$\begin{Bmatrix} y_{ts,h} \\ \theta_{ts,h} \\ y_{ts,s} \\ \theta_{ts,s} \end{Bmatrix} = \begin{bmatrix} \frac{L_{ts}}{2}K'_{ts,My} & \frac{L_{ts}}{2}K'_{ts,Vy} & \frac{L_{ts}}{2}K'_{ts,My} & \frac{L_{ts}}{2}K'_{ts,Vy} \\ -K'_{ts,M\theta} & -K'_{ts,V\theta} & -K'_{ts,M\theta} & -K'_{ts,V\theta} \\ -\frac{L_{ts}}{2}K'_{ts,My} & -\frac{L_{ts}}{2}K'_{ts,Vy} & -\frac{L_{ts}}{2}K'_{ts,My} & -\frac{L_{ts}}{2}K'_{ts,Vy} \\ -K'_{ts,M\theta} & -K'_{ts,V\theta} & -K'_{ts,M\theta} & -K'_{ts,V\theta} \end{bmatrix} \begin{Bmatrix} M_h \\ V_h \\ M_s \\ V_s \end{Bmatrix} + \begin{bmatrix} -\frac{L_{ts}}{2}K'_{p,p\theta} \\ K'_{p,p\theta} \\ \frac{L_{ts}}{2}K'_{p,p\theta} \\ K'_{p,p\theta} \end{bmatrix} \{P_h - P_s\} \tag{5.18}$$

The stiffnesses for pressure loads of the shell and head are calculated as cylinders according to [41]. The stiffness of the tubesheet is calculated according to ASME VIII div 2 [16] considering the equivalent solid plate elastic properties modifications (Young modulus and Poisson's ratio). The stress calculation is carried out estimating: (i) the shear forces and moments using the compatibility of the displacements; and (ii) the stress in cylindrical coordinates according the Equation 5.19 [41]. An equivalent stress is calculated according to von Mises equation to consider the stresses in other directions [16].

$$\begin{Bmatrix} \sigma_z \\ \sigma_\theta \\ \tau_{rz} \end{Bmatrix} = \begin{Bmatrix} \dfrac{D^2 P}{4t(D+t)} \pm \dfrac{6M}{t^2} \\ \dfrac{2yE}{D} \pm \dfrac{6M\nu}{t^2} \\ \dfrac{V}{t} \end{Bmatrix} \tag{5.19}$$

The tubesheet junction stresses are normally calculated using FEA due to its complex geometry [42]. The analytical method proposed here is accurate for relations of $D/(2t_h) > 5$ and $D/(2L_{ts}) > 4$. As SH and PH are in the limit of the accurate range, it is convenient to compare the analytical model results with FEA. A SH FEA is performed using ABAQUS/CAE software [23]. The FEA is made in a similar way of RH model, using C3D20RT element type and assuming symmetry between geometry and loads to reduce the computational time. The perforated holes of the tubesheet are also included in the model. The boundary conditions used are the same that has been described in the RH model. Figure 5.12 shows the FEA results obtained for SH model considering only pressure load.

The comparison between the FEA and the analytical stress results of the SH tubesheet junction is summarized in Table 5.6. A pressure load of 10.6 MPa is applied on head side matching with the nominal conditions. As can be seen, the stresses produced in the head-tubesheet junction show that there is a good agreement between the analytical model (Equations 5.17 and 5.18) and FEA. The stress is underestimated by the analytical model by only 4% in the tubesheet junction at the no-tube-lane zone. However, the stresses obtained in the shell-tubesheet junction are overestimated by the analytical model.

An important shear stress point to take into account in SH junction is at the no-tube-lane zone. The stresses at this point are calculated using Equation 5.20. This equation is based on the theoretical solution presented by Slot [46] for a solid plate with a temperature difference between upper and lower half parts. The shear stress constant is equal to $K_\tau = 0.51$ at the junction with head and/or shell zone. This effect

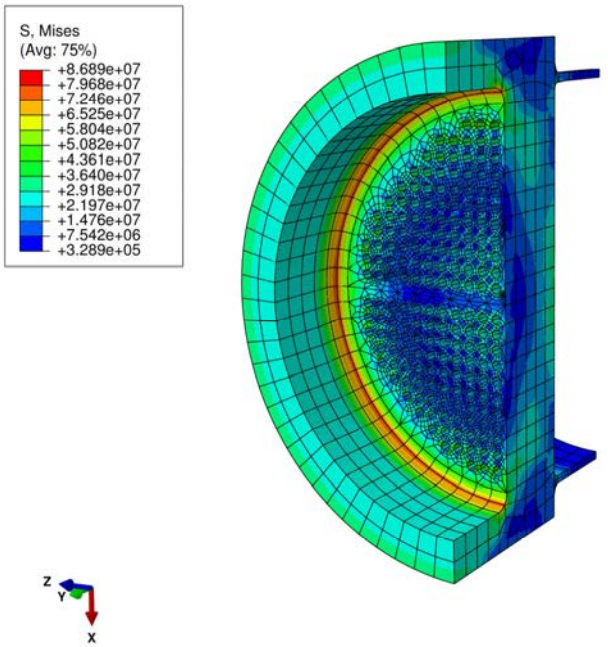

Figure 5.12: SH Tubesheet junction model.

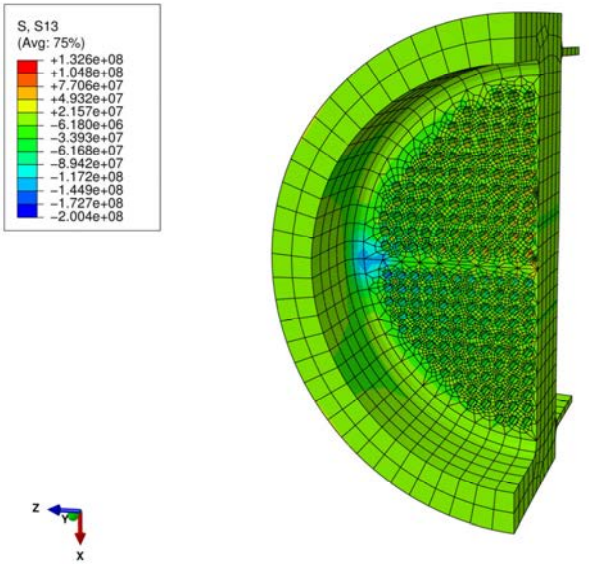

Figure 5.13: Stress results for tubesheet junction at no-tube-lane zone.

is also checked with FEA based on the SH model (Figure 5.13). The results show that the Equation 5.20 underestimates the shear stress by around 14 %.

$$\tau_{r\theta} = K_{\tau} \frac{(T_H - T_C)\beta_t E}{2} \tag{5.20}$$

Table 5.6: Comparison between analytical and FEA results obtained for SH tubesheet junction.

Load	Point	Analytical model, Equivalent stress, (MPa)	FEA, Equivalent stress, (MPa)
Pressure	Head-tubesheet junction, Equation 5.19	82.9	86.9
Pressure	Shell-tubesheet junction, Equation 5.19	29.8	25.6
Thermal	Tubesheet junction no-tube-lane, Equation 5.20	113.1	132.6

The tubesheet junction is formed by the joint of thick metal walls, especially for head and tubesheet. In this way, it is expected that the transient thermal stresses have a significant role on the tubesheet junction damage. For this reason, a two dimensional transient thermal model based on Equation 5.17 is performed to calculate the temperature field on the tubesheet junction. The model is built assuming axis-symmetric conditions. Convective boundary conditions are used for the surface with fluid contact: head, tube and shell. Insulation conditions are assumed for the external walls. Finally, uni-dimensional heat transfer conditions are assumed for the zones of head and shell far of tubesheet (see Figure 4.10). Details of the model calculation procedure are described in Chapter 4. In order to validate the model, a comparison between the analytical model and the SH FEA transient simulation temperatures is illustrated in Figure 5.14.

The heat transfer coefficient has a great influence on the surface wall temperatures, and similarly, the surface wall temperature has a great influence on the thermal stress. For this reason, a convenient estimation of the heat transfer coefficient could be interesting to obtain accurate results. However, the calculation of the heat transfer coefficient on the tubesheet junction surfaces for head or shell sides is very complex and it should be calculated by means of CFD simulations and/or experimentally. Since these options are out of the scope of this work, the following assumptions are used: the heat transfer coefficient on the tubesheet junction on shell-side wall is calculated as one order of magnitude lower than the cross flow on shell-side; the heat

transfer coefficient on the tubesheet junction on head-side wall is calculated as one order of magnitude lower than the heat transfer coefficient of the tube side.

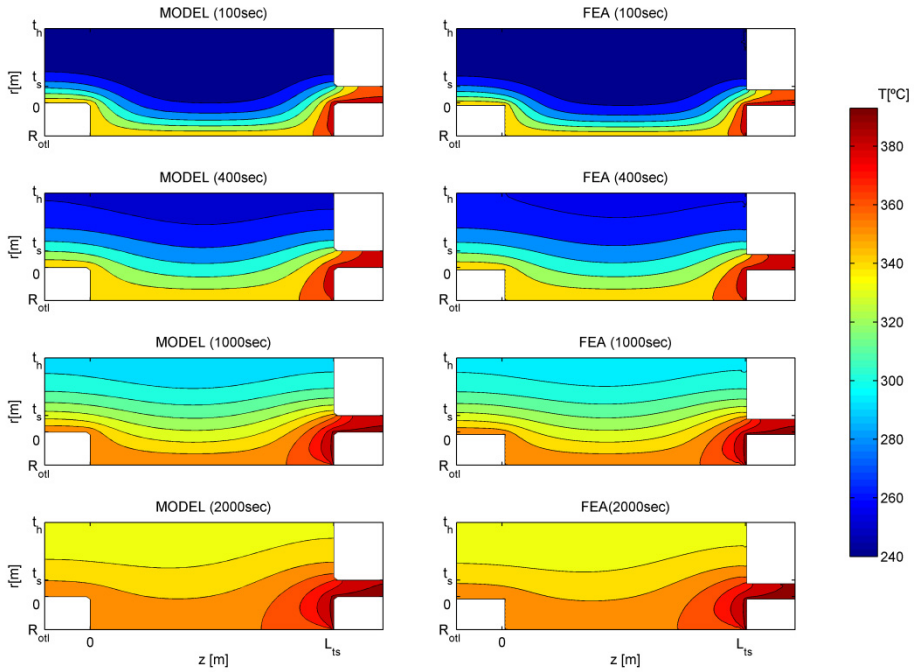

Figure 5.14: Comparison between the analytical model and FEA results obtained for SH.

Once the temperature field on tubesheet is known, the thermal stress is calculated for tubesheet-head junction according to [37], which considers only the radial thermal gradient. The thermal stress on tubesheet-shell junction is calculated according to Equation 5.14. Once the thermal stresses are calculated, they are combined with the mechanical stresses taking into account their corresponding sign. Then, the equivalent stresses are calculated using von Mises equation [16].

5.4.6. U-tube stress calculation

The U-tube design presents an economical solution to avoid the differential thermal expansion between tubes and shell. Another possible solution consists of using floating heads, which increases the heat exchanger cost by 10-20% [47]. However, the U-tube design presents some disadvantages: the mechanical tube

cleaning on the inlet side is difficult and the U-bend region presents a potential problem of vibrations on the outermost rows due to the long unsupported spam [48]. In addition, there is a differential thermal expansion between the hot and cold legs of the tube bundle [22].

The thermal stresses on U-tube due to the differential thermal expansion between cold and hot legs are calculated according to Singh et al. [49]. A linear equation system is built based on the relations between forces and moments with displacements and rotation angles, respectively. The calculation procedure is described in the following steps. Firstly, the tube is allowed to expand freely, where the displacement is calculated using Equation 5.21 considering the axial force $F = 0$. Secondly, the moment and forces are calculated using an iterative process to accomplish the compatibility of displacements. When the moments and forces are known, the moment law function, $M(\theta)$, can be calculated and then the stresses on U-bend are computed using the Equation 5.22.

$$\delta = (\overline{\beta_{hot}\Delta T_{hot}} - \overline{\beta_{cold}\Delta T_{cold}})L - \frac{2F}{AE}L \tag{5.21}$$

$$\sigma(\theta) = \frac{\psi\ M(\theta)\ r_o}{I} \tag{5.22}$$

It should be taken into account that the minimal U-bend radius is designed to not overpass the maximum allowable stress under nominal conditions. However, the thermal stresses on the U-bend are strongly related with the temperature profile of the heat exchangers. Since the temperature profiles change during the SG start, it is expected that the stresses change as well.

5.5. Results and discussion

The results of the dynamic analysis of the SG include:

- The analysis of the SG daily start-up assuming isothermal initial conditions.
- The stress analysis of the critical points of the SG such: tubesheets (see Figure 5.15) and T-junctions of the SG.
- The comparison of the dynamic response of two designs in the evaporator of the SG: TEMA X and kettle, during the start-up.

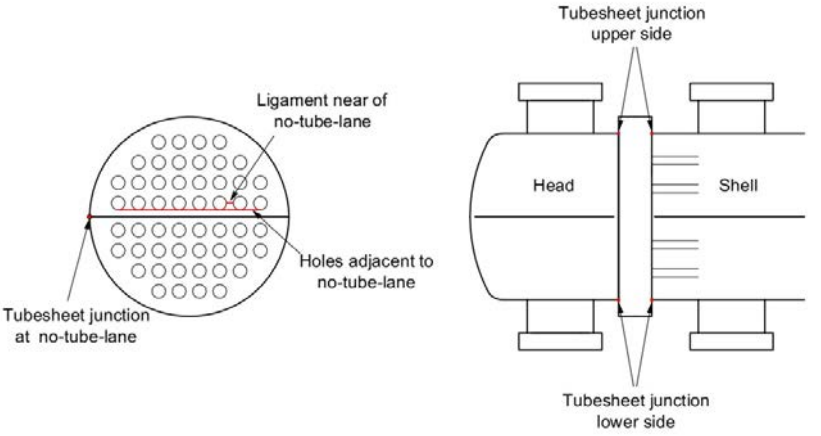

Figure 5.15: The five points selected for tubesheet stress analysis.

To carry out the dynamic study of the SG, a global script is built using the models described above allowing the estimation of the stress in real time. A global time step with higher size is selected to update the calculations of the models, which uses different time steps sizes.

5.5.1. Start-up simulation of the SG

A schematic of the start-up procedure is illustrated in Figure 5.16. Figure 5.17 shows the time evolution of the main thermodynamic variables during the start-up of the SG.

The dynamic analysis of the SG assumes that the storage system and/or solar field can provide the thermal oil inlet conditions to carry out the SG start-up. As mentioned before, isothermal initial conditions are considered for the SG heat exchangers, matching with the saturation temperature of the drum water (at around 240 ºC).

The thermal oil enters to the SG with a mass flow of 4% of its nominal value. The thermal oil is sent to the EV at 260 ºC (Figure 5.17-a), 20 ºC above to the saturation temperature of the drum water to avoid thermal shocks on thermal oil pipelines. The thermal oil also circulates through the PH. At the same time, the drum water ($T_d \approx 240$ ºC, Figure 5.17-c) circulates to heat-up the feed-water from the feed-water-heaters, which is assumed to be equal to 100 ºC at the beginning of the start-up. Then, the

feed-water enters to the PH at minimum temperature of 180 ºC to avoid potential thermal stresses in the tubesheet. Moreover, the steam generated is sent from the steam drum to the deaerator to heat-up the SG feed-water.

When around the 4% of the steam generation is produced, the thermal oil mass flow is sent to SH and RH. Now, the thermal oil mass flow is set to 5% of its nominal value with a temperature ramp-up rate of 8 ºC/min. The saturated steam from the steam drum is sent to the SH and the outlet steam is sent to the RH by the SH-RH by-pass line (Figure 5.2), where the attemperation system keeps the RH steam inlet temperature at around 250 ºC. The RH outlet steam is sent to the deaerator.

Around t = 20 min the SH and RH outlet steams achieves 320 ºC, which is the set point temperature at the inlet to start the turbine synchronization (Figure 5.17-b/d). The turbine inlet temperature is kept constant by using the attemperation system (Figure 5.2). The turbine synchronization takes around 8 min for a daily start-up [20].

After 28 min, the turbine synchronization is completed and the HP and LP steam inlet temperatures are increased to its nominal value (Figure 5.17-b/d). At the same time, the thermal oil mass flow ramp-up rate is set to obtain a ramp-up of 7 ºC/min in the evaporator. As a result, the steam drum pressure starts to rise. Since the turbine operation is set to sliding pressure mode, the steam mass flow increases as well.

After 45 min, full load conditions are achieved and the SG start-up is completed. The energy necessary to carry out the SG start-up is 36.4 MWh_{th}.

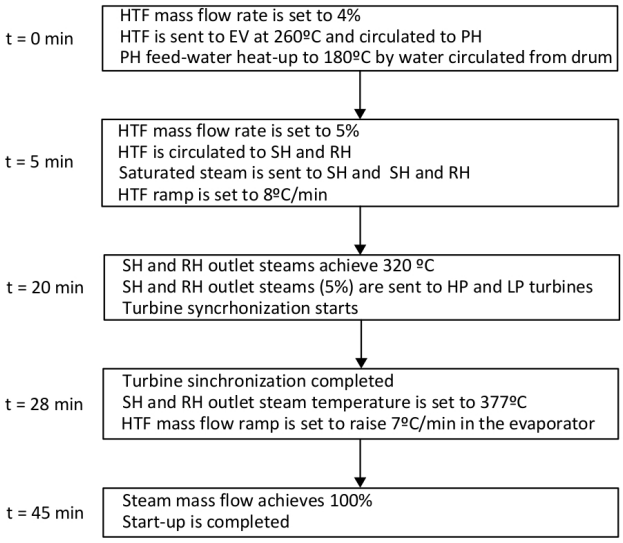

Figure 5.16: Schematic of the procedure of the start-up.

5.5.2. Stress analysis

According to the ASME code [50] the material lifetime is mainly reduced by two damage mechanisms: fatigue and creep. The fatigue damage is related to the magnitude of the stress cyclic variations, and the number of cycles to failure is computed as a function of the equivalent strain range. The creep damage is a function of the stress level and the temperature [51].

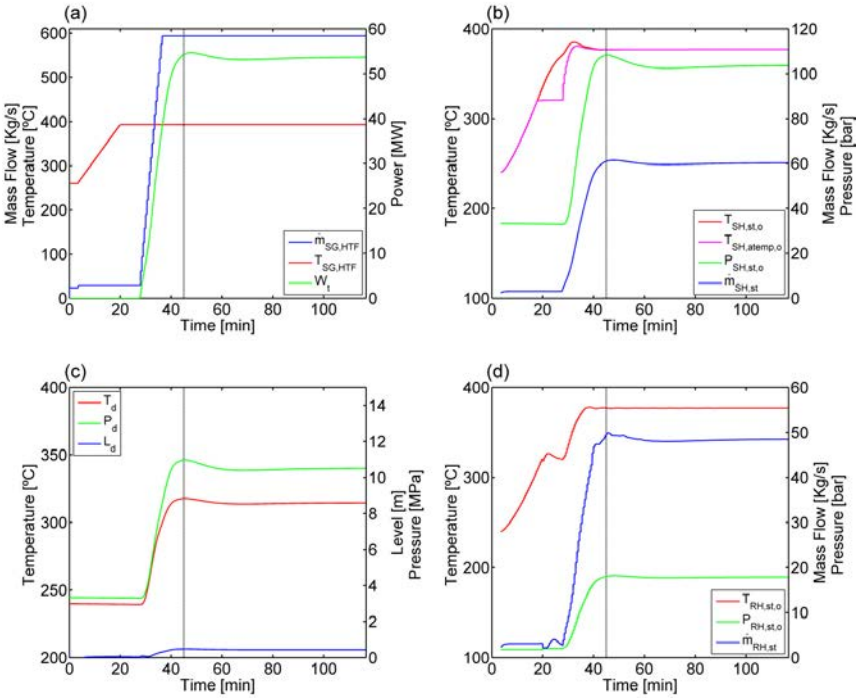

Figure 5.17: Daily start up simulation: a) thermal oil temperature and mass flow rate, turbine power output; b) SH performance; c) steam drum performance; d) RH performance.

The assessment against failure for cyclic loads is normally accomplished by fatigue analysis. However, a previous step should be considered according to ASME VIII div2 [16], where the maximum stress should be limited against ratcheting failure. In this way, the protection against ratcheting considering an elastic stress analysis should be accomplished by using this limitation: $\Delta S \leq S_{PS}$. If this limitation is not satisfied, a complex elastic-plastic analysis should be carried out [44]. The alternating stress ΔS is calculated considering primary membrane, primary bending and secondary stresses ($P_L + P_b + Q$). This means that the stresses due to local structural

discontinuities, i.e. the peak stresses (F) are not considered in this analysis. For this reason, the stresses concentration factors are not used in the stress analysis presented below.

The maximum allowable equivalent stress S_{PS} is calculated as the highest value between: i) three times the ASME VIII div 1 allowable stress limit S; ii) two times the yield stress of the material S_y. This limitation is imposed for the tubesheet and U-tube stress calculations.

In case of EN 12952-3 [6] the maximum stress is limited to avoid damage of the protective magnetite layer on the metal wall of the component. The maximum allowable stress is calculated 200 MPa above to the tangential pressure stress at nominal operating conditions: $\sigma_{a,\max} = \sigma_{\theta,p_o} + 200$. The minimum allowable stress is 600 MPa bellow to the tangential pressure stress at nominal operating conditions: $\sigma_{a,\min} = \sigma_{\theta,p_o} - 600$. As already mentioned, the stress calculations in the drum downcomer junction and SH head nozzle junction are made using EN 12952-3 [6] and therefore this limitation is imposed for this components.

Figure 5.18 shows the results of the stress analysis of the SG during the start-up. The vertical line at t = 45 min points out the end of the start-up process while the horizontal line identifies the maximum allowable stress. As can be seen, the stress evolution in all the components is in suitable stress ranges according to the aforementioned limits.

According to the stress nature, two stress groups can be identified. The first group considers the stress points where the thermal inertia are more significant, i.e. when the difference between the wall surface temperature and the average wall temperature are relatively high and this difference decay temporally. This group is formed by the following junction points: tubesheet-head, the tubesheet-shell, the steam drum-downcomer and SH head-nozzle (Figure 5.18-b/c/g/h). This group is more susceptible to high thermal stresses due to temperature ramp-up rates, and therefore establishes the minimum start-up time.

The second group considers the stress points where the thermal inertia can be neglected and then the stress can be estimated using the temperature and pressure states. This group is formed by the tubesheet ligaments, the tubesheet no-tube-lane zone (junction and near of holes) and the U-bend region (Figure 5.18-a/d/e/f).

During the daily start-up, the highest stress value is obtained on the U-bend in the SH (Figure 5.18-f). Nevertheless, this value does not represent any limitation since this stress can be easily reduced increasing the U-bend radius and/or the clearance in the last baffle. It is important to take into account that the U-bend radius design was

accomplished considering nominal operation conditions and for this reason the resulting stresses on the SH U-bend reach the safety value of 0.3 UTS.

The most limiting stresses are obtained in the tubesheet ligaments and the no-tube-lane zone (Figure 5.18-a/d). The most stressed point of the tubesheet ligament is obtained for RH in the point of high pressure at the end of the start-up. It is worth to mention that the ligaments that present the highest stress are those located near of the no-tube-lane (Figure 5.15). In contrast, the most stressed point in the no-tube-lane zone is obtained for the RH in nominal conditions, when the high temperature difference between the tube inlet and outlet is reached (Figure 5.18-d).

The most stressed points belong to the second group, in which thermal inertia can be neglected, pointing that higher temperature ramp-up rates could be used in the SG start-up. However, the temperature ramp-up rate selected for the thermal oil inlet (8 ºC/min) is very high compared with the literature data [19,20]. Therefore, an increment of the temperature ramp-up rate is considered as an unrealistic scenario.

In case of the evaporator ramp-up rate of 7 ºC/min is selected. It can be considered in the optimal range of the ramp-up rates suggested by Ferruzza et al. [2]. This means that higher evaporator ramp-up rates may not lead to a significant increment of the annual energy production.

The high thermal stresses obtained in the RH even under design conditions (Figure 5.18-d) suggest that the TEMA F design is susceptible to fatigue cycle failure. Therefore, another possible design option can be the U-shell/U-tube heat exchanger. Since this design has two tubesheets, the stresses in the no-tube-lane are eliminated. Another possible option consists of splitting the RH in two heat exchangers in series, reducing the temperature difference in the tubesheet. This design option is proposed by Aalborg CSP [52].

5.5.3. Comparison between kettle and TEMA X evaporators

Kettle evaporators have been used in pioneering parabolic trough plants due to the relatively low cost and successful operation [53]. For these reasons, this design has been installed in recent parabolic trough plants [54,55]. However, other references suggest that kettle evaporator design is susceptible of high stresses due to the high thicknesses (shell and tubesheet), and thus, it has a higher risk of fatigue failure.

In this Chapter, a TEMA X recirculation evaporator is used due to its expected good behavior against thermal stresses. This is mainly due to the fact that TEMA X evaporator is divided into three parts (two heat exchangers and one steam drum) whereas the kettle is formed only in one part. Thus, a significant reduction in the thicknesses is obtained due to the reduction on the shell diameters.

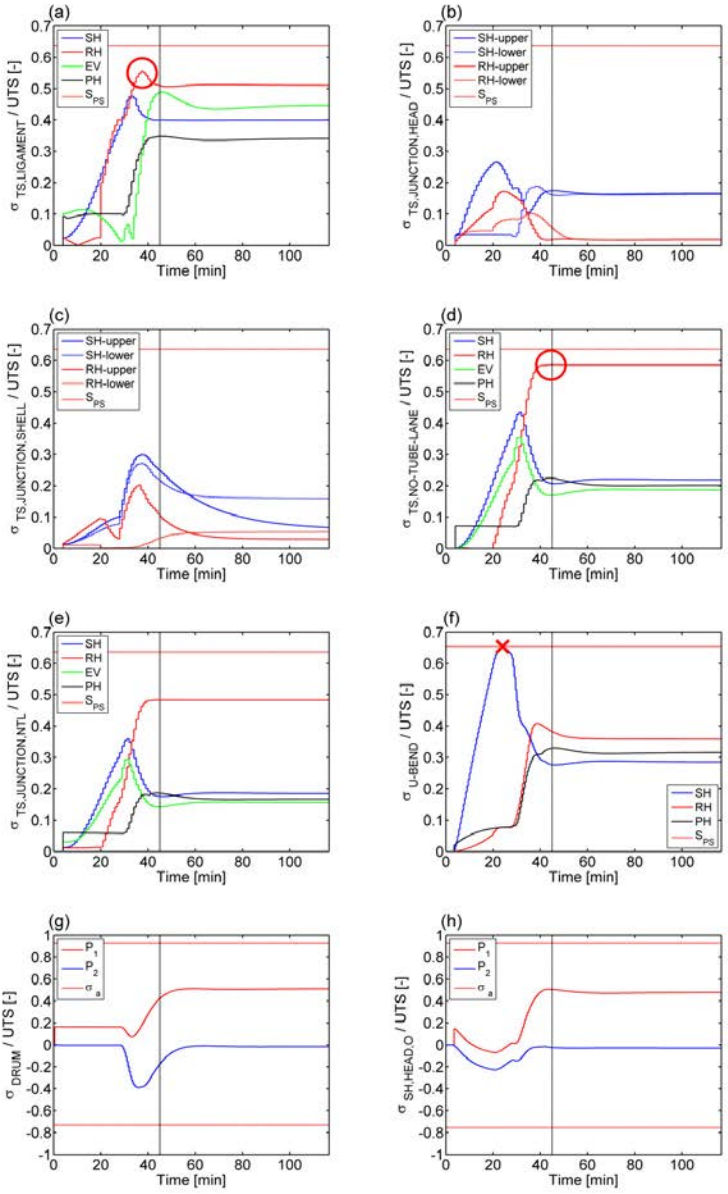

Figure 5.18: Stress evolution of the main components of the SG during daily start-up: a) tubesheet ligament stresses; b) tubesheet head junction stresses; c) tubesheet shell junction stresses; d) tubesheet no-tube-lane stresses; e) tubesheet junction at no-tube-lane zone; f) U-tube stresses; g) steam drum downcomer junction stresses; g) SH outlet head nozzle junction stresses.

In order to compare the dynamic behavior of both designs a new simulation is carried out using a kettle evaporator on the SG. The dynamic model for kettle is developed using a simplified second-order model based on Equations 5.4, 5.5 and 5.6. This model capture very well the dynamic response of the pressure against input changes of load, steam flow or feed-water flow [36]. However, high accurate models are necessary to capture the dynamic response of the water level.

Following the previous simulation, the ramp-up rates selected are 8ºC/min for thermal oil inlet and 7 ºC/min for evaporator. The kettle evaporator design is obtained following the procedure described in Chapter 2 (Table 2.3).

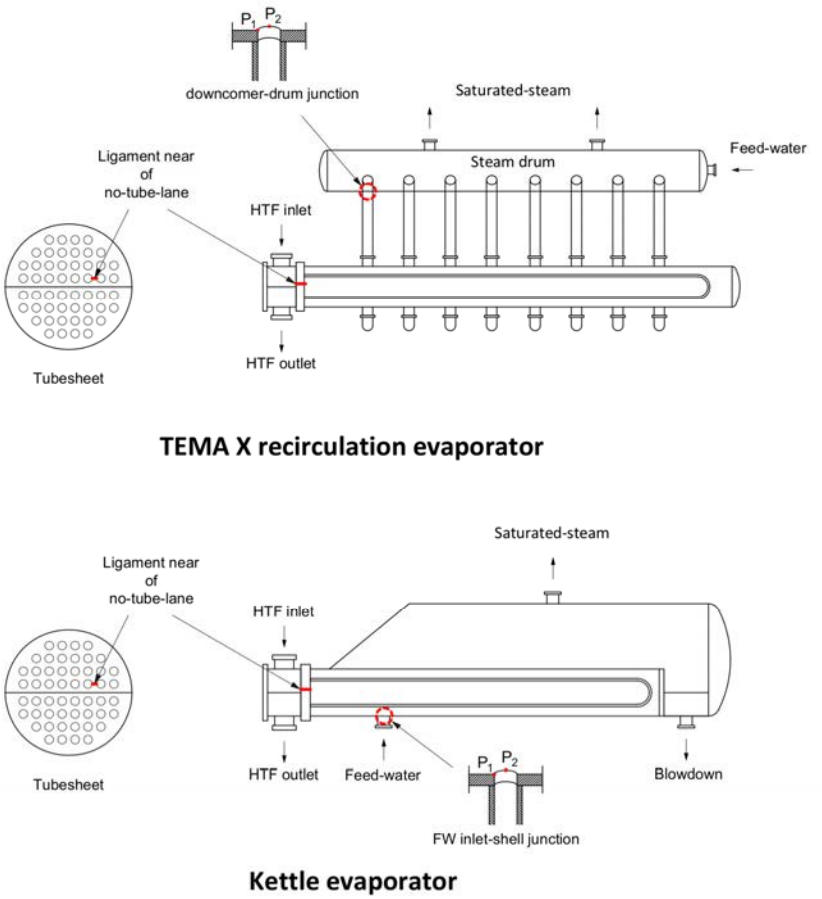

Figure 5.19: Critical points selected for the stress analysis of TEMA X recirculation and kettle evaporator.

The stress results of the most critical parts for both designs are presented in Figure 5.20. As it can be seen, the stresses obtained are placed within allowable ranges for both designs. As it is expected, the minimum thermal stresses on the drum (shell for kettle) are lower for kettle design (Figure 5.20-a). The maximum stress on tubesheet is in the same order of magnitude (Figure 5.20-b). However, the higher thermal inertia of the ligaments of kettle tubesheet leads to higher transient thermal stresses as it can be seen in Figure 5.20-b at t = 35 minutes.

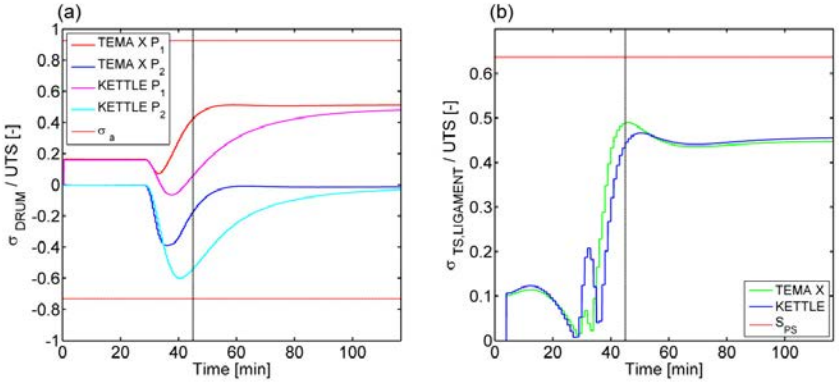

Figure 5.20: Results of the stress analysis for between TEMA X evaporator and kettle evaporator: a) drum downcomer junction (shell for kettle); b) tubesheet ligament stresses.

5.6. Conclusions

A dynamic analysis of the steam generator of a parabolic trough plant is carried out in this Chapter. The steam generator is based on shell-and-tube heat exchangers designed according to TEMA and ASME standards. Different transient models are proposed for the single phase heat exchangers TEMA F and TEMA H, and the TEMA X recirculation evaporator with steam drum. The temperature field and the stresses are calculated on the critical parts of steam generator such as: tubesheets, tubesheet junctions, head-nozzle junctions, steam drum-downcomer junction and U-bend regions. Furthermore, finite element simulations of different parts of the steam generator are developed to compare with the simplified analytical stress models.

A simulation of the steam generator start-up is performed using relatively high ramp-up rates for the thermal oil inlet and the evaporator. The stresses obtained in the steam generator are ranged within the allowable stress limits according to ASME Section VIII div 2 [16] and EN 12952-3 [6] standards. This means that the proposed

design of the steam generator is valid to carry out a future fatigue analysis to estimate its lifetime.

The results show that the start-up of steam generator takes around 45 minutes and the energy needed to start-up is around 36.4 MWh_{th}. The higher thermal stresses are obtained in the no-tube-lane of the U-tube tubesheets of the heat exchangers, especially in the reheater. The comparison between TEMA X and kettle evaporators shows a better behavior against thermal stresses, obtaining a reduction of 35% for the first design.

Nomenclature

Abbreviations

$CCPs$: combined-cycle plants
CSP : concentrating solar plants.
CT : cold tank.
EV : evaporator.
FW : feed-water.
HP : high pressure.
HPT : high pressure turbine.
$HRSG$: heat recovery steam generator.
HTF : heat transfer fluid.
HT : hot tank.
Hx : heat exchanger.
LP : low pressure.
LPT : low pressure turbine.
PH : preheater.
$PTPP$: parabolic trough power plant
RH : reheater.
SG : steam generator.
SH : superheater.
UTS : ultimate tensile strength.

Symbols

A : heat transfer area (m^2).
A_c : cross section area (m^2).

C_m^* : dimensionless thermal capacitance of metal wall (-).

D : diameter (m), characteristic time constant (-).

E : modulus of elasticity (MPa).

F : force (N).

I : moment of inertia (m^4).

K : stiffness (N/m).

K' : inverse of stiffness (m/N).

L : length (m), characteristic length constant (-), level (m).

L_{tp} : tube pitch (mm).

L_{ts} : tubesheet thickness (m).

M : mass (Kg), moment (N m).

P : pressure (Pa).

R : radius (m).

R_{otl} : radius of a circle circumscribed to outermost tube of a bundle (m).

T : temperature (ºC).

T^* : dimensionless temperature (-).

V : volume (m^3), vertical force (N).

W_t: turbine power (MWe).

a: thermal diffusivity (m/s^2).

h: convective coefficient (W/ m^2 ºC)

l_{ts}: tubesheet thickness (mm).

$\dot{m}$: mass flow rate (kg/s).

t : time(s).

t_j : thickness of component *j* (m).

t^*: dimensionless time(-).

r : radial coordinate (-).

u : specific internal energy (KJ/kg).

y : vertical displacement (m).

z : axial coordinate (-).

Greek Symbols

α_t : thermal stress concentration factor (-).

α_m :pressure stress concentration factor (-).

β_t :linear thermal expansion coefficient (1/K).

θ : rotation angle (rad), circumferential coordinate (-).

ν : Poisson's ratio (-).

ρ : density (kg/m^3).

σ : stress (MPa).

τ : shear stress (MPa).

ψ : U-tube stress concentration factor (-).

Subscripts

0 : nominal conditions.

ave : average.

$atemp$: attemperator.

b : bending.

cyl : cylinder.

d : drum.

dc : downcomer.

h : head.

i : inlet, inner

m : metal.

o : outlet, outer

r : riser.

rec : recirculated.

s : shell.

sat : saturated.

st : steam.

su : surface

t: tube.

tp : tube pitch.

ts: tubesheet.

w: water.

5.7. References

[1] Pelagotti L, Sørensen K, Condra TJ, Franco A. Modelling of a Coil Steam Generator for CSP applications 2014.

[2] Ferruzza D, Topel M, Basaran I, Laumert B. Start-Up Performance of Parabolic Trough Concentrating Solar Power Plants. SolarPACES Conf Procedings 2016.

[3] Mehos M, Turchi C, Vidal J, Wagner M, Ma Z, Ho C, et al. Concentrating Solar Power Gen3 Demonstration Roadmap 2017.

[4] Taler J, Weglowski B, Taler D, Sobota T, Dzierwa P, Trojan M, et al. Determination of start-up curves for a boiler with natural circulation based on the analysis of stress distribution in critical pressure components. Energy 2015;92:153–9. doi:10.1016/j.energy.2015.03.086.

[5] Taler J, Dzierwa P, Taler D, Harchut P. Optimization of the boiler start-up taking into account thermal stresses. Energy 2015;92:160–70. doi:10.1016/j.energy.2015.03.095.

[6] European Standard EN12952-3. Water-tube Boiler and Auxiliary Installations - Part 3: Design and Calculation for Pressure Parts 2001.

[7] Taler J. A new method for optimum heating of steam boiler pressure components. Int J Energy Res 2010;31:135–47. doi:10.1002/er.

[8] Alobaid F, Pfeiffer S, Epple B, Seon CY, Kim HG. Fast start-up analyses for Benson heat recovery steam generator. Energy 2012;46:295–309. doi:10.1016/j.energy.2012.08.020.

[9] Mertens N, Alobaid F, Starkloff R, Epple B, Kim HG. Comparative investigation of drum-type and once-through heat recovery steam generator during start-up. Appl Energy 2015;144:250–60. doi:10.1016/j.apenergy.2015.01.065.

[10] Benato A, Bracco S, Stoppato A, Mirandola A. LTE: A procedure to predict power plants dynamic behaviour and components lifetime reduction during transient operation. Appl Energy 2016;162:880–91. doi:10.1016/j.apenergy.2015.10.162.

[11] Alobaid F, Mertens N, Starkloff R, Lanz T, Heinze C, Epple B. Progress in dynamic simulation of thermal power plants. Prog Energy Combust Sci 2017;59:79–162. doi:10.1016/j.pecs.2016.11.001.

[12] Casella F, Pretolani F. Fast Start-up of a Combined-Cycle Power Plant : a Simulation Study with Modelica. 6th Model Conf 2006:3–10.

[13] González-Gómez PA, Petrakopoulou F, Briongos JV, Santana D. Cost-based design optimization of the heat exchangers in a parabolic trough power plant. Energy 2017;123:314–25.

[14] González-Gómez PA, Gómez-Hernández J, Briongos JV, Santana D. Thermo-economic optimization of molten salt steam generators. Energy Convers Manag 2017;146:228–43. doi:10.1016/j.enconman.2017.05.027.

[15] TEMA, Standards of the tubular exchangers manufacturers association, 9th ed. Tubular Exchanger Manufactures Association, 2007.

[16] American Society of Mechanical Engineers. ASME boiler and pressure vessel code, Section VIII 2010.

[17] Dzierwa P. Optimum heating of pressure components of steam boilers with regard to thermal stresses. J Therm Stress 2016;39:874–86. doi:10.1080/01495739.2016.1189773.

[18] Petrova N, Bouzid A-H. Deflections of A Multipass Shell-and-Tube Heat Exchanger Bolted Joint Subjected to Nonaxisymmetric Thermal Loading. J Press Vessel Technol 2012;134:11207. doi:10.1115/1.4004623.

[19] Hirsch T, Fabian Feldhoff J, Schenk H. Start-Up Modeling for Annual CSP Yield Calculations. J Sol Energy Eng 2012;134:31004. doi:10.1115/1.4006268.

[20] Schenk H, Dersch J, Hirsch T, Polklas T. Transient Simulation of the Power Block in a Parabolic Trough Power Plant. Proceeding 11 Th Int Model Conf 2015:605–14. doi:10.3384/ecp15118605.

[21] DYMOLA Systems Enginering: Multi-Engineering Modeling and Simulation bason on Modelica and FMI 2017. https://www.3ds.com/products-services/catia/products/dymola/ [accesed 08/07/2017].

[22] Sandia Natl. Lab., Molten Salt Receiver Subsystem Research Experiment Phase 1 - Final Report, Volume 1. Foster Wheeler Solar Development Corporation, Sandia Natl. Lab. Report SAND82-8179 1984.

[23] Abaqus/CAE Software Dassault Systèmes: https://www.3ds.com/products-services/simulia/products/abaqus/abaquscae/. 2017 n.d.

[24] National Renewable Energy Laboratory (NREL) 2016. http://www.nrel.gov/csp/solarpaces/by_project.cfm.

[25] Developments in pressure equipment - where to next? Press. Syst. Gr. instituion Mech. Eng., 2004.

[26] Zavoico AB. Solar Power Tower - Design Basis Document, Sandia Natl. Lab. Report, SAND2001-2100 2001.

[27] Stodola A, Lowenstein LC. Steam and Gas Turbines, vol. I. New York: McGraw-Hill Book Company; 1945.

[28] Alobaid F, Karner K, Belz J, Epple B, Kim H-G. Numerical and experimental study of a heat recovery steam generator during start-up procedure. Energy 2014;64:1057–70. doi:10.1016/j.energy.2013.11.007.

[29] Rayaprolu K. Boilers for Power and Process 2009.

[30] Pacheco JE. Final Test and Evaluation Results from the Solar Two Project, Sandia Natl. Lab. Report, SAND2002-0120 2002.

[31] Ansari MR, Mortazavi V. Simulation of dynamical response of a countercurrent heat exchanger to inlet temperature or mass flow rate change. Appl Therm Eng 2006;26:2401–8. doi:10.1016/j.applthermaleng.2006.02.015.

[32] Serth RW, Lestina TG. Process Heat Transfer: Principles, Applications and Rules, 2014.

[33] Smith R. Chemical process design and integration. John Wiley & Sons; 2005.

[34] Taborek J. Shell and Tube Heat Exchangers: single phase flow. In Heat Exchanger Design Handbook. Hemisph Publ Corp 1983.

[35] Singh KP, Holtz M. A Method to Design Shell-Side Pressure Drop Constrained Tubular Heat Exchangers. Eng Power 1977:441–8.

[36] Astrom KJ, Bell RD. Drum-boiler dynamics. Automatica 2000;36:363–78.

[37] Kim TS, Lee DK, Ro ST. Analysis of thermal stress evolution in the steam drum during start-up of a heat recovery steam generator. Appl Therm Eng 2000;24:137–49. doi:10.1002/(SICI)1099-114X(200002)24.

[38] Holmgren M. X steam for Matlab 2006. www.x-eng.com.

[39] Dzierwa P, Taler J. Optimum Heating of Pressure Vessels With Holes. J Press Vessel Technol 2014;137:11202. doi:10.1115/1.4027584.

[40] Taler J, Dzierwa P, Taler D. Determining optimum temperature changes during heating of pressure vessels with holes 2013:1–8.

[41] Young WC, Budynas RG. Roark's Formulas for Stress and Strain. McGraw-Hill Book Company; 2002.

[42] Ando M, Hasebe S, Kobayashi S, Kasahara N, Toyoshi A, Ohmae T, et al. Thermal transient test and strength evaluation of a tubesheet structure made of Mod.9Cr-1Mo steel. Part II: Creep-fatigue strength evaluation. Nucl Eng Des 2014;275:422–32. doi:10.1016/j.nucengdes.2014.04.029.

[43] O'Donnell WJ, Langer BF. Design of perforated plates. J Eng Ind 1962;84:307–19. doi:10.1115/1.3667483.

[44] Reinhardt W, Kizhatil R, Mcclellan GH. Analysis of a Tubesheet Undergoing Rapid Transient 2016;122:476–81.

[45] Soler A, Caldwell SM, Singh KP. Tubesheet Analysis—A Proposed ASME Design Procedure. Heat Transf Eng 1987;8:40–9. doi:10.1080/01457638708962801.

[46] Slot T. Photoelastic Simulation of Thermal Stresses by Mechanical Prestraining 1965.

[47] Purohit GP. Estimating costs of shell-and-tube heat exchangers. Chem Eng 1983:56–67.

[48] Thulukkanam K. Heat Exchanger Design Handbook, Second Edition. 2013. doi:10.1201/b14877.

[49] Singh KP, Holtz M. On Thermal Expansion Induced Stresses in in U-Bends of Shell-and- Tube Heat Exchangers. Eng Power 1979;101:634–9.

[50] American Society of Mechanical Engineers. ASME boiler and pressure vessel code, Section III 2010.

[51] Taira S. Lifetime of structures subjected to varying load and temperature, Creep in structures 1962.

[52] Aalborg CSP. Aalborg CSP Concentrated Solar Power steam generators 2016. http://www.aalborgcsp.com.

[53] Sandia .Natl. Lab., Betchel. Corporation, Investigation of Thermal Storage and Steam Generator Issues, Sandia Natl. Lab. Report SAND 93-7084 1993.

[54] Kelly B, Kearney D. Thermal Storage Commercial Plant Design Study for a 2-Tank Indirect Molten Salt System Final Report 2006.

[55] Kelly B. Nexant Parabolic Trough Solar Power Plant Systems Analysis Task 1 : Preferred Plant Size. Contract 2006.

CHAPTER

SIX

Fatigue analysis of the steam generator of parabolic trough power plants

Contents

6.1. Abstract 167

6.2. Introduction 168

6.3. Methodology for the fatigue analysis 170

6.3.1. Lifetime estimation according ASME Section VIII Div 2 [23] 171

6.4. Results of the fatigue analysis 175

6.4.1. Fatigue analysis for the evaporator temperature ramp operation during the SG start-up 176

6.4.2. Fatigue analysis for the HTF inlet temperature ramp operation during the SG start-up 179

6.4.3. Fatigue analysis for a 50% load change operation of the SG 181

6.5. Conclusions 183

6.6. References 186

6.1. Abstract

The increment of the flexibility has become a critical objective of concentrating solar power plants to improve their competitiveness. The steam generator has an important role on the flexibility of concentrating solar power plants. This is mainly for the stress limitation on thick-walled components, which limit the start-up and load

change ramps. In this way, the development of lifetime estimation models is required to optimize the design and operation of these plants.

In this Chapter, a fatigue analysis of the steam generator of a parabolic trough power plant is performed following ASME code. Two operations of the start-up of the steam generator are analyzed: the evaporator temperature ramp and the heat transfer fluid inlet temperature ramp. Furthermore, a load change operation is also studied. The stress models used for fatigue analysis have been validated using finite element analysis described in Chapter 5. The results show that the most compromised parts of the steam generator are the reheater tubesheet, the drum-downcomer junction and the SH nozzle.

6.2. Introduction

In current electricity markets a significant percentage of the total energy production comes from renewable energies such wind or photovoltaic's. However, these kind of energy sources are considered as non-dispatchables and therefore it may lead to unbalanced grid problems [1]. For this reason, dispatchable power plants are pushed to increase its flexibility in order to meet the electricity demand and compensate the unpredictable fluctuations of this renewable energy sources [2].

Concentrating solar power (CSP) plants has been positioned as a potential alternative to conventional plants since they can be considered as dispatchable under certain conditions [3]. This is mainly due to the capacity of these plants to integrate a cost-effective thermal storage system, the possibility of hybridization with fossil fuels and the use of steam turbines. Thus, the flexibility of the CSP plants is a critical issue to increase their competitiveness. In this way, faster start-ups and load changes have become an important feature in order to guarantee the flexibility. Furthermore, fast start-ups are especially important for CSP plants because increase the annual electricity production [4]. On the other hand, fast transient operations lead to higher stresses on thick-walled components. Thus, a good management requires a good estimation of the potential lifetime reduction/increment driving to the increment/reduction of the flexibility of the plant. The steam generator (SG) has a important role on the flexibility because the thermal stresses on thick-walled components limit the temperature change rates [5]. The SG is formed by four heat exchangers with a coupled performance. For these reasons, a dynamic simulation of the SG is a essential previous step in a fatigue analysis in order to identify realistic critical points. Moreover, the dynamic simulation helps to a better understating on the SG operation.

Several researchers has been focused on the investigation of the critical stress points of combined cycle power plants (CCPPs) [6–9]. A dynamic model is usually developed using software to calculate the thermodynamic quantities (pressure, temperature, mass flow, etc). Most of those works estimate the mechanical and thermal stress are calculated using European Standards [6–8]. Only some of them accomplished a fatigue analysis. For example, Benato et al. [6] performed a fatigue analysis of a heat recovery steam generator (HRSG). They developed a dynamic simulator tool in MATLAB to estimate the trends of the main thermodynamic parameters (flow rates, temperatures and pressures). To validate this model, they also developed a HRSG model based on Modelica language using DYMOLA software [10]. A comparison study of both models for single pressure level HRSG can be found in [11]. They carried out a fatigue analysis using the European Standard EN 13445 [12]. They identified that the most critical stress points are the high pressure steam drum and the superheater (SH) collectors. The fatigue results show that the higher lifetime reduction is obtained in the SH collector for a load change of 50%. However, details of the geometric locations of the stress critical points and their respective stress concentration factors or even the number of allowable cycles are not available. Angerer et al. [7] performed a fatigue analysis of the SH header using European Standard EN 12952-3 [13]. They studied a novel buffer storage system for the thermal decoupling of the gas turbine form the HRSG. The results show that this innovative system reduce around a 90% the fatigue damage in the SH header. Tonti et al. [8] presented some guidelines for calculation of in-service creep-fatigue damage of steam generators following European standard EN 12952-4 [14]. Furthermore, an example of fatigue analysis of the SH outlet header is also presented.

Most of the literature focused in steam generation, which combines dynamic simulation and stress analysis, use European standards. Nevertheless, some works can be found using ASME code. For example, Mirandola et al. [15] analyzed the residual lifetime a SH of a 320 MW coal-fired steam power plant. They studied the creep-fatigue damage on the SH pipes using ASME Section III [16]. The structural analysis to obtain deformations and stresses is performed using ANSYS software [17]. Two operation management cases are also compared economically.

Commercial CSP plants typically use an indirect steam generator system based on conventional shell-and-tube heat exchangers [18–20]. The most common methodology for the design of shell-and-tube heat exchangers is based on TEMA standards [21] and ASME Section VIII Div 1 [22] considering continuous operation. However, the intermittent operation of the SG with daily start-ups, shutdowns and load changes, makes necessary a sought alternative standards that considers a fatigue assessment, as ASME Section VIII Div 2 [23] or ASME Section III Subsection NH [16].

Different studies can be found about fatigue analysis focusing in heat exchangers and/or pressure vessels. The ASME VIII Div 2 approach is used in Refs. [24,25] for the fatigue analysis. Shen et al. [24] presented a fatigue analysis of a tubesheet subjected to thermal-shock. The results show that the most critical point is the tubesheet junction on shell-side. Dong et al. [25] studied the lifetime of pressure vessel focusing in welded points. They also performed a comparison study of the fatigue calculations using different standards.

In this Chapter, a fatigue analysis of the SG of a parabolic trough power plant (PTPP) is carried out. Several critical points of the SG are considered: tubesheets, tubesheet junctions, head-nozzle junctions and drum-downcomer junction. Two transient operations of the SG start-up are studied for the fatigue analysis. The first considers five different evaporator temperature ramps whereas the second considers five heat transfer fluid inlet temperature ramps. In addition, a SG load change operation is also analyzed. The stress calculations are made using the models presented in Chapter 5, which have been validated with finite element analysis. The fatigue calculations are performed following ASME Section VIII Div 2 [23].

6.3. Methodology for the fatigue analysis

The fatigue is defined as the damage of a structural component due to cyclic loads that involve cycles of stresses and strains. The fatigue failure is produced as the accumulation of the damage at localized zones, where the nucleation of cracks is extended until material fracture. There are two types of fatigue mechanisms: high cycle fatigue (HCF) and low cycle fatigue (LCF) [26]. In LCF, the peak stresses are above of the yield tensile strength, obtaining in this way a plastic strains. The allowable number of cycles are typically suited below of 1 or 5 10^4. In HCF, the stresses are below of the yield tensile strength and hence the strains produced are in elastic region.

Creep is anelastic deformation mechanism produced by the constant stress working at relatively high temperatures. The creep damage is mainly function of the stress, time and temperature. Normally, the creep damage becomes significant for temperatures above of the 40% of the melting temperature, in the case of low alloy steels this temperature is around 380 ºC whereas for austenitic steels is around 540 ºC [26]. The creep and fatigue damage can be combined by using Palmgren-Miner equation [27], where it can be seen that the damage is much higher if the creep and fatigue are take place at the same time.

Creep and fatigue analysis are normally accomplished by using design standards. Some of the most important are: ASME Section III [16] and VIII [23], UNE EN 13445-3 [12], UNE EN 12952-3 [13].

6.3.1. Lifetime estimation according ASME Section VIII Div 2 [23]

The assessment under cycling operation of the heat exchangers for standard industrial applications at low temperatures (<427ºC) can be made following ASME Section VIII Div 2 [23]. Two assessments should be considered for the protection against cycling operation: ratcheting and fatigue. The equivalent stresses are calculated considering operating load cycles, instead of design loads. Note that this method does not take into account creep damage.

According to AME Section VIII Div 2 [23] the structural stresses can be classified in three categories. The first category is formed by the primary stresses, which are: general membrane (P_m), local membrane (P_L) and primary bending (P_b). They are calculated considering only mechanical loads and excluding local stress discontinuities. The second category is formed by secondary membrane and bending (Q). They are calculated considering mechanical loads and/or thermal loads which produce thermal differential expansion. The local stress concentration factor are excluded. The third category is the peak stresses (F). These stresses are calculated considering mechanical loads and/or thermal loads that do not produce distortion of vessel shape, and also considering local stress concentrations. Figure 6.1 illustrates an schematic of the stresses classification.

Typically the first step in the heat exchanger design consists of the estimation of the thicknesses of the main parts (shell, tubes, head, tubesheet, nozzles, etc) using ASME Section II [28] and Section VIII Div 1 [22], considering design loads, primary membrane and bending stresses, and the maximum allowable stress S defined in ASME Section II [28] (See Figure 6.1).

In the case of assessment under cycling operation must be used operating loads instead of design loads. In addition, it must be considered the stresses due to thermal expansion and local discontinuities. For example, for ratcheting assessment must be considered membrane, bending and secondary stresses (P_L+P_b+Q). Moreover, the maximum allowable stress S_{PS}, which is calculated as the highest value between: i) three times the allowable stress limit S; ii) two times the yield stress of the material S_y. The results of the ratcheting assessment of the SG can be shown in Chapter 5.

In case of fatigue assessment the peak stress must be included (F), and hence, the local stress concentration factors must be used. The allowable stress amplitude for

fatigue analysis S_a is calculated according the *S-N* curves from ASME Section VIII Div 2 [23].

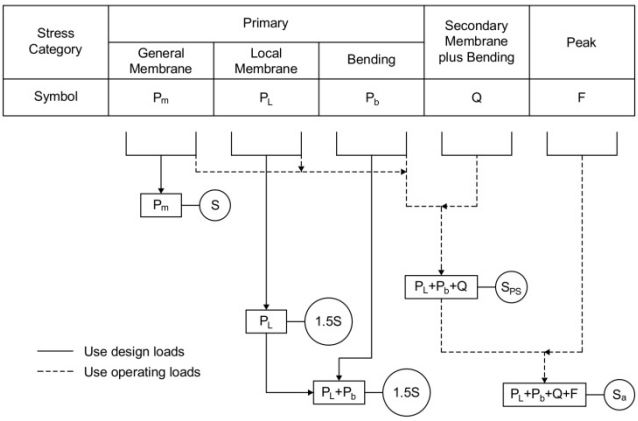

Figure 6.1: Stress classification according to ASME Section VIII Div 2 [23].

According to the ASME linearization method, the stress can be classified mainly in three types: membrane, bending and peak. And they can be defined analytically as follows [25]:

$$\begin{aligned}
\sigma_m &= \frac{1}{t}\int_0^t \sigma_x(y)\,dy \\
\sigma_b &= \frac{6}{t^2}\int_0^t \sigma_x(y)\cdot\left(\frac{t}{2}-y\right)dy \\
\sigma_p &= \sigma_x(y)-\sigma_m-\sigma_b\cdot\left(1-\frac{2y}{t}\right)
\end{aligned} \tag{6.1}$$

where the $\sigma_x(y)$ is the normal stress (normal to fissure propagation plane) obtained from shell theory neglecting the local stresses due to singularities. When finite element analysis is used, the solution obtained is the total stress distribution. Therefore, a linearization of the stresses should be carried out to classify the stress type.

The fatigue analysis is normally is accomplished by using time series of load cycles, also called Remaining Sequence of Extremes (RSE) [8]. There are different

possibilities to estimate the number of cycles in a fatigue analysis based on RSE. The main idea of these methods consists of counting the maximum and minimum relative extremes. They can be reduced assuming a minimum amplitude value. Figure 6.2 are shown some of these methods. As can be seen, there are different ways to consider the load cycles and the pattern to link an extreme with other. The fatigue results can vary around 25 % depending of the method selected [8]. In this work, the method b is selected in order to obtain conservative results.

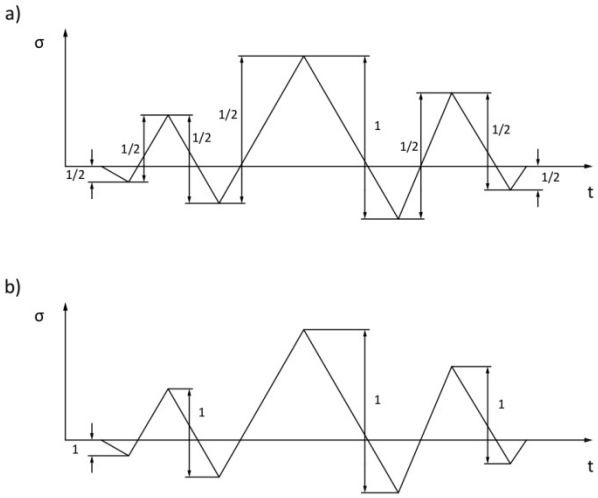

Figure 6.2: Possible calculations of the extremes in case of RSE [8].

The elastic-fatigue analysis according to ASME Section VIII Div 2 [23] should be made by following steps:

- Determine the load history: This is calculated according to the results of the SG simulations where the stresses of the main components are calculated for each step time. The critical points of the SG are chosen according the results of the Chapter 5.
- Calculation of the stress range $\Delta\sigma_{ij}$ for the principal stress directions considering their respective signs.
- Use the counting cycle method to the stress range $\Delta\sigma_{ij}$ to estimate the maximum relative stress ${}^{m}\sigma_{ij,k}$ and minimum relative stress ${}^{n}\sigma_{ij,k}$ of each *k* cycle. On the other

hand, it is also calculated the total M fatigue cycles (k=1,..,M) and the actual number of repetitions n_k of each k cycle.

- Calculation of the equivalent stress range considering normal and shear stresses:

$$\Delta\sigma_{ij,k} = {}^{m}\sigma_{ij,k} - {}^{n}\sigma_{ij,k}$$
$$\Delta S_k = \frac{1}{\sqrt{2}}\left[\begin{array}{c}(\Delta\sigma_{11,k} - \Delta\sigma_{22,k})^2 + (\Delta\sigma_{11,k} - \Delta\sigma_{33,k})^2 + \\ (\Delta\sigma_{22,k} - \Delta\sigma_{33,k})^2 + 6(\Delta\sigma_{12,k}{}^2 + \Delta\sigma_{13,k}{}^2 + \Delta\sigma_{23,k}{}^2)\end{array}\right]^{0.5} \quad (6.2)$$

- The effective alternating stress amplitude is calculated as follows:

$$\Delta S_{alt,k} = \frac{K_f K_e(\Delta S_{P,k} - \Delta S_{LT,k}) + K_{v,k}\Delta S_{LT,k}}{2} \quad (6.3)$$

where the equivalent stress range, $\Delta S_{P,k}$, is calculated considering primary, secondary and peak stresses. The equivalent thermal stress range, $\Delta S_{LT,k}$, is calculated considering secondary and peak stresses produced by thermal loads. The fatigue strength reduction, K_f, should be included to take into account local notch or weld effects. The fatigue penalty factor, K_e, is calculated as a function of the material and the equivalent alternative stresses, $\Delta S_{n,k}$, which is calculated considering only primary and secondary stresses. Lastly, the Poisson correction factor due to thermal loads, $K_{v,k}$, is computed as function of the elastic and the equivalent plastic Poisson's ratios.

- The allowable number of cycles is calculated according to *S-N* curves according to ASME Section VIII Div 2 [23]:

$$N_k = 10^{X(E,UTS,\Delta S_{alt})} \quad (6.4)$$

- Finally, the total fatigue damage for k cycles is calculated as follows:

$$D = \sum_{k=1}^{M} \frac{n_k}{N_k} \leq 1 \quad (6.5)$$

Further details about the elastic-fatigue calculations can be found in Sowoniski et al. [29]. In addition, they presented a wide variety of design calculations examples following ASME Section VIII Div 2 [23].

6.4. Results of the fatigue analysis

The fatigue analysis is performed for the SG start-up and shutdown with different ramp rates on the evaporator temperature and HTF inlet temperature. In addition, the fatigue damage of the 50% load change operation is also studied. A reference transient case ("Ref.") is used for comparison. This transient case was previously analyzed in Chapter 5. In addition, four transient cases are considered: two faster than the reference case, "25% Faster" and "50% Faster", and two slower than the reference case, "25% Slower" and "50% Slower". Table 6.1 shows the temperature ramps of each transient case.

Table 6.1: Transient cases for SG fatigue analysis.

Transient case	50% Slower	25% Slower	Ref.	25% Faster	50% Faster
Evaporator temperature ramp (ºC/min)	3.5	5.2	7	8.7	10.5
HTF inlet temperature ramp (ºC/min)	4	6	8	10	12

To carry out the fatigue analysis on the SG are necessary numerous dynamic and stress models. The heat exchangers are discretized along the tube length at least to the baffle spacing (see Table 2.3) in order to obtain enough accurate results. To estimate the thermal stresses on the steam drum and the heat exchanger heads, firstly it is calculated the temperature field along the wall thickness where the radial coordinate is discretized to obtain radial increments not higher than $5 \cdot 10^{-3}$ m. The axisymmetric temperature models for the tubesheet ligament and the tubesheet junction are discretized in a grid of nodes where the radial and axial increments are not higher than 10^{-2} m. Further details of these models are described in deep in Chapter 5.

6.4.1. Fatigue analysis for the evaporator temperature ramp operation during the SG start-up

Figure 6.3 shows the start-up simulation results for the different evaporator temperature transient cases selected. The transient response of the SG using the model described in Chapter 5. As it can be seen, a significant increment of the drum pressure must be accomplished during the start-up from 34 bar to 106 bar (Figure 6.3-a), whereas the temperature varies from 240 ºC to 314ºC (Figure 6.3-b). In Figure 6.3-c/d are illustrated the HTF inlet conditions to SG during the SG start-up.

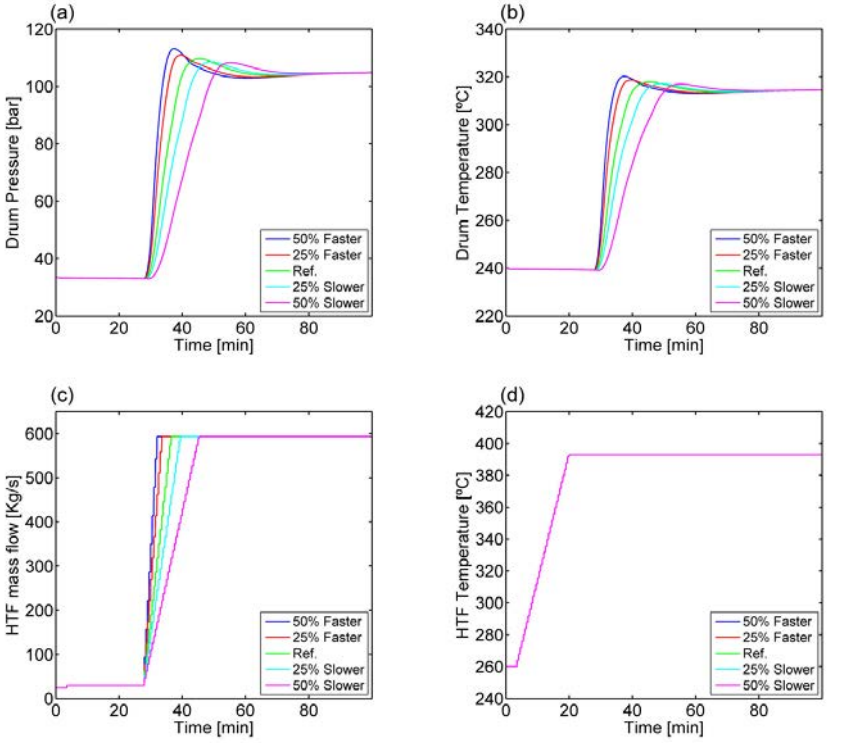

Figure 6.3: Simulation results for different evaporator temperature ramps. a) Drum pressure; b) Drum temperature; c) HTF mass flow; d) HTF inlet temperature.

According to the results shown in Chapter 5, the critical points of the SG for the fatigue analysis are: tubesheet ligaments, tubesheet junctions, SH nozzle-head junction and steam drum-downcomer junctions. Among these points, the most sensitive to the evaporator temperatures ramps are the SH nozzle and drum

junctions. Figure 6.4 shows the stress evolution of these points for the different ramps considered. Note that the two points are analyzed in the T-junctions, as was explained in the stress model shown in Chapter 5.

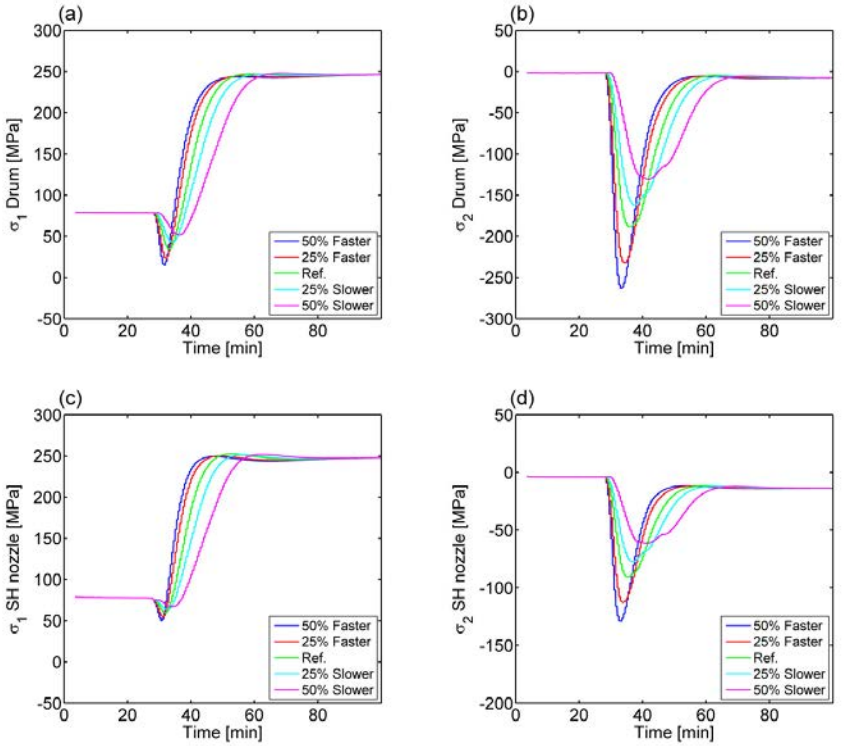

Figure 6.4: Stress results for different evaporator temperature ramps: a) Point 1 of the drum-downcomer junction; b) Point 2 of the drum-downcomer junction; c) Point 1 of the SH inlet nozzle-head junction; d) Point 2 of the SH inlet nozzle-head junction.

The fatigue analysis and the consequent lifetime estimation are computed in accordance to ASME VIII Div 2 [23]. Five transient cases are considered for the evaporator temperature ramp. In Figure 6.5 are shown the fatigue results. The lifetime is calculated by dividing the number of allowable cycles into 300 start-ups and shutdowns per year. In addition to TEMA X evaporator, the kettle evaporator is also included in the fatigue analysis.

The results show that the kettle does not achieve the minimum lifetime required of 25 years for the reference case. Since this case is the minimal value of the optimal range of evaporator ramps considered by Ferruzza et al. [4], it can be concluded that

kettle evaporator is not appropriate design for a PTPP. In contrast, the TEMA X evaporator achieves the 25 years lifetime condition even for the "50% faster" transient case.

The other critical point of the SG is the reheater (RH). This is because the high stresses are obtained due to the temperature difference across the no-tube-lane zone of the tubesheet, as it can be seen in Chapter 5. Note that the RH stress is not sensitive to the evaporator temperature ramps, as was shown in the results. This means that the critical stress is obtained according to the load state. The results show that the lifetime obtained is around 18 years, violating the design condition of 25 years in spite of the satisfactory results obtained in the stress analysis performed in Chapter 5. This issue can be solved by two alternative design options: i) dividing the RH into two heat exchangers in series or ii) using a U-shell/U-tube heat exchanger design to avoid the high temperature difference in the no-tube-lane zone.

For the SH nozzle-head junction, a slightly lifetime variation is observed for the transient cases studied. In a first step, it is expected a similar lifetime behavior of the drum-downcomer junction. This makes sense since both parts showed similar stress values for point P_1 (Figure 6.4-a/c). However, a significant difference was obtained on the stress on P_2 (Figure 6.4-b/d), being more sensitive for the drum-downcomer junction and hence this leads to higher variations on the lifetime calculations (Figure 6.5).

In case of EV, SH and PH tubesheets the calculations shows not significant variations in the lifetime for the evaporator temperature ramps. Furthermore, their lifetime is above 25 years with enough safety margin.

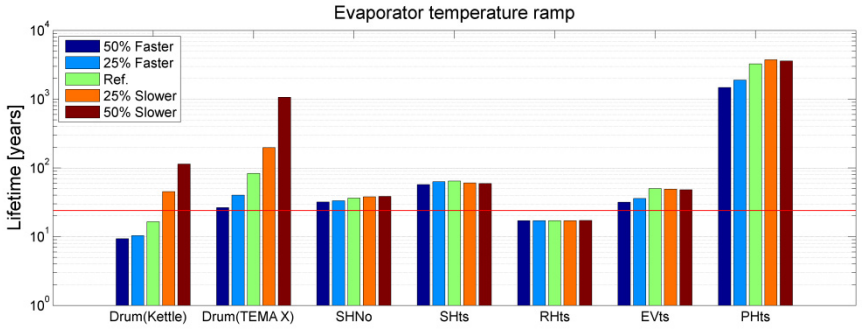

Figure 6.5: Fatigue results for different evaporator temperature ramps.

6.4.2. Fatigue analysis for the HTF inlet temperature ramp operation during the SG start-up

Figure 6.6 shows the start-up simulation results for the different HTF inlet temperature ramps. The temperature increment from 260 ºC to around 393 ºC. In the transient case "Ref." is considered a evaporator temperature ramp around of 8 ºC/min, this means that the faster cases are around 10 and 12 ºC/min, whereas the slow cases are around 6 and 4 ºC/min. It should be note, that HTF temperature rates are normally below of 8 ºC/min according to data reported in [30,31]. This is due to the high thermal inertia of the solar field, combined with the lower solar radiation in the morning. However, higher HTF temperatures of 8 ºC/min would be possible for PTPPs with HTF heaters.

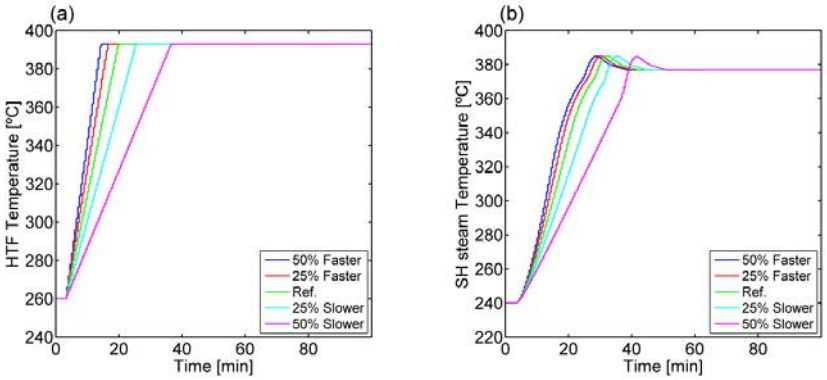

Figure 6.6: Simulation results for different HTF inlet temperature ramps: a) HTF inlet temperature; b) SH outlet steam temperature.

Figure 6.7 shows the stress points most sensitive to the HTF inlet temperature ramps, which are P_1 and P_2 of the SH nozzle-head junction. Although the temperature step is similar for HTF and steam sides, the lower thickness of the SH nozzle on shell-side compared to the nozzle of head-side, leads to significant thermal stress reduction. As it can be seen, the point P_1 has significant stress variation compared with point P_2.

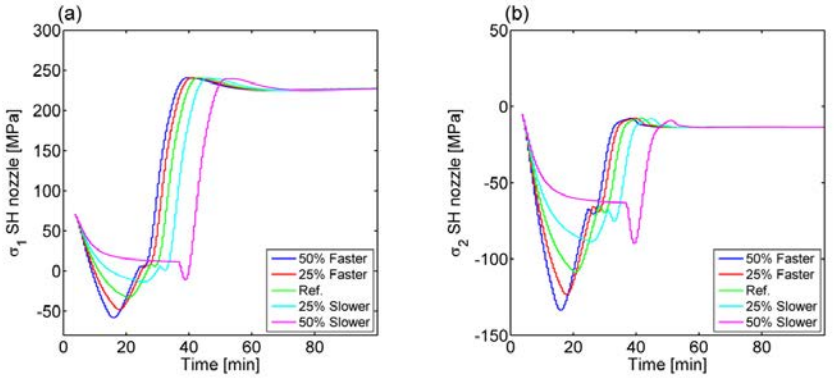

Figure 6.7: Stress results for different HTF inlet temperature ramps: a) Point 1 of the SH outlet nozzle-head junction; b) Point 2 of the SH outlet nozzle-head junction.

The results of the fatigue analysis for the different HTF temperature ramps are shown in Figure 6.8. As it can be seen, the majority of the critical points of the SG are insensitive for the HTF temperature ramps, except the SH nozzle-head junction. The results show that the HTF temperature rates equal and lower to 8ºC/min obtain lifetimes higher than 25 years for the SH nozzle-head junction.

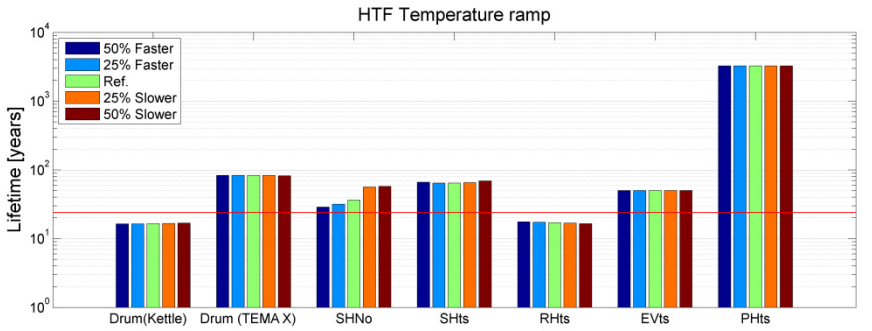

Figure 6.8: Fatigue results for different HTF temperature ramps.

6.4.3. Fatigue analysis for a 50% load change operation of the SG

Figure 6.9 illustrates the 50% load change simulation results for different evaporator temperature ramps. The evaporator temperature ramps studied are the same as in the start-up case. The part load performance of the turbine is modeled as sliding pressure operation mode. In addition, the steam turbine inlet temperatures are kept constant during the load change operation. The 50% load change leads to a pressure variation of 55 bar and the drum temperature variation is around 50ºC. The transient cases studied here are the same as considered for the evaporator temperature ramps.

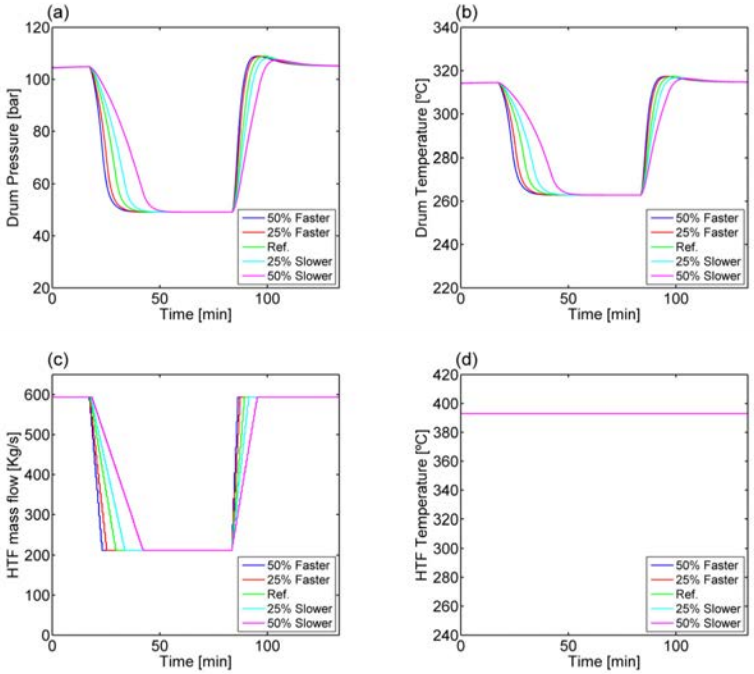

Figure 6.9: Simulation results for a 50% load change: a) Drum pressure; b) Drum temperature; c) HTF mass flow; d) HTF inlet temperature.

Figure 6.10 shows the most sensitive stress points for the load change operation: the SH nozzle and steam drum junctions. As it can be seen, for the stress points P_1 is more sensitive to pressure changes, whereas stress point P_2 are more sensitive for

transient thermal stresses. This can be easily checked because the pressure stress are always positive whereas the thermal stresses are positive for a cooling processes and negative for a heating processes.

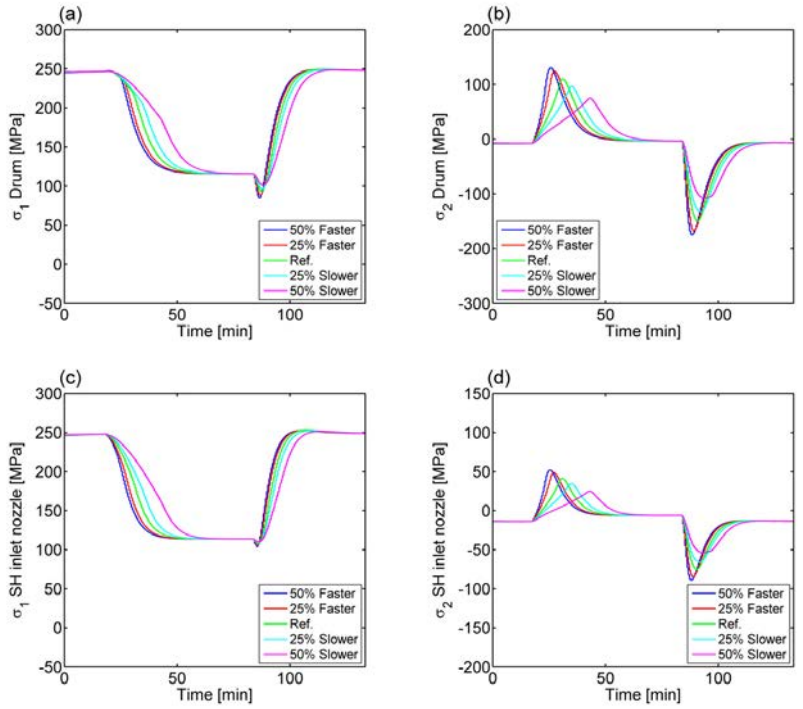

Figure 6.10: Stress results for 50% load change: a) Point 1 of the drum-downcomer junction; b) Point 2 of the drum-downcomer junction; c) Point 1 of the SH inlet nozzle-head junction; d) Point 2 of the SH inlet nozzle-head junction.

The fatigue results of the 50% load change are shown in Figure 6.11. The results are expressed as the fatigue damage equivalent to the start-up reference case (Equation 6.6). As it can be seen, the highest fatigue damage is obtained for the SH nozzle and steam drum junctions. The results follow a similar tendency to the start-up fatigue results showed for the evaporator temperature ramp (Figure 6.5). This makes sense because the load change operation is accomplished by means of a steam drum pressure variation, which involves an evaporator temperature ramp. On the other hand, the damage on the SH, RH, EV and PH tubesheets presents a low sensitivity for a load change. This is because the steam turbine inlet temperatures are kept constant during the load change. As explained in Chapter 5, the damage in tubesheets is

dominated by the thermal stresses. Since the temperature variations are higher for the start-up than the 50% load change operation, the thermal stress variations are higher as well. As a result, the tubesheet fatigue damages are one or two orders of magnitude higher for the start-up transient case.

$$D_{eq,j} = \frac{D_{load-change,j}}{D_{start-up,\mathrm{Ref}}} \quad j = 1,2,..,5. \tag{6.6}$$

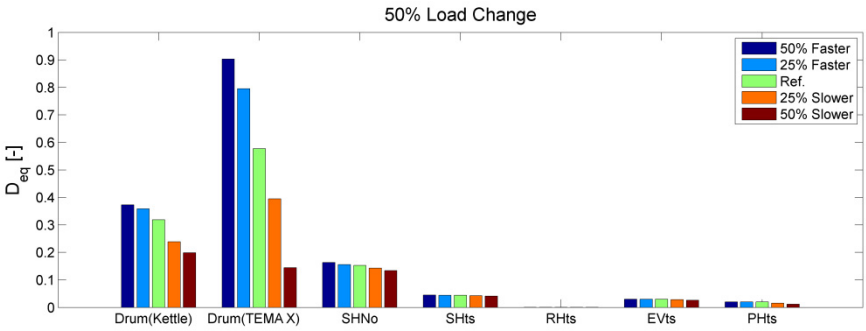

Figure 6.11: Fatigue results for a 50% load change transient case.

6.5. Conclusions

A fatigue analysis of the steam generator of a parabolic trough power plant is carried out using ASME Section VIII Div 2 [23]. Two transient operations of steam generator start-up are investigated: the evaporator temperature ramp and the heat transfer fluid temperature ramp. In addition, a 50% load change of steam generator is also studied. The stresses are calculated using the models described in Chapter 5, which have been validated with finite element simulations.

The results of the fatigue analysis for the steam generator start-up and shutdown show significant variations on the lifetime of the steam generator components when different evaporator temperature ramps are used. An extremely low lifetime (18 years considering 300 start-ups per year) is obtained for the reheater due to the high thermal stress obtained on the tubesheet. This push the need to sought other design alternatives for the reheater. The results show that the load change operation produces the higher fatigue damage on SH nozzle and steam drum junctions. In addition, it is observed a very low fatigue damage on heat exchangers tubesheets during the load change operation.

As a result of the fatigue analysis, it is shown that the TEMA X evaporator provides a very good alternative against kettle evaporator. The TEMA X evaporator allows the reduction of the steam generator start-up time with temperature ramps until 9 ºC/min obtaining a enough safe margin on its lifetime.

Nomenclature

Abbreviations

CCPs: combined-cycle plants.

CSP: concentrating solar plants.

EV: evaporator.

EVts: evaporator tubesheet.

HCF: high cycle fatigue.

HRSG: heat recovery steam generator.

HTF: heat transfer fluid.

LCF: low cycle fatigue.

PH: preheater.

PHts: preheater tubesheet.

PPTP: parabolic trough power plant

RH: reheater.

RHts: reheater tubesheet.

SG: steam generator.

SH: superheater.

SHNo: superheater nozzle outlet.

SHts: superheater tubesheet.

UTS: ultimate tensile strength.

Symbols

D : fatigue damage (-).

D_{eq} : fatigue damage equivalent to the start-up reference case (-).

E : modulus of elasticity (MPa).

F : peak stress (MPa).

K_e : fatigue penalty factor (-).

K_f : fatigue strength reduction (-).

$K_{v,k}$: Poisson's correction factor (-).

N_k : number of allowable cycles (-).

P_L : primary local membrane stress (MPa).

P_m : primary general membrane stress (MPa).

P_b : primary bending stress (MPa).

Q : secondary stress (MPa).

S : maximum allowable stress defined in ASME Section II [28] (MPa).

S_a : allowable stress amplitude for fatigue analysis (MPa).

S_{PS} : maximum allowable stress for ratcheting analysis (MPa).

S_y : yield stress limit (MPa).

P_b : primary bending stress (MPa).

t : thickness (m).

y : vertical coordinate (m).

Greek Symbols

$\Delta S_{alt,k}$: effective alternative stress (-).

$\Delta S_{n,k}$: equivalent alternative stress (-).

$\Delta S_{LT,k}$: equivalent thermal stress (-).

$\Delta S_{P,k}$: equivalent peak stress (-).

σ :stress (MPa).

6.6. References

[1] Laumert B. Csp Roadmap Wp1 2012:1–9.

[2] Turconi R, O'Dwyer C, Flynn D, Astrup T. Emissions from cycling of thermal power plants in electricity systems with high penetration of wind power: Life cycle assessment for Ireland. Appl Energy 2014;131:1–8. doi:10.1016/j.apenergy.2014.06.006.

[3] Usaola J. Participation of CSP plants in the reserve markets: A new challenge for regulators. Energy Policy 2012;49:562–71. doi:10.1016/j.enpol.2012.06.060.

[4] Ferruzza D, Topel M, Basaran I, Laumert B. Start-Up Performance of Parabolic Trough Concentrating Solar Power Plants. SolarPACES Conf Procedings 2016.

[5] Pelagotti L, Sørensen K, Condra TJ, Franco A. Modelling of a Coil Steam Generator for CSP applications 2014.

[6] Benato A, Bracco S, Stoppato A, Mirandola A. LTE: A procedure to predict power plants dynamic behaviour and components lifetime reduction during transient operation. Appl Energy 2016;162:880–91. doi:10.1016/j.apenergy.2015.10.162.

[7] Angerer M, Kahlert S, Spliethoff H. Transient simulation and fatigue evaluation of fast gas turbine startups and shutdowns in a combined cycle plant with an innovative thermal buffer storage. Energy 2017;130:246–57. doi:10.1016/j.energy.2017.04.104.

[8] Tonti A. Cyclic capability of steam generators, EN12952-4, other codes and experimental results. Int J Press Vessel Pip 2010;87:650–5. doi:10.1016/j.ijpvp.2010.08.003.

[9] Mertens N, Alobaid F, Starkloff R, Epple B, Kim HG. Comparative investigation of drum-type and once-through heat recovery steam generator during start-up. Appl Energy 2015;144:250–60. doi:10.1016/j.apenergy.2015.01.065.

[10] DYMOLA Systems Enginering: Multi-Engineering Modeling and Simulation based on Modelica and FMI 2017. https://www.3ds.com/products-services/catia/products/dymola/ [accesed 08/07/2017].

[11] Benato A, Stoppato A, Bracco S. Combined cycle power plants: A comparison between two different dynamic models to evaluate transient behaviour and residual life. Energy Convers Manag 2014;87:1269–80. doi:10.1016/j.enconman.2014.06.017.

[12] European Committee For Standardization, EN 13345-Part3, Unfired Pressure Vessels 2014.

[13] European Standard EN12952-3. Water-tube Boiler and Auxiliary Installations - Part 3: Design and Calculation for Pressure Parts 2001.

[14] European Standard EN12952-4. Water-tube Boiler and Auxiliary Installations - Part 4: in-service boiler life expectancy calculations 2001.

[15] Mirandola a., Stoppato a., Lo Casto E. Evaluation of the effects of the operation strategy of a steam power plant on the residual life of its devices. Energy 2010;35:1024–32. doi:10.1016/j.energy.2009.06.024.

[16] American Society of Mechanical Engineers. ASME boiler and pressure vessel code, Section III, Division 1, Subsection NH 2010.

[17] ANSYS Inc. ANSYS Mechanical Enterprise - Structural Analysis Software for FEA :http://www.ansys.com/about-ansys 2017.

[18] Kelly B, Kearney D. Thermal Storage Commercial Plant Design Study for a 2-Tank Indirect Molten Salt System Final Report 2006.

[19] Kelly B. Nexant Parabolic Trough Solar Power Plant Systems Analysis Task 1 : Preferred Plant Size. Contract 2006.

[20] Kelly B. Advanced Thermal Energy Storage for Central Receivers with supercritical coolants, Abengoa Solar Inc., 2010.

[21] TEMA. Standards of the tubular exchangers manufacturers association, 9th ed. Tubular Exchanger Manufactures Association, 2007.

[22] American Society of Mechanical Engineers. ASME boiler and pressure vessel code, Section VIII- Division1 2010.

[23] American Society of Mechanical Engineers. ASME boiler and pressure vessel code, Section VIII- Division2 2010.

[24] Shen J, Tang Y, Xu J, Liu Y. Strength and fatigue analysis of tubesheet subjected to thermal shock. Proc ASME 2016 2016:1–8.

[25] Dong P, Hong JK, De Jesus AMP. Analysis of Recent Fatigue Data Using the Structural Stress Procedure in ASME Div 2 Rewrite. J Press Vessel Technol 2007;129:355. doi:10.1115/1.2748818.

[26] Lu Y. High-temperature low-cycle-fatigue and crack-growth behaviors of three superalloys: HASTELLOY X, HAYNES 230, and HAYNES 188 2005;Ph.D.:329.

[27] Oakey JE. Power plant life management and performance improvement. Woodhead Publishing; 2011.

[28] American Society of Mechanical Engineers. ASME boiler and pressure vessel code, Section II 2010.

[29] Sowinski J, Osage D, Brown R. ASME Section VIII - Division2 : Example Problem Manual 2013.

[30] Schenk H, Dersch J, Hirsch T, Polklas T. Transient Simulation of the Power Block in a Parabolic Trough Power Plant. Proceeding 11 Th Int Model Conf 2015:605–14. doi:10.3384/ecp15118605.

[31] Hirsch T, Fabian Feldhoff J, Schenk H. Start-Up Modeling for Annual CSP Yield Calculations. J Sol Energy Eng 2012;134:31004. doi:10.1115/1.4006268.

CHAPTER

SEVEN

Conclusions

In this thesis the design and the dynamic analysis of the heat exchangers of the steam generator for parabolic trough and solar tower power plants was presented. The heat exchanger design was made following TEMA standards and ASME Pressure Vessel code. Genetic algorithms were used to obtain feasible and optimized heat exchanger designs. Several analytical models were proposed to estimate the dynamic response and the stresses of the heat exchangers. This approach based on low-time consumption models can be considered a powerful tool as it can be used to optimize the steam generator operation, allowing the estimation of the lifetime material consumption in real time.

In Chapter 2 a methodology for the design of the heat exchangers of the steam generator and oil-to-salt heat exchangers in a 50 MWe parabolic trough power plant was presented. The economic analysis obtained the global optimum for 4.85 ºC for the evaporator pinch point and 293 ºC for the outlet temperature of the heat transfer fluid. The best steam generator design consists of TEMA H shell for superheater and preheater and TEMA F shell for reheater. A TEMA X recirculation evaporator was proposed as alternative of kettle evaporator. The best design for the oil-to-salt heat exchanger consists of six TEMA F shell heat exchanger in series with a log mean temperature difference of 7 ºC and the molten-salt placed on the shell-side.

In Chapter 3 a methodology for the design of the heat exchangers of the steam generator of 110 MWe solar power tower plant was presented. The preliminary economic analysis shows that the forced circulation evaporator design presented lower annual costs (capital and operation) than natural circulation design. The proposed designs for the steam generator consist of U-shell type for superheater and

reheater, TEMA E shell forced circulation evaporator and TEMA F shell for preheater. Two configurations were analyzed: with one or two parallel trains. The economic analysis reveals the optimum evaporator pinch points of 2.6 ºC and 3 ºC, respectively.

A daily start-up simulation of the steam generator of solar power tower plant was performed in Chapter 4. Two initial start-up conditions were analyzed. The first assumes non-isothermal temperature profiles on the heat exchangers at the beginning of the start-up. The steam generator start-up takes around 50 minutes with a thermal energy consumption of 70 MWh_{th}. The second approach assumes isothermal initial conditions in the heat exchangers as a result of the cold salt circulation through the steam generator during the night to reduce the risk of salt freeze. In this case, the start-up time is around 110 minutes with a thermal energy consumption of 80 MWh_{th}. For both start-ups the most limiting stresses are obtained at the tubesheet junction. Furthermore, two start-up feedwater heat-up systems were analyzed. The first one consists of water circulation from steam drum, whereas the second one consists of steam circulation. It is observed that the second system provides suitable outlet preheater salt temperatures reducing the potential salt freeze risk.

A dynamic analysis of the steam generator of a parabolic trough plant was presented in Chapter 5. A start-up simulation is performed using relatively high temperature ramps for the thermal oil inlet and evaporator. The results are successful for the proposed steam generator design because the ratcheting and magnetite protection stress limits are not violated. The start-up requires around 45 minutes and a thermal energy of 36.4 MWh_{th}. The higher thermal stresses are obtained on the no-tube-lane of the U-tube tubesheets of the heat exchangers, especially in the reheater. The comparison study between TEMA X recirculation and kettle evaporators reveals a thermal stress reduction about 35% for the first design.

Lastly, a fatigue analysis of the steam generator of a parabolic trough plant was performed in Chapter 6. Two transient operations of steam generator start-up were studied: the evaporator temperature ramp and the heat transfer fluid temperature ramp. In addition, a 50% load change of steam generator was also studied. The stresses were calculated using the models described in Chapter 5, which have been validated with finite element simulations. The results showed an extremely low lifetime for the reheater due to the high thermal stress obtained on the tubesheet. This pushes the need to improve the reheater design. On the other hand, it was shown that the TEMA X evaporator provides a very good alternative against kettle evaporator. The TEMA X evaporator allows the reduction of the steam generator start-up time with temperature ramps until 9 ºC/min obtaining a enough safe margin on its lifetime.

Appendix

Appendix A. Evaporator calculations

The properties of the two phase flow on the tube side have great changes along the tube length, therefore the evaporator is discretized with $N = N_b$ and $M = N_{tp}$. Figure A.1 shows the heat exchanger discretization cell model.

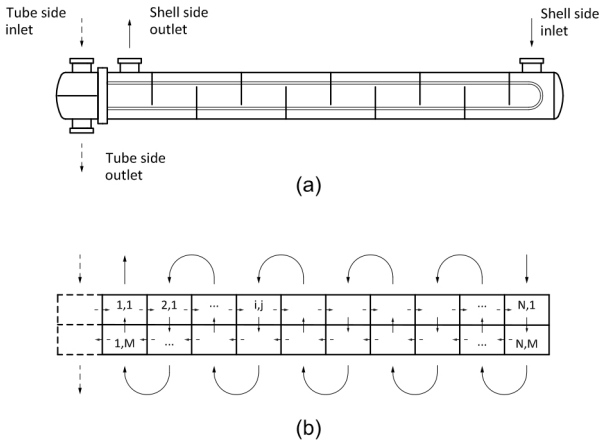

Figure A.1: Heat exchanger discretization cell model.

The energy balance in each cell leads to Equations A.1, A.2 and A.3. In the first step, the two-phase heat transfer coefficient on tube side $h_{t,local}$ and the overall heat

transfer coefficient U_{local} are calculated by means of the initial conditions (the inlet salt temperature and the inlet steam quality). Then, the local heat flux, the salt outlet temperature and the outlet steam quality are calculated using Equations A.1, A.2 and A.3. Furthermore, local properties are evaluated in each cell: the two-phase zone ($zone_{tp}$), the critical heat flux (q_{crit}), the two-phase velocity (v_{tp}), the two-phase pressure drop (ΔP_{tp}). The process is repeated until the sum of local heat flux is $\sum \Delta q = Q_{ev}$. Then the evaporator heat transfer area is calculated as: $A = \Delta A \cdot N \cdot M$ and the pressure drop on tube side: $\Delta P_{t,EV} = \sum \Delta P_{tp}$. A schematic of the evaporator calculations is shown in Figure A.2.

$$\Delta q(i,j) = U_{local}(i,j)\Delta A(\overline{T}_{sa}(i,j) - T_{sat}) \tag{A1}$$

$$T_{sa,out}(i,j) = \frac{\Delta q(i,j)}{\dot{m}_{sa} C_{p,sa}} + T_{sa,in}(i,j) \tag{A2}$$

$$x_{out}(i,j) = x_{in}(i,j) + \frac{\Delta q(i,j)}{h_{fg}\dot{m}_{rec}} \tag{A3}$$

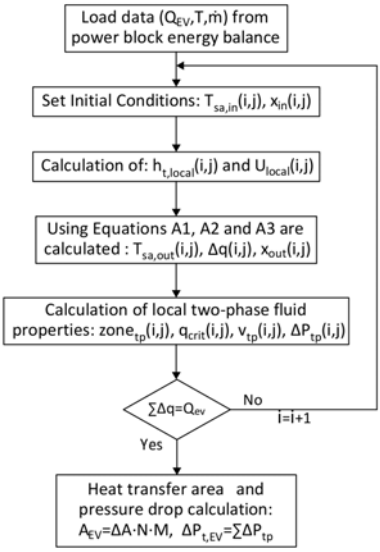

Figure A.2: Scheme of the evaporator calculation.

Appendix B. Tubesheet stress calculations

Since ASME Section VIII-Division 1 or/and TEMA standards does not takes into account thermal loads, the method proposed by O'Donnell et al. [36] is used for tubesheet thickness calculation. The main equations for the stress calculations proposed by O'Donnell et al. [36] are shown in Table B.1. Also, an schematic of the main tubesheet zones is illustrated in Figure B.1.

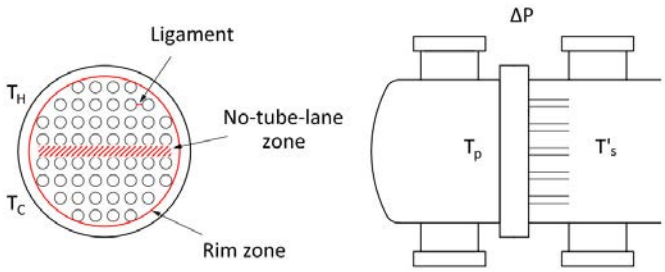

Figure B.1: Schematic of Tubesheet zones.

The calculation process of the tubesheet stresses is described in the following steps:

- Calculation of the effective elastic constants according to O'Donnell et al. [36].
- Calculation of the stresses due to the pressure load in an equivalent solid plate in the radial, σ_r^p, and tangential, σ_θ^p directions.
- Calculation of the stress due to the thermal loads using Equation B.5 where: $\sigma_\theta^t = \sigma_r^t = \sigma_{skin}$.
- The stress of an equivalent solid plate, σ_1, is calculated considering only the pressure load where : $\sigma_1 = \max(|\sigma_\theta^p|, |\sigma_r^p|)$. Then, the average stress across

ligament at either surface of plate is calculated using Equation B.1 which must be lower than: $\sigma_{eff} \leq 1.5\, S_m$.

- Calculation of the average stress across ligament and through thickness using Equation B.2 which must be lower than: $S_{eff} \leq S_m$.

- The stress of an equivalent solid plate, σ_1 , is calculated combining pressure and thermal loads where: $\sigma_1 = \max(\left|\sigma_\theta^p + \sigma_\theta^t\right|, \left|\sigma_r^p + \sigma_r^t\right|)$ .Then, the average stress across ligament at either surface of plate is calculated using Equation B.1 which must be lower than: $\sigma_{eff} \leq 3\, S_m$.

Table B.6.2: Main equations for stress calculations proposed by O'Donnell et al. [1].

Load	Stress intensity	Equation
Pressure and thermal	Average across ligament at either surface of plate	$\sigma_{eff} = K\frac{R}{h}\left\|\sigma_1\right\|$ (B.1)
Pressure	Average across ligament and through thickness	$S_{eff} = \frac{R}{h}\left[\left(\frac{\Delta P r}{H}\right)^2 + \left(\sigma_r\right)^2\right]$ (B.2)
Pressure and thermal	Peak in ligaments	$\sigma_{\max} = Y\sigma_1 + P$ (B.3)
Pressure and thermal	Peak at perforations adjacent to rim	$\sigma_{\max} = K_r\sigma_{rim} + P$ (B.4)
Thermal (skin effect)	Peak at surface	$\sigma_{\max} = \frac{E\,\alpha_T (T_P - T_s')}{1-\nu}$ (B.5)
Thermal (temperature difference across no-tube-lane zone)	Peak in ligaments	$\sigma_{\max} = \frac{K_u E^*\,\alpha_T (T_H - T_C)}{2}$ (B.6)
Thermal (temperature difference across no-tube-lane zone)	Peak at holes adjacent to no-tube-lane zone	$\sigma_{\max} = \frac{K_D E\,\alpha_T (T_H - T_C)}{2(1-\nu)}$ (B.7)

Appendix C. U-Tube stress calculations

The U-tube stress calculations are performed following the methodology proposed by Singh et al. [2].

Based on the elasticity theory, the energy deformation of the tubes in the straight and curve sections can be calculated as follows:

$$U = \int \frac{N^2}{2EA} ds + \int \frac{V^2}{2GA} ds + \int \frac{M^2}{2EI} ds \tag{C.1}$$

The forces and displacements can be related using Castigliano's theorem:

$$\frac{\partial U}{\partial P} = u; \qquad \frac{\partial U}{\partial R} = v; \qquad \frac{\partial U}{\partial M} = \alpha; \tag{C.2}$$

Then, the moment on a generic point (M_i) can be written as function of the stiffness K_i and the rotation angle α_i as: $M_i = K_i \alpha_i$. The stiffness is expressed as function of $K_i = f(\alpha_i, L, L_{bc}, E, I)$. Since the rotation angles (α_i) are unknown, initial values must be set for the stiffness calculation (K_i^0), and then the matrix $[B]$ can be calculated. The rotation angle (α_2), the vertical force (R) and the axial force (P) in leg 2 are calculated as follows:

$$\begin{Bmatrix} \alpha_2 \\ R \\ P \end{Bmatrix} = [B]^{-1} \begin{Bmatrix} \delta \\ 2\Delta - \varepsilon_1 - \varepsilon_2 \\ 0 \end{Bmatrix} \tag{C.3}$$

where δ is free thermal expansion of leg1 over leg 2, Δ is the increase in the radius of the U-bend due to its temperature rise, ε_1 and ε_2 are the vertical displacements of leg 1 and 2, respectively. The rotation angle in leg 1 is calculated by means of the moment equilibrium on U-bend:

$$\alpha_1 = \frac{1}{K_1^0}(K_2^0 \alpha_2 + 2Pr - R(S_1 - S_2)) \tag{C.4}$$

where r is the U-bend radius, S_1 and S_2 are the overhang longitudes. At this point, the rotation angles are known, and then the values of stiffness can be recalculated obtaining K_i^1. The process is repeated until the convergence of stiffness values is achieved: $\Delta K_i = K_i^1 - K_i^0 \leq tol$. Once the problem is converged, the stress on the U-bend is calculated as follows:

$$M(\theta) = M_2 + R(S_2 + r\sin\theta) + Pr(1-\cos\theta) \tag{C.5}$$

$$\sigma(\theta) = \frac{\psi \; M(\theta) \; C_o}{I} \tag{C.6}$$

where ψ is the stress intensification factor for the U-bend and C_o is the outer tube radius.

References

[1] W.J. O'Donnell, B.F. Langer, Design of perforated plates, J. Eng. Ind. 84 (1962) 307–319. doi:10.1115/1.3667483.

[2] K.P. Singh, M. Holtz, On Thermal Expansion Induced Stresses in in U-Bends of Shell-and- Tube Heat Exchangers, Eng. Power. 101 (1979) 634–639.

List of Publications

The results of this PhD thesis have been published in the following papers:

- González-Gómez PA, Petrakopoulou F, Briongos JV, Santana D. Cost-based design optimization of the heat exchangers in a parabolic trough power plant. Energy 2017;123:314–25.

- González-Gómez PA, Gómez-Hernández J, Briongos JV, Santana D. Thermo-economic optimization of molten salt steam generators. Energy Conversion and Management 2017;146:228–43.

- González-Gómez PA, Gómez-Hernández J, Briongos JV, Santana D. Steam generator daily start-up for solar power tower plants. *Submitted for publication in Applied Energy*.

- González-Gómez PA, Gómez-Hernández J, Santana D., Ferruzza D., Haglind F., Steam generator daily start-up for parabolic trough power plants. *Submitted for publication in Applied Energy*.

The following conference presentations are also an outcome of the thesis:

- González-Gómez PA, Petrakopoulou F, Briongos JV, Santana D. Steam Generator Design for Solar Towers using Solar Salt as Heat Transfer Fluid. SolarPaces Conference 2016.

- González-Gómez PA, Gómez-Hernández J, Briongos JV, Santana D. Evaporator optimization for solar tower power plants. CNIT 10, Lleida, Spain, 2017.

- González-Gómez PA, Gómez-Hernández J, Briongos JV, Santana D. Assesment of evporators using solar salt as heat transfer fluid. SolarPaces Conference 2017.

Other works not directly linked to this PhD thesis are:

- Rodríguez-Sánchez MR, Sanchez-Gonzalez A, González-Gómez PA, Marugán-Cruz C, Santana D. Thermodynamic and economic assessment of a new generation of subcritical and supercritical solar power towers. Energy 2016;1–11.

- Gómez-Hernández J, González-Gómez PA, Ni-Song T, Briongos JV, Santana D. Design of a solar linear particle receiver placed at the ground level. SolarPaces Conference 2017.

- Gómez-Hernández J, González-Gómez PA, Briongos JV, Santana D. Influence of the steam generator on the exergetic and exergoeconomic analysis of solar tower plants. *Submitted for publication in Energy*.